PROBABILISTIC DESCRIPTION OF FATIGUE CRACK GROWTH UNDER CONSTANT-AND VARIABLE-AMPLITUDE LOADING

by

H. Ghonem and M. Zeng

THE UNIVERSITY OF RHODE ISLAND
Solid Mechanics Laboratory
Department of Mechanical Engineering and Applied Mechanics

MARCH 1989

Prepared For
DEPARTMENT OF AIR FORCE
AIR FORCE OFFICE OF SCIENTIFIC RESEARCH
BOLLING AIR FORCE BASE, DC 20032

Contract AFOSR-85-0362

Unclassified

SECURITY CLASSIFICATION OF THIS PAGE

19 MAY

19 MAY 1989

REPORT DOCUMENTATION PAGE

1a REPORT SECURITY CLASSIFICATION: UNCLASSIFIED	1b RESTRICTIVE MARKINGS
2a SECURITY CLASSIFICATION AUTHORITY	3 DISTRIBUTION/AVAILABILITY OF REPORT: Approved for Public Release; Distribution is unlimited
2b DECLASSIFICATION/DOWNGRADING SCHEDULE	
4 PERFORMING ORGANIZATION REPORT NUMBER(S)	5 MONITORING ORGANIZATION REPORT NUMBER(S): AFOSR-TR- 89-0716
6a NAME OF PERFORMING ORGANIZATION: UNIVERSITY OF RHODE ISLAND; 6b OFFICE SYMBOL (If applicable)	7a NAME OF MONITORING ORGANIZATION: AFOSR/NA
6c ADDRESS (City, State and ZIP Code): Dept of Mechanical Engineering, Solid Mechanics Laboratory, Kingston, RI 02881	7b ADDRESS (City, State and ZIP Code): Building 410, Bolling AFB, Washington, DC 20332-6448
8a NAME OF FUNDING/SPONSORING ORGANIZATION: AFOSR/NA; 8b OFFICE SYMBOL (If applicable): NA	9 PROCUREMENT INSTRUMENT IDENTIFICATION NUMBER: AFOSR-85-0362
8c ADDRESS (City, State and ZIP Code): Building 410, Bolling AFB, Washington DC 20332-6448	10 SOURCE OF FUNDING NOS.

PROGRAM ELEMENT NO	PROJECT NO	TASK NO.	WORK UNIT NO.
61102F	2302	B2	

11 TITLE (Include Security Classification): [U] Prob. Descrip. of Fatigue Crack Growth under Constant-and Variable-Amplitude Loading

12. PERSONAL AUTHOR(S): H. Ghonem and M. Zeng

13a TYPE OF REPORT	13b TIME COVERED	14 DATE OF REPORT (Yr., Mo., Day)	15. PAGE COUNT
FINAL	FROM 85-1-16 TO 88-11-15	89-4-15	180

16. SUPPLEMENTARY NOTATION

17 COSATI CODES			18 SUBJECT TERMS (Continue on reverse if necessary and identify by block number)
FIELD	GROUP	SUB GR	CRACK; OVERLOAD; STOCHASTIC PROCESS; RETARDATION

19. ABSTRACT (Continue on reverse if necessary and identify by block number)

This report is concerned with the discription of the development and application of a stochastic crack growth model. It is built as a discontinuous Markov process and is inhomogeneous with respect to the number of cycles required for the crack to reach a specified crack length. The model is then used to describe the evolution of the crack length in terms of growth curves, each of whose points possess equal probability of advancing from one position to another forward position. The validity of the model is established by applying it to constant-as well as to variable amplitude loading. In those applications the theoretical constant probability crack growth curves generated by the model compared to those experimentally obtained using Al 7075-T6 and Al 2024-T3 material for constant-amplitude loading while Ti-6Al-4V was used in single overload application. Results of these comparisons indicate the ability of the proposed model when fitted with parameters whose values can be obtained from a limited numbers of experimental tests, to predict the crack growth statistics under different loading conditions.

20 DISTRIBUTION/AVAILABILITY OF ABSTRACT	21 ABSTRACT SECURITY CLASSIFICATION
UNCLASSIFIED/UNLIMITED ☐ SAME AS RPT ☒ DTIC USERS ☐	UNCLASSIFIED

22a NAME OF RESPONSIBLE INDIVIDUAL	22b TELEPHONE NUMBER (Include Area Code)	22c OFFICE SYMBOL
G. Haritos	202-767-0463	NA

DD FORM 1473, 83 APR EDITION OF 1 JAN 73 IS OBSOLETE

SECURITY CLASSIFICATION OF THIS PAGE

1. REPORT NO.	2. GOVERNMENT AGENCY	3. RECIPIENT'S CATALOG NO.
4. TITLE AND SUBTITLE Probabilistic Description of Fatigue Crack Growth Under Constant- and Variable - Amplitude Loading		5. REPORT DATA March 1989 6. PERFORMING ORG. CODE
7. AUTHORS H. Ghonem and M. Zeng		8. PERFORMING ORG. REPT NO. URI-MSL-891
9. PERFORMING ORG NAME AND ADDRESS University of Rhode Island Department of Mechanical Engineering Solid Mechanics Laboratory Kingston, RI 02881		10. WORK UNIT NO. 11. CONTRACT OR GRANT NO. AFOSR-85-0362
12. SPONSORING AGENCY NAME AND ADDRESS U.S. Air Force Office of Scientific Research Bolling Air Force Base Washington, DC 20032		13. TYPE REPT. /PERIOD COVERED Final Report 14. SPONSORING AGENCY CODE

15. SUPPLEMENTARY NOTES

This report is concerned with the discription of the development and application of a stochastic crack growth model. It is built as a discontinuous Markov process and is inhomogeneous with respect to the number of cycles required for the crack to reach a specified crack length. The model is then used to describe the evolution of the crack length in terms of growth curves, each of whose points possess equal probability of advancing from one position to another forward position. The validity of the model is established by applying it to constant-as well as to variable amplitude loading. In those applications the theoretical constant probability crack growth curves generated by the model compared to those experimentally obtained using Al 7075-T6 and Al 2024-T3 material for constant-amplitude loading while Ti-6Al-4V was used in single overload application. Results of these comparisons indicate the ability of the proposed model when fitted with parameters whose values can be obtained from a limited numbers of experimental tests, to predict the crack growth statistics under different loading conditions.

17. KEYWORDS (SUGGESTED BY AUTHORS)	18. DISTRIBUTION STATEMENT
Crack, Overload, Stochastic Process, Retardation	

19. SECURITY CLASS THIS(REPT)	20. SECURITY CLASS THIS(PAGE)	21. NO PGS.	22. PRICE
Unclassified	Unclassified	180	

ABSTRACT

This report is concerned with the discription of the development and application of a stochastic crack growth model. It is built as a discontinuous Markov process and is inhomogeneous with respect to the number of cycles required for the crack to reach a specified crack length. The model is then used to describe the evolution of the crack length in terms of growth curves, each of whose points possess equal probability of advancing from one position to another forward position. The validity of the model is established by applying it to constant as well as to variable amplitude loading. In those applications the theoretical constant probability crack growth curves generated by the model were compared to those experimentally obtained using Al 7075-T6 and Al 2024-T3 materials for constant-amplitude loading while Ti-6Al-4V was used in single overload application. Results of these comparisons indicate the ability of the proposed model, when fitted with parameters whose values can be obtained from a limited numbers of experimental tests, to predict the crack growth statistics under different loading conditions.

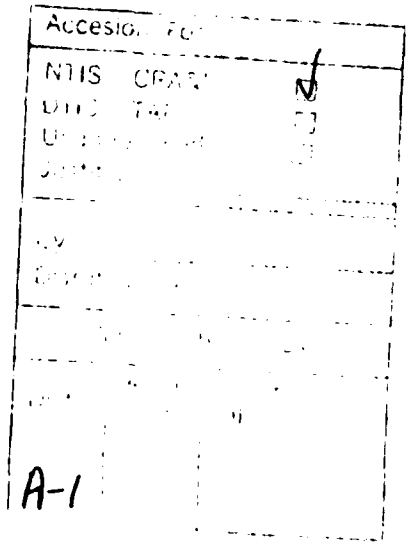

ACKNOWLEDGEMENT

This work was supported by the U.S. Air Force Office of Scientific Research under contract AFOSR 85-0362 monitored by Dr. G. Haritos. This support is gratefully acknowledged.

TABLE OF CONTENTS

LIST OF TABLES

LIST OF FIGURES

CHAPTER I

INTRODUCTION

Prediction of the fatigue crack growth process is generally made by using one of the deterministic crack growth laws which views the process as continuous in time and state. Under these laws the growth rate is calculated from the experimental knowledge of the applied stress, current crack length and other influencing parameters. As pointed out by Lauschmann[1], three applications of the mean-value operator on the crack growth are implicitly invalued in standard concepts of the growth law: averaging along the crack front, averaging in the direction of crack propagation close to the given crack length and averaging over individual realization of the process. This averaging technique provides the advantage of simplicity and the ability to respond to changes in the process's physical conditions. It suffers, however, from the inability to express the process's inherent random properties, a factor critical to engineering design and reliability management. The use of statistical distributions or probabilistic models thus becomes a necessary tool for a more reliable prediction of crack growth. In this approach one can distinguish three different groups of probabilitic models. The first group, see for example references[2-7], depends on the introduction of random variables to replace the constants in the appropriate deterministic law. The second group, examples of which are shown in references[8-10], introduces a joint probability distribution whose

variables are crack length and number of loading cycles. The last group of probabilistic models assigns a non-decreasing evolutionary feature to the growth process by using the concepts of the stochastic theory, in particular, the Markov process. Detailed analysis of these different types of models is given in reference[11]. The work in this research program falls within the definition of the last group, i.e. the stochastic Markov model. The first generation of these models, represented in the work of Bogdanoff et al[12-15], Ghonem et al[16,17] and Sedlacek[18], while having the ability to describe the random crack growth process in defined cases, has difficulty in estimating its predictive ability to cases where no experimental data is available. In recent years a different generation of stochastic models has evolved. In these models, variability in the process is taken into account by means of generalizing the growth law, using the stochastic theory, into a probability form. The work of Ghonem and Dore[19] and others[20-23] are examples of this approach. The purpose of this report is to describe the theoretical and experimental work that has been carried out in developing the model of Ghonem and Dore[19] termed the constant probability crack growth model. This description will be covered in the following three chapters. The mathematical elements of the model are introduced in chapter II, which will also deal with the correlation between the elements and the micro-physical condition of the growth process. The experimental set-up and procedure used for verifying the model in the case of constant-amplitude loading will be discussed in this chapter. Chapter III deals with an extension of the model base to include the case of random loading by utilizing a simple single overload spectrum. In

this chapter retardation experiments and their relation to the estimation of the crack growth law in the delayed zone will be described. The last chapter summarizes the findings of this research program and suggests avenues for further model refinement and application. Mathematical derivations and experimental procedures which have been published in literature during the course of this research program will not be repeated in the main text of the report. Reference will be made to these publications, some of which will be included as appendices.

CHAPTER II

COSTANTANT PROBABILITY CRACK GROWTH MODEL

2.1 Mathematical Elements

Formulations of this model and its theoretical development have been detailed in references [11, 19], see appendix A and C. In brief summary, the model is based on the view that the crack front is identified as having a large number of arbitrarily chosen points. While each of these points can propagate under repeated cyclic loading in three dimensional geometry. The model considers only the mode I crack propagation along a plane perpendicular to that of the externally applied load. The fracture surface is divided into equally spaced states each of which has a width equal to the expected experimental error Δx. Adhering to the mechanistic properties of a propagation crack and considering the growth process to be evolutionary discrete state and time-inhomogeneous, the model yields a crack survival probability which is written as:

$$\ln P_r(i) = - \int \lambda_r di + L \qquad (1)$$

where $P_r(i)$ is the probability of the crack tip being in the state r when Δi cycles elapsed, λ_r is the transition intensity parameter at state r and L is an integration constant.

The solution of equation (1) depends on the mathematical definition of λ_r. Earlier work of Ghonem and Provan[16, 17] considered λ_r linearly dependent on r in the form

$$\lambda_r = r\lambda \tag{2}$$

where λ is a material constant. This yields a growth process well described as a Markovian linear birth process. Difficulties in this approach have been analyzed in the reference[11].

In the present program, λ_r was established as a crack length, cycle and stress dependent parameter in the form

$$\lambda_r = L(r)\, e^{ki} \tag{3}$$

where L and k are state position dependents (see Appendix A). This equation in conjuction with equation (1) yields a probabilistic crack growth equation in the form

$$\begin{aligned} \ln P_r(i) &= B(e^{KI_0} - e^{Ki}) && i \geq I_0 \\ \ln P_r(i) &= 0 && i < I_0 \end{aligned} \tag{4}$$

the parameter B, K and I_0 depend on state r through the experimental functional forms

$$B = c_1 r^{n1}$$
$$K = c_2 r^{n2} \qquad (5)$$
$$I_0 = c_3 \left((r-1)^{n3} - r^{n3} \right)$$

where c_j and n_j are constants depending on load conditions, enviroment, etc. Equations (4) and (5) are the basic results. They are used to construct constant probability crack growth curves. The constants in equation (5) can be calculated by considering the crack growth curve obtained by using a continuous equation as the $P_r(i)=0.5$ curve. This can be done numerically and the constant probability crack growth curves can be established under any loading conditions without the need to perform a large number of fatigue tests. The results of this approach, when applied to data proceeded by Virckler et al[24] on Al 2024-T3, were in agreement with the experimental curves with an average error in the theoretical curves estimated at 5% (see reference[19] and Appendix A for detailes of this application).

2.2 Experimental Verification

In order for the model to have a wider scope of application, a verification of the model was carried out for different loading conditions on the same material. An in-house experimental program was followed, during 1985 and 1986, on Al 7075-T6. In this program, tests were conducted at three different stress levels (R=4,5,6), and at each stress level sixty replications were employed, crack length versus number of cycles was measured using a

photographic technique. The crack length measurements obtained were from 9mm to 23mm on center crack retangular specimens with dimensions of 320mm x 101mm and the thickness of 3.175mm. Diagrams of sample functions were obtained and converged into constant probability crack growth curves for each test condition. Equations (4) and (5) were then employed to obtain the theoretical constant probability crack growth curves for each corresponding test loading condition. Comparision with experimental data yielded very good correlation. The experimental program, procedure, measurement technique and analysis are described in detail in reference[11, 25] and Appendix B.

CHAPTER III

VARIABLE-AMPLITUDE LOAD APPLICATION

3.1 Introduction

A practical load spectrum contains overloads or underloads which bring about crack retardation or acceleration respectively. Single tensile overload represents the most basic and simplest situation involving retardation, see Fig. 1. Various researchers have attempted to develop predictive crack growth models involving random loading by correlating the transient effects of retardation with a wide range of variables associated with loading, metallurgical properties, environment, etc. The models are generally built around one of serveral suggested retardation mechanisms. While no one mechanism can offer interpretations of all retardation characteristics. It is possible to identifiy the principal mechanisms as:

1. Compressive residual stress created in the overload plastic zone due to the clamping action of the elastic material surrounding this zone[25-29].

2. Crack tip blunting, especially in materials with work hardening properties, which leads to a decrease of the actual ΔK at the crack tip [30].

3. Crack closure due to crack surface contact above minimum load as a result of the residual tensile strain in the material element in the wake of the crack tip. This mechanism is predominant under a plane strain condition[31, 32].

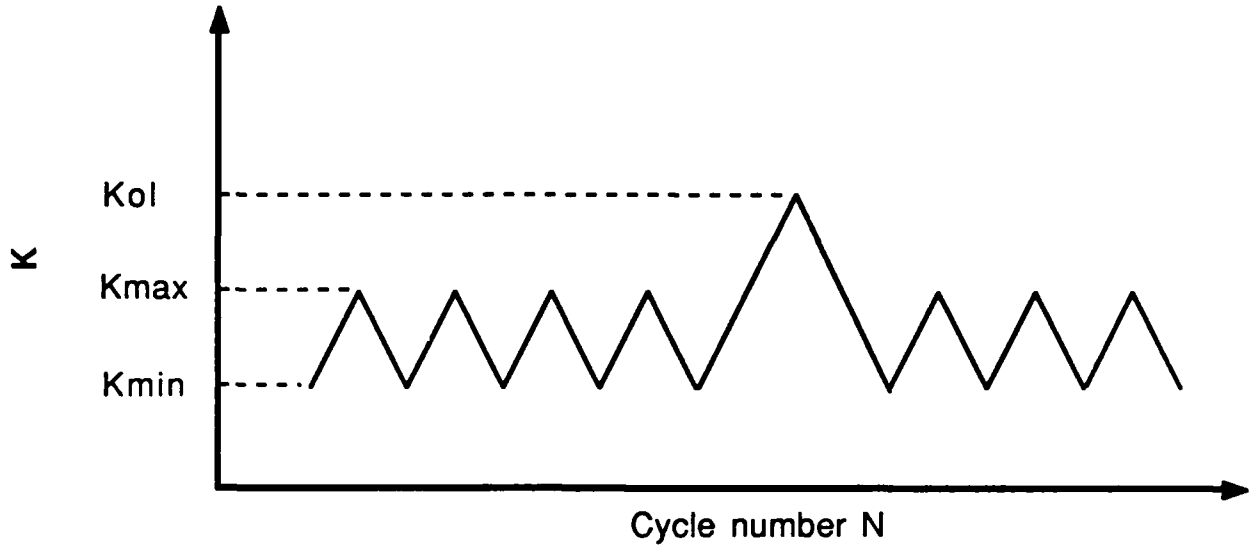

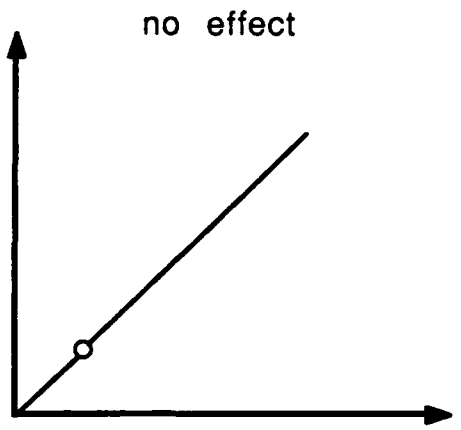

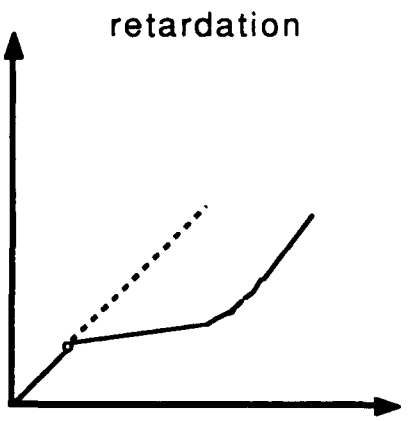

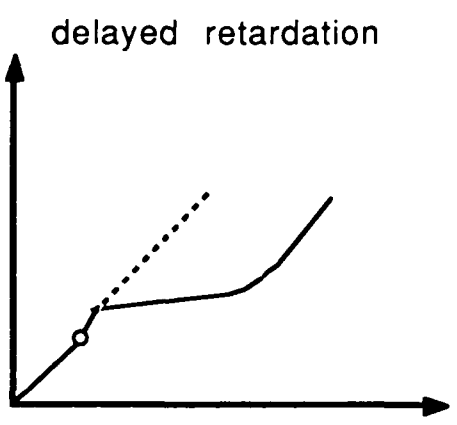

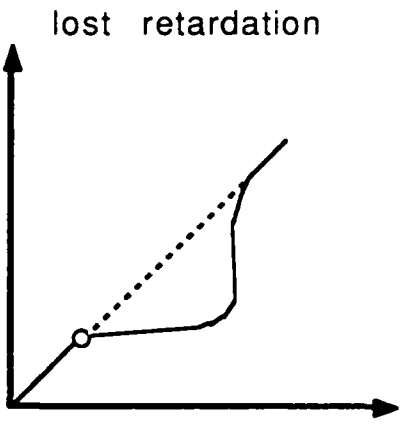

Fig. 1 Different cases of transient crack growth behavior following a tensile peak ovdrload

4. Crack plane orientation; the plane of a mode I fatigue crack has a specific orientation in relation to the applied stress. Under overload condition there can be a change of crack plane orientation producing transient effects[33].

5. Metallurgical factors, such as yield strength[34], type of precipitates[35] and strain hardening / softening characteristics[36].

As pointed out by Arone[37], almost all these mechnism can be expressed in term of the effective stress intensity factor concept which permits the calculation of the crack growth rate after overload in the same form as for the constant-amplitude loading except that the stress intensity factor is replaced by its effective value. The value is generally expressed in terms of load parameters, environmental conditions, material properties and specimen (or component) geometry. The defficiency in this approach is that, again, it does not take into account the inherent randomness of the retardation phenomenon[39] which is manifested in the high degree of scatter observed in retardation experiments[38]. The work presented in this chapter is an attempt to extend the concept of the constant-probability crack growth model to include the transient retardation effects. This is achieved by introducing an effective stress intensity parameter, ΔK_{eff}, into the definition of the transition intensity of the stochastic crack growth process. By considering the load interaction effects in an appropriate expression of ΔK_{eff}, the model generates a unified probability growth law that can be used to

predict scatter in complex random load history.

3.2 Proposed Model

3.2.1 Mathematical Elements

The constant-probability crack growth equation (1) depends on the determination of the transition intensity parameter λ_r. In Appendix C it has been shown that

$$\lambda_r = L\ \Delta i^{\alpha} \tag{6}$$

where L depends on the material, the crack position (r) and stress conditions ($\Delta\sigma$ and R).

One can thus be more specific in the above definition by rewriting it as :

$$\lambda_r = C_1\, f_1(\Delta\sigma, R)\ f_2(a)\ \Delta i^{\alpha} \tag{7}$$

both f_1 and f_2 can be expressed as a joint function expressing the effective crack tip stress intensity factor at position r. i.e.

$$\lambda_r = C_1\, f_3(\Delta K_{eff}, R)\ \Delta i^{\alpha} \tag{8}$$

where C_1 and α are material constants.

This transition intensity is, in fact, similar to that proposed by Ditlersen and Sobczyk[39]. By substituting (8) in (1) and setting a boundary condition that Pr(i)=1 when $\Delta i = 0$, one obtains

$$\Delta i = f(\Delta K_{eff}, R)\,(-\ln P_r(i))^{\beta} \qquad (9)$$

where $f(\Delta K_{eff},R)=\left(\frac{1+\alpha}{-c_1}\right)^{\beta}\,[f_3(\Delta K_{eff},R)]^{-\beta}$ and $\beta=\frac{1}{1+\alpha}$

The equation above defines the number of cycles required for the crack tip, under the driving force of $f(\Delta K_{eff}, R)$ to advance from state r to state r+1 (i.e. from crack length a to $a+\Delta a$) with a survival probability $P_r(i)$. When $P_r(i)$ is kept constant, while incremental values of Δx, i.e. crack length increments, are substituted in an appropriate form of $f(\Delta K_{eff}, R)$ a crack growth curve whose points posses the same propagation probability, can be generated.

The critical element in equation (9) is the determination of an approriate $f(\Delta K_{eff}, R)$ which includes the effects of overload. This is the subject of the following section.

3.2 $f(\Delta K_{eff}, R)$ During Retardation

From the introduction of this chapter and the extensive review on the subject of overload[41], the principal would-be mechanism responsible for crack retardation is the closure stress resulting from the induced plasticity in the wake of the crack and the constraining compressive residual stress in the overload plastic zone in front of the crack tip. If one recognizes that these two effects act simultaneously, effects to define the corresponding effective stress-

intensity factor would be more difficult than operating in a region where only one effect plays the major role. Closure stress is defined as the stress required to fully open the crack. If an externally applied load is set above the closure stress level, one can assume that $f(\Delta K_{eff}, R)$ can be calculated by accounting only for the crack tip compressive residual stress. This condition was achieved by carrying out closure experiments on compact tension specimen made of rolled and annealed Ti-6Al-4V material sheets. Specimen geometry is shown in Appendix D while material composition is listed in table 1.

C	Fe	N	Al	V	H	O
0.026	0.09	0.011	5.8	5.8	0.008	0.14

Table 1 Chemical Composition of Ti-6Al-4V Material in WT%

The notch-mounted COD gauge technique was used to measure the crack opening displacement. The experiments were carried out under constant ΔP defined by maximum and minimum load, P_{max} and P_{min} respectively, with the frequency of 15 Hz. A single overload P_{ol} was applied at crack length of 18mm, 25mm and 29mm with frequency of about 0.5 Hz. The interval crack length is large enough to avoid the overload interaction. This was carried out for different P_{min}, P_{max} and

P_{OL}. In all these test, while a permanent increase in COD measurments was registered following the overload application, no closure could be detected. This was attributed to the possible insensitivity of COD gauge resulting from the long distance between the crack tip and the position of the gauge at the mouth of the crack, which in all tests was more than 20 mm. A new set of experiments was then executed. In these a series of pairs of hardness indentations were made along two lines parallel to and equal distance from the expected nominal crack path(Fig. 2). Each pair measures 3mm apart. A strain extensometer, with an accuracy of $5x10^{-5}$, was used with the tips of its head resting in the pair of indentations whose connecting line was perpendicular

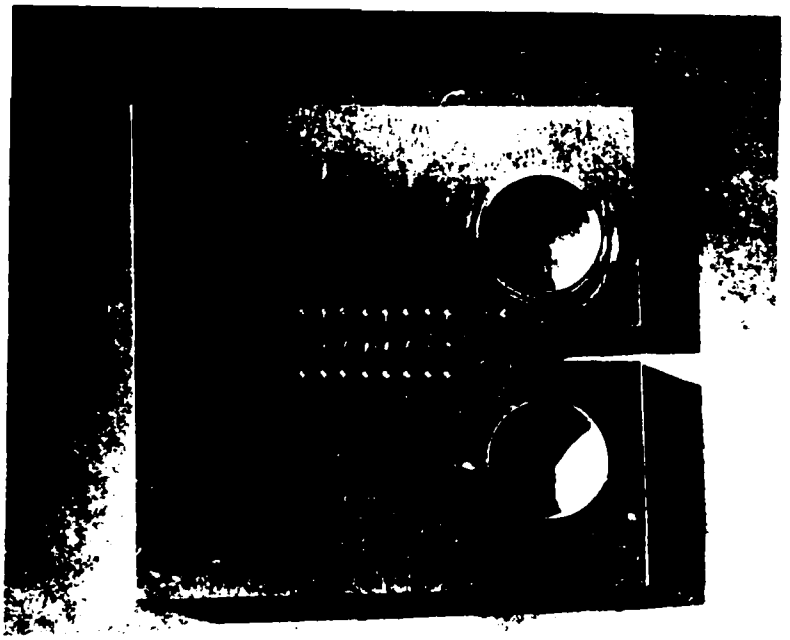

Fig. 2 A series of pairs of hardness indentations made along two lines parallel to and equal distance from the expected nominal crack path

to the crack plane. The position of the extensometer followed behind the advancing crack tip. Closure measurements were made in the same pattern discribed above, but only at the distance of 3mm behind the crack tip. A schematic of this surface measurement procedure and an illustrative photograph are shown in Figure 3 and Figure 4 respectively. Output from this experiment, in the form of load versus displacement curves for different crack lengths a and different P^{ol}_{max}/P_{max}, is shown in Figures 5(a) and (b); the indication being that, for this material, the onset of the closure depends on P_{min}. No closure was observed for $P_{min} > 1KN$. Thus it was assumed that for these Ti-6Al-4V specimens and load conditions with Pmin > 1KN, the governing retardation mechanism is the crack tip constraining compressive residual stress.

A number of models accounting for the effect of residual stress due to overloading have been suggested. The modified Willenberg et al[36] appeared to be the one most frequently referenced. According to this model, the stress intensity for crack growth is modified by a residual stress intensity factor K_R that decays linearly with crack extension. This K_R is written as:

$$K_R = \left[\frac{1 - K_{th}/K_{max}}{S - 1} \right] \left[K_{max} \left(1 - \frac{\Delta a_{ol}}{Z_{ol}}\right) - Kol \right] \qquad (10)$$

K_{th} is the maximum stress intensity factor associated with fatigue crack growth threshold at R=0; Δa_{ol} is crack growth following the overload and S is defined as a shut off ratio corresponding to that

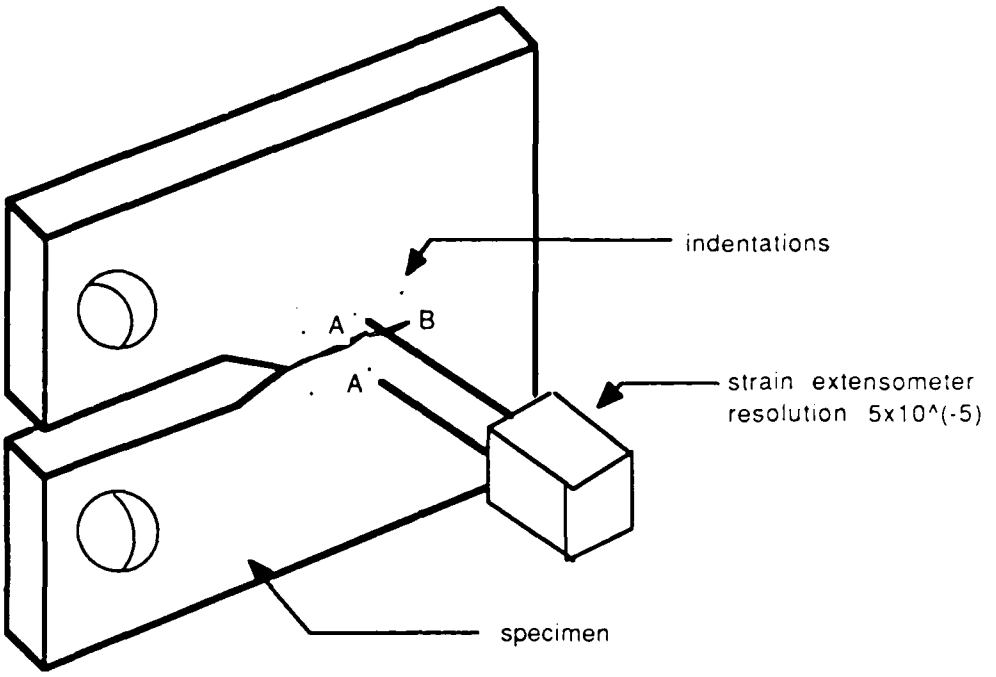

Fig. 3 Schematic sketch of closure measurement
(the position of the gauge leads A are maintained at 3mm behind the crack tip B at the moment of applying overload)

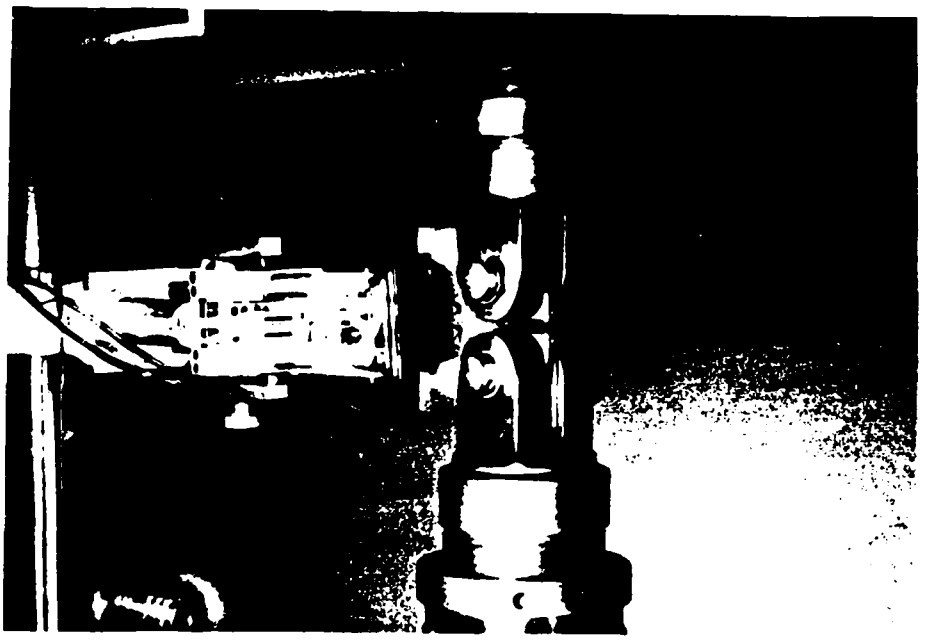

Fig. 4 Photograph of the schematic sketch shown in Fig. 3

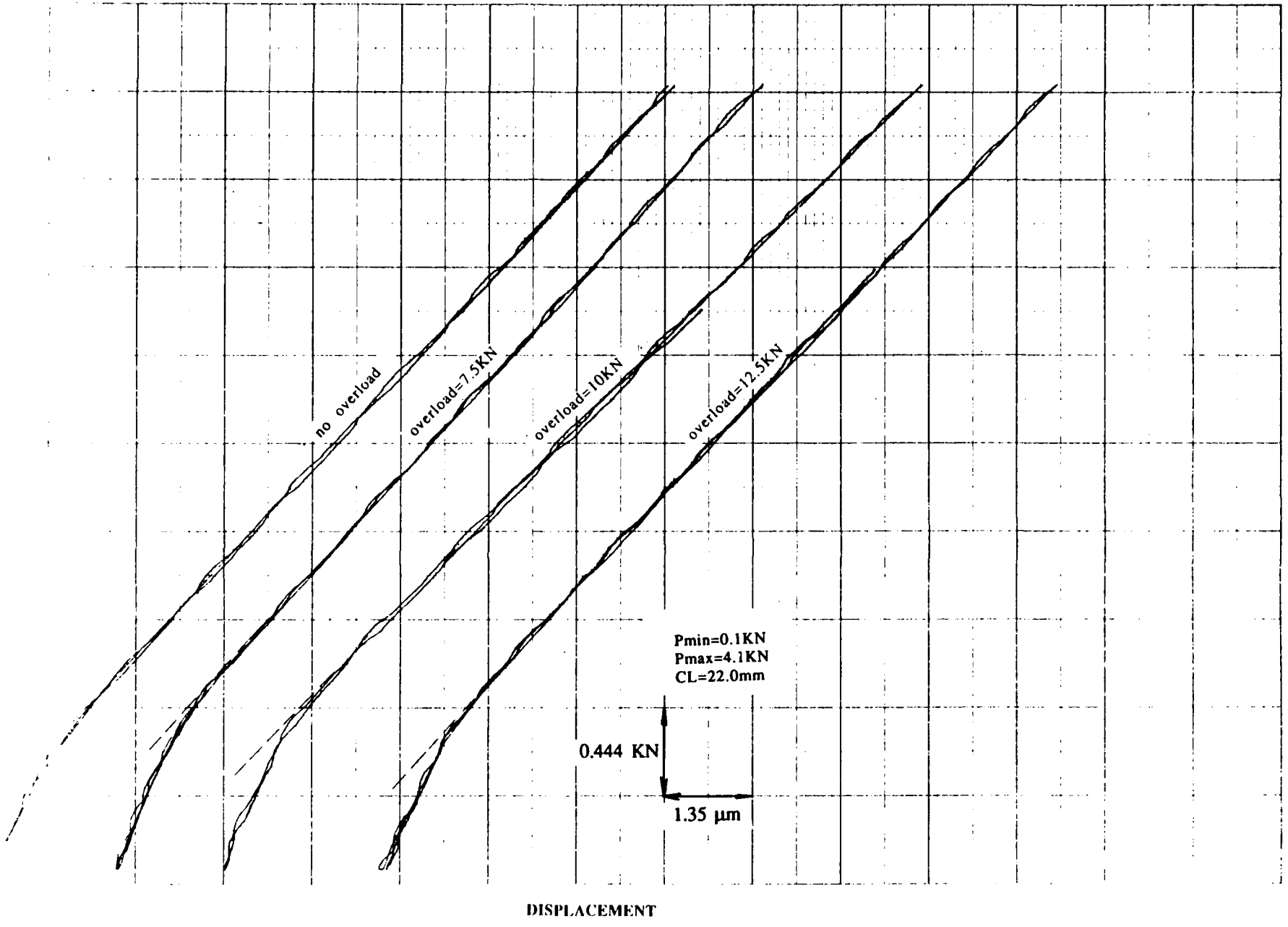

Fig. 5(a) Load-displacement measurements for crack opening displacement (displacement between extensometer and crack tip is 3mm)

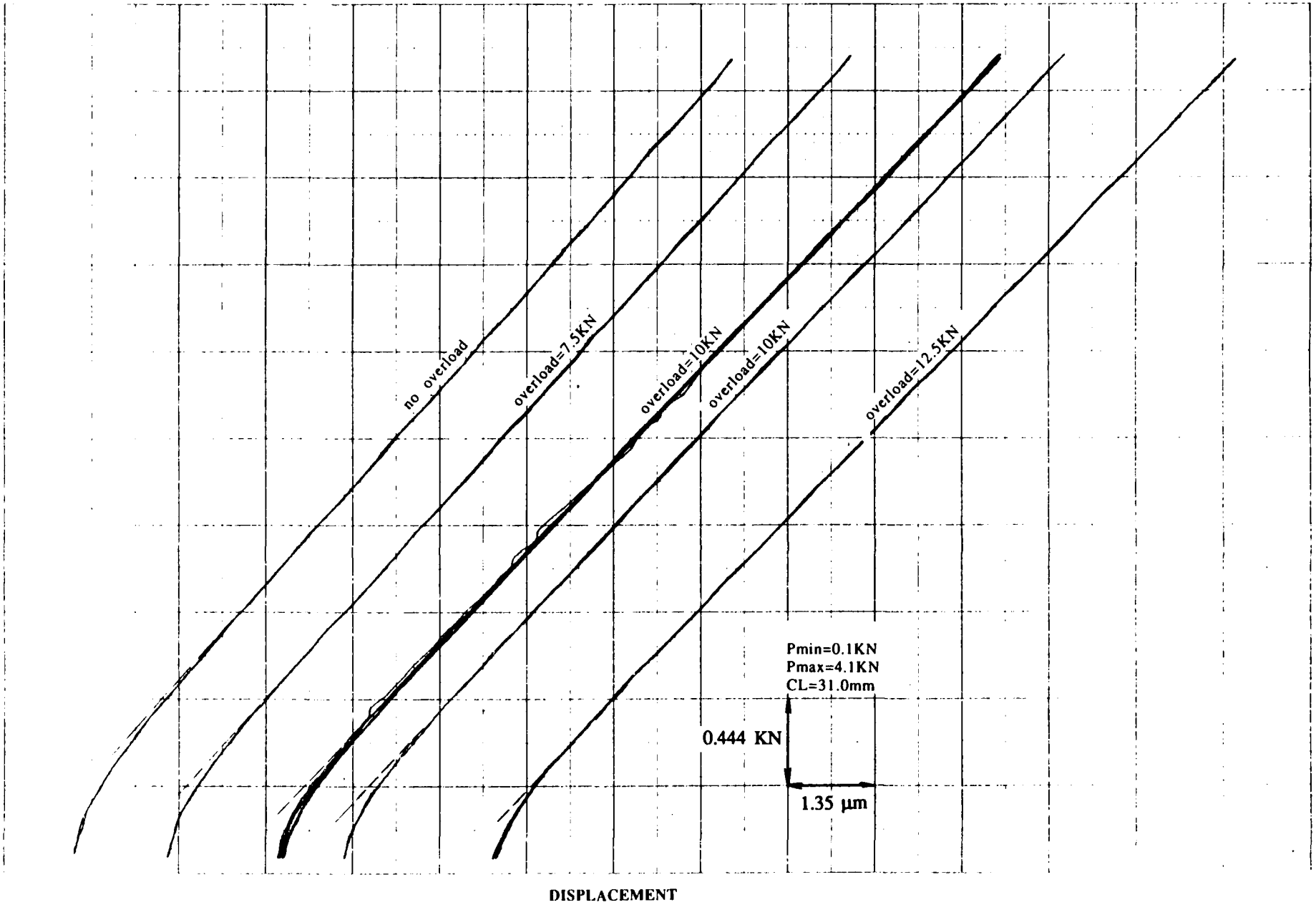

Fig. 5(b) **Load-displacement measurements for crack opening displacement (displacement between extensometer and crack tip is 3mm)**

value of the ratio K^{ol}_{max}/K_{max}, where crack arrest is expected to result; Z_{ol} is the overload affected zone and equal to

$$Z_{ol} = \frac{\gamma}{2\pi}(K^{ol}_{max} / \sigma_y)^2 \qquad (11)$$

where γ is an experimental constant; For Ti-6Al-4V material γ and S are expected to be 4 and 2.8, respectively[43,44] while σ_y is 924 N/mm^2. Additional work by Wei et al[42] suggests that further modifications be made to the above equations. These modifications preserve the basic concept that a residual stress intensity factor K_R is produced by the overload. The rate of decay is, however, assumed to be proportional to $(1 - \Delta a_{ol}/Z_{ol})^2$ over the range of Δa_{ol} from Z^*_{ol} to Z_{ol}. This is expressed as:

$$K_R = K^0_R (1 - \frac{\Delta a_{ol}}{Z_{ol}})^2 \qquad Z^*_{ol} \le a_{ol} \le Z_{ol} \qquad (12)$$

Z^*_{ol} indicates the delayed zone and is assumed to be equal to the appropriate cyclic plastic zone size. Z_{ol} is the overload effected zone. $K_R{}^0$ is the residual stress indensity factor immediately following the overload, i.e. at $\Delta a_{ol} = 0$; it is given as:

$$K^0_R = \frac{1 - K_{th}/K_{max}}{S - 1} (K^{ol}_{max} - K_{max}) \qquad (13)$$

In a deterministic sense, equation (12) could be used in conjuction with a Paris type crack growth law to calculate the crack growth rate in the overload affective zone. One of these laws, which exibits a strong dependency on R, is what developed by Walker[46] in the form:

$$\frac{da}{dN} = C\, K_{max}^{m}\, \Delta K^{n}$$

which could be further expressed as

$$\frac{da}{dN} = C\, K_{max}{}^{m+n}\, (1-R)^{n} \qquad (14)$$

where C and m are material constants.

The above equation is, in fact, identical to the equation derived by Fitzgerald[47] on the basis of empirical data fitting. In his form however, the value of ΔK is reduced by ΔK_0 which is defined as a parameter indicating an apparent threshold value.

Now, by assuming that the compressive residual stress at the crack tip due to the overloading is the main mechanism, equation (14) could then be modified as

$$\frac{da}{dN} = C\, K_{eff}{}^{m+n}\, (1-R_{eff})^{n} \qquad (15)$$

where $K_{eff} = K_{max}-K_R$, $R_{eff} = \frac{K_{min}-K_R}{K_{max}-K_R}$, and substituting these into eq.(15) we will get

$$\frac{da}{dN} = C\,(K_{max}-K_R)^m\,\Delta K^n \qquad (16)$$

There is no available information in the literature indicating the validity of the above equation for overload conditions which do not promote closure by crack tip plasticity. Therefore experimental tests were carried out on specimens of Ti-6Al-4V, having the compact tension geometry previously described, to test equations (12) and (16) in the overload affected region. These tests included varying parameters of stress ratio, overload and ΔK as shown in table 2. In each test crack length and the associated growth rate were measured during base loading as well as during the delayed zone after the overload application. N_D was also measured and listed in table 2. Some experimental results of this work, in the form of da/dN versus crack length during retardation, are shown in Figures 6(a)-6(d). Results using [12] and [16] for the same loading conditions are also presented in these figures. It was observed, however that by modifying Wei and Shih's form, i.e., equation [12], to

$$K_R = \frac{1-K_{th}/K_{max}}{S-1}(K^{ol}_{max} - K_{max})\,\frac{K^{ol}_{max}}{K_{max}} \qquad (17)$$

(Pol-Pmax)/Pmax (%)	50%		70%		109%	
Overload(KN)	16.5		18.7		23.0	
	ΔK $(N \cdot mm^{-\frac{3}{2}})$	Nd	ΔK $(N \cdot mm^{-\frac{3}{2}})$	Nd	ΔK $(N \cdot mm^{-\frac{3}{2}})$	Nd
Pmin=2.2KN	685.2	532	581.5	1763	678.7	12,267
Pmax=11KN	875.0	376	873.6	1502	871.1	10,940
R=0.20	1037.0	135			1007.0	8,549
Pmin=5KN	465.1	1,218	464.3	2,810	463.5	88,208
Pmax=11KN	596.1	898	594.8	2,481	593.5	48,615
R=0.46	748.5	563	686.0	2,264	686.5	38,267
Pmin=6.6KN	339.4	4,080	340.2	45,120	343.1	
Pmax=11KN	440.6	1,094	439.7	17,788	435.2	18,388
R=0.6	559.1	936	501.8	16,217	500.4	13,332

Table 2 **Effect of Varying R, overload ratio and ΔK on CracK Growth Delay (Nd) in Ti-6Al-4V**

A closer fitting, as shown also in the above mentioned figures can be achieved. This empirical modification emphasizes the influence of the overload ratio. Several other observations obtained from this experimental program will be discussed in the following chapter. The major conclusion drawn from this work, however, is that the effective stress intensity factor for the overload affected zone could be determined. Once this has been achieved, the next step is to generate experimentally the scatter crack growth curves. From these, constant probability crack growth curves could be established and compared with those theoretically obtained using the proposed model. This will be detailed in the following section.

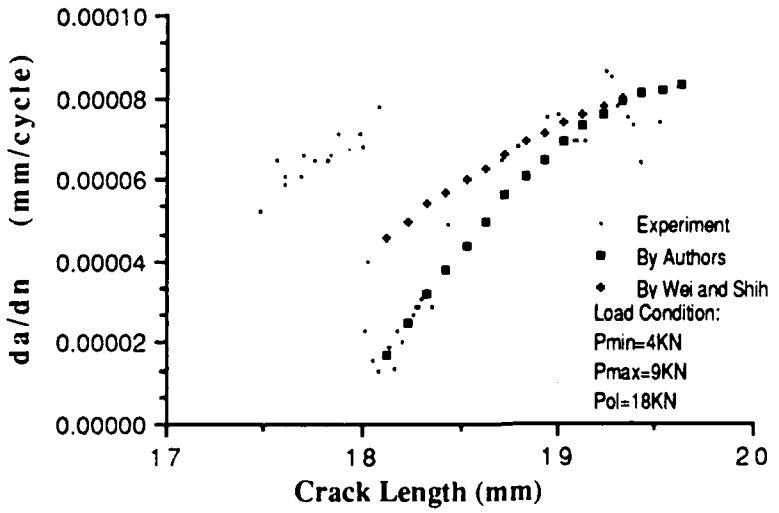

Fig. 6-(a) KR model test

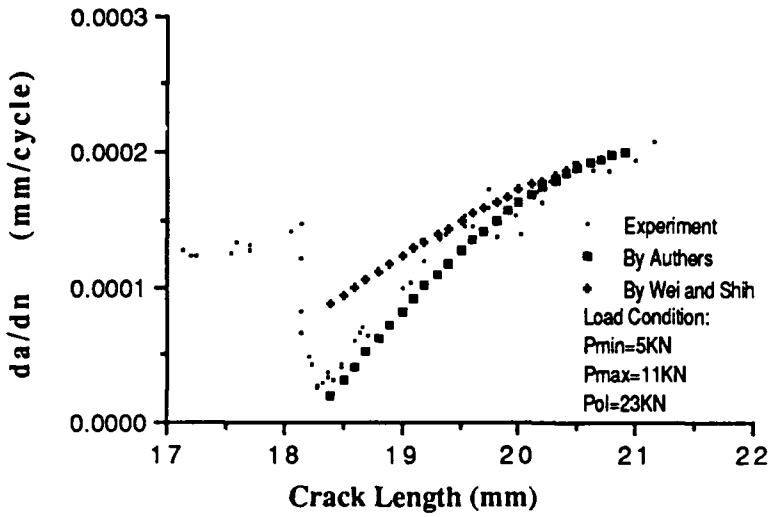

Fig. 6-(b) KR model test

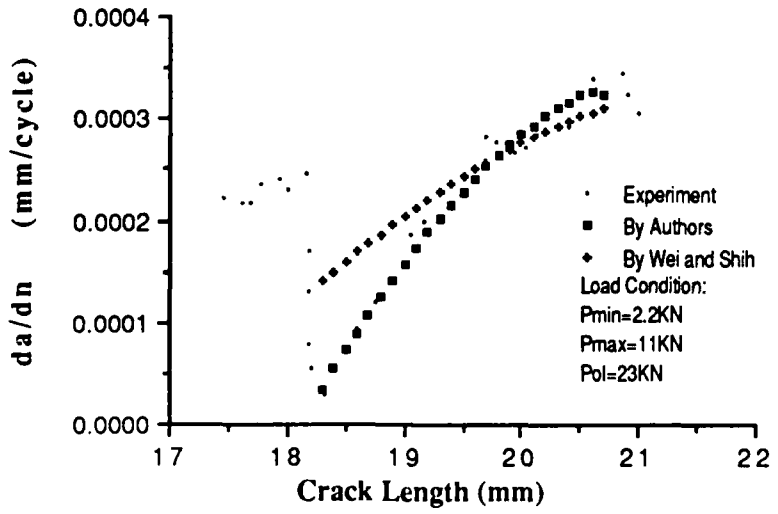

Fig. 6-(c) KR model test

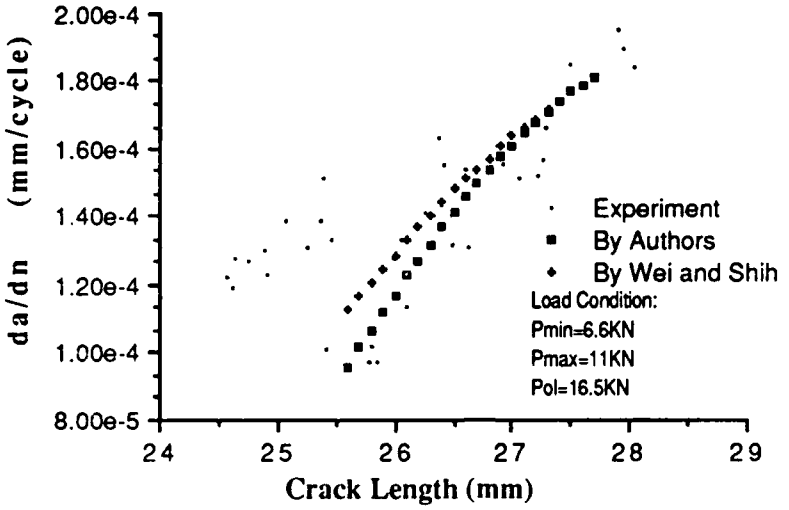

Fig. 6-(d) KR model test

3.3 Single Overload Application

3.3.1 Experimental Crack Growth Curves

Crack growth scatter curves, including durations of delayed zones, were generated by using sixty-five identical compact-tension specimens of Ti-6Al-4V material which are used throughout this program. Each specimen supplied one sample crack growth curve containing three overload regions at crack lengthes of 18, 25 and 29 mm. These intervals were seleted so that no one overload region could interact with any other overload region on the same curve. Basic load conditions were P_{min} = 4 KN and P_{max}= 9 KN; overload P_{ol} was 18 KN. Load frequency was 15 Hz and the base loading as well as

the overloads was applied by using an automatic function generator system linked to the servohydraulic material testing machine which was run by the same operator in a temperature-controlled room during the entire test program. Data was collected in the form of number of cycles and corresponding crack length at intervals of 1,500 cycles with each data point representing an average of three measurements taken with a frequency of 500,000 points per second. Crack length was measured using a current reversing potential drop system developed by the authors and decribed in Appendix D. Typical results of crack length a vs number of cycles N are shown in Figure 7. Each of these sixty-five sample curves, which are shown in Figure 8, corresponding to initial and final crack lengths of 16 and 32mm, respectively, was divided into 160 segments; each representing a crack state position with a width of 0.1 mm. Number of cycles in each state was calculated as i_{rj} where $1 \leq r \leq 160$ and $1 \leq j \leq 65$. This data was then utilized in a manner identical to that described in references[11, 27] to generate experimental constant probability crack growth curves which include retardation zones. The curves are shown in Figures 9(a) and 9(b).

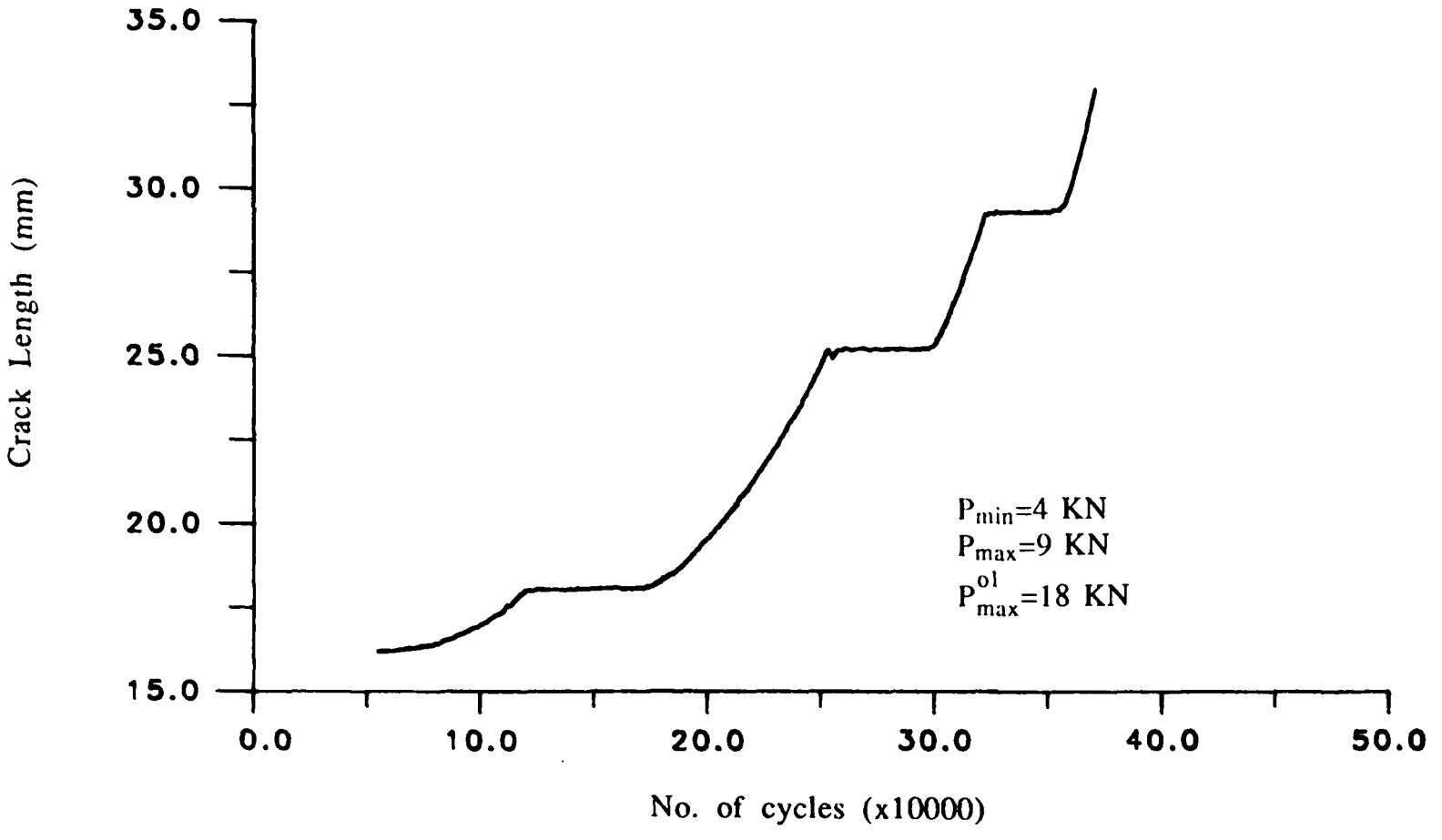

Fig. 7 Typical results of crack length vs number of cycles

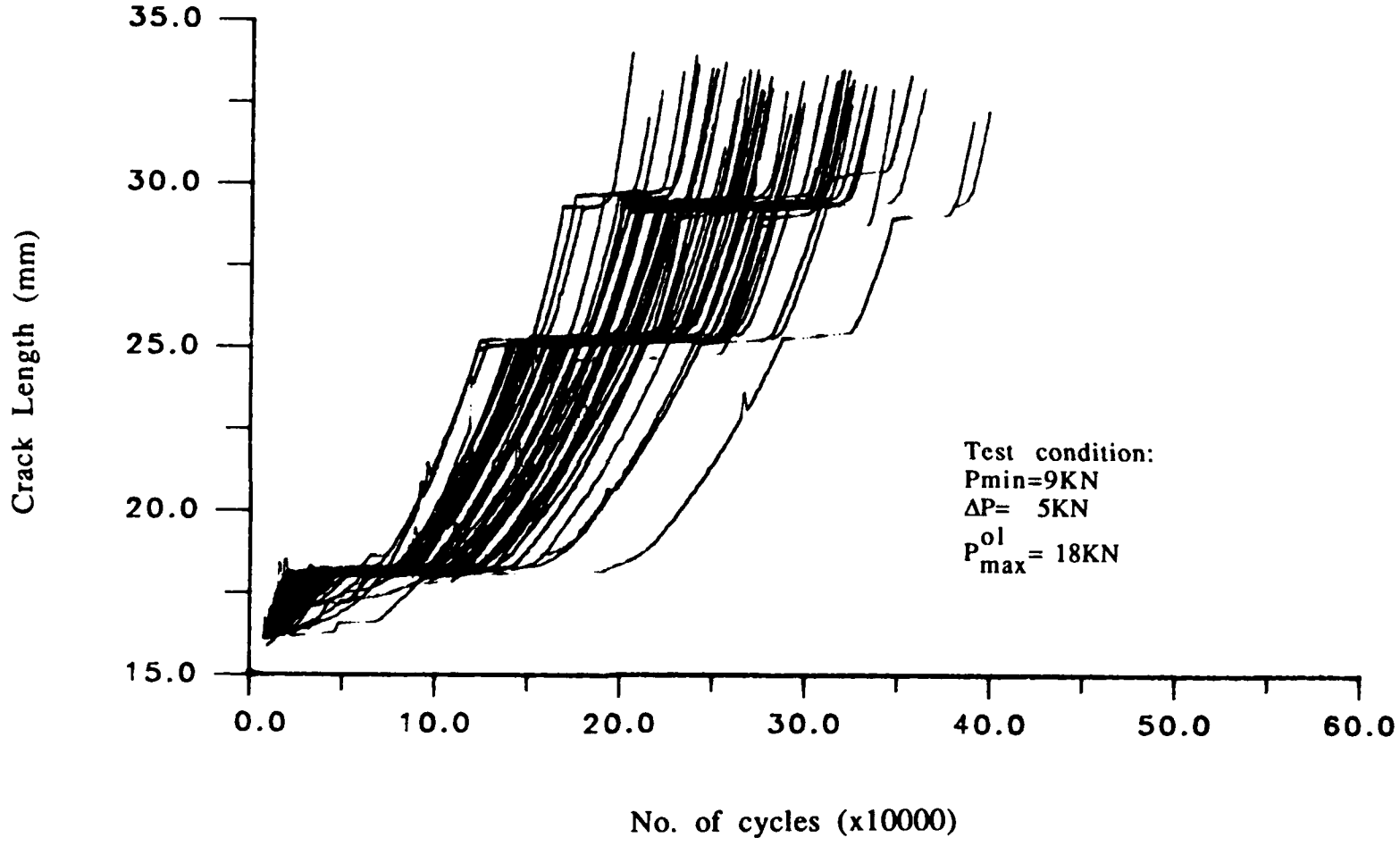

Fig. 8 Crack growth sample curves (from 65 Ti-6Al-4V specimen)

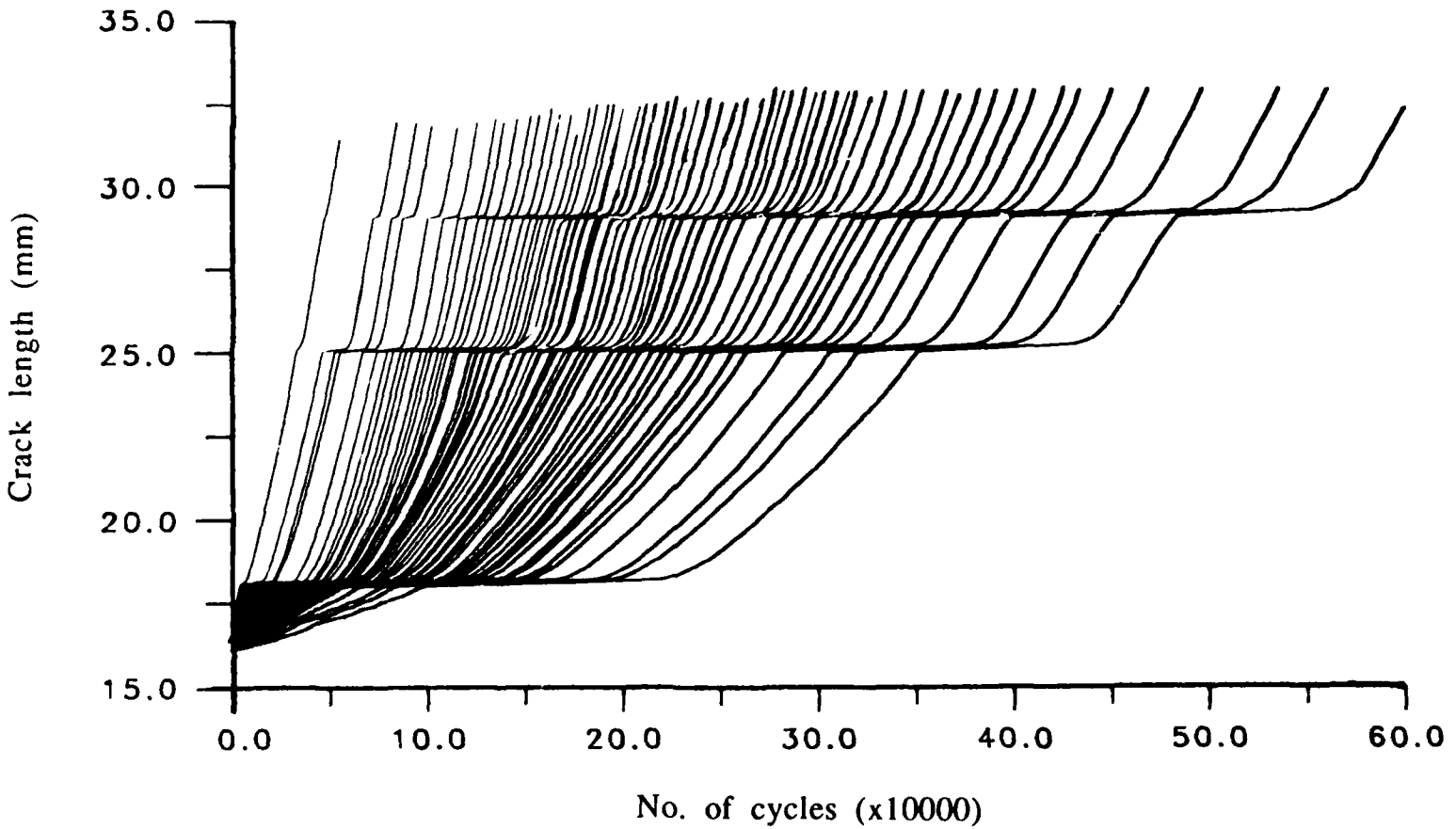

Fig. 9(a) Constant probability crak growth curves (generated from 65 sample curves using method described in reference [11])

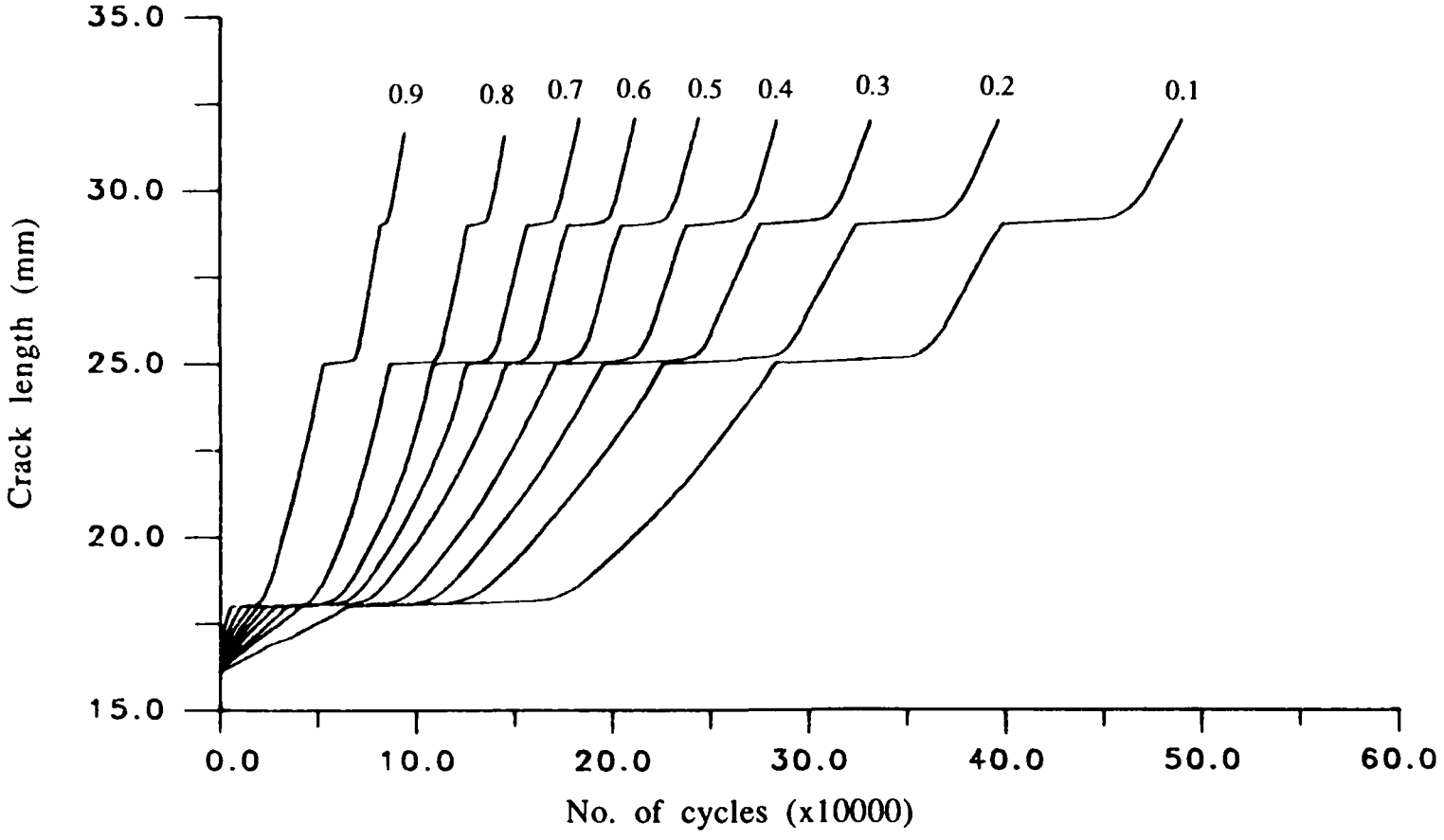

Fig. 9(b) **Nine of the experimental constant probability crack growth curves shown in Fig. 9(a)**

3.3.2 Theoretical Crack Growth Curves

The next step was to produce the corresponding theoretical curves using the proposed model. This was achieved in the following combined form by employing equations (7), (9) and (16) and considering the threshold level

$$\Delta i = C\,(K_{max}-K_R)^{-m}\,(\Delta K-\Delta K_0)^{-n}\,(-\ln P)^{\beta} \qquad (18)$$

By maintaining the value of P constant and calculating K_{max}, K_R and ΔK for a crack length a; $a=\Sigma\,\Delta x$, one obtains the number of cycles ΔN corresponding to increament Δa at a crack length a. This yields an individual constant probability crack growth curve. The length Z_{ol} of the overload affected zone was determined by using equation (11).

The full solution of equation (18) requires the knowledge of the parameters c, m, n and β. As the objective of this part of the study was to predict the overload delayed zone, use was made of the portions of the experimental constant-probability curves corresponding to the constant amplitude load cycles to estimate the constants using minimum least square curve fitting method. If the unit of stress intensity factor is $N\cdot mm^{-1.5}$ and $\Delta x=0.1mm$ the results are

$$C = 9.881\times10^{10}$$

$$m = 0.93$$

$$n = 2.03$$

and $$\beta = 0.46$$

Those constants were used in equation (18) to generate the theoretical constant probability crack growth curves for the delayed regions. Eight of those are shown in Figure 10(a)-Figure 10(h) and compared with constant probability curves from the experiment (Figure 9(b)). Furthermore, delayed cycles obtained both experimentally and theoretically are presented in table 3, in which the degree of error between the two sets of results was listed. The average error in data predicted by the proposed model is 8%.

Discussion of the results and observations concerning the retardation process are the subject of the following chapter.

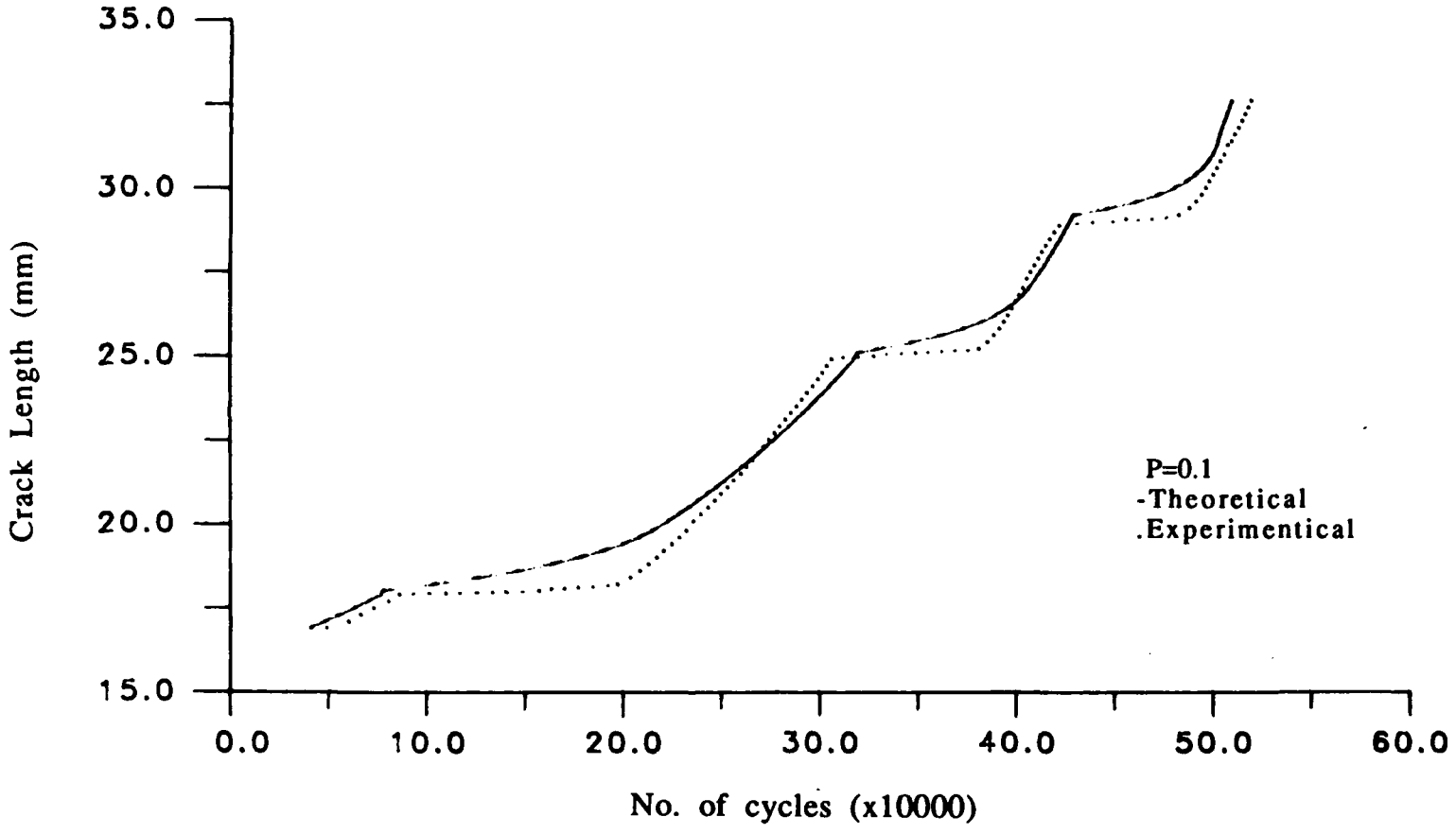

Fig. 10 (a) Comparision of theoretical and experimental crack growth curves (P=0.1)

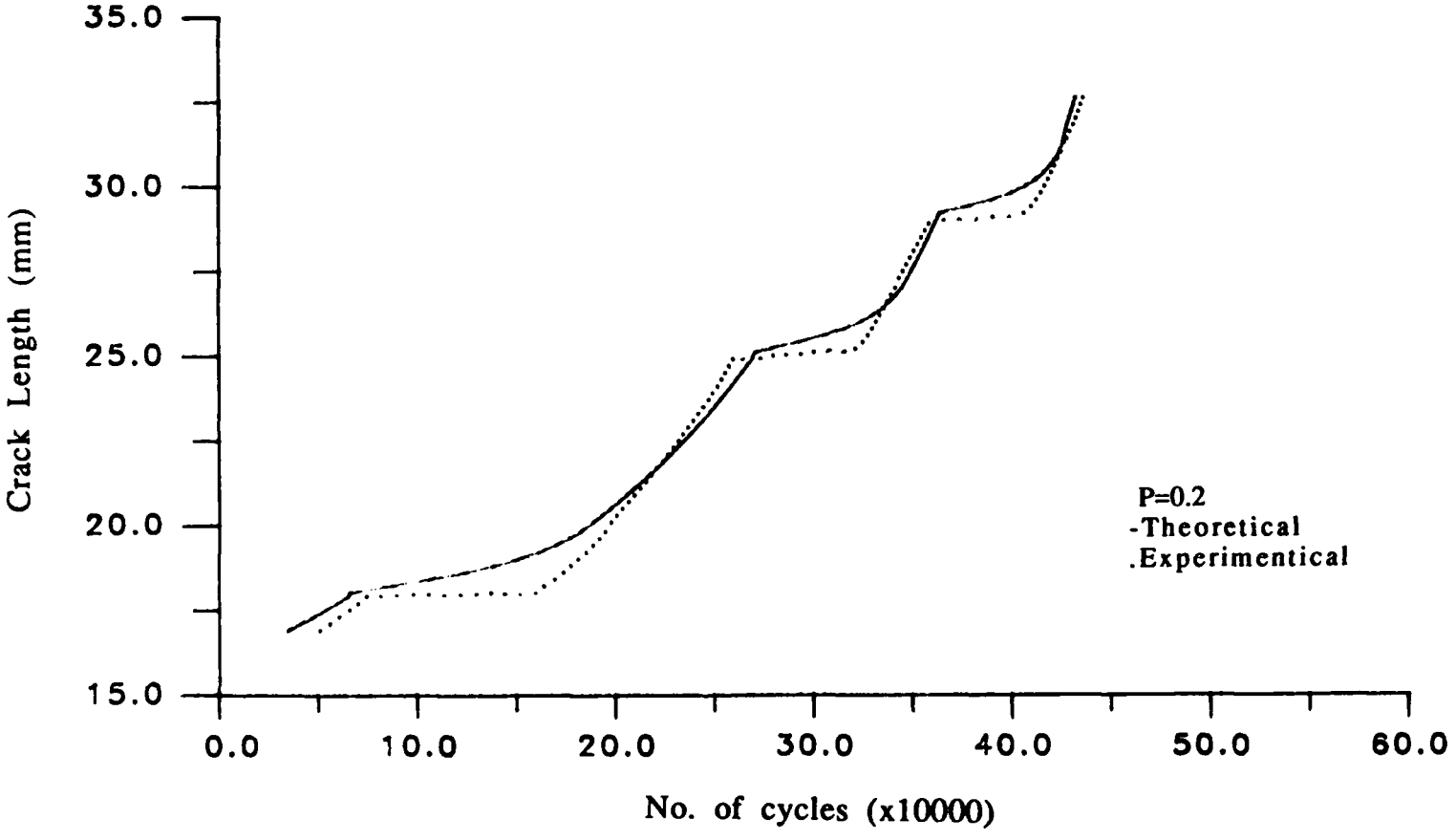

Fig. 10 (b) Comparision of theoretical and experimental crack growth curves (P=0.2)

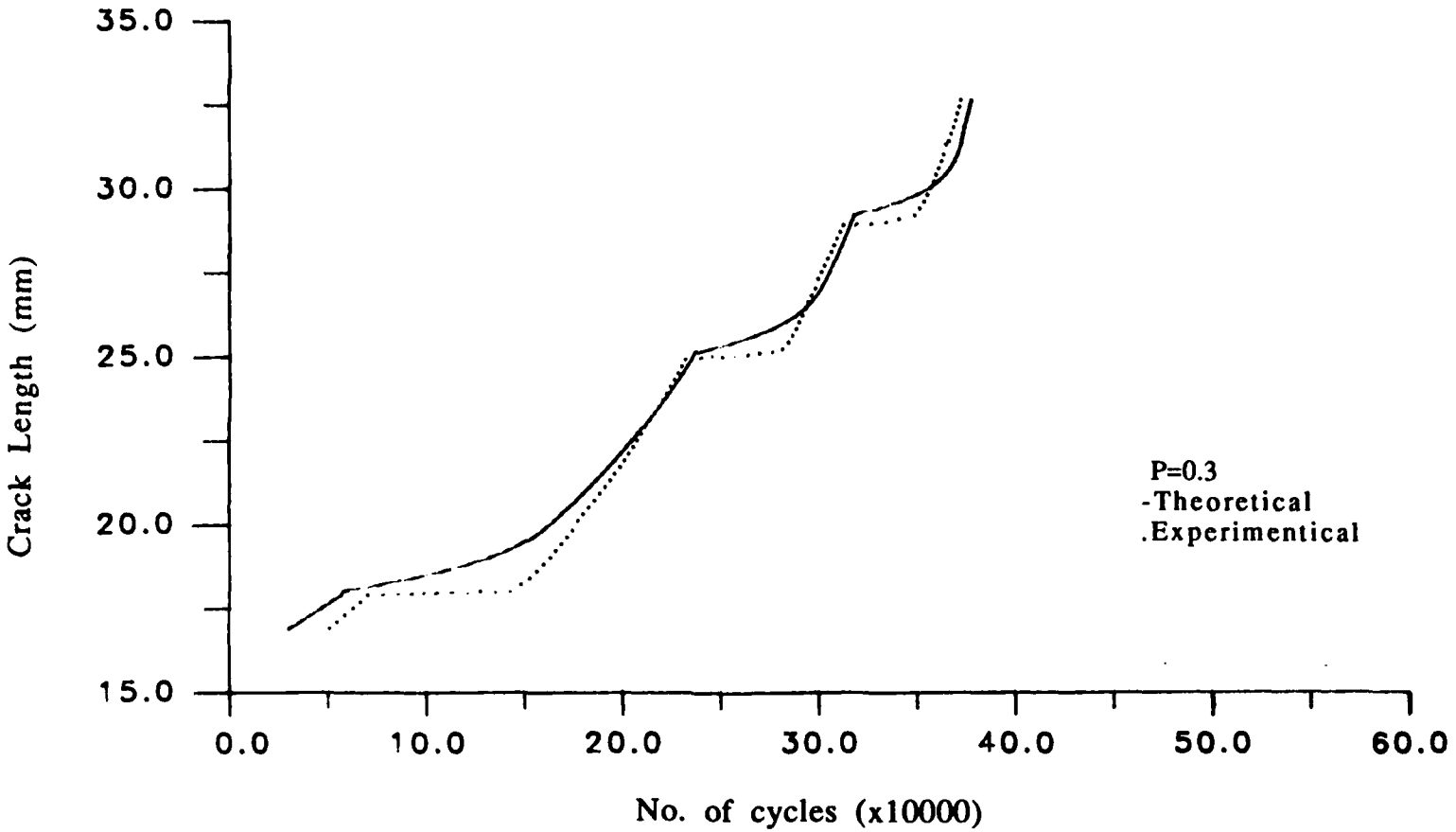

Fig. 10 (c) Comparision of theoretical and experimental crack growth curves (P=0.3)

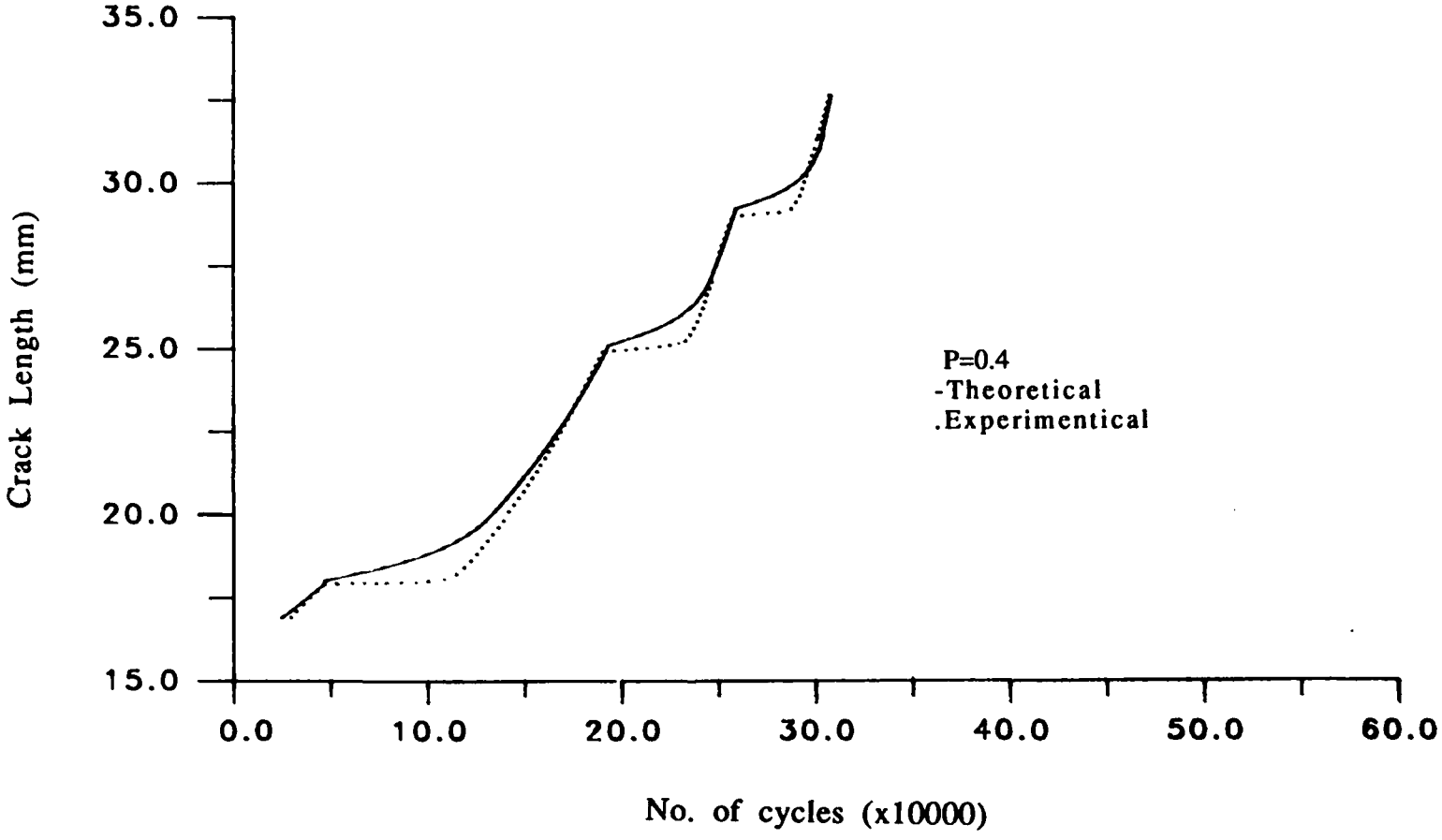

Fig. 10 (d) Comparision of theoretical and experimental crack growth curves (P=0.4)

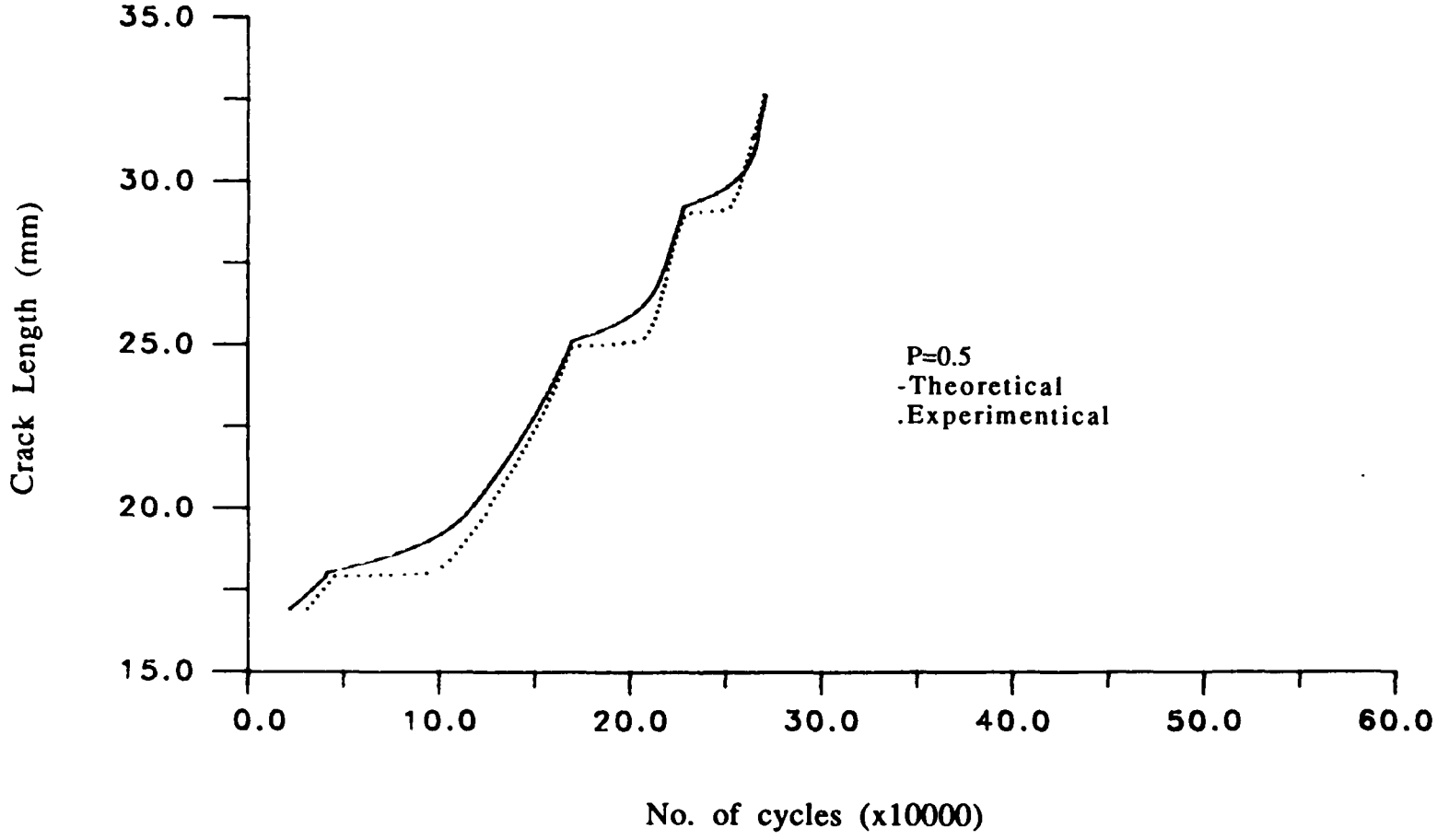

Fig. 10 (e) Comparision of theoretical and experimental crack growth curves (P=0.5)

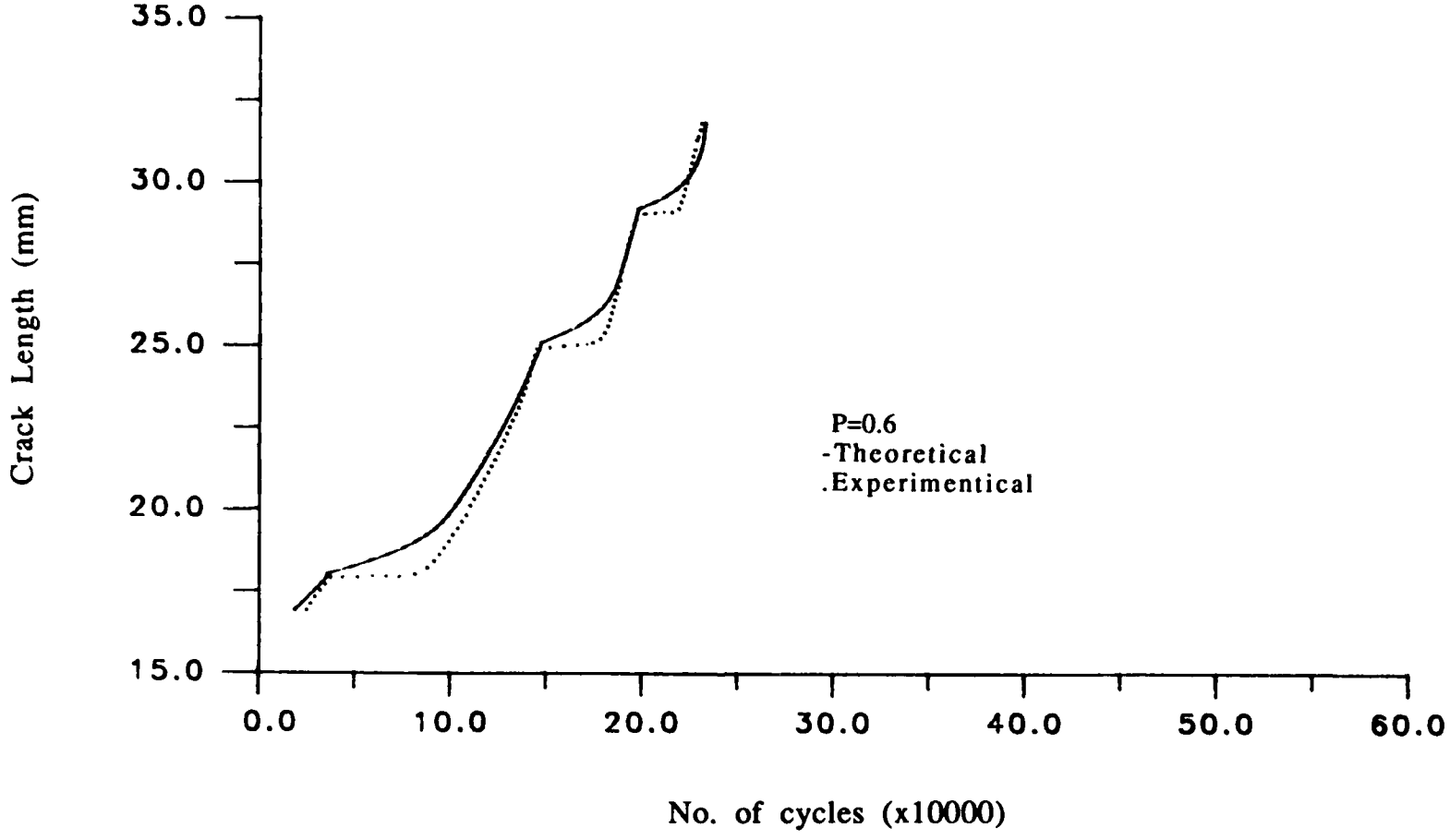

Fig. 10 (f) Comparision of theoretical and experimental crack growth curves (P=0.6)

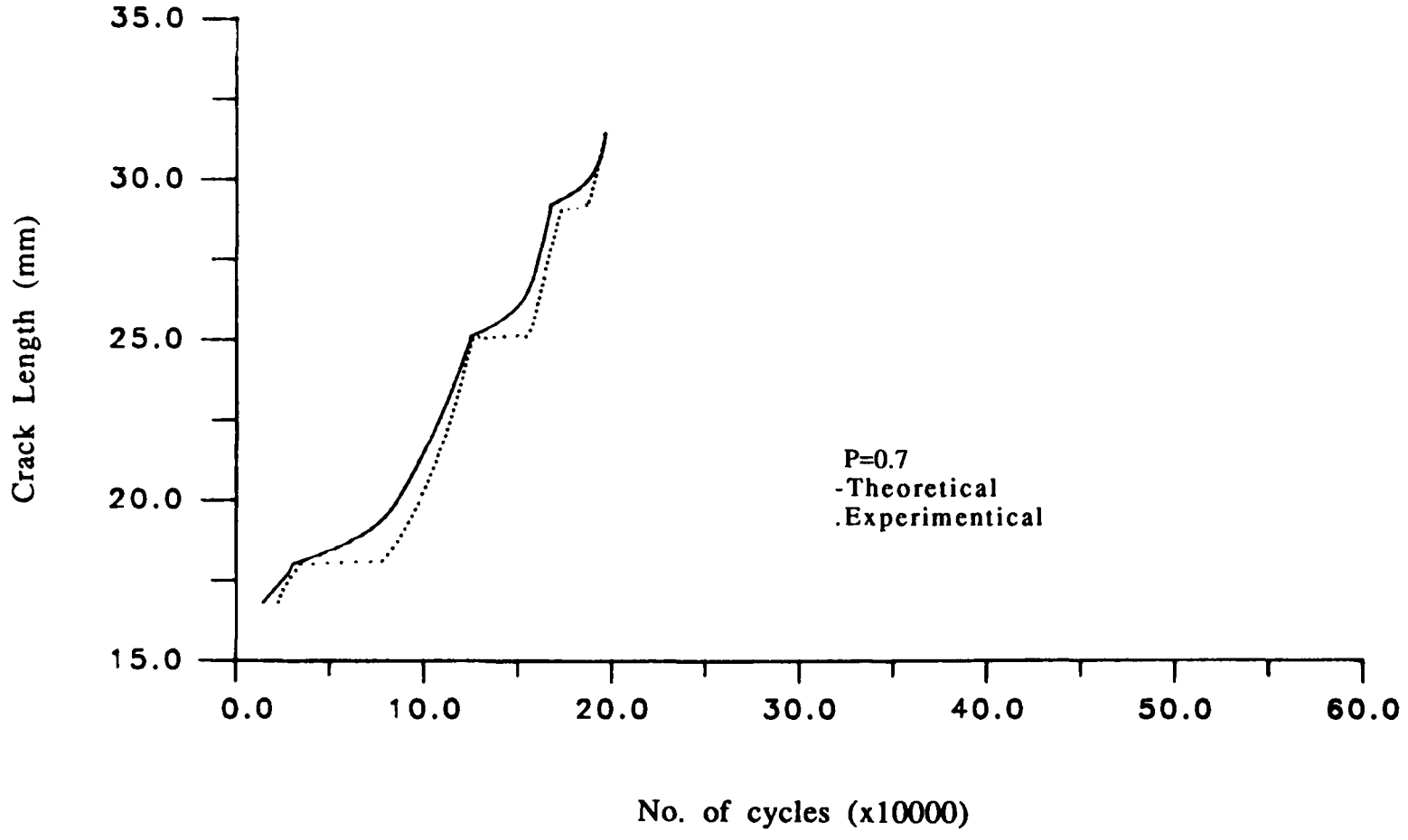

Fig. 10 (g) Comparision of theoretical and experimental crack growth curves (P=0.7)

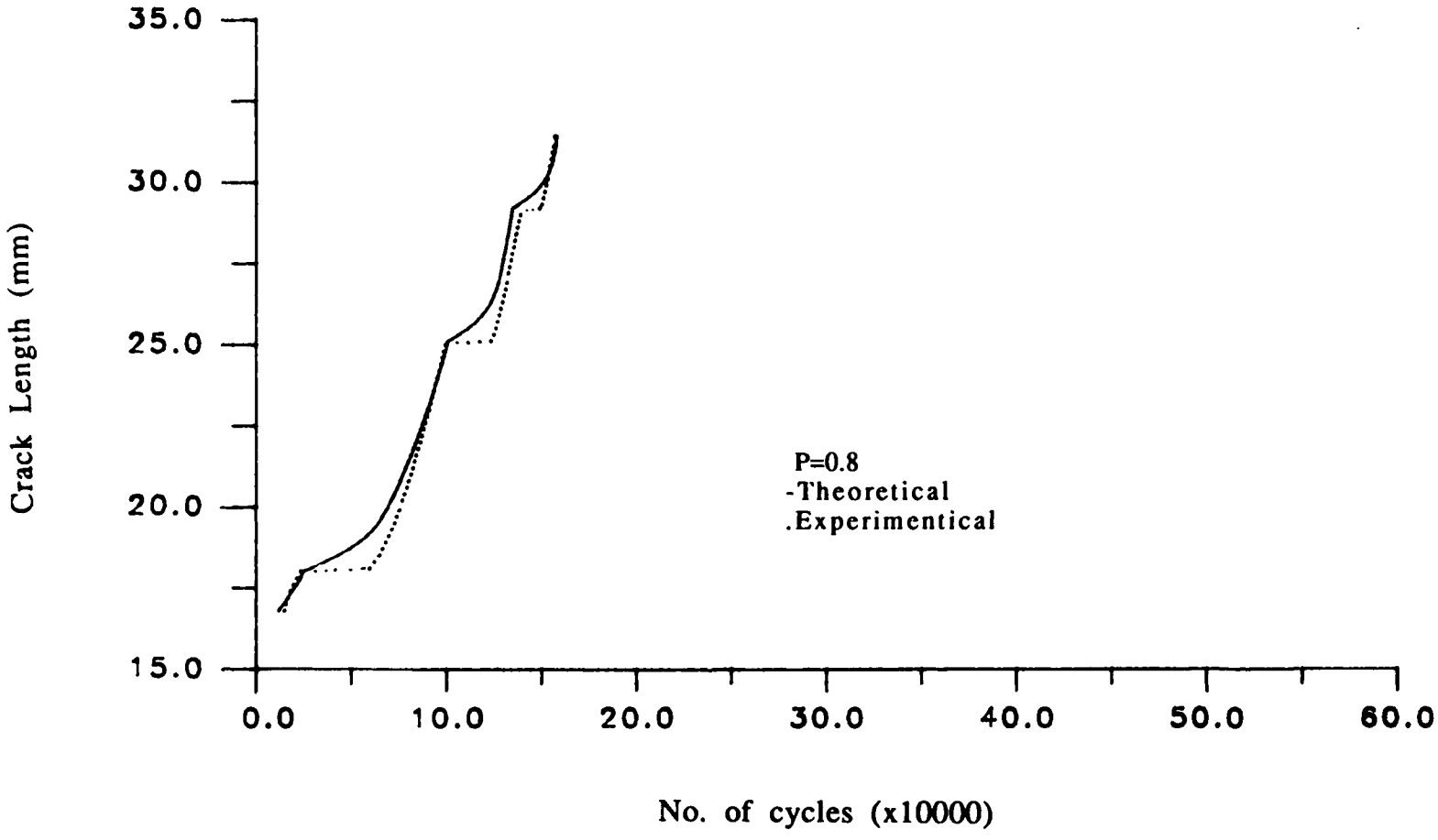

Fig. 10 (h) Comparision of theoretical and experimental crack growth curves (P=0.8)

P=0.1

	CL (MM)	ΔN (THEORY) (CYCLES)	ΔN (EXPERIMENT) (CYCLES)	% ERROR
	16.9	3093	2625	17.83
	17.0	3055	3425	-10.80
	17.1	3019	3645	-17.69
	17.2	2983	3322	-10.20
	17.3	2947	2896	1.76
	17.4	2913	3070	-5.11
	17.5	2878	2897	-0.66
	17.6	2844	3211	-11.43
	17.7	2810	3314	-15.21
	17.8	2778	2897	-4.11
	17.9	2745	2647	3.70
retardation zone	18.0	2713	3096	-12.37
	19.6	103154	105209	-1.95
	19.7	2524	2256	11.88
	19.8	2470	2172	12.06
	19.9	2445	2170	12.67
	20.0	2241	1922	16.59
	20.1	2131	1862	14.45
	20.2	2108	1870	12.73
	20.3	2084	1866	11.68
	20.4	2061	1871	10.15
	20.5	2038	1869	9.04
	20.6	2015	1874	7.52
	20.7	1993	1828	9.03
	20.8	1971	1826	7.94
	20.9	1949	1865	4.50
	21.0	1927	1823	5.70
	21.1	1906	1730	10.17
	21.2	1885	1731	8.90
	21.3	1865	1728	7.93
	21.4	1843	1850	-0.38
	21.5	1824	1847	-1.25
	21.6	1803	1727	4.40
	21.7	1784	1721	3.66
	21.8	1764	1722	2.44
	21.9	1745	1719	1.51

Table 3 **Percentage error between the theoretical and experimental constant-probability crack growth curves**

	CL (MM)	ΔN(THEORY) (CYCLES)	ΔN(EXPERIMENT) (CYCLES)	% ERROR
	22.0	1725	1714	0.64
	22.1	1707	1726	-1.10
	22.2	1688	1710	-1.29
	22.3	1670	1717	-2.74
	22.4	1652	1733	-4.67
	22.5	1633	1712	-4.61
	22.6	1616	1719	-5.99
	22.7	1599	1621	-8.77
	22.8	1581	1619	-2.35
	22.9	1563	1517	-3.03
	23.0	1547	1510	2.45
	23.1	1530	1532	-0.13
	23.2	1514	1533	-1.24
	23.3	1497	1517	-0.06
	23.4	1481	1434	3.28
	23.5	1465	1422	3.02
	23.6	1449	1418	2.19
	23.7	1434	1425	0.63
	23.8	1418	1316	7.75
	23.9	1403	1319	6.37
	24.0	1387	1416	-2.05
	24.1	1373	1396	-1.65
	24.2	1358	1404	-3.28
	24.3	1343	1304	2.99
	24.4	1329	1294	2.70
	24.5	1315	1286	2.26
	24.6	1300	1300	0.00
	24.7	1287	1283	0.03
	24.8	1272	1194	6.53
	24.9	1259	1305	-3.52
retardation zone →	25.0	1246	1418	-12.13
	26.9	79515	90133	-11.78
	27.0	1134	1048	8.21
	27.1	1035	979	5.72
	27.2	981	952	3.05
	27.3	971	956	1.57
	27.4	961	956	0.52
	27.5	950	974	-2.46
	27.6	940	963	-2.39

Table 3 (continued)

	CL (MM)	ΔN (THEORY) (CYCLES)	ΔN (EXPERIMENT) (CYCLES)	% ERROR
	27.7	930	960	-3.13
	27.8	920	950	-3.16
	27.9	910	975	-6.67
	28.0	900	970	-7.22
	28.1	890	971	-8.34
	28.2	881	967	-8.89
	28.3	871	967	-9.93
	28.4	861	889	-3.14
	28.5	852	944	-9.74
	28.6	843	976	-13.63
	28.7	834	921	-9.45
	28.8	824	938	-12.15
	28.9	816	935	-12.72
retardation zone	29.0	807	896	-9.93
	31.1	70242	77076	-8.87
	31.2	658	731	-9.13
	31.3	624	732	-14.75
	31.4	618	724	-14.64
	31.5	610	725	-15.86
	31.6	604	722	-16.34
	31.7	597	702	-14.96
	31.8	590	700	-15.71
	31.9	583	697	-16.35
	32.0	576	696	-17.24
	32.1	571	698	-18.19
	32.2	563	680	-17.20
	32.3	557	662	-15.86
	32.4	551	660	-16.50
	32.5	545	657	-11.70
	32.6	538	657	-18.11
	32.7	532	623	-14.61
	32.8	526	610	-13.77
	32.9	520	601	-13.48
	33.0	513	598	-14.21

Table 3 (continued)

P=0.2

	CL (MM)	ΔN(THEORY) (CYCLES)	ΔN(EXPERIMENT) (CYCLES)	% ERROR
	16.9	2623	2203	19.06
	17.0	2591	2324	11.49
	17.1	2561	2682	-4.51
	17.2	2529	2432	3.99
	17.3	2500	2331	7.25
	17.4	2470	2623	-5.83
	17.5	2441	2542	-3.97
	17.6	2412	2428	-0.06
	17.7	2384	2364	0.85
	17.8	2356	2322	1.46
	17.9	2328	2320	0.03
retardation zone	18.0	2301	2329	-1.20
	19.6	90204	100892	-10.59
	19.7	2480	2229	11.26
	19.8	2265	2231	1.52
	19.9	2073	2026	2.32
	20.0	1901	2014	-5.61
	20.1	1808	1927	-6.17
	20.2	1787	1917	-6.78
	20.3	1768	1822	-2.96
	20.4	1748	1823	-4.11
	20.5	1728	1827	-5.42
	20.6	1709	1856	-7.92
	20.7	1690	1813	-6.78
	20.8	1672	1817	-7.98
	20.9	1653	1768	-6.50
	21.0	1634	1610	1.49
	21.1	1617	1603	0.87
	21.2	1598	1612	-0.87
	21.3	1582	1611	-1.80
	21.4	1563	1613	-3.10
	21.5	1547	1598	-3.19
	21.6	1529	1416	7.98
	21.7	1513	1411	7.23
	21.8	1496	1308	14.37
	21.9	1480	1404	5.41
	22.0	1463	1311	10.39
	22.1	1448	1387	4.40
	22.2	1432	1314	8.98

Table 3 (Continued)

	CL (MM)	ΔN (THEORY) (CYCLES)	ΔN (EXPERIMENT) (CYCLES)	% ERROR
	22.3	1416	1402	1.00
	22.4	1401	1326	5.66
	22.5	1385	1394	-0.65
	22.6	1371	1406	-2.49
	22.7	1355	1400	-3.21
	22.8	1341	1403	-4.42
	22.9	1326	1404	-5.55
	23.0	1312	1380	-4.93
	23.1	1298	1315	-1.29
	23.2	1283	1410	-9.01
	23.3	1270	1356	-6.63
	23.4	1256	1316	-4.56
	23.5	1243	1298	-4.24
	23.6	1229	1309	-6.11
	23.7	1216	1305	-6.82
	23.8	1202	1296	-7.25
	23.9	1190	1290	-8.18
	24.0	1177	1305	-9.81
	24.1	1164	1284	-9.35
	24.2	1152	1003	14.86
	24.3	1139	988	15.28
	24.4	1127	986	14.30
	24.5	1115	983	13.43
	24.6	1103	987	11.75
	24.7	1091	963	13.29
	24.8	1079	977	10.44
	24.9	1068	985	8.43
retardation zone	25.0	1056	1102	-4.17
	26.9	66908	76760	-12.83
	27.0	961	971	-1.03
	27.1	877	952	-7.88
	27.2	833	943	-11.66
	27.3	824	930	-11.40
	27.4	814	901	-9.65
	27.5	806	889	-9.34
	27.6	798	841	-5.11
	27.7	788	849	-7.18
	27.8	780	839	-7.03
	27.9	772	849	-9.06

Table 3 (continued)

	CL (MM)	ΔN (THEORY) (CYCLES)	ΔN (EXPERIMENT) (CYCLES)	% ERROR
	28.0	763	862	-11.48
	28.1	755	850	-11.17
	28.2	747	825	-9.45
	28.3	739	858	-13.87
	28.4	730	847	-13.81
	28.5	723	804	-10.07
	28.6	715	760	-5.92
	28.7	707	770	-8.18
	28.8	699	754	-7.29
	28.9	692	767	-9.78
retardation zone	29.0	684	824	-16.99
	31.1	55293	60602	-8.76
	31.2	558	622	-10.28
	31.3	530	607	-12.68
	31.4	523	604	-13.41
	31.5	518	615	-15.77
	31.6	512	559	-8.41
	31.7	506	598	-15.38
	31.8	500	517	-3.28
	31.9	495	556	-10.97
	32.0	489	558	-12.36
	32.1	484	499	-3.00
	32.2	478	545	-12.29
	32.3	472	418	-12.92
	32.4	467	468	-0.02
	32.5	462	519	-10.98
	32.6	457	511	-10.56
	32.7	451	459	1.77
	32.8	446	405	10.12
	32.9	441	402	9.70
	33.0	435	416	4.57

Table 3 (continued)

P=0.3

	CL (MM)	ΔN (THEORY) (CYCLES)	ΔN (EXPERIMENT) (CYCLES)	% ERROR
	16.9	2295	1879	22.14
	17.0	2267	1879	20.65
	17.1	2240	1894	18.27
	17.2	2214	2321	-4.61
	17.3	2187	1880	16.33
	17.4	2161	1884	14.70
	17.5	2136	2011	6.22
	17.6	2111	1976	6.83
	17.7	2086	1937	7.69
	17.8	2061	1890	9.05
	17.9	2037	1884	8.12
retardation zone	18.0	2014	1947	3.44
	19.6	88950	96093	-7.43
	19.7	2001	1844	8.51
	19.8	1982	1833	8.12
	19.9	1814	1814	0.00
	20.0	1663	1759	-5.46
	20.1	1582	1725	-8.29
	20.2	1564	1719	-9.02
	20.3	1547	1749	-11.55
	20.4	1529	1415	8.06
	20.5	1513	1416	6.85
	20.6	1495	1424	4.99
	20.7	1479	1304	13.42
	20.8	1463	1409	3.83
	20.9	1446	1311	10.30
	21.0	1430	1426	0.28
	21.1	1415	1307	8.26
	21.2	1398	1310	6.72
	21.3	1384	1312	5.49
	21.4	1368	1310	4.43
	21.5	1353	1300	4.31
	21.6	1339	1394	-3.95
	21.7	1323	1387	-4.61
	21.8	1309	1396	-6.23
	21.9	1295	1309	-1.07
	22.0	1281	1303	-1.69
	22.1	1267	1328	-4.59

Table 3 (Continued)

	CL (MM)	ΔN (THEORY) (CYCLES)	ΔN (EXPERIMENT) (CYCLES)	% ERROR
	22.2	1252	1310	-4.42
	22.3	1240	1318	-5.92
	22.4	1225	1301	-5.84
	22.5	1213	1303	-6.91
	22.6	1199	1308	-8.33
	22.7	1186	1259	-5.80
	22.8	1173	1179	-0.51
	22.9	1161	1097	5.83
	23.0	1147	1005	14.13
	23.1	1136	986	15.21
	23.2	1123	1203	-6.65
	23.3	1111	966	15.01
	23.4	1099	1007	9.14
	23.5	1087	1000	8.70
	23.6	1076	999	7.71
	23.7	1064	992	7.26
	23.8	1052	973	8.12
	23.9	1041	974	6.88
	24.0	1030	1018	1.18
	24.1	1019	980	3.98
	24.2	1007	985	2.23
	24.3	997	960	3.85
	24.4	986	974	1.23
	24.5	976	962	1.46
	24.6	965	973	-0.82
	24.7	955	957	-0.21
	24.8	944	960	-1.67
	24.9	934	972	-3.91
retardation zone →	25.0	925	1075	-13.95
	26.9	55587	62279	-10.74
	27.0	842	933	-9.75
	27.1	767	846	-9.33
	27.2	729	675	8.00
	27.3	721	677	6.50
	27.4	712	845	-15.74
	27.5	706	802	-11.97
	27.6	697	706	-1.27
	27.7	690	741	-6.88

Table 3 (continued)

	CL (MM)	ΔN (THEORY) (CYCLES)	ΔN (EXPERIMENT) (CYCLES)	% ERROR
	27.8	683	672	1.64
	27.9	675	773	-12.68
	28.0	668	749	-10.81
	28.1	660	681	-3.08
	28.2	654	684	-4.39
	28.3	646	671	-3.72
	28.4	640	674	-5.04
	28.5	632	634	-0.31
	28.6	625	637	-1.88
	28.7	619	685	-9.64
	28.8	612	681	-10.13
	28.9	605	632	-4.27
retardation zone	29.0	599	668	-10.32
	31.1	44706	46274	-3.39
	31.2	488	497	-1.81
	31.3	464	481	-3.53
	31.4	458	500	-8.40
	31.5	453	501	-9.58
	31.6	448	421	6.41
	31.7	443	451	-1.77
	31.8	438	485	-9.69
	31.9	432	419	3.10
	32.0	428	417	2.64
	32.1	423	463	-8.63
	32.2	419	418	0.24
	32.3	413	410	0.73
	32.4	409	456	-10.30
	32.5	404	407	-0.74
	32.6	399	404	-1.24
	32.7	395	409	-3.42
	32.8	390	399	-2.25
	32.9	386	396	-2.52
	33.0	382	397	-3.78

Table 3 (continued)

P= .4

	CL (MM)	ΔN(THEORY) (CYCLE)	ΔN(EXPERIMENT) (CYCLE)	% ERROR
	16.90	2023	1832	10.43
	17.00	2000	1835	8.99
	17.10	1976	1835	7.68
	17.20	1952	1888	3.39
	17.30	1930	1848	4.44
	17.40	1906	1828	4.27
	17.50	1884	1880	0.21
	17.60	1861	1836	1.36
	17.70	1840	1880	-2.13
	17.80	1818	1849	-1.68
	17.90	1796	1878	-4.37
retardation zone	18.00	1776	1880	-5.53
	19.60	69614	76566	-9.08
	19.70	1753	1615	8.54
	19.80	1748	1619	7.97
	19.90	1600	1517	5.47
	20.00	1467	1309	12.07
	20.10	1395	1350	3.33
	20.20	1379	1311	5.19
	20.30	1365	1307	4.44
	20.40	1348	1344	0.30
	20.50	1334	1311	1.75
	20.60	1319	1413	-6.65
	20.70	1305	1394	-6.38
	20.80	1290	1313	-1.75
	20.90	1275	1303	-2.15
	21.00	1262	1414	-10.75
	21.10	1247	1284	-2.88
	21.20	1234	1137	8.53
	21.30	1220	1104	10.51
	21.40	1207	1195	1.00
	21.50	1193	1092	9.25
	21.60	1181	1119	5.54
	21.70	1167	1058	10.30
	21.80	1155	1043	10.74
	21.90	1142	1095	4.29
	22.00	1129	1072	5.32
	22.10	1117	1075	3.91
	22.20	1105	1068	3.46

Table 3 (continued)

	CL (MM)	ΔN(THEORY) (CYCLE)	ΔN(EXPERIMENT) (CYCLE)	% ERROR
	22.30	1093	1108	-1.35
	22.40	1081	989	9.30
	22.50	1069	990	7.98
	22.60	1058	1000	5.80
	22.70	1046	973	7.50
	22.80	1035	986	4.97
	22.90	1023	972	5.25
	23.00	1013	990	2.32
	23.10	1001	979	2.25
	23.20	991	999	-0.80
	23.30	980	940	4.26
	23.40	969	1002	-3.29
	23.50	959	980	-2.14
	23.60	948	972	-2.47
	23.70	939	981	-4.28
	23.80	928	867	7.04
	23.90	918	982	-6.52
	24.00	908	990	-8.28
	24.10	899	876	2.63
	24.20	888	907	-2.09
	24.30	880	816	7.84
	24.40	869	965	-9.95
	24.50	861	796	8.17
	24.60	851	958	-11.17
	24.70	842	866	-2.77
	24.80	833	872	-4.47
	24.90	824	858	-3.96
retardation zone →	25.00	815	887	-8.12
	26.90	49499	52846	-6.33
	27.00	743	708	4.94
	27.10	676	605	11.74
	27.20	643	647	-0.62
	27.30	635	670	-5.22
	27.40	629	608	3.45
	27.50	622	669	-7.03
	27.60	615	630	-2.38
	27.70	609	671	-9.24
	27.80	602	631	-4.60
	27.90	596	631	-5.55

Table 3 (continued)

	CL (MM)	ΔN (THEORY) (CYCLE)	ΔN (EXPERIMENT) (CYCLE)	% ERROR
	28.00	589	671	-12.22
	28.10	582	547	6.40
	28.20	577	604	-4.47
	28.30	570	580	-1.72
	28.40	563	532	5.83
	28.50	558	581	-3.96
	28.60	552	581	-4.99
	28.70	545	554	-1.62
	28.80	540	573	-5.76
	28.90	534	576	-7.29
retardation zone	29.00	528	513	2.92
	31.10	42429	40755	4.11
	31.20	431	469	-8.10
	31.30	409	418	-2.15
	31.40	404	418	-3.35
	31.50	399	402	-0.75
	31.60	395	415	-4.82
	31.70	391	416	-6.01
	31.80	386	362	6.63
	31.90	382	413	-7.51
	32.00	377	412	-8.50
	32.10	373	402	-7.21
	32.20	369	410	-10.00
	32.30	365	406	-10.10
	32.40	360	390	-7.69
	32.50	357	391	-8.70
	32.60	352	350	0.57
	32.70	348	334	4.19
	32.80	344	316	8.86
	32.90	340	313	8.63
	33.00	337	311	8.36

Table 3 (continued)

P= .5

	CL (MM)	ΔN (THEORY) (CYCLE)	ΔN (EXPERIMENT) (CYCLE)	% ERROR
	16.90	1780	1616	10.15
	17.00	1759	1622	8.45
	17.10	1737	1679	3.45
	17.20	1718	1644	4.50
	17.30	1696	1620	4.69
	17.40	1677	1633	2.69
	17.50	1657	1618	2.41
	17.60	1637	1537	6.51
	17.70	1618	1648	-1.82
	17.80	1599	1537	4.03
	17.90	1580	1604	-1.50
retardation zone	18.00	1562	1431	9.15
	19.60	63381	71592	-11.47
	19.70	1683	1503	11.98
	19.80	1537	1454	5.71
	19.90	1408	1310	7.48
	20.00	1290	1187	8.68
	20.10	1227	1122	9.36
	20.20	1213	1107	9.58
	20.30	1200	1101	8.99
	20.40	1186	1105	7.33
	20.50	1173	1101	6.54
	20.60	1160	1219	-4.84
	20.70	1148	1188	-3.37
	20.80	1134	1102	2.90
	20.90	1122	1108	1.26
	21.00	1109	1104	0.45
	21.10	1098	1082	1.48
	21.20	1085	1079	0.56
	21.30	1073	1079	-0.56
	21.40	1061	1063	-0.19
	21.50	1050	1095	-4.11
	21.60	1038	975	6.46
	21.70	1027	998	2.91
	21.80	1015	972	4.42
	21.90	1005	993	1.21
	22.00	993	879	12.97
	22.10	983	874	12.47

Table 3 (continued)

	CL (MM)	ΔN(THEORY) (CYCLE)	ΔN(EXPERIMENT) (CYCLE)	% ERROR
	22.20	971	888	9.35
	22.30	962	983	-2.14
	22.40	950	966	-1.66
	22.50	941	877	7.30
	22.60	930	975	-4.62
	22.70	920	917	0.33
	22.80	910	963	-5.50
	22.90	900	880	2.27
	23.00	891	958	-6.99
	23.10	881	919	-4.13
	23.20	871	966	-9.83
	23.30	862	911	-5.38
	23.40	852	885	-3.73
	23.50	844	881	-4.20
	23.60	834	821	1.58
	23.70	825	872	-5.39
	23.80	816	824	-0.97
	23.90	808	795	1.64
	24.00	799	775	3.10
	24.10	790	714	10.64
	24.20	782	687	13.83
	24.30	773	739	4.60
	24.40	765	776	-1.42
	24.50	757	696	8.76
	24.60	748	688	8.72
	24.70	741	677	9.45
	24.80	732	689	6.24
	24.90	725	669	8.37
retardation zone	25.00	717	658	8.97
	26.90	43217	46671	-7.40
	27.00	653	632	3.32
	27.10	595	631	-5.71
	27.20	565	631	-10.46
	27.30	559	630	-11.27
	27.40	553	629	-12.08
	27.50	548	631	-13.15
	27.60	541	628	-13.85
	27.70	535	583	-8.23

Table 3 (continued)

	CL (MM)	ΔN (THEORY) (CYCLE)	ΔN (EXPERIMENT) (CYCLE)	% ERROR
	27.80	529	528	0.19
	27.90	524	527	-0.57
	28.00	518	531	-2.45
	28.10	513	528	-2.84
	28.20	506	531	-4.71
	28.30	502	569	-11.78
	28.40	496	428	15.89
	28.50	490	435	12.64
	28.60	486	468	3.85
	28.70	479	441	8.62
	28.80	475	466	1.93
	28.90	470	456	3.07
retardation zone	29.00	464	468	-0.85
	31.10	34678	32033	8.26
	31.20	379	412	-8.01
	31.30	359	415	-13.49
	31.40	356	414	-14.01
	31.50	351	407	-13.76
	31.60	347	413	-15.98
	31.70	344	414	-16.91
	31.80	340	353	-3.68
	31.90	335	409	-18.09
	32.00	332	408	-18.63
	32.10	328	402	-18.41
	32.20	325	394	-17.51
	32.30	321	298	7.72
	32.40	317	305	3.93
	32.50	313	297	5.39
	32.60	310	293	5.80

Table 3 (continued)

P= .6

	CL (MM)	ΔN(THEORY) (CYCLE)	ΔN(EXPERIMENT) (CYCLE)	% ERROR
	16.90	1547	1394	10.98
	17.00	1528	1393	9.69
	17.10	1510	1290	17.05
	17.20	1492	1205	23.82
	17.30	1475	1202	22.71
	17.40	1457	1248	16.75
	17.50	1440	1415	1.77
	17.60	1422	1317	7.97
	17.70	1406	1321	6.43
	17.80	1390	1340	3.73
	17.90	1373	1410	-2.62
retardation zone	18.00	1357	1325	2.42
	19.60	57403	64368	-10.82
	19.70	1462	1280	14.22
	19.80	1336	1310	1.98
	19.90	1223	1292	-5.34
	20.00	1121	1196	-6.27
	20.10	1067	996	7.13
	20.20	1054	970	8.66
	20.30	1043	979	6.54
	20.40	1030	1003	2.69
	20.50	1020	976	4.51
	20.60	1008	1002	0.60
	20.70	997	987	1.01
	20.80	986	975	1.13
	20.90	975	873	11.68
	21.00	964	981	-1.73
	21.10	953	893	6.72
	21.20	943	879	7.28
	21.30	933	867	7.61
	21.40	922	894	3.13
	21.50	913	883	3.40
	21.60	902	879	2.62
	21.70	892	967	-7.76
	21.80	882	867	1.73
	21.90	873	881	-0.91
	22.00	864	819	5.49
	22.10	853	822	3.77
	22.20	845	794	6.42

Table 3 (continued)

	CL (MM)	ΔN (THEORY) (CYCLE)	ΔN (EXPERIMENT) (CYCLE)	% ERROR
	22.30	835	875	-4.57
	22.40	826	826	0.00
	22.50	818	784	4.34
	22.60	808	859	-5.94
	22.70	800	740	8.11
	22.80	790	783	0.89
	22.90	783	784	-0.13
	23.00	774	766	1.04
	23.10	765	703	8.82
	23.20	757	691	9.55
	23.30	749	739	1.35
	23.40	741	695	6.62
	23.50	733	644	13.82
	23.60	725	641	13.10
	23.70	717	618	16.02
	23.80	709	641	10.61
	23.90	702	639	9.86
	24.00	694	676	2.66
	24.10	687	639	7.51
	24.20	679	642	5.76
	24.30	672	636	5.66
	24.40	665	639	4.07
	24.50	658	637	3.30
	24.60	650	640	1.56
	24.70	644	638	0.94
	24.80	636	633	0.47
	24.90	630	673	-6.39
retardation zone	25.00	623	583	6.86
	26.90	37575	40279	-6.71
	27.00	568	528	7.58
	27.10	517	527	-1.90
	27.20	491	529	-7.18
	27.30	486	506	-3.95
	27.40	481	485	-0.82
	27.50	475	440	7.95
	27.60	470	445	5.62
	27.70	465	428	8.64
	27.80	460	426	7.98

Table 3 (continued)

	CL (MM)	ΔN(THEORY) (CYCLE)	ΔN(EXPERIMENT) (CYCLE)	% ERROR
	27.90	456	425	7.29
	28.00	450	429	4.90
	28.10	445	426	4.46
	28.20	441	427	3.28
	28.30	435	430	1.16
	28.40	431	425	1.41
	28.50	427	428	-0.23
	28.60	421	412	2.18
	28.70	417	426	-2.11
	28.80	413	433	-4.62
	28.90	408	411	-0.73
retardation zone	29.00	403	402	0.25
	31.10	32136	30647	4.86
	31.20	329	320	2.81
	31.30	312	312	0.00
	31.40	309	313	-1.28
	31.50	306	318	-3.77
	31.60	302	309	-2.27
	31.70	298	309	-3.56
	31.80	295	316	-6.65
	31.90	292	305	-4.26
	32.00	288	271	6.27
	32.10	286	303	-5.61
	32.20	282	298	-5.37
	32.30	278	295	-5.76
	32.40	276	296	-6.76
	32.50	272	294	-7.48

Table 3 (continued)

P= .7

	CL (MM)	ΔN (THEORY) (CYCLE)	ΔN (EXPERIMENT) (CYCLE)	% ERROR
	16.90	1312	1154	13.69
	17.00	1295	1084	19.46
	17.10	1280	1120	14.29
	17.20	1265	1190	6.30
	17.30	1250	1085	15.21
	17.40	1235	1198	3.09
	17.50	1221	1103	10.70
	17.60	1206	1118	7.87
	17.70	1192	1211	-1.57
	17.80	1178	1113	5.84
	17.90	1164	1120	3.93
retardation zone	18.00	1150	1207	-4.72
	19.60	48744	50186	-2.87
	19.70	1240	1184	4.73
	19.80	1132	1103	2.63
	19.90	1037	1080	-3.98
	20.00	950	973	-2.36
	20.10	904	977	-7.47
	20.20	894	881	1.48
	20.30	884	883	0.11
	20.40	874	884	-1.13
	20.50	864	825	4.73
	20.60	855	877	-2.51
	20.70	845	846	-0.12
	20.80	835	790	5.70
	20.90	827	819	0.98
	21.00	817	870	-6.09
	21.10	808	821	-1.58
	21.20	800	820	-2.44
	21.30	790	820	-3.66
	21.40	782	804	-2.74
	21.50	773	748	3.34
	21.60	765	762	0.39
	21.70	756	769	-1.69
	21.80	749	739	1.35
	21.90	739	769	-3.90
	22.00	732	741	-1.21
	22.10	724	741	-2.29
	22.20	716	698	2.58

Table 3 (continue)

	CL (MM)	ΔN (THEORY) (CYCLE)	ΔN (EXPERIMENT) (CYCLE)	% ERROR
	22.30	708	618	14.56
	22.40	700	640	9.38
	22.50	693	644	7.61
	22.60	685	685	0.00
	22.70	678	636	6.60
	22.80	671	613	9.46
	22.90	663	639	3.76
	23.00	656	614	6.84
	23.10	649	636	2.04
	23.20	641	642	-0.16
	23.30	635	637	-0.31
	23.40	628	614	2.28
	23.50	622	639	-2.66
	23.60	614	635	-3.31
	23.70	608	639	-4.85
	23.80	601	637	-5.65
	23.90	595	635	-6.30
	24.00	589	637	-7.54
	24.10	582	635	-8.35
	24.20	576	636	-9.43
	24.30	569	582	-2.23
	24.40	564	584	-3.42
	24.50	557	584	-4.62
	24.60	552	585	-5.64
	24.70	545	575	-5.22
	24.80	540	570	-5.26
	24.90	534	573	-6.81
retardation zone →	25.00	528	578	-8.65
	26.90	32479	37184	-12.65
	27.00	481	425	13.18
	27.10	438	423	3.55
	27.20	417	427	-2.34
	27.30	412	425	-3.06
	27.40	407	420	-3.10
	27.50	403	426	-5.40
	27.60	398	423	-5.91
	27.70	395	424	-6.84
	27.80	390	423	-7.80

Table 3 (continue)

	CL (MM)	ΔN (THEORY) (CYCLE)	ΔN (EXPERIMENT) (CYCLE)	% ERROR
	27.90	386	424	-8.96
	28.00	381	421	-9.50
	28.10	378	424	-10.85
	28.20	373	426	-12.44
	28.30	370	424	-12.74
	28.40	365	420	-13.10
	28.50	361	423	-14.66
	28.60	358	401	-10.72
	28.70	353	389	-9.25
	28.80	350	367	-4.63
	28.90	346	396	-12.63
retardation zone	29.00	342	387	-11.63
	31.10	24646	20704	19.04
	30.60	515	518	-0.58
	30.70	461	479	-3.76
	30.80	414	413	0.24
	30.90	373	397	-6.05
	31.00	338	348	-2.87
	31.10	306	312	-1.92
	31.20	279	315	-11.43
	31.30	265	304	-12.83
	31.40	262	304	-13.82
	31.50	259	315	-17.78
	31.60	256	274	-6.57
	31.70	253	276	-8.33
	31.80	250	311	-19.61
	31.90	247	280	-11.79
	32.00	245	266	-7.89
	32.10	241	266	-9.40
	32.20	239	266	-10.15
	32.30	237	261	-9.20

Table 3 (continued)

P= .8

	CL (MM)	ΔN(THEORY) (CYCLE)	ΔN(EXPERIMENT) (CYCLE)	% ERROR
	16.90	1057	941	12.33
	17.00	1044	943	10.71
	17.10	1031	942	9.45
	17.20	1020	1004	1.59
	17.30	1007	986	2.13
	17.40	996	966	3.11
	17.50	983	926	6.16
	17.60	972	928	4.74
	17.70	961	893	7.61
	17.80	949	883	7.47
	17.90	938	925	1.41
retardation zone	18.00	928	987	-5.98
	19.60	39254	48723	-19.43
	19.70	999	893	11.87
	19.80	913	807	13.14
	19.90	835	818	2.08
	20.00	766	802	-4.49
	20.10	729	822	-11.31
	20.20	720	792	-9.09
	20.30	712	743	-4.17
	20.40	705	787	-10.42
	20.50	696	741	-6.07
	20.60	689	676	1.92
	20.70	681	640	6.41
	20.80	674	642	4.98
	20.90	666	640	4.06
	21.00	658	674	-2.37
	21.10	652	642	1.56
	21.20	644	643	0.16
	21.30	637	641	-0.62
	21.40	630	641	-1.72
	21.50	623	640	-2.66
	21.60	617	639	-3.44
	21.70	609	617	-1.30
	21.80	603	633	-4.74
	21.90	597	622	-4.02
	22.00	589	637	-7.54
	22.10	584	636	-8.18

Table 3 (continued)

	CL (MM)	ΔN (THEORY) (CYCLE)	ΔN (EXPERIMENT) (CYCLE)	% ERROR
	22.20	577	639	-9.70
	22.30	570	668	-14.67
	22.40	565	636	-11.16
	22.50	558	636	-12.26
	22.60	552	597	-7.54
	22.70	547	535	2.24
	22.80	540	537	0.56
	22.90	534	537	-0.56
	23.00	529	537	-1.49
	23.10	523	531	-1.51
	23.20	517	536	-3.54
	23.30	512	532	-3.76
	23.40	506	535	-5.42
	23.50	501	534	-6.18
	23.60	495	533	-7.13
	23.70	490	537	-8.75
	23.80	485	533	-9.01
	23.90	479	533	-10.13
	24.00	474	533	-11.07
	24.10	470	531	-11.49
	24.20	464	532	-12.78
	24.30	459	529	-13.23
	24.40	454	532	-14.66
	24.50	449	530	-15.28
	24.60	445	482	-7.68
	24.70	439	481	-8.73
	24.80	435	467	-6.85
	24.90	430	412	4.37
retardation zone	25.00	426	430	-0.93
	26.90	27758	31478	-11.82
	27.00	388	349	11.17
	27.10	353	375	-5.87
	27.20	336	374	-10.16
	27.30	332	309	7.44
	27.40	328	306	7.19
	27.50	325	321	1.25
	27.60	321	306	4.90
	27.70	318	319	-0.31

Table 3 (continued)

	CL (MM)	ΔN (THEORY) (CYCLE)	ΔN (EXPERIMENT) (CYCLE)	% ERROR
	27.80	314	308	1.95
	27.90	311	306	1.63
	28.00	308	337	-8.61
	28.10	304	306	-0.65
	28.20	301	305	-1.31
	28.30	298	320	-6.88
	28.40	294	306	-3.92
	28.50	291	304	-4.28
	28.60	288	288	0.00
	28.70	285	302	-5.63
	28.80	282	307	-8.14
	28.90	279	331	-15.71
retardation zone	29.00	275	332	-17.17
	31.10	21589	17284	24.91
	31.20	225	272	-17.28
	31.30	213	271	-21.40
	31.40	211	250	-15.60
	31.50	209	225	-7.11
	31.60	206	228	-9.65
	31.70	204	208	-1.92
	31.80	202	206	-1.94
	31.90	199	205	-2.93
	32.00	197	203	-2.96

Table 3 (continued)

P= .9

	CL (MM)	ΔN(THEORY) (CYCLE)	ΔN(EXPERIMENT) (CYCLE)	% ERROR
	17.50	696	592	17.57
	17.60	688	607	13.34
	17.70	681	643	5.91
	17.80	672	682	-1.47
	17.90	664	643	3.27
retardation zone	18.00	657	617	6.48
	19.60	25363	24362	4.11
	19.70	707	644	9.78
	19.80	646	606	6.60
	19.90	592	638	-7.21
	20.00	542	640	-15.31
	20.10	516	564	-8.51
	20.20	510	541	-5.73
	20.30	505	537	-5.96
	20.40	498	541	-7.95
	20.50	493	539	-8.53
	20.60	488	518	-5.79
	20.70	482	538	-10.41
	20.80	477	535	-10.84
	20.90	472	533	-11.44
	21.00	466	518	-10.04
	21.10	462	534	-13.48
	21.20	456	504	-9.52
	21.30	451	487	-7.39
	21.40	446	454	-1.76
	21.50	441	435	1.38
	21.60	437	434	0.69
	21.70	431	435	-0.92
	21.80	427	411	3.89
	21.90	423	439	-3.64
	22.00	417	431	-3.25
	22.10	413	411	0.49
	22.20	409	433	-5.54
	22.30	404	432	-6.48
	22.40	400	433	-7.62
	22.50	395	433	-8.78
	22.60	391	432	-9.49
	22.70	387	431	-10.21
	22.80	382	394	-3.05

Table 3 (continued)

	CL (MM)	ΔN(THEORY) (CYCLE)	ΔN(EXPERIMENT) (CYCLE)	% ERROR
	22.90	379	360	5.28
	23.00	374	375	-0.27
	23.10	370	355	4.23
	23.20	367	535	-31.40
	23.30	362	410	-11.71
	23.40	358	329	8.81
	23.50	355	408	-12.99
	23.60	351	351	0.00
	23.70	347	332	4.52
	23.80	343	337	1.78
	23.90	339	310	9.35
	24.00	336	329	2.13
	24.10	332	310	7.10
	24.20	329	329	0.00
	24.30	325	308	5.52
	24.40	321	309	3.88
	24.50	319	303	5.28
	24.60	314	327	-3.98
	24.70	312	308	1.30
	24.80	308	308	0.00
	24.90	304	330	-7.88
retardation zone	25.00	302	332	-9.04
	26.90	19422	22168	-12.39
	26.60	410	405	1.23
	26.70	368	404	-8.91
	26.80	333	306	8.82
	26.90	302	304	-0.66
	27.00	274	304	-9.87
	27.10	251	284	-11.62
	27.20	237	284	-16.55
	27.30	235	273	-13.92
	27.40	233	273	-14.65
	27.50	230	274	-16.06
	27.60	227	273	-16.85
	27.70	225	274	-17.88
	27.80	223	273	-18.32
	27.90	220	272	-19.12
	28.00	218	273	-20.15

Table3 (continued)

	CL (MM)	ΔN (THEORY) (CYCLE)	ΔN (EXPERIMENT) (CYCLE)	% ERROR
	28.10	215	272	-20.96
	28.20	213	272	-21.69
	28.30	211	273	-22.71
	28.40	208	272	-23.53
	28.50	207	271	-23.62
	28.60	204	273	-25.27
	28.70	201	271	-25.83
	28.80	200	273	-26.74
	28.90	197	273	-27.84
retardation zone	29.00	196	272	-27.94
	31.10	14578	11642	25.22
	30.60	294	298	-1.34
	30.70	263	299	-12.04
	30.80	236	278	-15.11
	30.90	213	278	-23.38
	31.00	193	237	-18.57
	31.10	175	227	-22.91
	31.20	159	217	-26.73
	31.30	151	196	-22.96
	31.40	149	196	-23.98
	31.50	148	196	-24.49
	31.60	146	196	-25.51
	31.70	145	195	-25.64
	31.80	142	193	-26.42
	31.90	142	194	-26.80

Table 3 (continued)

CHAPTER IV

CONCLUSIONS

1. The goal of this research program was to develop a crack growth model which takes into account the random nature of the crack evolution in real solids. This was achieved by viewing the growth process as a Markovian stochastic process, discrete in state and inhomogenous with respect to time. This led to the derivation of a law that predicts the crack jump from one state to the following state with a specified probability, i.e. yielding constant probability crack growth curves. In the model, the transition intensity of the process is identified as a function of the effective stress intensity factor. This permits the consideration of the load interaction history and makes the model a valuable design and reliablity tool for constant, as well as, random load applications. A fundamental concept of the model is the assumption that the crack growth curve produced by an appropriate continuum law is identical to the median probability curve which corresponds to the value of $P_r(i)=0.56$; this was sufficient to identify the remaining constant probabilitty crack growth curves.

2. An in-house experimental program was executed to generate constant probability crack growth curves for three different loading conditions by using 180 Al 7075-T6 center-notched flat specimen. A comparison was then made between these curves and those theoretically obtained for each corresponding test condition; full analysis of this application is provided in Appendices A-C.

3. An in-house experimental program was carried out to generate constant probability crack growth curves for conditions of overload application. In these tests sixty-five Ti-6Al-4V compact tension specimens were used under the same base loading and for the same overload ratio applied to three different crack lengths. The corresponding theoretical constant probability crack growth curves were calculated using the proposed model. A critical step in these calculations was the determination of the effective stress intensity factor during retardation. This was accomplished by separating the retardation mechanisms and setting up experimental load conditions so that the only governing mechanism was the crack tip compressive residual stress. Comparision between experimental and theoretical crack growth curves indicated prediction error of average 8%.

Several remarks concerning the experimental observations are called for here:

A- Following an overload, two separate zones can be distinguished in front of the crack tip as shown in Fig. 11. The first is a ductile rupture zone and coincides with the sudden peak in the crack growth rate. The width of this zone increases as the crack length, at which the overload is applied, increases; see figure 12. The second region is the retardation zone; it was observed that for the same stress ratio, R, and the same overload ratio, the number of cycles, Nd, spent in this region decreases as the crack length increases. This is contrary to observations made by Arone[37]. Also results of the current experiments seem to validate the conclusions drawn by Lankford and Davidson[45] that Nd decreases as R increases.

B- In several tests an apparent temporary crack tip arrest was observed in the retardation zone. In each case the crack succeeded in crossing this zone and regaining an accelerated growth equal to that existing prior to the overload. Further investigation of these arrrest regions showed, in all test specimens, traces of crack growth striations indicating that growth existed in duration of apparent arrest. The failure to detect this behavior could be due to the inability to measure the associated very small crack growth using the potential drop measurement system. Examples of these types of striations, before overload application as well as in the region of apparent arrest, are shown in figure 13.

C- The test specimens, all of which were made of Ti-6Al-4V, a highly textured material, responded to the application of the overload by instantaneous crack tip extension via ductile rupture on a plane inclined to the normal-to-load plane, see figure 14. The length of the defected crack component and its angle, b and q, respectively, in Figure 15 were found to depend on the crack length at which the defection occurs; as the crack length increases, b increases while q decreases. Due to the orientation of the deflected component, the governing stress intensity factor at its tip is viewed as a combination of K_I and K_{II}. As the loading cycle returns to its base form, the value of K_{II} decays gradually as the deflected crack tip orients itself back towards the original fracture plane, see Figure 15. The length of the deflected crack and its transition coincides with the combined length of the overload rupture and delayed zones. It must however, be noted that this crack deflection phenomenon is limited to the surface

layer, i.e. the plain stress condition with a depth of less than 500 μm as illustrated in Figure 16.

Finally, while the work in this program encourages the validity of the proposed model's ability to predict scatter in the crack growth behavior, it also emphasizes a specific shortcoming:

On the basis of the extensive experimental work carried out during this program, it has been observed that crack growth scatter could be divided into two stages; the first corresponding to short crack lengths and the second corresponding to long cracks. Short lengths promote the highest scatter reflecting the fact that at this length the microstructural parameters, such as grain size and slip system dominate. As the crack length increases scatter tends to decrease, an indication that the growth process becomes a stress controlled phenomenon. The use of stochastic models should therefore, be directed primarily towards short crack applications. In this respect the proposed model should be further developed to include, in an explicit form, parameters that indentify the role of microstructure.

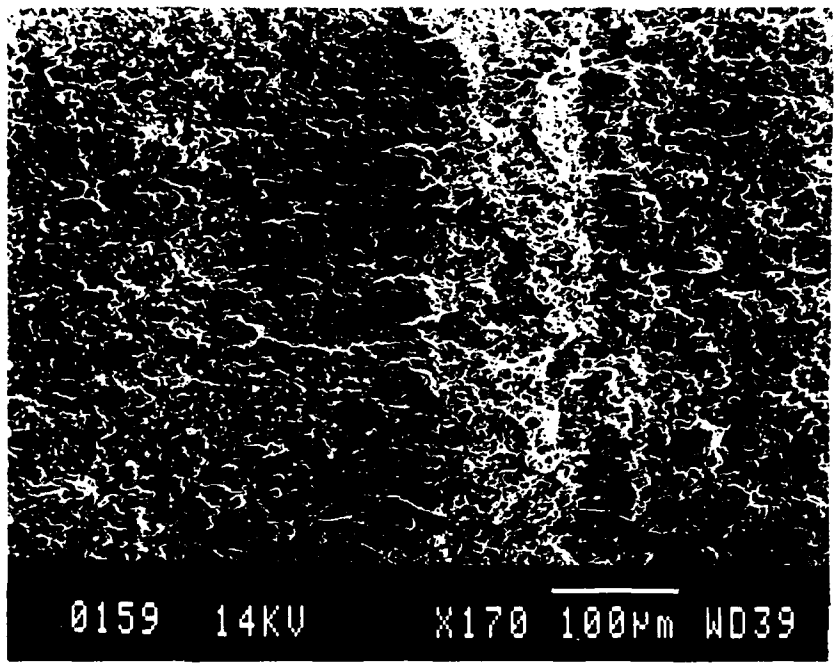

Figure 11(a) Overview of an overload zone showing the ductile repture area and delayed zone

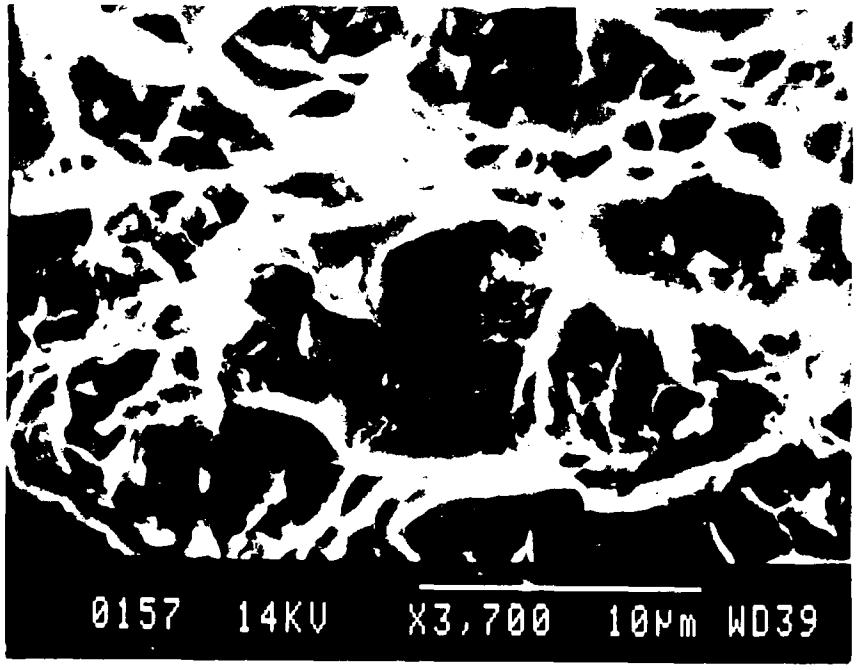

Figure 11(b) Details of the repture area shown above

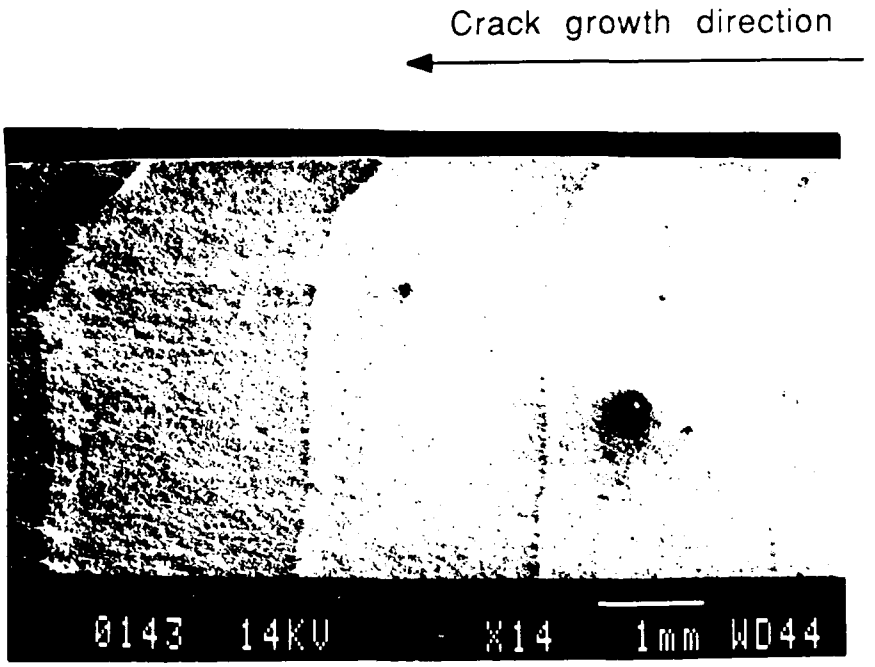

Figure 12 Ductile rupture zones following overload application at different crack length

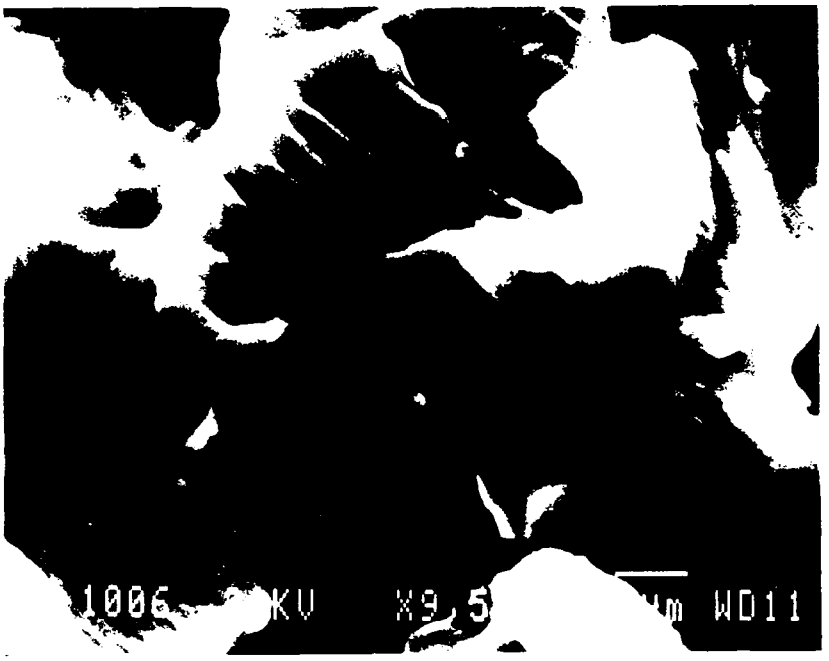

Figure 13(a) Striation of the fracture surface before overload application

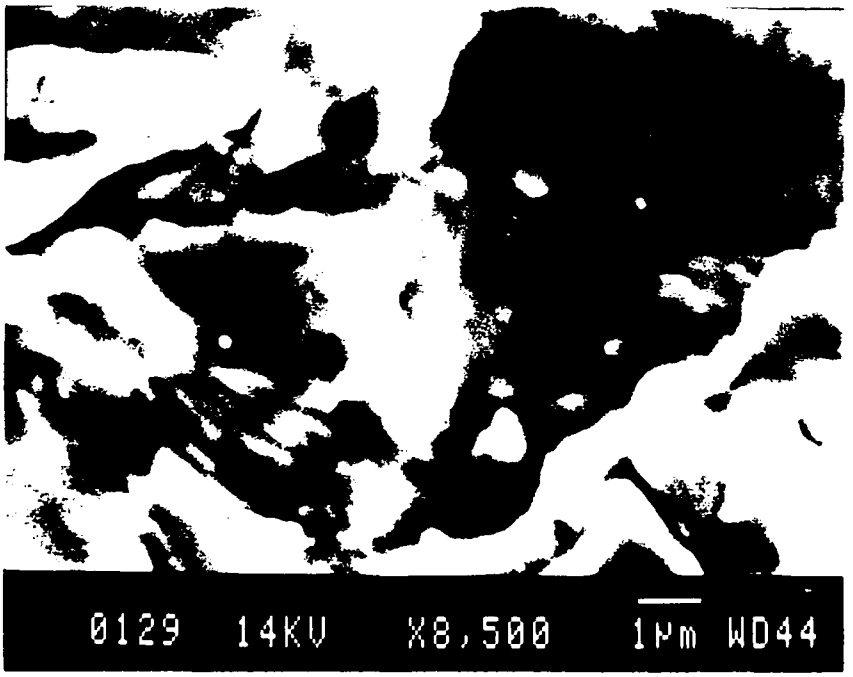

Figure 13(b) Striation in the delayed zone following an overload application in the same specimen of the above figure

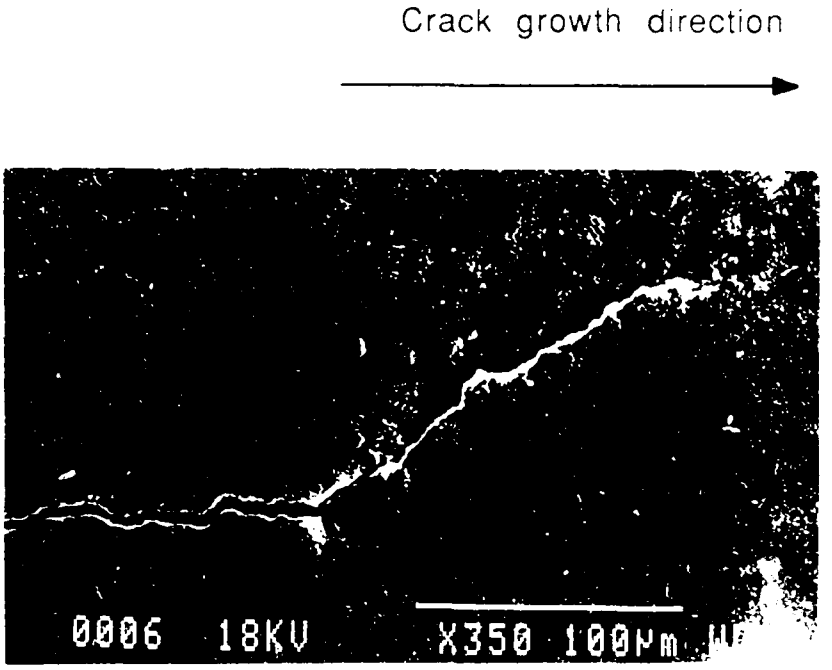

Figure 14(a) Change in the crack orientation due to overload

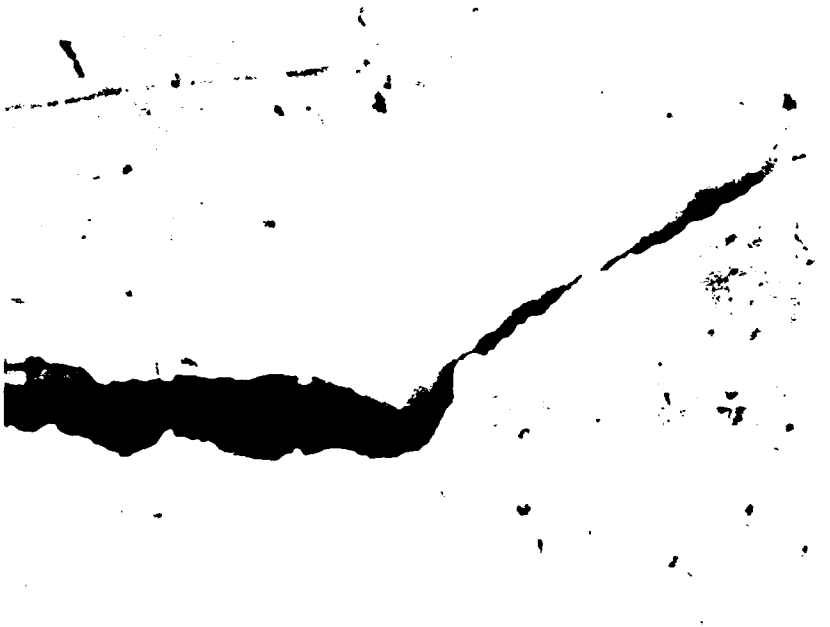

Figure 14(b) Close up of the deflected zone

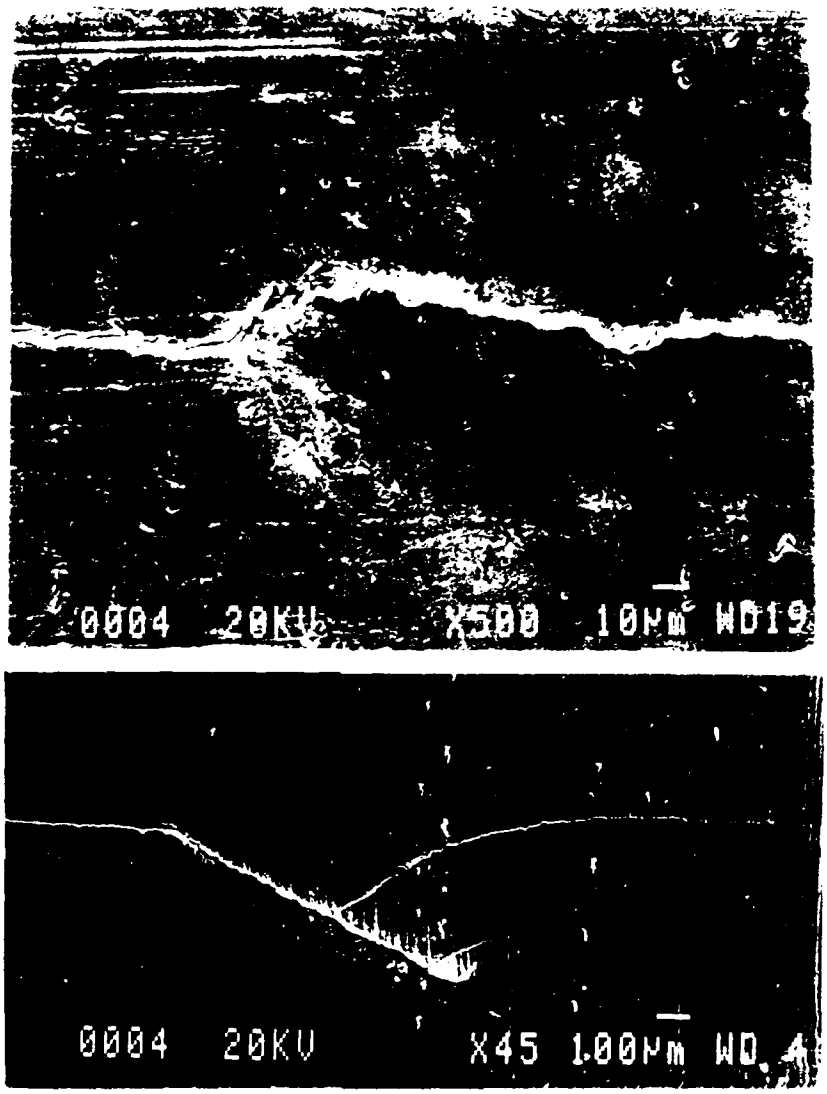

Figure 15 Scanning and optical microscope patterns of the transition of the kinked crack in a increases, b decreases and c decreases

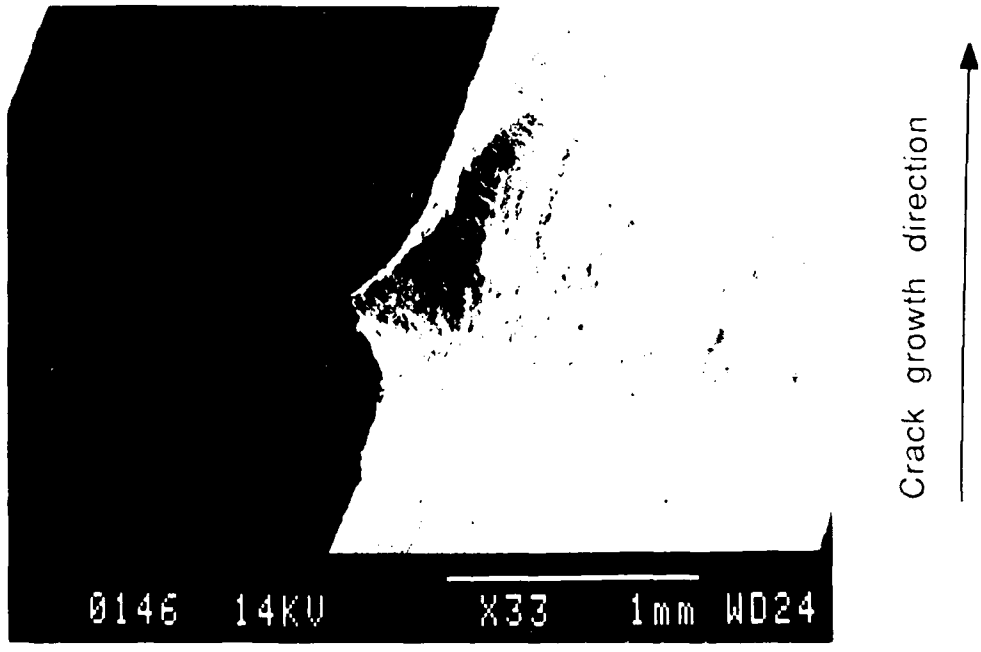

Figure 16 The deflected part of the surface crack after the overload application and the depth of this transition in the interior of the specimen

REFERENCES

[1] H. Lauschmann, A stochastic model of fatigue crack growth in heterogeneous material, Engng Fracture Mech. **26**, (1978)

[2] D.W. Hoeppner and W. E. Krupp, Prediction of component life by application of fatigue crack growth knowledge, Engng Fracture Mech. **6**, (1974)

[3] Karl-Heinz Schwalbe, Comparison of several crack propagation laws with experimental results, Engng Fracture Mech. **6**, (1974)

[4] S. Chand and S. B. L. Garg, Propagation under constant Amplitude loading, Engng Fracture Mech. **21**, (1985)

[5] S. C. Saunder, On the probability determination of scatter factors using Miner's rule in fatigue life studies, ASTM STP **511**

[6] J. N. Yang and R. C. Donath, Statistics of a superalloy under sustained load, J. Engng Mater. Tech. **106**, (1984)

[7] S. Tauaka, M. Ichickawa and S. Akita, Variability of m and C in fatigue crack propagation law $da/dn=C(\Delta K)^m$, Int. J. Fract. **17**, (1981)

[8] K. P. Oh, A weakest-link model for the prediction of fatigue crack growth rate, J. Engng Mater. Tech. **100**. (April 1978)

[9] W. Weibull, A statistical representation of fatigue failure in solids, Trans. Roysl Inst. Tech. (Stockholm), No. 27, (1949)

[10] A. Tsurui and A. Igarashi, A probabilistic approach to fatigue crack growth rate. J. Engng Mater. Tech. **102**, (July 1980)

[11] H. Ghonem and S. Dore, Probabilistic description of fatigue crack growth in aluminum alloys. AFOSR-83-0323, (April 1986)

[12] J. L. Bogdanoff, A new cumulation damage model-Part I, J. Appl. Mech. **45**, (1987)

[13] J. L. Bogdanoff and W. Krieger, A new cumulative damage model-Part II, J. Appl. Mech. **45**, (1978)

[14] J. L. Bogdanoff, A new cumulative fatigue model-Part III, J. Appl. Mech. **45**, (1978)

[15] J. L. Bogdanoff and F. Kozin, A new cumulative damage model-Part IV, J. Appl. Mech. **47**, (1980)

[16] H. Ghonem and J. M. Provan, Micromechanics theory of fatigue crack initiation and propagation. Engng Fracture Mech.**13**, (1980)

[17] J. Provan and H. Ghonem, Probabilistic description of microstructual fatigue failure, continuum model of discrete systems. University of Waterloo Press, (1977)

[18] J. Sedlacek, The stochastic interpretation of service strength and reliability of mechanical systems. Monographs and Memoranda **6**, National Institute of Machine Design, Prague, (1968)

[19] H. Ghonem and S. Dore, Probabilistic description of crack growth in polycrystalline solids. Engng Fracture Mech. **21**, (1985)

[20] H. Lauschmann, To the probabilistic description of fatigue crack growth. C. Sc. Dissertation, Technical University of Prague, (1985)

[21] F. Ellyin and C. O. Fakinlede, Probabilistic simulation of fatigue crack growth by damage accumulation, Engng Fracture Mech. **22**, (1985)

[22] O. Ditlevsen, Random fatigue crack growth-a first passage problem. Engng Fracture Mech. **23**, (1986)

[23] H. Alawi, A probabilistic model for fatigue crack growth under random loading. Engng Fracture Mech. **23**, (1986)

[24] D. A. Virckler, B. M. Hillberry and P. K. Goel, The statistical nature of fatigue crack propagation. ASME, J. Engng Mater. Tech. **101**, (April 1979)

[25] H. Ghonem and S. Dore, Experimental study of the constant probability crack growth curves under constant amplitude loading. Engng Fracture Mech. **27**, (1987)

[26] J. Willenborg, R. M. Engle and H. A. Wood, A crack growth retardation model using an effectivestress concept. AFFDL-TM-FBR-81-1, Air Force Dynamics lab, (1971)

[27] O. Wheeler, Spectrum loading and crack growth. J. Basic Engng, 94 D, 181, (1972)

[28] S. Matsuoka and K. Tauaka, Delayed retardation phenomenon of fatigue crack growth resulting from a single application of overload. Engng Fracture Mech.**10**, (1978)

[29] T. D. Gray and J. P. Gallagher, Predicting fatigue crack retardation following a single overload using a modified wheeler model. Mechanics of Crack Growth, ASTM, STP**590**, (1976)

[30] R. H. Christensew, Metal Fatigue, McGraw Hill, New York, (1959)

[31] W. Elber, The significance of crack clousure. ASTM STP **486**, (1971)

[32] C. Bathias and M. Vancon, Mechanics of overload effect on fatigue crack propagation in Al alloys. Engng Fracture Mech. **10**, (1978)

[33] J. Schijue, Fatigue damage accumulation and incompatible crack front orientation. Engng Fracture Mech. **6**, (1974)

[34] R. J. Bucci A. B. THakker, T. H. Sanders, R. R. Sawtell and J. T. Rankinging, 7075 Al alloys fatigue crack growth resistance under constant amplitude and spectrum loading. ASTM STP **714**, (1980)

[35] J. Petit and S. Suresh, Constant amplitude and post overload fatigue crack growth in Aluminum-Lithium alloys. Division of Engineering, Brown University, Providence, Rhode Island, (1985)

[36] R. Hertzberg, Micromechanisms of fatigue crack advance in PVC. J. Mater. Sci. **8**, Nov. 1973

[37] R. Arone, Fatigue crack gorwth under random overloads superimposed on constant-amplitude cyclic loading. Engng Fracture Mech **24**, (1986)

[38] W. J. Mills and R. W. Hertzberg, Load interaction effect on fatigue crack propagation in 2024-T3 Aluminum alloy. Engng Fracture Mech. **8**, (1976)

[39] O. Ditlevsen and K. Sobczyk, Random fatigue crack growth with retardation. Engng Fracture Mech. **24**, (1986)

[40] H. Ghonem, Constant probability crack growth curves. Engng Fracture Mech. **30**, (1988)

[41] Crack growth analysis for arbitrary specimen loading, Volume I-results and discussion, Final Report, Air Force Danamics Laboratory

[42] R. P. Wei, N. E. Fenelli, K. D. Unangst and T. T. Shih, Fatigue crack growth responce following a high-load excursion in 2219-T851 Aluminum alloy. Transaction of the ASTM, Vol. 102, (July 1980)

[43] O. Jonas and R. P. Wei, An exploratory study of delay in fatigue-crack growth, Int. J. Fract. Mech. **7**, (1971)

[44] R. P. Wei and T. T. Shih, Delay in fatigue crack growth, Int. J. Fract. Mech. **10**, (1974)

[45] J. Lankford and D. L. Davidson, Fatigue crack tip plasticity associated with overloads and subsequent cycling. J. Engng Mat. Tech. (Jan. 1976)

[46] K. Walker, The effect of stress ratio during crack propagation and fatigue for 2024-T3 and 7075-T6 Aluminum. ASTM STP **462**, (1970)

[47] J. H. Fitzgerald, Empirical formulations for the analysis and prediction of trends for steady-state fatigue crack growth rates. J. of Testing and Evalution, JTEVA, Vol. 5, No. 5, Sept. 1977

APPENDIX A

PROBABILISTIC DESCRIPTION OF FATIGUE CRACK GROWTH IN POLYCRYSTALLINE SOLIDS

Engineering Fracture Mechanics Vol. 21, No. 6, pp. 1151–1168, 1985
Printed in the U.S.A.

0013-7944/85 $3.00 + .00

PROBABILISTIC DESCRIPTION OF FATIGUE CRACK GROWTH IN POLYCRYSTALLINE SOLIDS

H. GHONEM and S. DORE
Mechanics of Solids Laboratory, Department of Mechanical Engineering and Applied Mechanics, University of Rhode Island, Kingston, RI 02881, U.S.A.

Abstract—A stochastic model describing the crack evolution and scatter associated with the crack propagation process has been built on the basis of the discontinuous Markovian process. The evolution and scatter are identified in terms of constant probability curves whose equation is derived as $\ln P_r(i) = B(e^{Ki_0} - e^{Ki})$, $i \geq I_0$, where i is the number of cycles, B and K are crack-length-dependent variables, $P_r(i)$ is the probability of the crack being at position r along the fracture surface after i cycles elapse and I_0 is the minimum number of cycles required for the crack to advance from one position on the fracture surface to the next. The validity of the model is established by comparing the crack growth curves generated for Al 2024-T3 at a specific loading condition with those experimentally obtained.

INTRODUCTION

LABORATORY TESTS conducted on different polycrystalline materials exhibited considerable variation in the crack growth characteristics data. This variation, or scatter, is considered a major factor in the gap that exists between theoretical predictions of existing continuum crack propagation models and experimental observations.

Several studies, employing theory of probability concepts, have been developed to predict and characterize the variation in crack propagation data. These studies generally follow two approaches. The first approach is based on the introduction of random variables encompassing the scatter sources to replace the deterministic parameters in continuum crack propagation rules such as the Paris–Erdogan Equation [1] which is widely studied and used. The result of this operation is viewed as a sample crack growth equation by which mean crack position and associated variance can be calculated. Examples of models belonging to this approach are those of Hoeppner and Krupp [2], Gurney [3], Ostergaard and Hillberry [4] and others [5–7].

The second approach is based on the assumption that the crack propagation process could be formulated in terms of a particular discontinuous Markovian process. This leads to the description of the crack length in the form of its probability distribution whose evolution in time characterizes the nondeterministic nature of the crack propagation process. Examples of these models are found in the work of Ghonem and Provan [8] and Bogdanoff and Kozin [9].

This paper is an attempt to extend the concepts presented in Ref. [8] to produce a theoretical method which will estimate the crack growth scatter at any stress level. This is achieved by developing the sample functions of the crack growth process in terms of a constant-probability crack growth criterion. Mathematical elements of this criterion are detailed in the first part of this paper while the second part deals with the use of the model in a numerical example to estimate crack growth scatter in Aluminum 2024-T3. Emphasis is placed on the adherence of the model to the physical aspects of the crack growth process and the degree of agreement between the theoretical results of the model and corresponding experimental data.

MATHEMATICAL ELEMENTS OF THE MODEL

The stochastic model of the fatigue crack propagation as briefly described in [8] is developed in terms of a general pure birth, discontinuous Markovian stochastic process. The model is based on the assumption that the crack front can be approximated, as shown in Fig. 1, by a large number of elements α, $\alpha = 1, \ldots, M$, each of which, in terms of the theory of probability, identifies a statistical trial or experiment. The fracture state of the αth trial at cycle i is given by the crack length or the random variable ${}^{\alpha}a_i$ whose evolution with time shall then be established. ${}^{\alpha}a_i$ will hereafter be referred to as a_i.

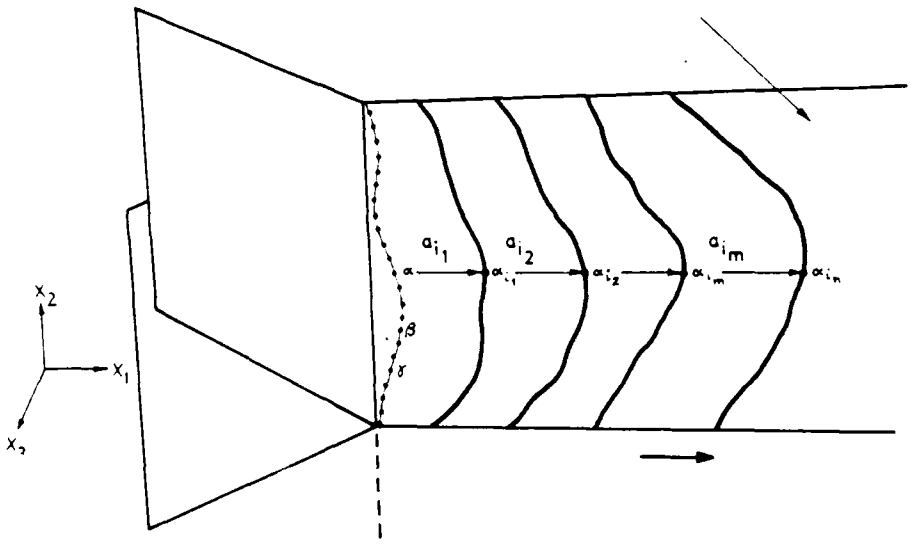

Fig. 1. Schematic of Mode I crack propagation fracture surface.

Due to the built-in limitations of all experimental techniques the observed value of a_i can only be specified within the range of

$$x < a_i < x + \Delta x, \tag{1}$$

where Δx is the experimental error and x is the crack position calculated as (see Fig. 2)

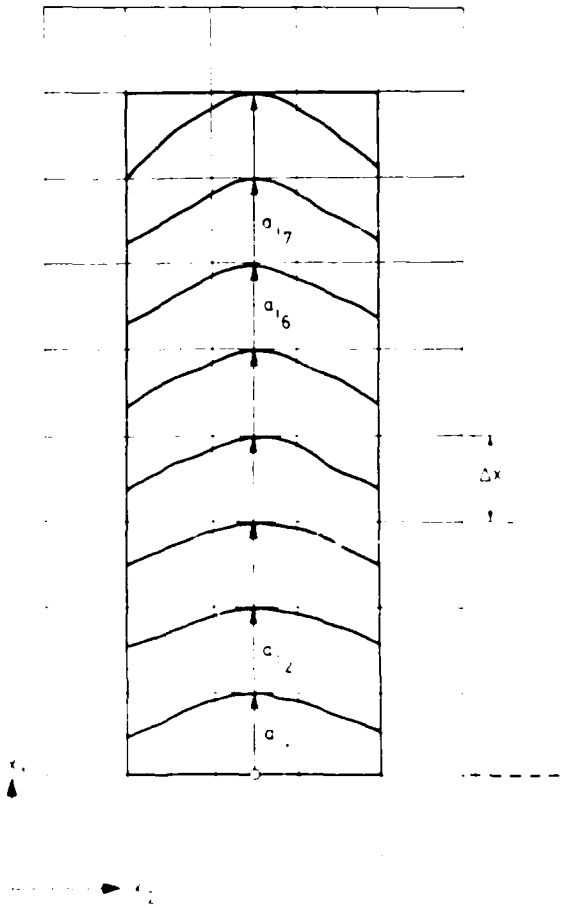

Fig. 2. Schematic of the proposed fatigue crack propagation model.

$$x = r\Delta x; \qquad r_0 < r < r_f. \tag{2}$$

Here r identifies the observable zone or state along the fracture surface; r_0 is the initial propagation state, r_f is the state just prior to catastrophic failure of the specimen and $r_1, r_2, \ldots, r_{f-1}$ are the intermediate zones.

Given that the crack is in state r, then after i cycles have elapsed from the instant of reaching r, one of two events would occur: a_i would remain in state r (event ${}^{r}E_i$) or a_i would not be in state r (event ${}^{\backslash}E_i$). The following observations can now be made:

1. Due to the fact that the propagation process is an irreversible one, the crack, if it does not stay in r, must exist in a state greater than r.

2. Since it is not possible for the crack to propagate from one state to any other state without penetrating the immediate neighboring state, each crack could then be identified by the number of cycles required to advance from a given state to the following one.

Based on these observations the two events ${}^{r}E_i$ and ${}^{\backslash}E_i$ can be seen as the element of a measurable sample space Ω, see Ref. [9], and the following definition of the probability measure of a_i becomes possible. At any fatigue cycle i the probability that a_i is in state r, i.e. the probability of ${}^{r}E_i$, is defined as

$$P\{a_i \epsilon {}^{r}E_i\} = P\{x < a_i < x + \Delta x\},$$

i.e.

$$P({}^{r}E_i) = P_r(i). \tag{3}$$

Therefore the probability of a_i not falling within r is

$$P({}^{\backslash}E_i) = P_{\backslash}(i) = 1 - P_r(i). \tag{4}$$

Here $P_{\backslash}(i)$ continuously increases as the number of cycles increase.

Furthermore, it is known that the existence of the crack front at a particular position inside the material depends on its present mechanical and microstructure details and is not directly influenced by the details of any of its other previous positions. More specifically, the probability of a_i propagating from state r to $r + 1$ in the cycle interval $(i, i + \Delta i)$ depends on the event ${}^{r}E_i$ and is independent of any event ${}^{q}E_j, \ldots, {}^{p}E_0$ occurring prior to i; $0 < j < i$. This can be expressed as

$$P\{{}^{t}E_{\Delta i}/{}^{r}E_i, \ldots, {}^{q}E_j, \ldots, {}^{p}E_0\} = P\{{}^{t}E_{\Delta i}/{}^{r}E_i\} = P_{rt}(i) \tag{5}$$

where $t = r + 1$ and '/' denotes a conditional probability measure. These characteristics together with the evolution of a_i within the two-event space Ω, describe a discontinuous Markovian process. The function $P_{rt}(i)$ could then be considered the transition probability linking the probability measures of two consecutive states r and t; $t = r + 1$, along the fracture surface.

It is now possible to describe the propagation process of the crack front in terms of the following criteria:

1. The probability of a_i propagating to a state different than r in Δi cycles is given by

$$\begin{aligned} P_{\backslash}(\Delta i) &= P\{{}^{t}E_{\Delta i}/{}^{r}E_i\} + 0(\Delta i) \\ &= \lambda_r \Delta i + 0(\Delta i), \end{aligned} \tag{6}$$

where λ_r is a positive parameter describing the crack transition rate from state r to t in Δi cycles and is thus considered a material- and time-dependent variable; see Bharucha-Reid [11].

2. The corresponding probability that a_i will be in state r during the cycle interval Δi is

$$\begin{aligned} P_r(\Delta i) &= P\{{}^{r}E_{\Delta i}/{}^{r}E_i\} + 0(\Delta i) \\ &= (1 - \lambda_r \Delta i) + 0(\Delta i). \end{aligned} \tag{7}$$

3. The probability that a_i is in a state different from $r + 1$ is

$$P_{rt}(\Delta i) = P\{{}^{r}E_{\Delta i}/{}^{r}E_i\} = 0(\Delta i); \quad t > r + 1. \tag{8}$$

Since

$$P\{{}^{r}E_{i+\Delta i}\} = P\{{}^{r}E_{\Delta i}/{}^{r}E_i\} \cdot P\{{}^{r}E_i\}, \tag{9}$$

therefore substituting eqns (6), (7) and (8) in eqn (9), the probability of the event ${}^{r}E_{\Delta i}$ can be obtained as

$$P_r(i + \Delta i) = (1 - \lambda_r \Delta i)P_r(i) + 0(\Delta i). \tag{10}$$

By transposing and taking the limit $\Delta i \to 0$, eqn (10) becomes

$$\frac{dP_r(i)}{di} = -\lambda_r P_r(i). \tag{11}$$

The solution of this equation is

$$\ln P_r(i) = -\int \lambda_r \, di + L_1, \tag{12}$$

where L_1 is a constant.

An important element in solving this equation is the parameter λ_r which is seen here as a measure of the crack growth rate. This measure is assumed to have the following properties:

1. In the presence of continuous cyclic loading the longer the cycle duration during which the crack is in a specific state, the higher the probability that the propagation threshold of the crack tip is satisfied and the higher the probability that the crack will advance. This indicates that in a general case, λ_r increases monotonically with an increase in the number of cycles i.

2. λ_r being a material-dependent variable should then possess a nonzero positive value at cycle $i = 0$.

Based on these observations λ_r is chosen to have the form

$$\lambda_r = L_2 e^{Ki}, \tag{13}$$

where L_2 and K are crack-position independent and time dependent parameters. Substituting (13) in (12) one obtains

$$\ln P_r(i) = -Be^{Ki} + L_1, \tag{14}$$

where

$$B = \frac{L_2}{K}.$$

Upper and lower limits of $P_r(i)$ in the above equation are

$$1 \geq P_r(i) \geq 0.$$

The form of eqn (14) suggests that i has a lower boundary which satisfies the upper limit of $P_r(i)$. This means that eqn (14) will be valid only for $i \geq I_0$, where I_0 is the lower boundary of i or simply the minimum number of cycles required for the crack to advance from state r. In this approach, concepts such as those of the weakest-link theory by Weibull [12] and others

[13, 14] have not been taken into consideration. Hence, the upper limit condition for $P_r(i)$ can be expressed as

$$P_r(i) = 1; \qquad i < I_0.$$

By invoking this upper limit condition on eqn (14) the constant L_1 is obtained as

$$L_1 = Be^{KI_0} \tag{15}$$

Equation (14) could then be written in the form

$$\begin{aligned} P_r(i) &= e^{B(e^{Ki} - e^{KI_0})}; \qquad i \geq I_0. \\ P_r(i) &= 1; \qquad\qquad\quad i < I_0. \end{aligned} \tag{16}$$

This result, illustrated in Fig. 3, describes a set of curves which can be obtained by varying $P_r(i)$. Each of these curves is a constant probability curve identifying the discrete crack position and the corresponding number of cycles. Since the variables B, K and I_0 are functions of the crack length, they are related to the crack length through certain constants. These constants can be determined by using one known constant probability crack growth curve and eqn (16) consequently becomes fully defined. The significance of this concept is that if the crack growth curve obtained by using a continuum model is considered as being the mean growth curve, i.e. the $P_r(i) = 0.5$ curve, a view that is consistent with the application of the majority of the continuum models, the parameters B, K and I_0 can then be calculated and eqn (16) becomes sufficient to identify the crack length and associated scatter in number of cycles at any stress level without the need to perform scatter experiments. In the next part of the paper this model will be employed in a numerical example to estimate the crack growth curves of Aluminum 2024-T3 and results will be compared to available experimental data.

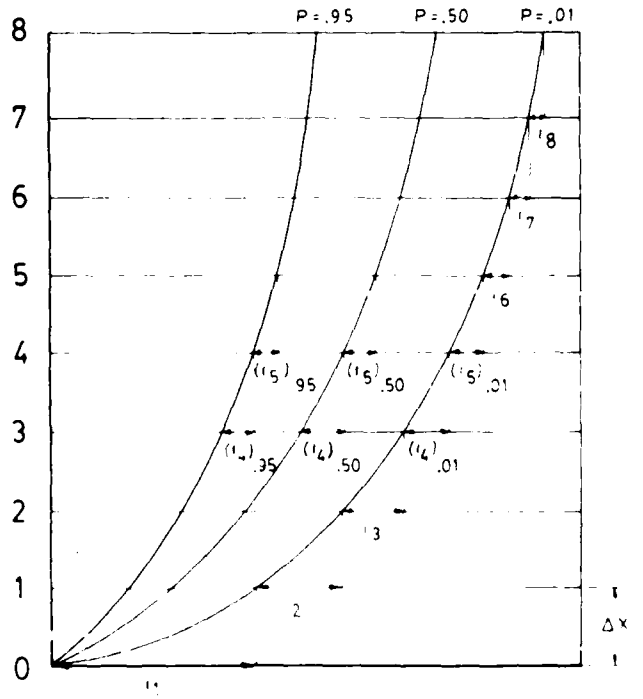

Fig. 3. Schematic of constant-probability crack growth curves as generated by eqn (16).

APPLICATION

The first step to be dealt with here is the determination of the unknown variables B, K and I_0 in eqn (16). To achieve this the authors utilized experimental crack growth scatter data obtained by Virkler, Hillberry and Goel [15] and Yang, Donath and Salivar [16].

The first set of data [15] is obtained from 68 identically prepared Aluminum 2024-T3 tension specimens with a central slot perpendicular to the loading axis. The data consists of the number of cycles necessary to reach the same specified crack length for each specimen; 164 crack lengths are recorded ranging from 9 mm to 49.8 mm for a half crack length. The 68 sample crack growth curves are shown in Fig. 4. These curves were utilized to obtain constant probability crack growth curves as follows: The total crack length was divided into 204 states; each with a width of 0.2 mm. The number of cycles spent in each state was calculated and arranged in ascending order; the largest number was assigned a probability of

$$P_r(i) = 1 - (x/68); \qquad x = 68,$$

and so on, up to a probability of

$$P_r(i) = 1 - (x/68); \qquad x = 1,$$

for the shortest number of cycles. Points with equal probability were connected and a set of ten constant probability curves was generated as shown in Fig. 5. Data points representing the number of cycles corresponding to similar discrete crack positions along three different constant probability growth curves, $P_r(i) = 0.05$, 0.50 and 0.95, were used as input for eqn (16) to determine the variables B, K and I_0. The values obtained are listed in Table 1. These values are plotted versus the crack length position, i.e. state r in Figs. 6(a, b, c); and by using regression analysis the following relationships were constructed:

$$\begin{aligned} B &= 0.018r^{0.28}, \\ K &= 2.498 \times 10^{-7} r^{1.95}, \\ I_0 &= 0.94 \times 10^{7}[(r-1)^{-1.01} - r^{-1.01}]. \end{aligned} \tag{17}$$

To confirm these relationships, another set of crack growth scatter data of IN 100, a superalloy

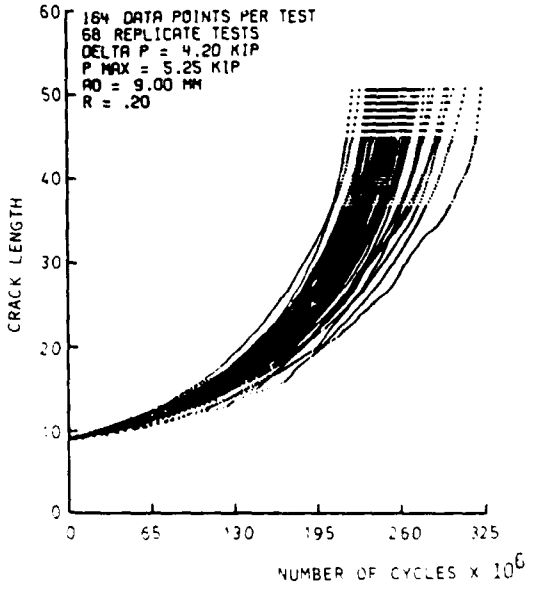

Fig. 4. Replicate a versus t data set from Virkler's study [15]

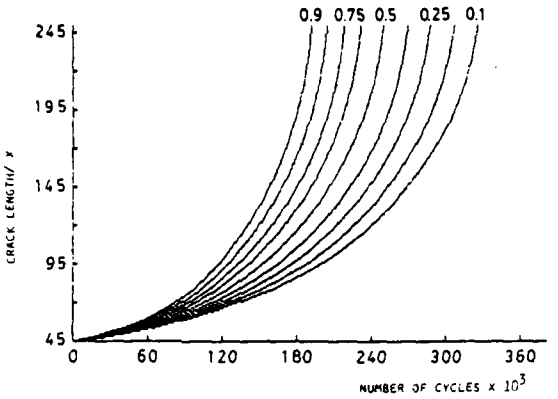

Fig. 5. Experimental constant-probability crack growth curves generated from data in Ref. [15].

used in certain gas turbine engines, was used [16]. The data consisted of the distribution of crack size as function of load cycles for two different load conditions as shown in Figs. 7(a,b). Analysis similar to that done on the work of Virkler and co-workers was carried out, yielding two sets of values for B, K and I_0. They are shown in Table 2. These values are again plotted vs the crack length position as shown in Figs. 8(a,b,c) and 9(a,b,c) and the following relationships were obtained.

Test condition I

$$B = 0.055r^{0.76},$$
$$K = 1.362 \times 10^{-6}r^{2.34}, \tag{18}$$
$$I_0 = 2.743 \times 10^5[(r-1)^{-0.71} - r^{-0.71}].$$

Test condition II

$$B = 0.059r^{0.73},$$
$$K = 6.68 \times 10^{-7}r^{2.015}, \tag{19}$$
$$I_0 = 1.843 \times 10^6[(r-1)^{-1.45} - r^{-1.45}].$$

Table 1. Values of B, K and I_0 for different crack length position r (Δx = 0.2 mm)

Crack length position r	I_0 (cycles)	B ($\times 10^{-2}$)	K ($\times 10^{-3}$)
55	3166	5.5	0.617
65	2269	5.8	0.856
75	1706	6.0	1.133
85	1330	6.2	1.446
95	1066	6.4	1.796
105	873	6.6	2.183
115	729	6.8	2.604
125	618	6.9	3.063
135	530	7.1	3.555
145	460	7.2	4.086
155	403	7.3	4.647
165	356	7.5	5.249
175	317	7.6	5.885
185	283	7.7	6.549
195	255	7.8	7.249
205	231	8.0	7.984
215	210	8.1	8.751
225	192	8.2	9.547
235	176	8.3	11.040
245	162	8.4	11.127

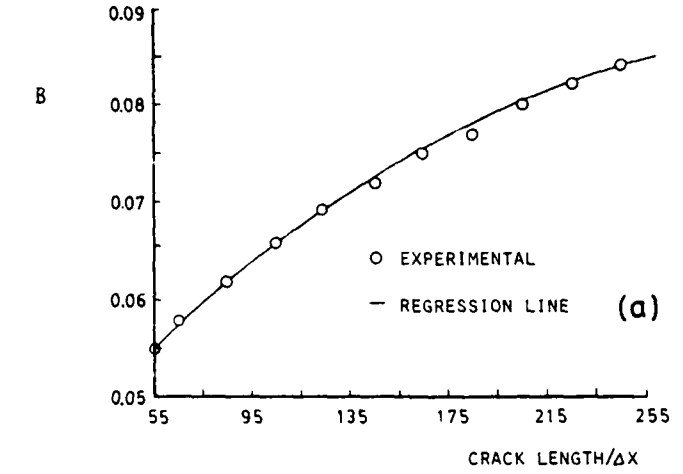

Figure 6(a)

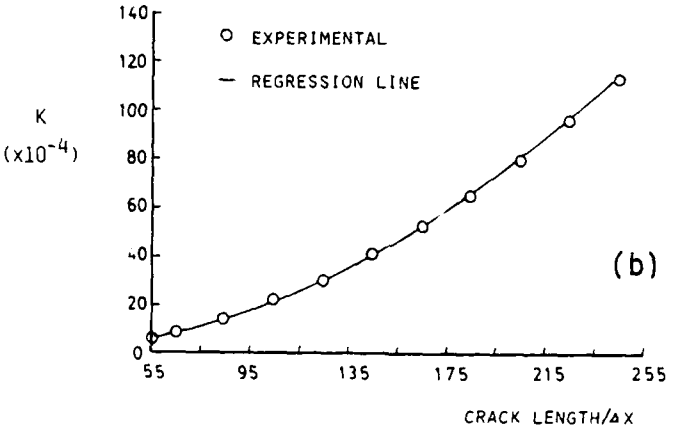

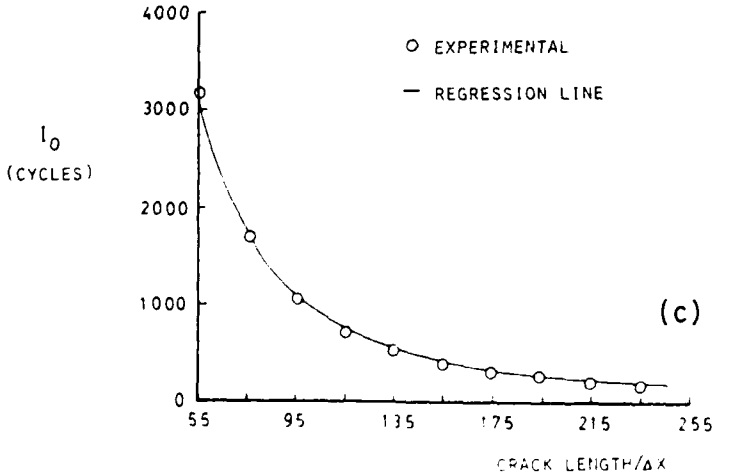

Fig. 6. Relationship between B, K and I_0 and crack length based on experimental data from Ref. [15].

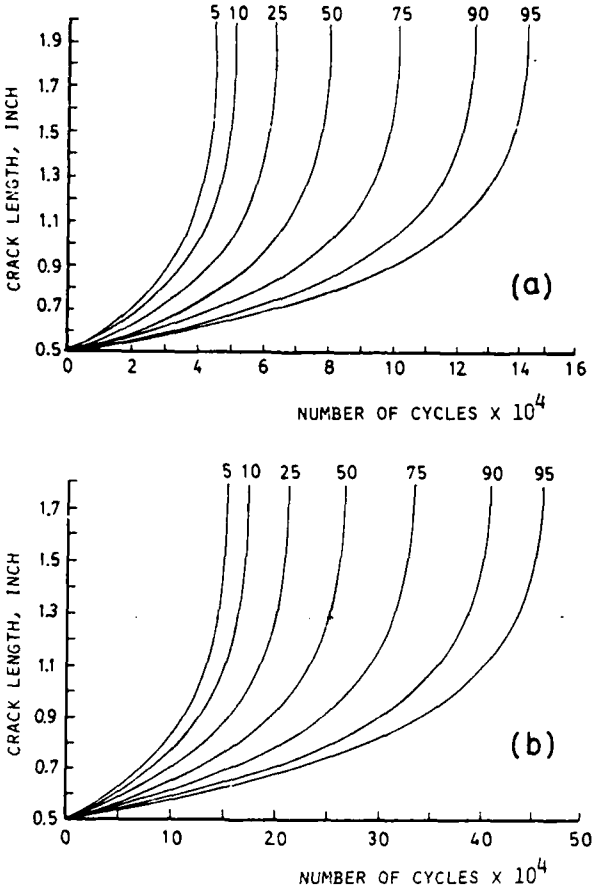

Fig. 7. Experimental constant-probability crack growth curves for (a) Test Condition I and (b) Test Condition II (Ref. [16]).

Table 2. Values of B, K and l_0 for different crack length positions (Δx = 0.1 in)

Crack length position	l_0 (cycles)	B ($\times 10^{-1}$)	K ($\times 10^{-4}$)
	Test Condition I		
6	10280	1.915	0.946
7	8036	2.715	1.117
8	7203	2.836	1.719
9	5460	3.014	2.144
10	4169	3.143	3.206
11	3387	3.263	3.777
12	2806	3.518	4.407
13	2326	3.981	5.150
	Test Condition II		
6	39940	2.189	0.268
7	28870	2.423	0.333
8	24050	2.688	0.427
9	14410	2.998	0.467
10	9275	3.228	0.669
11	7618	3.308	1.014
12	6402	3.637	1.017
13	5204	3.834	1.136

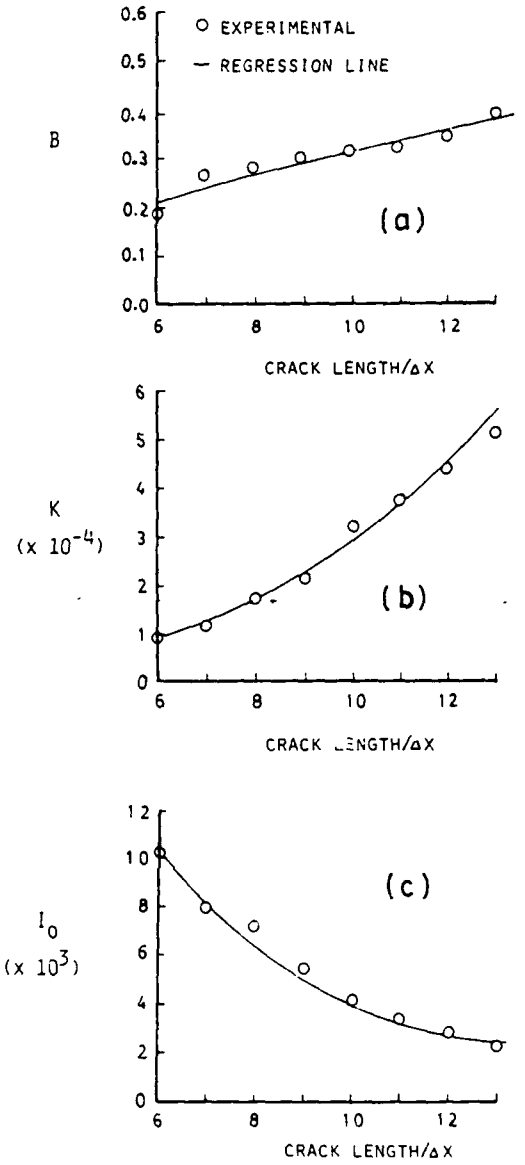

Fig. 8. Relationship between B, K and I_0 and crack length position for Test Condition I for Ref. [16].

By observing eqns (17), (18), (19) general forms of B, K and I_0 in terms of crack length a, could be written as

$$B = C_1 a^{m_1},$$
$$K = C_2 a^{m_2}, \tag{20}$$
$$I_0 = C_3[(a - \Delta x)^{m_3} - a^{m_3}].$$

An attempt can now be made using eqn (16) in conjunction with eqn (20) to generate constant probability curves for the test conditions of Virkler *et al.* [15]. These curves could then be compared to those experimentally obtained in Fig. 5. The first step is to obtain the mean crack growth curve utilizing, as mentioned before, a continuum crack growth equation. In this application the Paris–Erdogan equation in the following form is used to generate such a curve

$$\Delta t = \frac{1}{C(\Delta\sigma\sqrt{\pi})^m} \frac{1}{m-1}[a_0^{1-m} - a_f^{1-m}]; \qquad m = \frac{n}{2}. \tag{21}$$

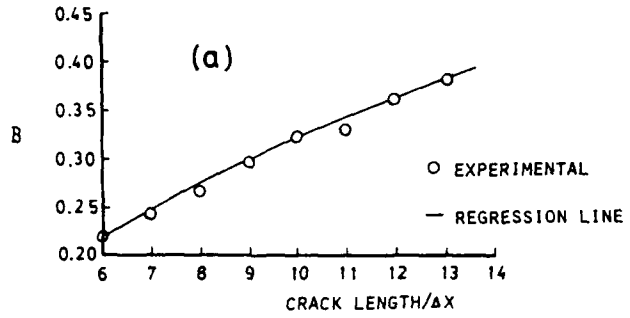

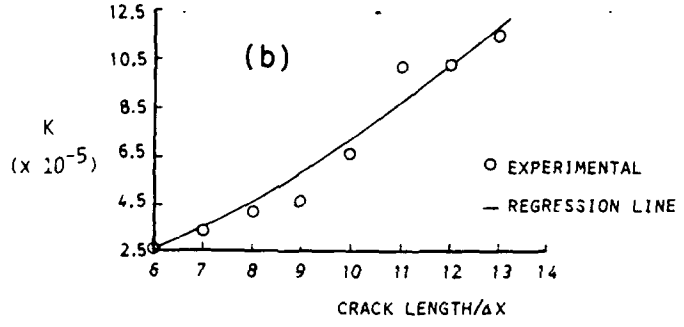

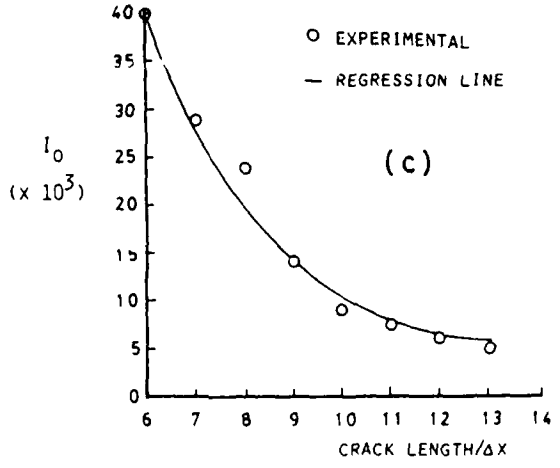

Fig. 9. Relationship between B, K and I_0 and crack length position for Test Condition II in Ref. [16]

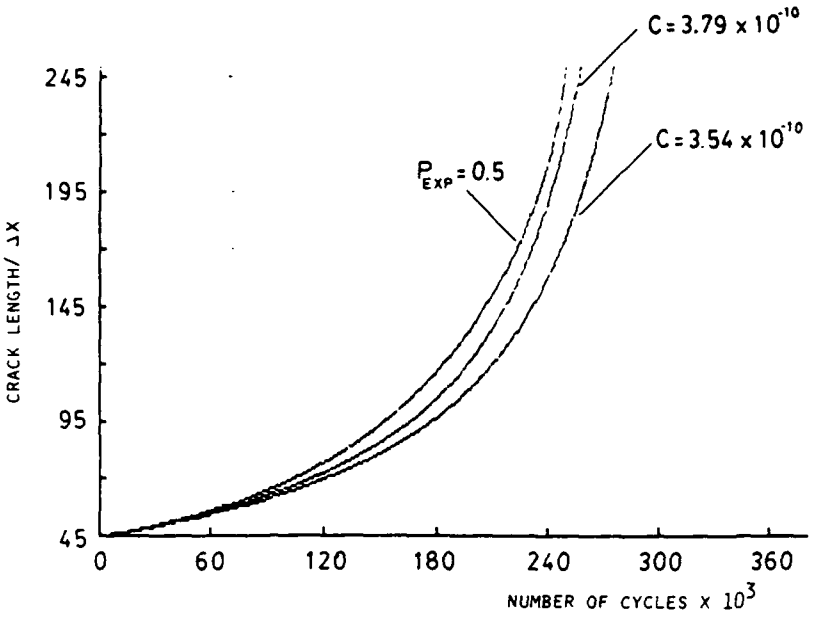

Fig. 10. The experimental mean crack growth curve ($P_f(i) = 0.5$) and the corresponding theoretical curves using the P-F equation with different C values.

for Al 2024-T3 the index n is equal to 4 while the parameter C attains values ranging from 3.5×10^{-10} to 3.79×10^{-10}. Equation (21) was then used to obtain the crack growth curve as shown in Fig. 10 ($C = 3.79 \times 10^{-10}$, $a_0 = 9$ mm and $\Delta\sigma = 7$Ksi). This curve is viewed here as equivalent to the experimental mean curve, i.e. the $P_f(i) = 0.5$ curve.

The number of cycles corresponding to six discrete crack positions along the Paris–Erdogan curve was then used as input for eqns (16) and (20), where $P_f(i) = 0.5$. These six equations were solved by an iterative technique employing Newton–Raphson's method. Converging values for the six constants were found as followed:

$$C_1 = 0.0563; \quad C_2 = 2.04 \times 10^{-7}; \quad C_3 = 1.022 \times 10^{-7},$$

$$n_1 = 0.298; \quad n_2 = 1.917; \quad n_3 = -1.0.$$

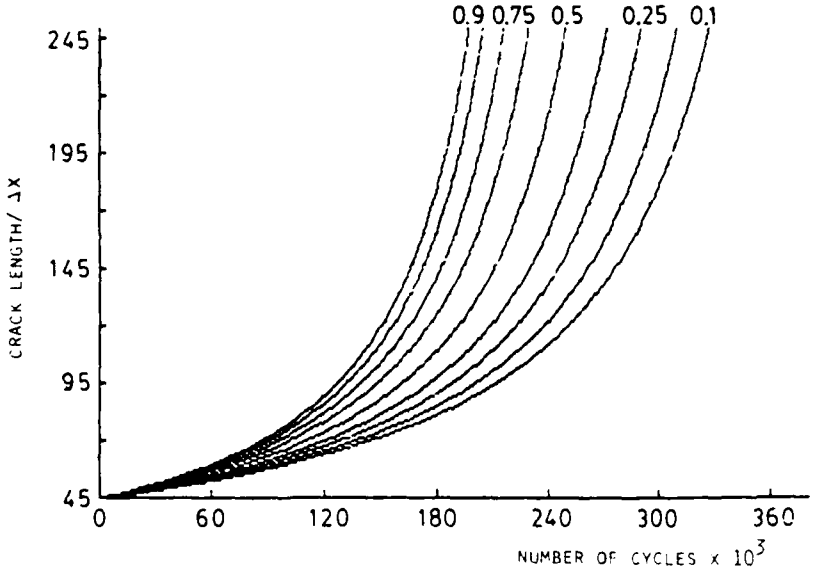

Fig. 11. Theoretical constant-probability crack growth curves generated for the test condition reported in Ref. [15].

Table 3 Percentage error between the theoretical and experimental constant-probability crack growth curves

	P = 0.897			P = 0.838			P = 0.750		
State	No. cycles (exptl.)	No. cycles (theor.)	% Error	No. cycles (exptl.)	No. cycles (theor.)	% Error	No. cycles (exptl.)	No. cycles (theor.)	% Error
46	5529.0	5335.0	3.509	5911.0	5550.0	6.107	6232.0	5873.0	5.761
47	10749.0	10443.0	2.847	11431.0	10864.0	4.960	12183.0	11495.0	5.647
48	15793.0	15338.0	2.881	16613.0	15956.0	3.955	17782.0	16883.0	5.056
49	20480.0	20033.0	2.183	21586.0	20840.0	3.456	22953.0	22051.0	3.930
50	24835.0	24540.0	1.188	26298.0	25529.0	2.924	27806.0	27012.0	2.855
51	28920.0	28870.0	0.173	30750.0	30034.0	2.328	32530.0	31778.0	2.312
52	32960.0	33034.0	0.225	35030.0	34365.0	1.898	36957.0	36360.0	1.615
53	36747.0	37040.0	0.797	39005.0	38532.0	1.213	41217.0	40769.0	1.087
54	40317.0	40898.0	1.441	42789.0	42545.0	0.570	45166.0	45015.0	0.334
55	43763.0	44615.0	1.947	46302.0	46412.0	0.238	48858.0	49106.0	0.508
56	47090.0	48199.0	2.355	49656.0	50140.0	0.975	52402.0	53056.0	1.237
57	50288.0	51658.0	2.724	52896.0	53738.0	1.592	55937.0	56856.0	1.643
58	53443.0	54997.0	2.908	56129.0	57211.0	1.928	59322.0	60530.0	2.036
59	56236.0	58223.0	3.533	59174.0	60566.0	2.352	62616.0	64080.0	2.338
60	58971.0	61341.0	4.019	62037.0	63809.0	2.856	65646.0	67511.0	2.841
70	81344.0	87617.0	7.712	86113.0	91137.0	5.834	91434.0	96417.0	5.450
80	97397.0	107316.0	10.184	103634.0	111621.0	7.707	110266.0	118080.0	7.086
90	110576.0	122630.0	10.901	117827.0	127540.0	8.243	125616.0	134914.0	7.402
100	122030.0	134876.0	10.527	129916.0	140269.0	7.969	138682.0	148370.0	6.986
110	131667.0	144893.0	10.045	140358.0	150676.0	7.351	149920.0	159370.0	6.303
120	140420.0	153235.0	9.126	149576.0	159344.0	6.530	159779.0	168528.0	5.476
130	147991.0	160292.0	8.312	157713.0	166674.0	5.682	168564.0	176270.0	4.572
140	155049.0	166336.0	7.280	165122.0	172952.0	4.742	176448.0	182901.0	3.657
150	161046.0	171573.0	6.537	171606.0	178392.0	3.954	183346.0	188645.0	2.890
160	166576.0	176155.0	5.751	177447.0	183147.0	3.212	189547.0	193667.0	2.174
170	171394.0	180194.0	5.134	182531.0	187341.0	2.635	195017.0	198095.0	1.578
180	175477.0	183786.0	4.735	186888.0	191067.0	2.236	199731.0	202028.0	1.150
190	179242.5	186997.0	4.326	190881.5	194399.0	1.843	203948.0	205543.0	0.782
200	182494.0	189885.0	4.050	194329.0	197396.0	1.578	207702.0	208705.0	0.483
210	185287.0	192497.0	3.891	197308.5	200106.0	1.418	210858.0	211565.0	0.335
220	187594.0	194872.0	3.880	199733.5	202568.0	1.419	213446.0	214162.0	0.335
230	189482.5	197037.0	3.987	201686.0	204818.0	1.553	215517.5	216534.0	0.472
240	190895.3	199022.0	4.203	203290.3	206876.0	1.764	217205.8	218706.0	0.691

Table 3. (*continued*)

P = 0.647				P = 0.500				P = 0.352			
State	No. cycles (exptl.)	No. cycles (theor.)	% Error	State	No. cycles (exptl.)	No. cycles (theor.)	% Error	State	No. cycles (exptl.)	No. cycles (theor.)	% Error
46	6579.0	6256.0	4.910	46	7160.0	6831.0	4.595	46	7586.0	7475.0	1.463
47	12820.0	12246.0	4.477	47	13764.0	13371.0	2.855	47	14513.0	14633.0	0.827
48	18582.0	17986.0	3.207	48	19944.0	19638.0	1.534	48	20966.0	21493.0	2.514
49	24079.0	23491.0	2.442	49	25805.0	25650.0	0.601	49	27321.0	28073.0	2.752
50	29117.0	28776.0	1.171	50	31221.0	31421.0	0.641	50	33093.0	34390.0	3.919
51	34140.0	33853.0	0.841	51	36398.0	36965.0	1.558	51	38486.0	40459.0	5.127
52	38760.0	38735.0	0.064	52	41237.0	42296.0	2.568	52	43649.0	46295.0	6.062
53	43316.0	43432.0	0.268	53	45970.0	47426.0	3.167	53	48680.0	51911.0	6.637
54	47444.0	47955.0	1.077	54	50394.0	52365.0	3.911	54	53460.0	57319.0	7.218
55	51371.0	52313.0	1.834	55	54558.0	57125.0	4.705	55	58000.0	62530.0	7.810
56	55167.0	56515.0	2.443	56	58504.0	61714.0	5.487	56	62311.0	67555.0	8.416
57	58831.0	60570.0	2.956	57	62310.0	66142.0	6.150	57	66383.0	72404.0	9.070
58	62333.0	64484.0	3.451	58	66045.0	70417.0	6.620	58	70384.0	77085.0	9.521
59	65881.0	68265.0	3.619	59	69760.0	74547.0	6.862	59	74221.0	81608.0	9.953
60	69102.0	71920.0	4.078	60	73251.0	78539.0	7.219	60	77907.0	85980.0	10.362
70	96499.0	102712.0	6.438	70	103215.0	112173.0	8.679	70	110375.0	122818.0	11.273
80	116986.0	125785.0	7.521	80	125695.0	137375.0	9.292	80	135245.0	150428.0	11.226
90	133386.0	143714.0	7.743	90	143921.0	156958.0	9.058	90	155181.0	171885.0	10.764
100	147313.0	158042.0	7.283	100	159193.0	172607.0	8.426	100	171665.0	189033.0	10.117
110	159244.0	169753.0	6.599	110	171894.0	185398.0	7.856	110	185504.0	203051.0	9.459
120	169732.0	179502.0	5.756	120	183197.0	196047.0	7.014	120	197615.0	214723.0	8.657
130	179030.0	187743.0	4.867	130	193126.0	205046.0	6.172	130	208376.0	224589.0	7.781
140	187308.0	194801.0	4.000	140	201932.0	212752.0	5.358	140	217928.0	233037.0	6.933
150	194553.0	200912.0	3.269	150	209728.0	219425.0	4.624	150	226365.0	240353.0	6.179
160	201128.0	206253.0	2.548	160	216804.0	225256.0	3.898	160	234018.0	246749.0	5.440
170	206875.0	210963.0	1.976	170	222998.0	230397.0	3.318	170	240733.0	252386.0	4.841
180	211880.0	215146.0	1.541	180	228413.0	234962.0	2.867	180	246708.0	257392.0	4.331
190	216421.5	218887.0	1.139	190	233200.5	239045.0	2.506	190	251879.0	261869.0	3.966
200	220380.0	222250.0	0.849	200	237419.0	242716.0	2.231	200	256352.5	265893.0	3.722
210	223699.5	225290.0	0.711	210	240980.5	246034.0	2.097	210	260165.5	269530.0	3.599
220	226445.0	228052.0	0.710	220	243921.0	249047.0	2.102	220	263334.5	272836.0	3.608
230	228605.3	230571.0	0.860	230	246261.5	251797.0	2.248	230	265885.8	275850.0	3.748
240	230391.5	232881.0	1.081	240	248183.0	254314.0	2.470	240	267913.5	278611.0	3.993

Table 3. (*continued*)

P = 0.250				P = 0.162				P = 0.103			
State	No. cycles (exptl.)	No. cycles (theor.)	% Error	State	No. cycles (exptl.)	No. cycles (theor.)	% Error	State	No. cycles (exptl.)	No. cycles (theor.)	% Error
46	8047.0	7998.0	0.609	46	8437.0	8556.0	1.410	46	8502.0	9050.0	6.446
47	15345.0	15657.0	2.033	47	16265.0	16750.0	2.982	47	16529.0	17717.0	7.187
48	22089.0	22997.0	4.111	48	23271.0	24604.0	5.728	48	23857.0	26025.0	9.087
49	28870.0	30038.0	4.046	49	30384.0	32138.0	5.773	49	31390.0	33995.0	8.299
50	34921.0	36798.0	5.375	50	37031.0	39372.0	6.322	50	38368.0	41648.0	8.549
51	40582.0	43294.0	6.683	51	42961.0	46323.0	7.826	51	44584.0	49002.0	9.909
52	45899.0	49546.0	7.933	52	48452.0	53008.0	9.403	52	50336.0	56075.0	11.401
53	51080.0	55551.0	8.753	53	53908.0	59441.0	10.264	53	55989.0	62882.0	12.311
54	55957.0	61339.0	9.618	54	59080.0	65637.0	11.099	54	61362.0	69438.0	13.161
55	60664.0	66917.0	10.308	55	64060.0	71608.0	11.783	55	66759.0	75756.0	13.477
56	65207.0	72296.0	10.872	56	68843.0	77366.0	12.380	56	71817.0	81849.0	13.969
57	69555.0	77487.0	11.404	57	73448.0	82922.0	12.899	57	76952.0	87729.0	14.005
58	73856.0	82499.0	11.703	58	77883.0	88287.0	13.358	58	81593.0	93407.0	14.479
59	77969.0	87341.0	12.020	59	82187.0	93471.0	13.730	59	86233.0	98893.0	14.681
60	81932.0	92021.0	12.314	60	86420.0	98482.0	13.957	60	90577.0	104197.0	15.037
70	116421.0	131469.0	12.926	70	123298.0	140727.0	14.136	70	129977.0	148919.0	14.573
80	144055.0	161043.0	11.793	80	153285.0	172411.0	12.477	80	162330.0	182477.0	12.411
90	165539.0	184032.0	11.171	90	176432.0	197049.0	11.686	90	187094.0	208577.0	11.482
100	183301.0	202410.0	10.425	100	195702.0	216750.0	10.755	100	207907.0	229452.0	10.363
110	198092.0	217437.0	9.766	110	211331.0	232861.0	10.188	110	224661.0	246528.0	9.733
120	211008.0	229949.0	8.976	120	225042.0	246280.0	9.437	120	239112.0	260753.0	9.051
130	222459.0	240528.0	8.122	130	237197.0	257627.0	8.613	130	251969.0	272785.0	8.261
140	232461.0	249586.0	7.367	140	247745.0	267346.0	7.912	140	263055.0	283094.0	7.618
150	241368.0	257430.0	6.655	150	257164.0	275763.0	7.232	150	273014.0	292022.0	6.962
160	249507.0	264289.0	5.924	160	265905.0	283123.0	6.475	160	282229.0	299829.0	6.236
170	256701.0	270335.0	5.311	170	273669.0	289610.0	5.825	170	290501.0	306713.0	5.581
180	263152.0	275704.0	4.770	180	280612.0	295374.0	5.261	180	297894.0	312830.0	5.014
190	268602.5	280305.0	4.431	190	286401.0	300527.0	4.932	190	304104.0	318300.0	4.668
200	273347.0	284821.0	4.198	200	291373.5	305160.0	4.732	200	309289.5	323218.0	4.503
210	277386.0	288724.0	4.087	210	295646.5	309352.0	4.636	210	313773.5	327666.0	4.428
220	280749.5	292269.0	4.103	220	299187.5	313158.0	4.669	220	317566.5	331706.0	4.452
230	283435.5	295505.0	4.258	230	302099.3	316631.0	4.810	230	320624.3	335393.0	4.606
240	285613.3	298467.0	4.500	240	304475.8	319813.0	5.037	240	323183.8	338770.0	4.823

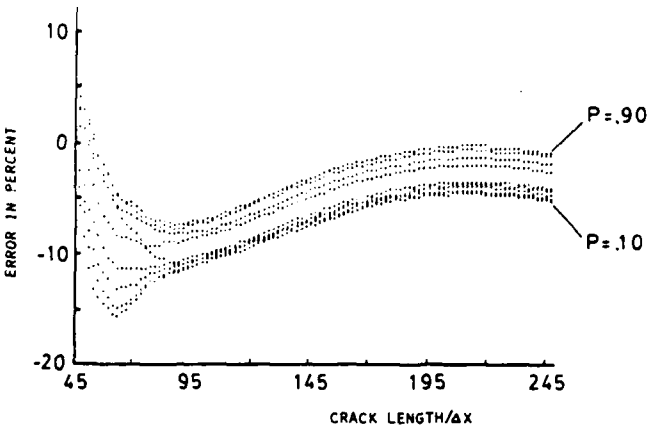

Fig. 12. Error in percent of the proposed model for C (in the Paris–Erdogan equation) = 3.79×10^{-10}.

Making use of these constants, eqns (16) and (20) were again utilized to generate a set of theoretical constant-probability crack growth curves as shown in Fig. 11. These curves were compared to those experimentally obtained in Fig. 5 and results of this comparison in the form of percentage of error of number of cycles corresponding to similar crack lengths are listed in Table 3 and summarized in Fig. 12. On the basis of these results the following observations can be made:

1 The present model succeeds in describing the evolution of the crack growth by estimating the number of cycles required for the crack to advance from one discrete position along the fracture surface to the following one. The evolution process was carried out for constant-probability crack growth curves. From these curves the scatter in the crack length at a specific fatigue as well as the scatter in the number of cycles required to advance the crack to a specific length, can be estimated. The results of the model, when applied to Al 2024-T3 that have been subjected to fatigue cycles with a constant stress amplitude, are in agreement with those experimentally obtained. Average error in the theoretical curves is estimated to be 5%, which is within the scatter limit of any experimental curve. The accuracy of the model, however, seems to depend on the degree of agreement between the crack growth curve obtained using a continuum theory and the experimental mean curve. To examine this effect in the present application, the value of the parameter C in the Paris–Erdogan Equation was changed from 3.79×10^{-10} to 3.51×10^{-10} so that the deviation of the theoretical mean curve from the experimental one is increased as shown in Fig. 10. As a result the average error in the prediction of the model, as illustrated in Fig. 13, is increased from 5% to 13%.

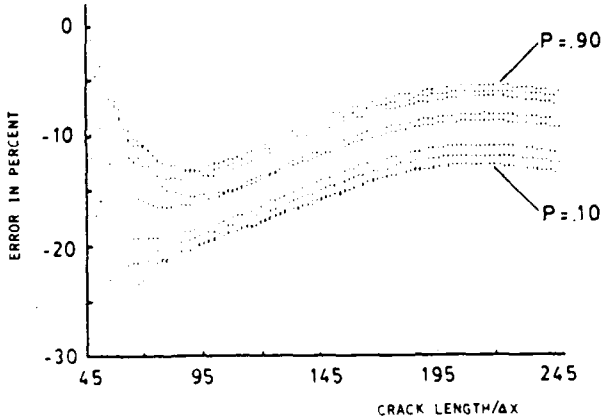

Fig. 13. Error (in percent) of the proposed model for C in the Paris–Erdogan equation) = 3.51×10^{-10}.

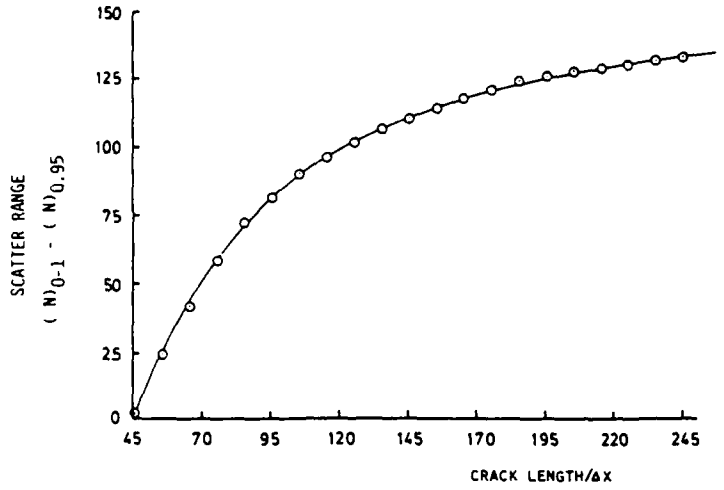

Fig. 14. Variation of scatter range as function of crack length position.

2. The degree of scatter in the number of cycles corresponding to a specified state is observed to decrease as the crack length increases. At higher crack lengths all the cracks require about the same number of cycles to advance from one discrete position to the following one. This may then lead to the conclusion that the degree of scatter in the number of cycles to failure depends on the large scatter observed in the early stages of crack propagation. This is illustrated in Fig. 14. The effect of scatter associated with "short" cracks on the variation in the number of cycles required for the crack to reach a critical length is currently under investigation by the authors.

3. The notion that there is a minimum number of cycles required for the crack to advance from one position on the fracture surface to the next immediate one has been theoretically derived in this model through the parameter I_0 in eqn (16). This concept of "incubation time" could be interpreted in relation to the time required for the crack tip propagation threshold (such as a specified mobile dislocation density, a thermodynamic activation level or any other criterion) to be satisfied. This concept warrants further study.

CONCLUDING REMARK

A model is presented here describing the crack propagation process as a discontinuous Markovian process. Based on this, the concept of constant-probability crack growth curves has been quantitatively derived. With the assumpotion that the crack growth curve given by any continuum crack growth model coincides with the experimental mean growth curve, the proposed model has demonstrated that it could sufficiently describe the evolution of the crack length and associated scatter at any stress level.

Acknowledgement—The authors wish to acknowledge support of this research program by the Air Force Office of Scientific Research through Contract No. AFOSR-84-0235TEF.

REFERENCES

[1] P. Paris and F. Erdogan, A critical analysis of crack propagation law, *J. Basic Engng Trans. ASME Ser. D* **85** (December 1963).
[2] D. W. Hoeppner and W. E. Krupp, Prediction of component life by application of fatigue crack growth knowledge *Engng Fracture Mech.* **6** (1974).
[3] T. R. Gurney, *Fatigue of Welded Structures*, Cambridge University Press (1979).
[4] D. F. Ostergaard and B. M. Hillberry, Characterization of the variability in fatigue crack propagation data *Probabilistic Fracture Mechanics and Fatigue Methods. Application for Structural Design and Maintenance* (Edited by J. M. Bloom and J. C. Ekvall), *ASTM STP* **798**, pp. 97–115. ASTM (1983).
[5] G. O. Johnston, Statistical scatter in fracture toughness and fatigue growth rate data, in *Probabilistic Fracture Mechanics and Fatigue Methods. Applications for Structural Design and Maintenance* (Edited by J. M. Bloom and J. C. Ekvall), *ASTM STP* **798**, pp. 42–66. ASTM (1983).

[6] L. N. McCartney and P. M. Cooper. A new method of analyzing fatigue crack propagation data. *Engng Fracture Mech.* **9**(2) (1977).
[7] R. G. Forman, V. E. Kearney and R. M. Engle. Numerical analysis of crack propagation in cyclic-loaded structures. *J. Basic Engng Ser. D* **89** (1967).
[8] H. Ghonem and J. M. Provan. Micromechanics theory of fatigue crack initiation and propagation. *Engng Fracture Mech.* **13**(4) (1980).
[9] F. Kozin and J. L. Bogdanoff. A critical analysis of some probabilistic models of fatigue crack growth. *Engng Fracture Mech.* **14** (1981).
[10] H. Ghonem. Stochastic fatigue crack initiation and propagation in polycrystalline solids. Ph.D. Thesis, McGill University (1978).
[11] A. T. Bharucha-Reid. *Elements of the Theory of Markov Processes and Its Applications*. McGraw–Hill, New York (1960).
[12] W. Weibull. A statistical theory of the strength of materials. *Ing. Vetenskaps Hkad. Handl.* (151) (1939).
[13] K. P. Oh. A weakest-link model for the prediction of fatigue crack growth rate. *ASME J. Engng Mater. Technol.* **100** (April 1978).
[14] A. Tsurui and A. Igarashi. A probabilistic approach to fatigue crack growth rate. *ASME J. Engng Mater. Technol.* **102** (July 1980).
[15] D. A. Virkler, B. M. Hillberry and P. K. Goel. The statistical nature of fatigue crack propagation. *ASME J. Engng Mater. Technol.* **101** (April 1979).
[16] J. N. Yang, R. C. Donath and G. C. Salivar. Statistical fatigue crack propagation of IN 100 at elevated temperatures. ASME Int. Conf. on Advances in Life Prediction Methods, Albany, NY (18–20 April 1983).

APPENDIX B

EXPERIMENTAL STUDY OF THE CONSTANT-PROBABILITY CRACK GROWTH CURVES UNDER CONSTANT AMPLITUDE LOADING

Engineering Fracture Mechanics Vol. 27, No. 1, pp. 1–25, 1987
Printed in Great Britain

0013–7944/87 $3.00 + 0.00
Pergamon Journals Ltd.

EXPERIMENTAL STUDY OF THE CONSTANT-PROBABILITY CRACK GROWTH CURVES UNDER CONSTANT AMPLITUDE LOADING

H. GHONEM AND S. DORE
Mechanics of Solids Laboratory, Department of Mechanical Engineering and Applied Mechanics, University of Rhode Island, Kingston, RI 02881, U.S.A.

Abstract — This paper is concerned with the application of a mathematical model that describes the fatigue crack growth evolution and associated scatter in polycrystalline solids. The model has been built on the basis that an analogy exists between a particular discontinuous Markovian stochastic process, namely the general pure birth process, and the crack propagation process. The, crack evolution and scatter were then defined in terms of material, stress and crack-length dependent properties and crack tip incubation time.

The application of the model is carried out by comparing the constant-probability crack growth curves generated for three different load levels with those obtained from testing sixty Al 7075-T6 specimens for each load level. A photographic method was utilized to measure the crack-length in this test program, by recording the residual deformation that accompanies the flanks of the crack during propagation.

INTRODUCTION

PREDICTION OF fatigue crack growth, even under constant amplitude loading, has not been an easy task. This is mainly because the manner in which the various parameters, such as loads, material properties and crack geometries, affect the crack propagation is not clearly understood[1]. This, consequently, had led to a proliferation of hypotheses and laws for describing fatigue crack propagation (see review articles in refs [1, 2 and 3]). Most of these models are based on concepts of the continuum theory with the assumption that cracks propagate in an ideal continuum media. Actual metallic materials, however, are composed of random microstructure described by various microparameters which can seriously affect the growth of a crack in these materials. As a result, the deterministic theories can only be accepted as an approximation of the actual random fatigue crack propagation process.

The use of statistical distributions or probabilistic models thus becomes necessary to make predictions of crack growth more reliable. The search for the "true" statistical distribution has been a difficult task since in any application, the amount of crack-growth data which has been collected for any particular case would not be sufficient to discriminate between the different types of distributions[4]. In addition, when a series of tests on identical specimens is performed to establish the scatter due to material properties, the uncertainties in load values and crack-length measurements are also included in the scatter data. Due to this limitation, it is difficult to isolate the scatter associated with material properties in any experiment. One is also hampered by the lack of an exact physical description of the fatigue process[5]. When taking these two factors into consideration, any probabilistic or statistical model can identify the variability of crack-length only in a comparative sense. This means that the absolute values of the variability at a specific load level predicted by a model may not be equal to those obtained experimentally. However, it is possible for a ratio of variabilities predicted for two different load conditions to be equal to that of the experimental results obtained at the same loading conditions. In this, the experimental errors being independent of the magnitude of the applied loads, are eliminated.

There are basically two kinds of mathematical models in existence to predict the variability in fatigue crack growth. The first employs a statistical approach in which random variables are introduced instead of the constants in the appropriate deterministic crack growth equation. While these models (see, for example refs [6–11]) are simple to use and versatile in application, they possess some disadvantages. First, all of them are based on Paris law[12] where it has been shown that other laws like the Forman's law[13] are more applicable. Secondly, the scatter parameters in these models have no physical description and no attempts have been made to link these parameters to the micro-structural properties. Lastly, though these models generate crack-growth

data that match the experimental data reasonably well in some cases, they do not provide any insight into the nature of the fatigue crack propagation process.

The second approach employs evolutionary methods in which the propagation of the crack is treated in a probabilistic or stochastic sense instead of a statistical one. Making use of a specific probability process, namely the Markovian process, the models with this approach strive to correlate the properties of this process with those of fatigue crack propagation.

Examples of this approach are the models by Ghonem *et al.*[14, 15], Kozin and Bogdanoff[16] and Aoki and Sakata[17]. The major disadvantage in using these models is the lack of crack-growth scatter data for different conditions which would have been helpful to check the validity of the probabilistic assumptions on which these models were built.

The objective of this paper is to examine the results of the stochastic model developed by Ghonem and Dore[15] when utilized for the prediction of the crack growth evolution, in the same material, at different loading conditions. Before proceeding on this application, a brief review of the fundamentals of the model is presented in the next section. This will be followed by the description of the experimental study and detailed analysis of the results.

REVIEW OF THE PROPOSED MODEL

In this model, the fracture surface is divided into a finite number of crack "states" of equal width; a probability space of two events was defined with the condition that the crack is in state "r" after i cycles have elapsed from the instant of reaching "r". They are, the event that the crack will remain in the state "r" and the event that the crack will not be in "r". Assuming that the crack propagation process is irreversible and utilizing the fact that under conditions of constant amplitude loading the existence of a crack at a particular state depends only on its present mechanical and microstructural details, a definition for the transition probability was arrived at. Using the criteria attached to the discontinuous Markovian process[18], a transition intensity (λ_r) could be defined. In this approach, λ is assumed to be a material parameter which in addition to being a function of the crack position "r", should explicitly depend on both the initial elapsed cycles i and the incremental duration Δi. The propagation process thus becomes time-inhomogeneous. This characteristic is a departure from the works of Ghonem and Provan[14] and Kozin and Bogdanoff[16].

The probability equation was then derived and can be written as:

$$\begin{aligned} \ln P_r(i) &= B(e^{KI_0} - e^{Ki}) \quad ; \quad i \geq I_0 \\ &= 0 \qquad\qquad\quad ; \quad i < I_0 \end{aligned} \tag{1}$$

where i is the number of cycles, B and K are crack-length and stress dependent variables, $P_r(i)$ is the probability of the crack being at a state "r" on the fracture surface after i cycles elapse and I_0 is the minimum number of cycles required for the crack to advance from one position on the fracture surface to the next and is also crack-length and stress dependent.

This derivation was made by defining the transition intensity λ_r and the Incubation time I_0 in the following form.

$$\lambda_r = \frac{B}{K} e^{Ki} \tag{2}$$

$$I_0 = C_3[(r-1)^{n_3} - r^{n_3}] \tag{3}$$

where (4)

$$B = C_1 r^{n_1} \tag{5}$$

$$K = C_2 r^{n_2}$$

and C_1, C_2, C_3, n_1, n_2 and n_3 are material, applied stress and environment dependent parameters. These functions (eqs 2 and 3) were verified with the available crack growth scatter data based on the works of Virkler *et al.*[19] and Yang *et al.*[6].

As can be seen, identification of the six constants is sufficient to define eq. (1) at any crack position so as to calculate the associated number of cycles elapsed for any probability ($P_r(i)$) value. Carrying out this operation for a given probability value at all the crack states in a cumulative manner, will generate a crack-position versus number-of-cycles curve representing the probability with which a crack spends a certain number of cycles at any state.

Here, one should observe that the constants in these mathematical functions can be calculated by considering the crack growth curve obtained by using a continuum equation as being the $P_r(i) = 0.5$ curve. This can be done numerically, and the crack growth scatter at any crack length and at any fatigue load can be defined without the need to perform large number of fatigue tests. As mentioned before, the results of the model, when applied to Al 2024-T3 that was subjected to load cycles of constant amplitude, were in agreement with those experimentally obtained with the average error in the theoretical curves estimated to be 5%.

In order for the model to have a wider scope of application, it has to be substantiated for different loading conditions and for different materials. The first step in that direction is the verification of the model for different loading conditions on the same polycrystalline material. The experimental set-up and procedure used for this purpose are described in the next section.

DESCRIPTION OF THE EXPERIMENTAL SET-UP

Tests were conducted on Aluminium 7075–T6 alloy and crack-length versus number of cycles data were collected at three different stress levels. Each level was tested by using 60 identical specimens to establish the degree of crack-length scatter during propagation.

A rectangular specimen (320 mm × 101 mm) with a thickness of 3.175 mm and a center-cracked tension geometry was used throughout the test program. The direction of the center-crack chosen was perpendicular to the rolling direction of the sheet from which the specimens were cut as shown in Fig. 1. The dimensions of the specimen and the crack initiating notch are based on the ASTM E647 recommendations and are shown in Figs 2 and 3 respectively. The specimen ends were fixed to the test system by flat end grips whose dimensions are also based on the ASTM E647 recommendations.

A study was carried out to compare the available crack-length measuring techniques namely,

(a) The Photographic Technique,
(b) The Drop Potential Method,
(c) The Mechanical Method,
(d) The Electrical Technique,
(e) The Acoustic Method,
(f) The Ultrasonic Method and
(g) The Visual Method.

The results of this study, based on refs [20, 21 and 22] are detailed in ref. [23]. The conclusion was that the method of photographing the crack during propagation was the one most suited for the present program, since it is capable of tracing the growth of one point along the crack-front as opposed to a technique that measures the average position of the crack front.

The photographic technique used in this study depends on the reproduction of a sharp image of the deformed material along the flanks of the crack to make it possible to locate the crack-tip image and, consequently, to determine the crack-length with an acceptable degree of resolution. Since it is certain that in ductile materials, a sizable plastically deformed zone accompanies the crack during its propagation, especially in plane stress applications (see Fig. 4), this zone can be utilized as an accurate crack-length indicator. An example of this deformed zone is shown in Fig. 5. It can be seen that the interface between the two fracture surfaces (the crack) is not present along with this image. As the crack increases in length, leading to a higher crack opening displacement, the separation of the fracture surfaces becomes visible as a dark line within the deformed zone. This is shown in Fig. 6.

The testing configuration included a camera and a continuous light source positioned on one side of the specimen. The camera was triggered by an electrical pulse sent by a microcomputer that kept track of the elapsed number of cycles. Also, a number of shutter speeds, aperture settings, developing solutions, processing times and film types were experimented with to achieve the best

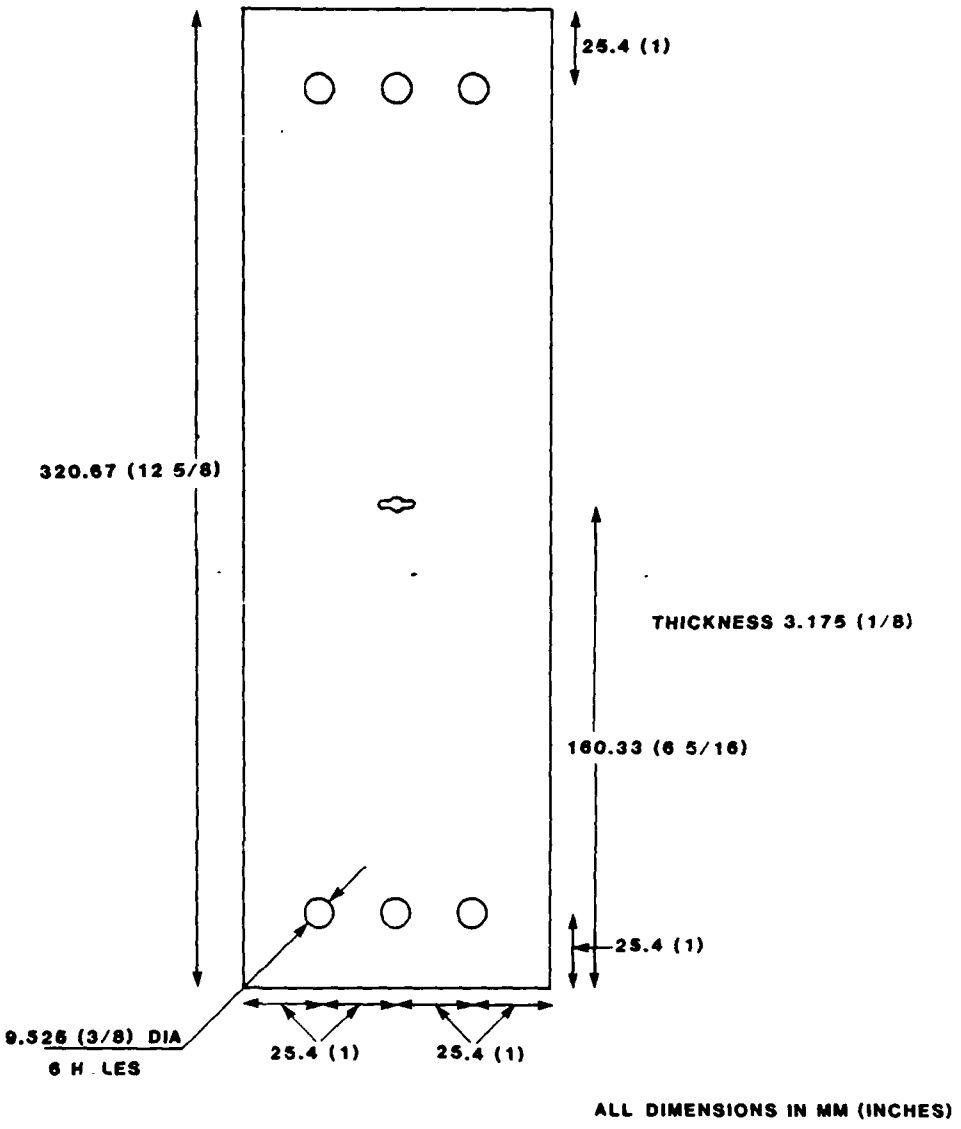

Fig. 2. Test specimen in the present study.

reproduction of this shear zone; these parameters are fully described in ref. [23].

A transmitted-light microscope equipped with a horizontal travelling table was used to determine the length of the image of the plastically deformed zone. The measurements were made by a digital micrometer having a resolution of 1 μm and transferred, after suitable interfacing, to a microcomputer for acquisition and subsequent analysis (see Fig. 7).

The error in these measurements was determined by comparing an actual crack-length, measured directly on the specimen's surface, and the length of its corresponding shear zone. This comparison, which was made in the cases of 1 × and 2 × magnifications (see in Table 1) indicated that the errors associated with the 2 × magnification, which was adopted throughout the test program, were lower. The region of interest used for recording the shear zone was limited to the central 28 mm on the 36 mm frame. Using a 2 × magnification, this meant that a maximum of 14 mm of crack growth was photographed in any test.

All the 180 tests carried out in this study were performed on a closed loop, servo-hydraulic Material Test System (MTS 880) capable of controlling loads within 0.2%.

Based on ASTM E647 recommendations, the initial crack-length, a_0 was chosen to be 10.00 mm; however, the crack-lengths were recorded from a length of 9.00 mm onwards. The final crack-length (a_f) for the purposes of this test program was limited to 23 mm measured from the center line of the test specimen. The loading parameters were then selected so that the crack transition from the normal mode to the shear mode could not occur before the crack reached this

specified length, i.e. 23 mm. This condition was imposed on the loading parameters in order to avoid the problem of defining the crack-length in the shear mode.

Tests were executed at three different stress ratios R; $R = P_{min}/P_{max}$, where P_{min} is the minimum load level and P_{max} is the maximum load level. The loading sequence for fatigue pre-cracking and the three test load conditions are detailed in Tables 2 and 3, respectively. A frequency of 10 Hz and a ramp waveform were selected for the loading cycle.

Figure 8 is an example of the results obtained in this test program showing the progress of the crack length at different loading cycles for one of the loading conditions.

EXPERIMENTAL RESULTS

As mentioned in the previous section sixty specimens were tested for three stress levels and crack-length (a) versus number-of-cycles (N); data was recorded from a length of 9 mm to a length of 23 mm. It may be recalled that the initial crack-length chosen for this test program was 10 mm and not 9 mm. Data between 9 mm and 10 mm will be used for future work on short crack. behaviour and the comparison between the theoretical probability crack-length versus number of cycles data. The experimental data will be made from the initial crack-length of 10 mm onwards. Crack-growth data (a vs N) for the three stress conditions is shown in Figs 9–11.

The next step in the analysis is the selection of the width-of-crack state for producing experimental data suitable for comparison with that generated by the mathematical model [15]. As can be seen from Table 1, the maximum error between the shear zone recorded on film and the crack-length measured from the specimen was estimated to be 0.163 mm. Using a conservative approach, the maximum error was assumed to be 0.2 mm and this was considered to be the state width.

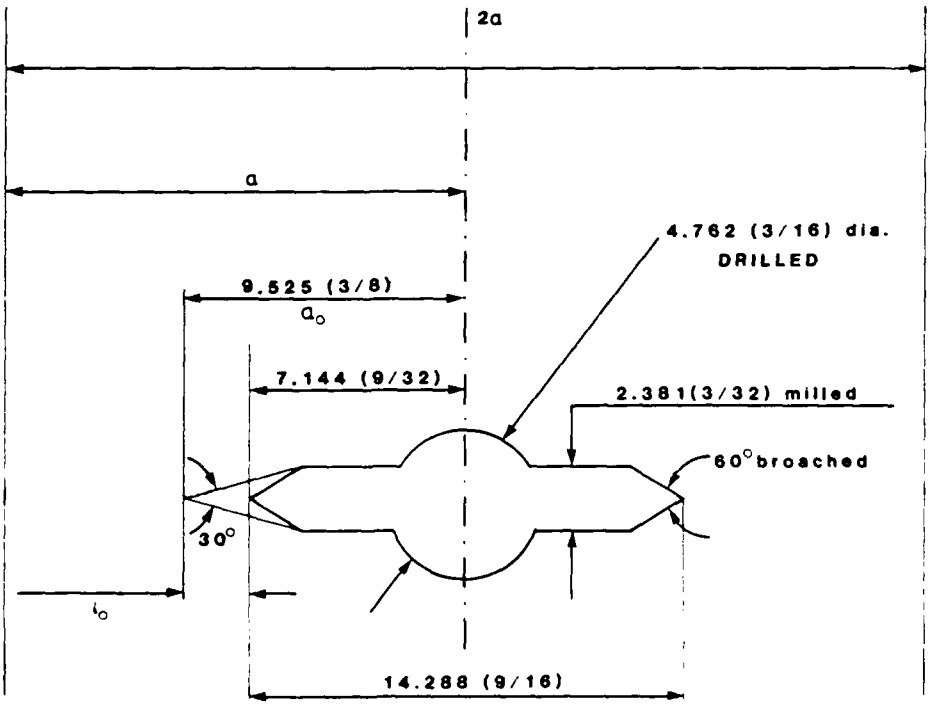

Fig. 3. Crack initiating notch

Table 1. Comparison of the actual crack-length with the length measured from the film (all dimensions in mm)

Measured value (M)	Magnification (m)	Corrected (C) ($C = M/m$)	Actual (A)	Error ($A-C$)
4.882	1.058	4.612	4.831	0.218
8.047	1.045	7.700	7.755	0.055
11.624	1.045	11.123	11.206	0.083
18.855	1.045	18.043	18.082	0.039
8.208	2.000	4.104	4.202	0.098
17.028	2.000	8.514	8.677	0.163
15.950	2.000	7.975	8.042	0.067
17.692	2.000	8.846	8.924	0.078
19.841	2.000	9.920	9.956	0.035
23.023	2.000	11.501	11.592	0.090
26.161	2.000	13.080	13.153	0.072
29.803	2.000	14.901	15.018	0.116
31.623	2.000	15.811	15.892	0.081

Table 2. Loading sequence for fatigue pre-cracking (all loads in kN)

Test Condition	Load level till crack was generated (20 Hz) P_{max}	P_{min}	ΔP	Load level till crack reached 7.5mm (20 Hz) P_{max}	P_{min}	ΔP
I	25.95	8.30	17.65	26.55	13.55	13.00
II	29.30	7.70	21.60	24.80	10.65	14.15
III	26.30	7.70	18.60	21.50	7.30	14.20

Table 3. Test load conditions (all loads in kN)

Test Condition	Test load level (10 Hz) P_{max}	P_{min}	ΔP	R
I	22.79	13.68	9.11	0.6
II	22.25	11.13	11.12	0.5
III	15.19	6.08	9.11	0.4

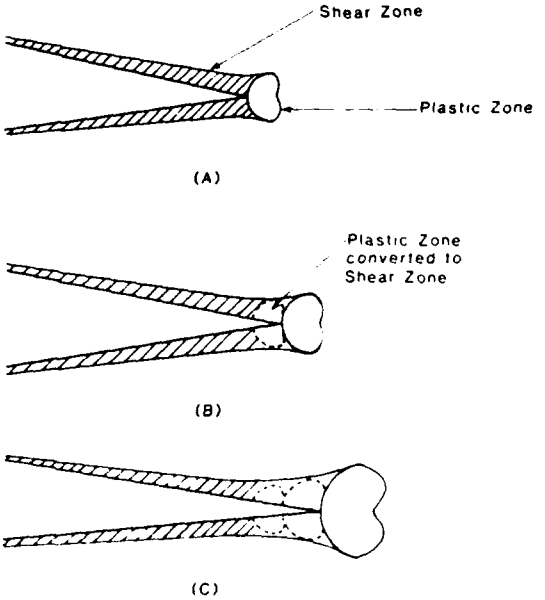

Fig. 4. Zone of plastic deformation in the vicinity of the fatigue crack[31]

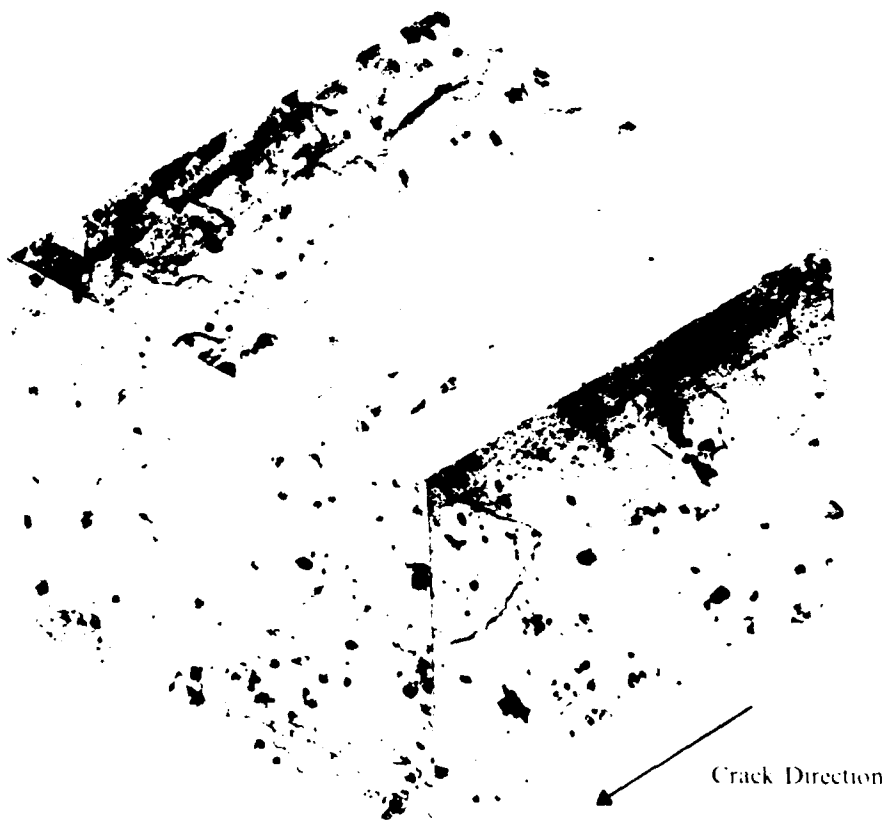

Fig. 1. Direction of crack with respect to the grain structure

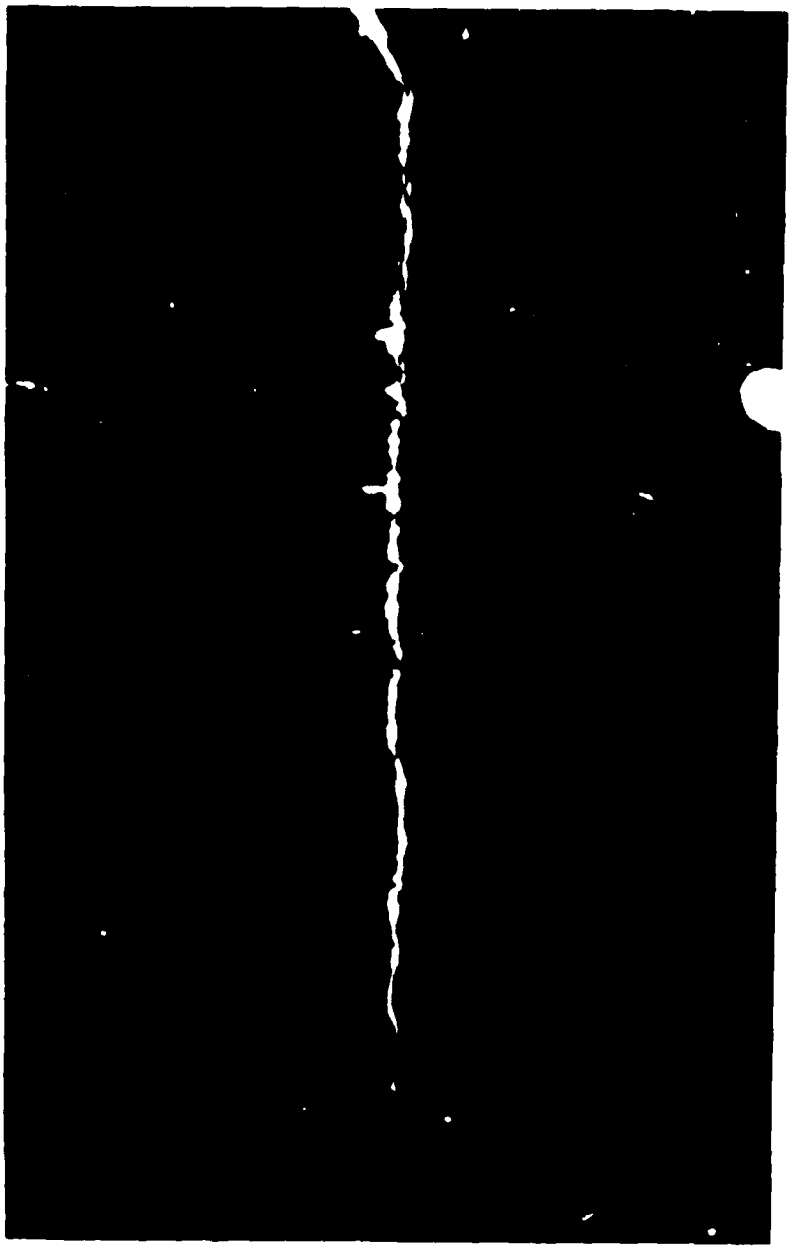

Fig. 8. Photograph of the shear zone accompanying the crack.

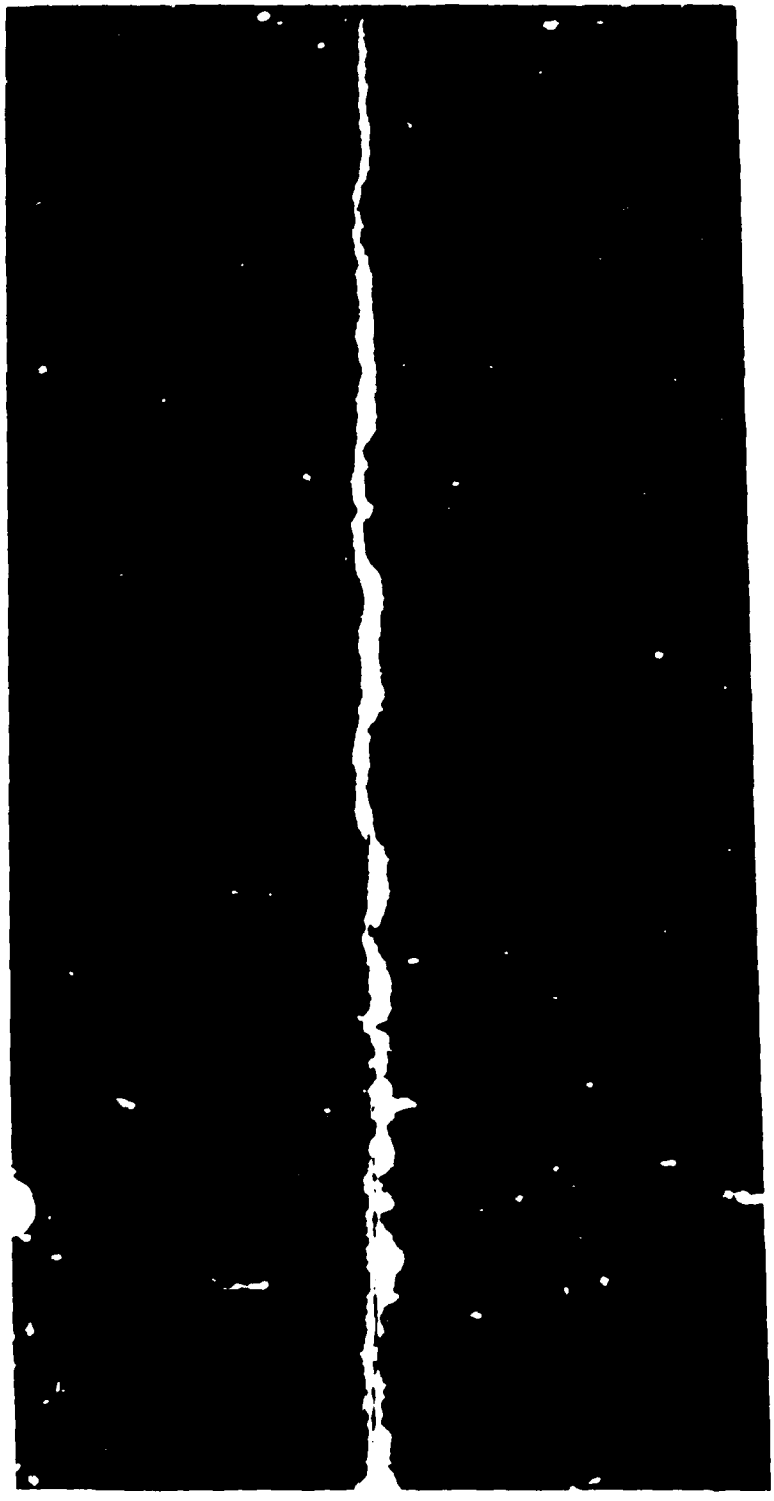

Fig. 6. Photograph of the shear zone with a visible separation of the crack surfaces

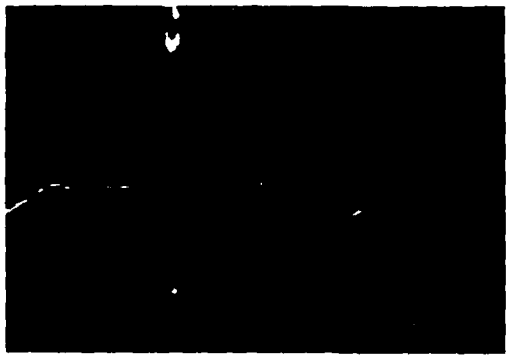

1. Crack length = 9.495 mm
Number of cycles = 6380

2. Crack length = 10.498 mm
Number of cycles = 15510

3. Crack length = 10.912 mm
Number of cycles = 18960

4. Crack length = 12.031 mm
Number of cycles = 25360

5. Crack length = 12.630 mm
Number of cycles = 28210

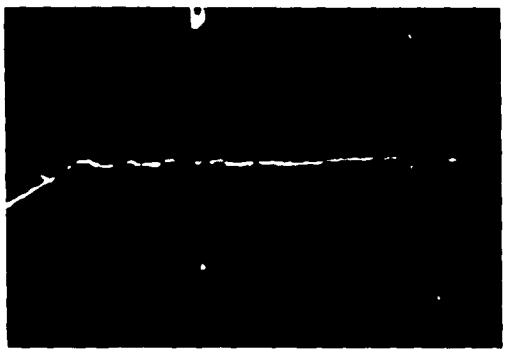

6. Crack length = 13.000 mm
Number of cycles = 29800

Fig. 8. Crack evolution as recorded from specimen number 1 subjected to Test Condition-II (Magnification 10X).

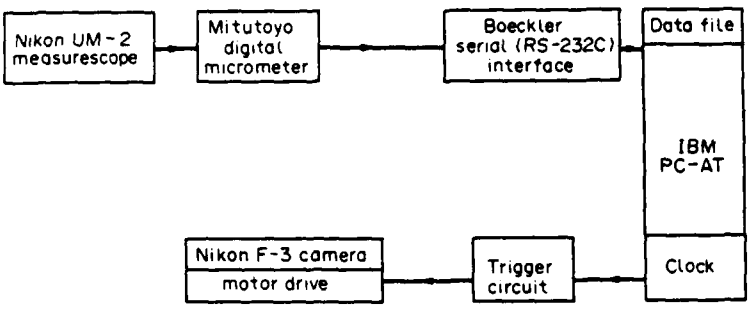

Fig. 7. Schematic of the camera-triggering and the crack-length measuring circuits.

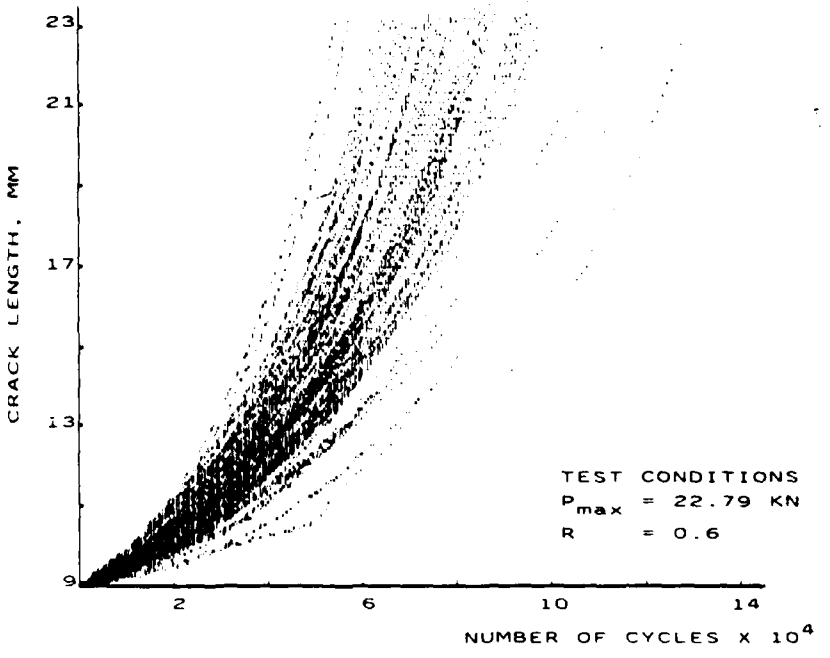

Fig. 9. Crack-length vs number of cycles data from 60 specimens for Test Condition I.

For a state width of 0.2 mm, the zone between 10 and 10.2 mm corresponded to an initial crack state (r_0) of 51 and the zone between 22.8 and 23 mm to a final crack state (r_f) of 115, leading to a total of 65 crack states. Similar to the approach discussed in ref. [15], the number of cycles spent by a crack in each of these 65 states was calculated by interpolation of the a vs N data. Thereupon, for all the stress levels, the interpolated values for each state in each of the sixty specimens was arranged in an ascending order. The lowest number of cycles was assigned a probability of:

$$P_r(i) = 1 - (x/60) \quad ; \quad x = 1$$

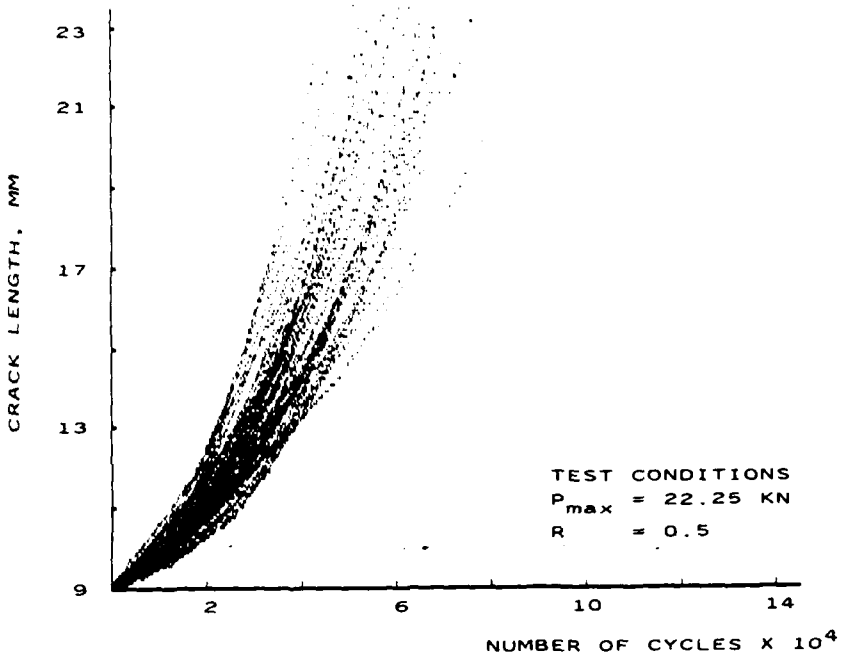

Fig. 10. Crack-length vs number of cycles data from 60 specimens for Test Condition II.

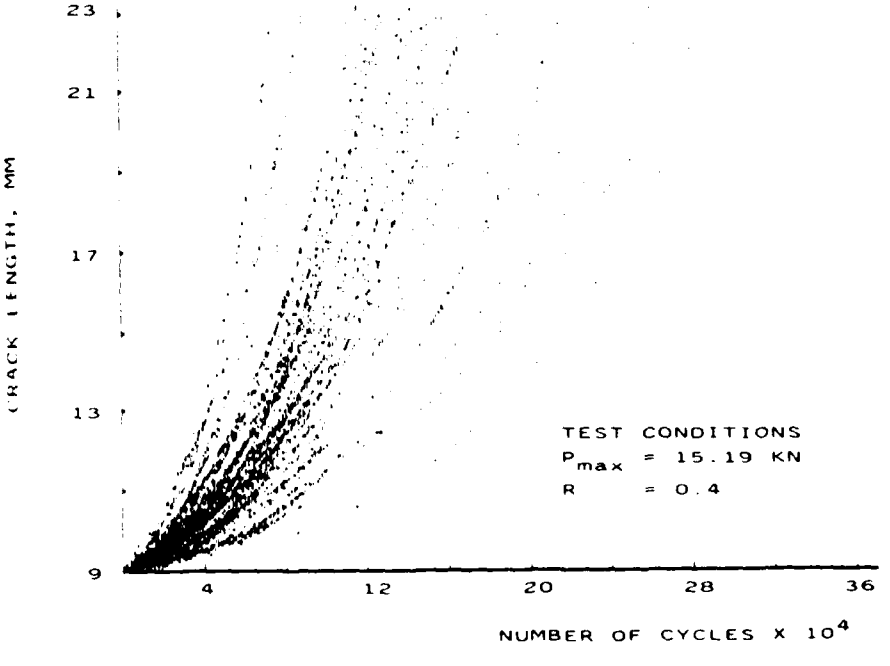

Fig. 11. Crack-length vs number of cycles data from 60 specimens for Test Condition III

and so on up until the highest number of cycles whose corresponding probability value was:

$$P_r(i) = 1 - (x/60) \quad ; \quad x = 60.$$

A probability range of 0.9–0.1 was selected for comparison of the experimental and the theoretical data. The curves obtained experimentally are plotted in Figs 12–14 with the probability values having decrements of 0.1.

In these figures it is observed that the widest scatter band is associated with the test condition that produced the smallest mean crack-growth rate, Test Condition III, while the narrowest scatter band is associated with the Test Condition II in which the mean crack growth rate is the highest. This is due to the fact that when loads are high, the influence of the microstructure on crack propagation is diminished so that the degree of scatter of the a vs N sample curves, in relation to the mean growth curve, tends to be limited. Similar observations were made by Yang *et al.*[7] and this is perceptible in Fig. 15.

THEORETICAL RESULTS

Firstly, the continuum growth law to be utilized in the mathematical model was arrived at by investigating a number of crack growth equations with known material constants which recognize the effect of the stress ratio. Forman's equations[13,24] and the equation derived by Hardath *et al.*[25] fall into this category.

Forman's equation is generally written as:

$$\frac{da}{dN} = \frac{C(\Delta K)^n}{(1 - R)K_c - \Delta K} \tag{6}$$

where a is the crack-length, N is the number of cycles, K is the stress intensity factor range, K_c is the critical stress intensity factor, R is the stress ratio and C and n are material constants.

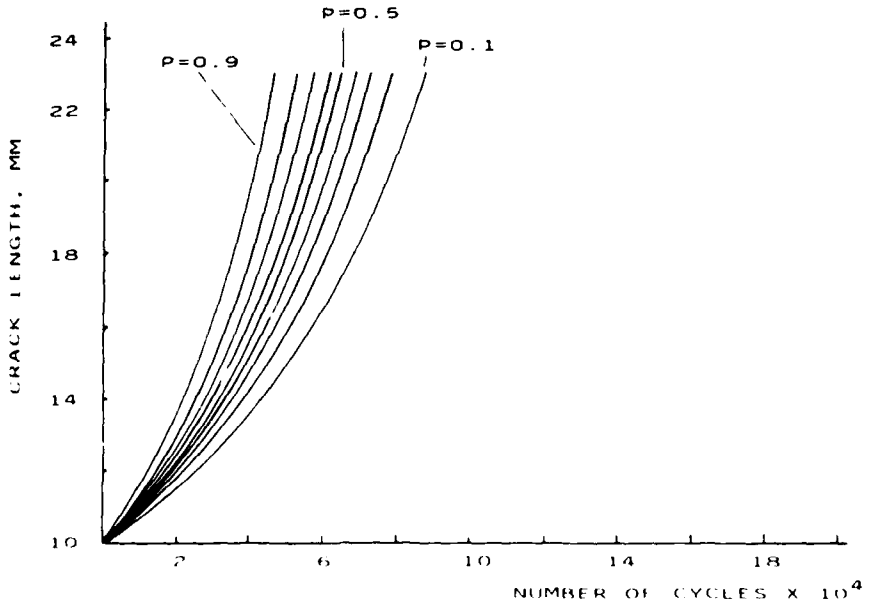

Fig. 12. Experimental constant-probability crack growth curves generated for Test Condition I.

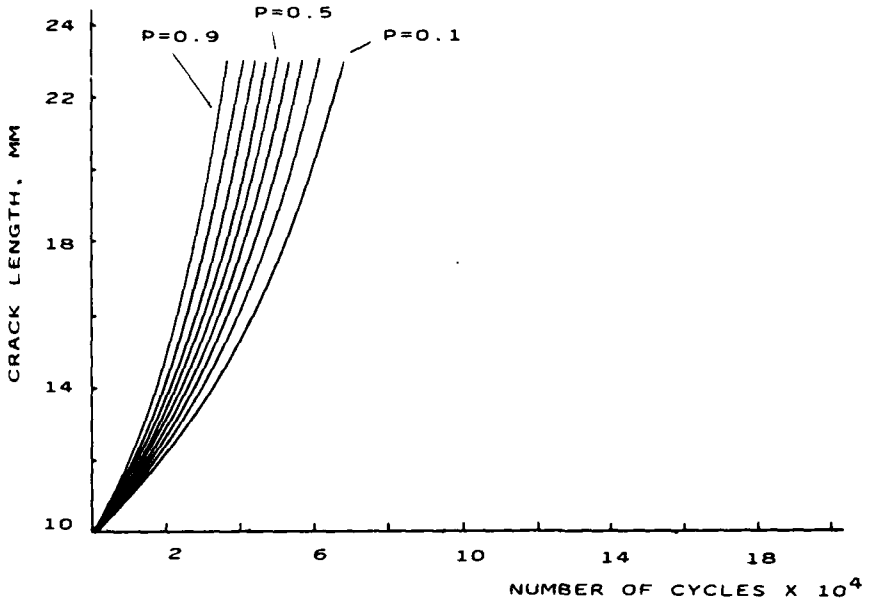

Fig. 13. Experimental constant-probability crack growth curves generated for Test Condition II.

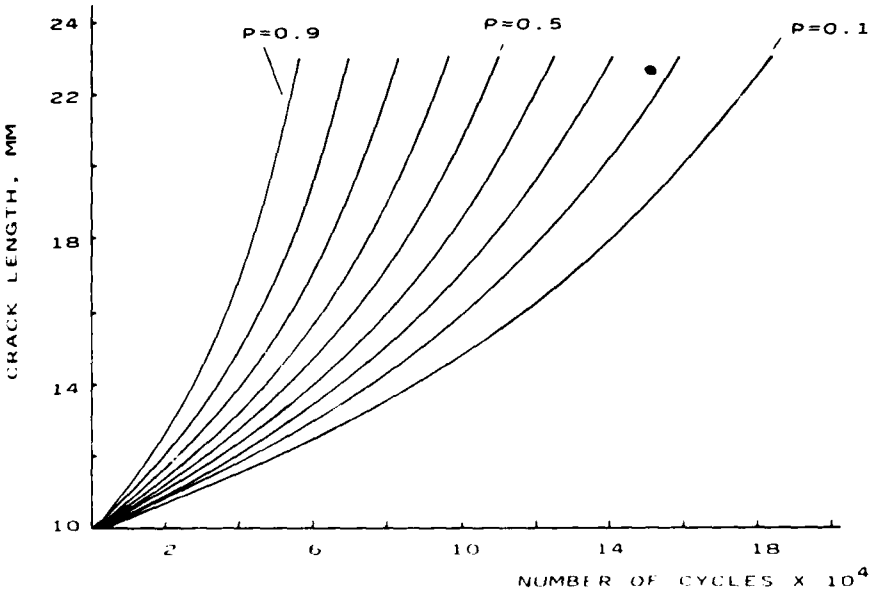

Fig. 14. Experimental constant-probability crack growth curves generated for Test Condition III

The values of K_c, C and n for Aluminium 7075–T6 are listed in ref.[13] as:

$$K_C = 68 \text{ Ksi-in}^{\frac{1}{2}} (74 \text{ M Pa-}m^{\frac{1}{2}}$$

$$C = 5 \times 10^{-13} \text{ U.S. Customary Units}$$

$$= 1.63 \times 10^{-17} \text{ SI Units}$$

$$n = 3$$

and in ref.[24] as:

$$K_C = 40 \text{ Ksi-in}^{\frac{1}{2}} (44 \text{ MPa-}m^{\frac{1}{2}})$$

$$C = 2.13 \times 10^{-13} \text{ U.S. Customary Units}$$

$$= 1.60 \times 10^{-18} \text{ SI Units}$$

$$n = 3.21.$$

The equation derived by Hardarth *et al.*[25] is:

$$\frac{da}{dN} = C(\Delta \bar{K})^n \tag{7}$$

where
$$\bar{K} = \frac{K_{\text{eff}}}{\left(1 - \frac{K_{\max}}{K_f}\right)^2} \tag{8}$$

and
$$K_{\text{eff}} = (s_{\max} - s_0)\sqrt{\pi a}\, F \tag{9}$$

s_{max} is the maximum stress, s_0 is the crack opening stress, $\sqrt{\pi a}$ F is the stress intensity parameter for specimen configuration, K_{max} is the maximum stress intensity factor, K_F is the fracture parameter [81 Ksi-in$^{\frac{1}{2}}$ (89 M Pa-$m^{\frac{1}{2}}$)], C and n are material parameters.

$$C = 3.83 \times 10^{-8} \text{ SI Units}$$

$$n = 3.17.$$

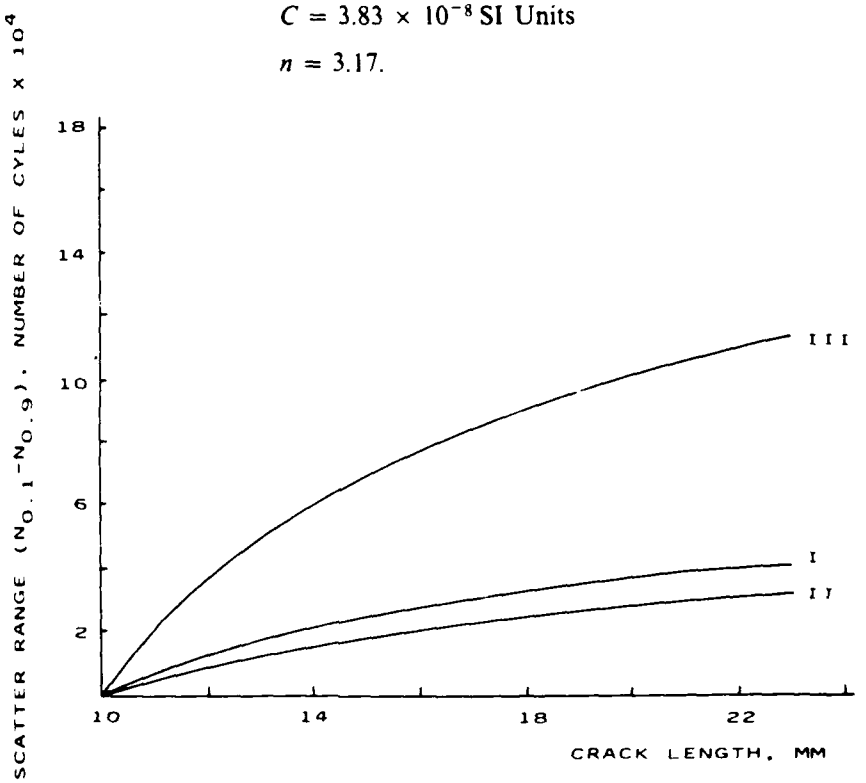

Fig. 15 Variation of the scatter range with crack length for the three Test Conditions.

Of the above two laws, the one provided by Forman *et al.*[13] was selected because it is based on data obtained from different laboratories as opposed to the equation of Hudson *et al.*[24] that was derived after correlation with one set of experimental data. The growth law of Hardarth *et al.*[25] was also not utilized because the present mean experimental growth rate was different from that predicted by the law, by an order of magnitude for all the three stress levels.

Having defined the continuum growth law and the corresponding material constants, the six constants C_1, C_2, C_3, n_1, n_2, n_3 were next calculated by obtaining their converged values using Newton–Raphson's method.

The six constants for each load condition are:

	I	II	III
C_1	0.015127	0.010064	0.010105
C_2	1.9371×10^{-6}	3.4055×10^{-6}	1.9758×10^{-6}
C_3	1.5940×10^{6}	1.0888×10^{6}	2.3151×10^{6}
n_1	0.8000	0.7957	0.8514
n_2	1.4946	1.4991	1.3501
n_3	−0.7000	−0.6820	−0.8537

Following the analysis presented in ref. [15] the theoretical probability curves were plotted making use of these constants, in Figs 16–18.

The percentage error of the number of cycles is plotted in Figs 19–21. The average value off the absolute errors was found to be 7%, 5% and 8% for the ', II and the III load conditions, respectively.

A remark is warranted on the six constants that characterize the crack growth scatter. Though these constants depend on the load parameters, no attempt has been made to derive an explicit relationship. In fact, there is no need for an explicit relationship since they are computed directly from the continuum growth law.

CONCLUSIONS

(1) The mathematical model developed here provides a physical description for fatigue crack propagation as well as capability of predicting crack growth scatter at different stress levels. While the model uses the crack growth data from a continuum law as its input, it does not depend on a specific law. The only requirement is that such a law must be a correct representation of the mean growth curve. The model has been validated for two aluminium alloys Al 2024–T3 and Al 7075–T6 subjected to four different stress levels and is in the process of being applied to steel and titanium alloys.

(2) The scatter data recorded for the second load condition ($\Delta P = 11.12$ kN, $P_{max} = 22.25$ kN) of the experimental program has been observed to be the least widespread when compared with that obtained from other load conditions with lower values of ΔP. This can be attributed to the following phenomenon. The crack transition from a specific state is governed by a critical threshold energy at the crack tip. When such a threshold is satisfied in one cycle or an accumulation of several cycles, depending on the load condition and crack-geometry, the crack tip can then advance from its present state to the following one. Hence for larger loads and longer crack-lengths, the probability that this propagation threshold is satisfied increases rapidly with the number of elapsed load cycles while, for smaller loads and shorter crack-lengths, the probability of discrete crack growth advancement increases gradually. In this hypothesis the degree of scatter in achieving the required threshold energy reflects on the degree of scatter of crack growth. Fractographic analysis of fracture surfaces shows that, at the same crack-length, more striations per unit distance are present along the fracture surface of specimens subjected to a large load level (Test Condition II, see Fig. 22b) than in the specimens subjected to a lower load level (the Test Conditions I and III, see Figs 22a and 22c). It is known that ductile fracture striations are formed due to a change in the orientation

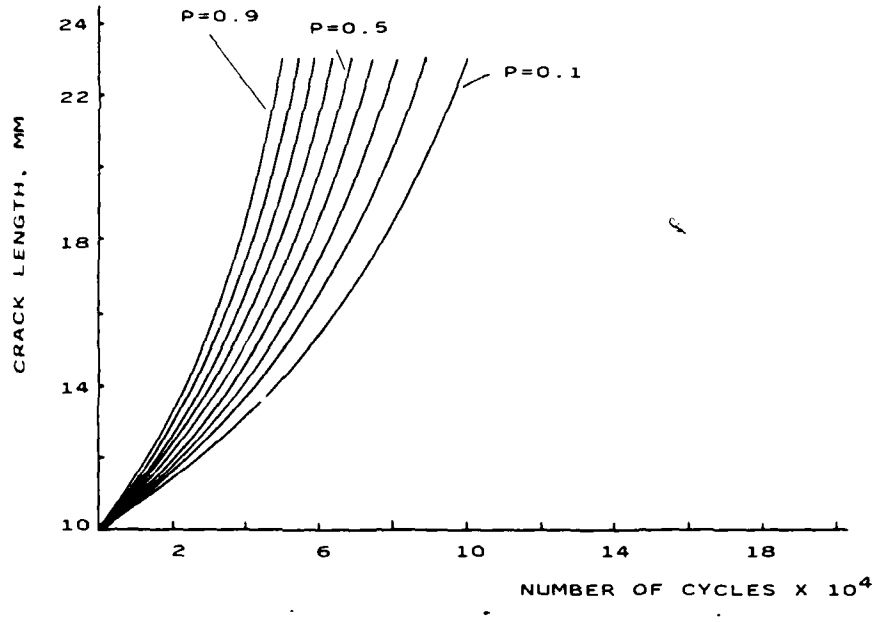

Fig. 16. Theoretical constant-probability crack growth curves generated for Test Condition I.

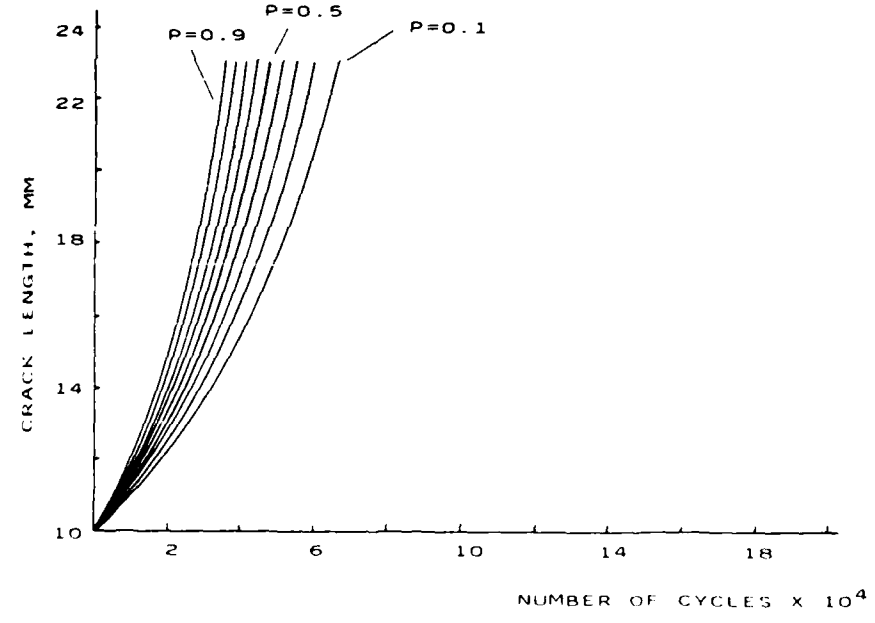

Fig. 17. Theoretical constant-probability crack growth curves generated for Test Condition II

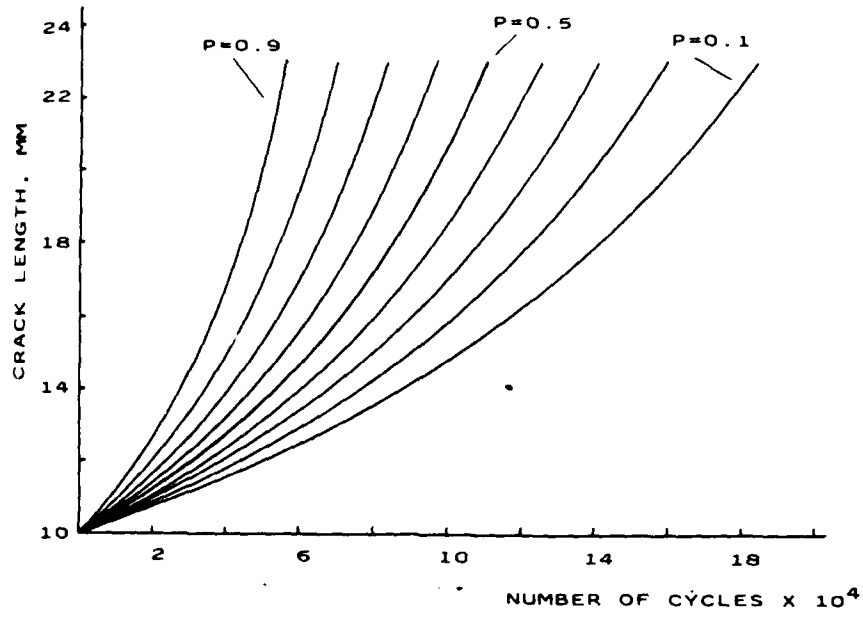

Fig. 18. Theoretical constant-probability crack growth curves generated for Test Condition III.

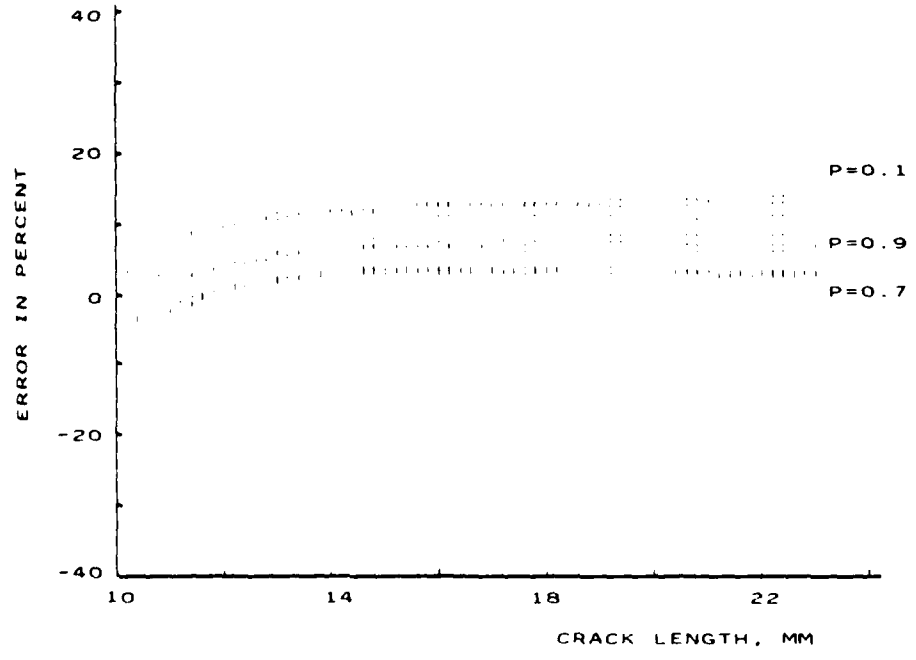

Fig. 19. Error in percent of the proposed model in the constant probability crack growth curves for Test Condition I

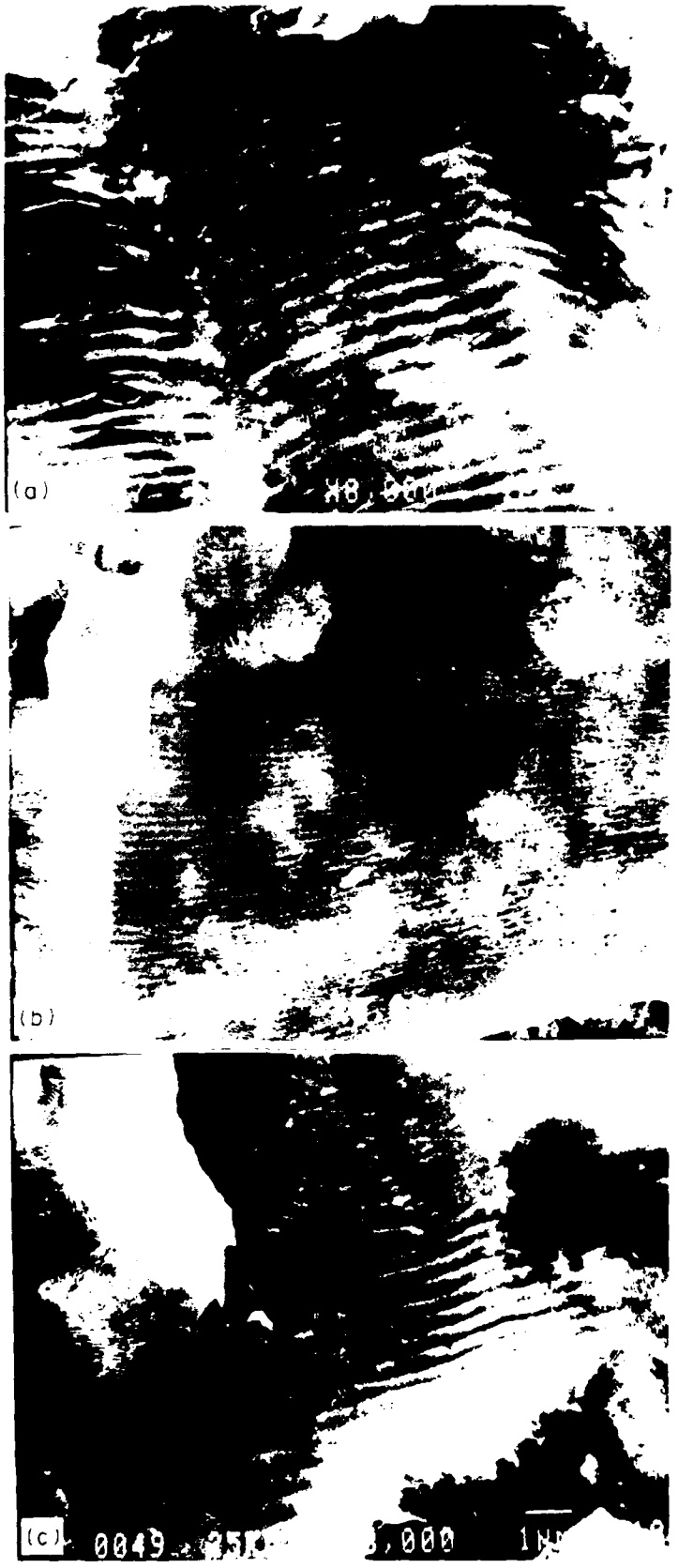

Fig. 22. (a) – (c)

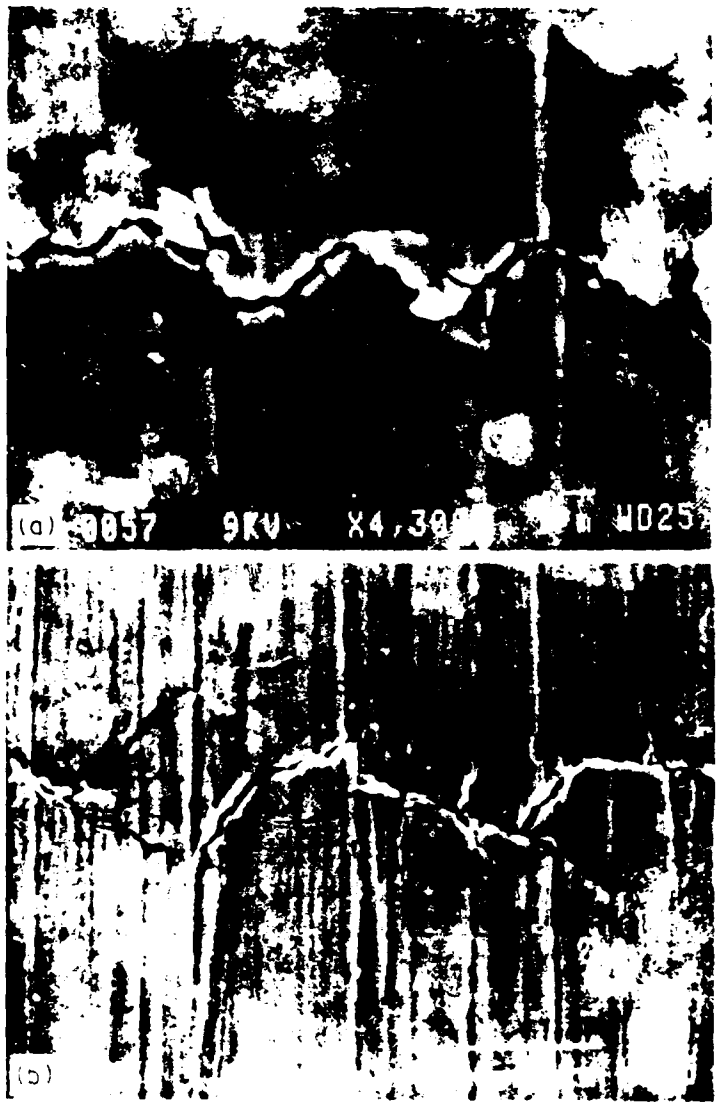

Fig. 23. (a) + (b)

Fig. 24. (a) — (b)

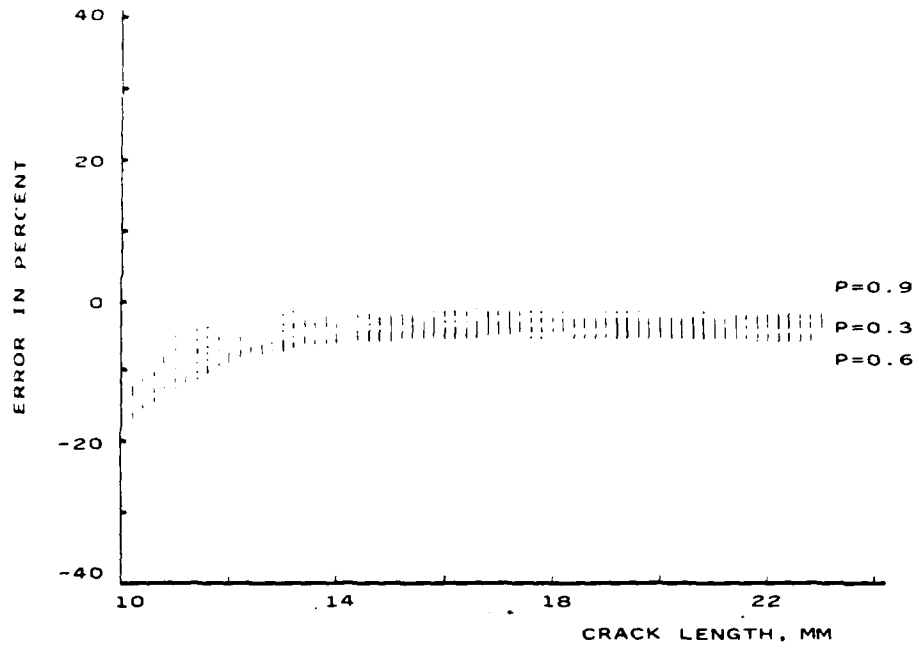

Fig. 20. Error in percent of the proposed model in the constant probability crack growth curves for Test Condition II.

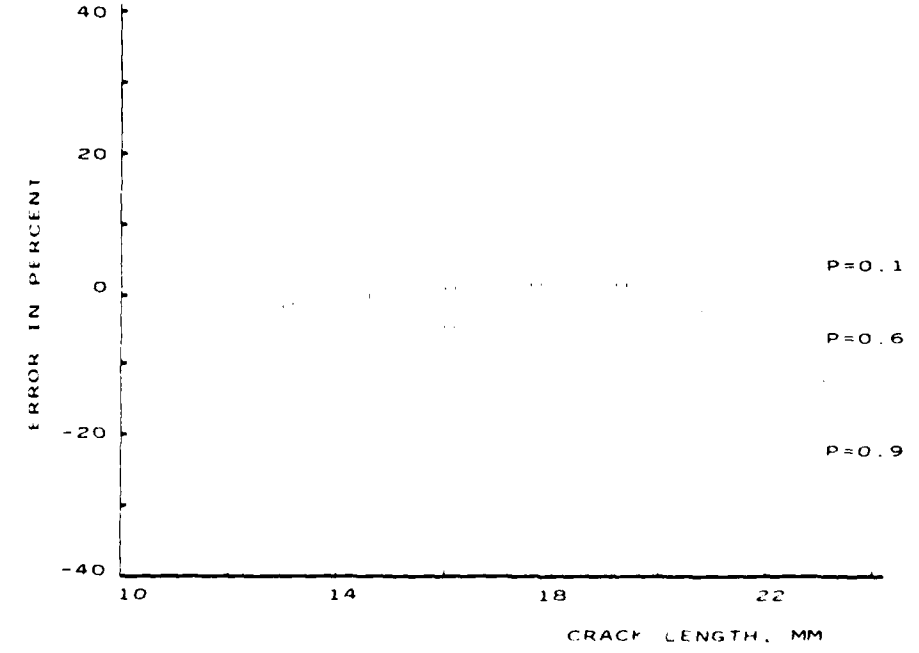

Fig. 21. Error in percent of the proposed model in the constant probability crack growth curves for Test Condition III

of the fracture surface along a specific slip plane[26, 27]. Therefore, a denser striation pattern is observed at loading conditions associated with higher growth rates because numerous orientation changes take place in a unit distance of the fracture surface. It follows that the energy required for these changes is achieved more frequently under these conditions. Using this analogy at a macroscopic level, it can be said that the crack tip propagation threshold is also achieved more often. These observations may act as another factor that substantiate the fact that larger loading conditions result in a smaller degree of crack-growth scatter.

The changes in the orientation of the fracture surface along a specific slip-plane are reflected as the waviness of the crack path on the specimen surface. This is shown in Figs 23(a) and (b). In view of the explanation given previously, increased waviness of the crack path (measured in terms of the horizontal distance required for the crack propagation direction to change) is related to increase in the externally applied load levels and thus the degree of crack growth scatter at a particular load level could be related to the wavines of the crack path. Quantification of this dependence has not been attempted here.

The phenomenon of crack-tip branching was also observed. Typical examples are shown in Fig. 24(a) and (b). While the existence of branching certainly contributes to the degree of crack growth scatter due to random loss of propagation energy at the crack tip, the extent of this contribution is not known. Both the effect of the waviness and that of the crack-tip branching on the degree of crack growth scatter are under study by the authors.

(3) The use of the present model is directed towards two applications. The first is the constant amplitude loading which, while representing a simple load spectrum, does occur in practice; e.g. pressurization cycles in transport aircraft cabins, rotating bending stresses in generators, thermal stress cycles in pressure vessels. This application has been examined in this paper. The second application is the variable amplitude loading which could be a two-step load sequence (low-high, high-low) or a spectrum of random loads. Variable amplitude loading is, however, a complex problem due to the fact that the crack tip damage per cycle under such loading is not only controlled by the stress amplitude of the current cycle, but also by the preceding load history. It is generally agreed[28–30] that this dependence is only transient in nature and should not exist after a certain duration of cycling.

Reflecting this concept on the fundamentals of the constant-probability crack growth model, one observes two areas where modifications can be made to account for the history dependence of the crack growth process due to load changes. The first, is the assignment of appropriate mathematical functions for the variables B, K and I_0 to take this phenomenon into consideration. The Markovian approach in the model is not violated because even though the crack tip conditions depend on the loading history, the propagation process is affected only by the present crack tip conditions. On the basis of the existing works on variable amplitude loading, it can be said that the mathematical functions cannot be arrived at by simple superimposition. However, quantification of the crack growth rates for variable amplitudes, even in the deterministic sense has not been accomplished so far. Only if that is achieved, will modifications for B, K and I_0 be possible.

The other area where modification must be made is the consideration of initial crack-length (a_0). In the present model, a_0 was a constant as a result of an imposed experimental condition. Thus, the model provides a distribution of the number of cycles required for a crack to reach a specified discrete state from a_0. No attempt has been made to consider an initial crack-length distribution and the manner in which it will affect the constant probability curves. Attempts to interpret the constant-probability growth curves in terms of a distribution of crack states after a specified number of cycles have elapsed from the instant the crack reached a_0 were also not made. Only this type of a distribution is useful for variable-amplitude loading application because the history of the fracture process is described in terms of the number of cycles. The recognition of this distribution is an important step since it represents the initial crack-length configuration which is a necessary boundary condition for the new load spectrum.

Acknowledgement—This work was supported by the U.S. Air Force Office of Scientific Research under Contract AFOSR 85-0362 monitored by Dr. G. Haritos and Dr. N. Pagano.

REFERENCES

[1] D. W. Hoeppner and W. E. Krupp, Prediction of component life by application of fatigue crack growth knowledge. *Engng Fracture Mech.* **6**, 47–70 (1974).
[2] Karl-He: .z Schwalbe, Comparison of several fatigue crack propagation laws with experimental results. *Engng Fracture Mech.* **6**, 325–341 (1974).
[3] S. Chand and S. B. L. Garg, Propagation under constant amplitude loading, *Engng Fracture Mech.* **21**, 1–30 (1985).
[4] S. C. Saunders, On the probabilistic determination of scatter factors using Miner's rule in fatigue life studies. *ASTM STP* **511**.
[5] W. J. Plumbridge, Review: fatigue crack propagation in metallic and polymeric materials. *J. Mater. Sci.* **7** (1972).
[6] J. N. Yang, R. C. Donath and G. C. Salivar, Statistical fatigue crack propagation of IN 100 at elevated temperatures, *ASME Int. Conf. on Advances in Life Prediction Methods*, Albany, New York (1983).
[7] J. N. Yang and R. C. Donath, Statistics of crack growth of a super-alloy under sustained load. *J. Engng Mater. Technol.* **106**, 79–83 (1984).
[8] S. Tanaka, M. Ichikawa and S. Akita, Variability of m and C in fatigue crack propagation law $da/dN = C(\Delta K)^m$. *Int. J. Fracture* **17**, R 121–124 (1981).
[9] T. R. Gurney, *Fatigue of Welded Structures*, Cambridge University Press (1979).
[10] D. F. Ostergaard and B. M. Hillberry, Characteristic of the variability in fatigue crack propagation data, *Probabilistic Fracture Mechanics and Methods: Applications for structural design and maintenance*, *ASTM STP* **798**, 97–115 (1983).
[11] B. R. Ellingwood, Probabilistic Assessment of low cycle fatigue behaviour of structural welds, *J. Press. Vess. Technol.* 26–29 (February 1976).
[12] P. Paris and F. Erdogan, A critical analysis of crack propagation law, *J. bas. Engng* 528–534 (December 1963).
[13] R. G. Forman, V. E. Kearney and R. M. Engle, Numerical analysis of crack propagation in cyclic loaded structures, *J. Bas. Engng* 459–464 (Septem.ber 1967).
[14] H. Ghonem and J. W. Provan, Micromechanics theory of fatigue crack initiation and propagation, *Engng Fracture Mech.* **13**, 963–977 (1980).
[15] H. Ghonem and S. Dore, Probabilistic description of fatigue crack propagation in polycrystalline solids. *Engng Fracture Mech.* **21**, 1151–1168 (1985).
[16] J. L. Bogdanoff and F. Kozin, *Probabilistic Models of Cumulative Damage*. John Wiley & Sons (1985).
[17] S. Aoki and M. Sakata, Statistical approach to delayed fracture of brittle materials, *Int. J. Fracture* **16**, 454–468 (1980).
[18] A. T. Bharucha-Reid, *Elements of the theory of Markov processes and its applications*. McGraw-Hill (1960).
[19] D. A. Virkler, B. M. Hillberry and P. K. Goel, The statistical nature of fatigue crack propagation, *J. Engng Mater. Technol.* **101**, 148–153 (1979).
[20] N. E. Frost, K. J. Marsh and L. P. Pook, *Metal fatigue*, Vol. 225. Clarendon Press, Oxford (1974).
[21] C. J. Beevers (Ed.), *Advances in Crack Length Measurement Techniques*. Chameleon Press, London, 1982.
[22] R. B. Thompson and D. O. Thompson, Ultrasonics in Nondestructive Evaluation. *Proc. IEEE*, 1716–1755 (December 1985).
[23] H. Ghonem and S. Dore, Probabilistic description of fatigue crack growth in aluminium alloys, AFOSR-83-0322, (April 1986).
[24] C. M. Hudson and J. T. Scardina, Effect of stress ratio on fatigue crack growth in 7075-T6 aluminium alloy sheet. *Engng Fracture Mech.* **1**, 429–446 (1969).
[25] H. F. Hardarth, J. C. Newman, Jr, W. Elber and C. C. Poe, Jr., Recent developments in analysis of crack propagation and fracture of practical materials, NASA TM-78766 (June 1978).
[26] R. W. Hertzberg and P. C. Paris, Application of electron fractography and fracture mechanics to fatigue crack propagation, *Proc. First Int. Conf. Fracture*, Sendai, Japan (1965).
[27] R. M. N. Pelloux and J. C. McMillan, Analysis of fracture surfaces by electron microscopy, *Proc. First Int. Conf. Fracture*, Sendai, Japan (1965).
[28] J. Schijve, Fatigue crack growth under spectrum loads, *ASTM STP* **595**, 3–23 (1976).
[29] W. Elber, Damage tolerance in aircraft structures, *ASTM STP* **486**, 230–242 (1971).
[30] R. Sunder, A mathematical model of fatigue crack propagation under variable amplitude loading, *Engng Fracture Mech.* **12**, 155–165 (1979).
[31] H. L. Ewalds and R. J. H. Wanhill, *Fracture Mechanics*, Vol. 176. Edward Arnold, London (1984).

(*Received* 29 *May* 1986)

APPENDIX C

CONSTANT-PROBABILITY CRACK GROWTH CURVES

Engineering Fracture Mechanics Vol. 30, No. 5, pp. 685–699, 1988
Printed in Great Britain.

0013-7944/88 $3.00 + .00
Pergamon Press plc.

CONSTANT-PROBABILITY CRACK GROWTH CURVES

H. GHONEM
Department of Mechanical Engineering and Applied Mechanics, University of Rhode Island, Kingston, RI 02881, U.S.A.

Abstract—This paper details a stochastic, time-inhomogeneous model that serves as a theoretical basis for the prediction of crack growth and its variability under constant-amplitude loading. Crack evolution is described as a set of constant probability curves, each of whose points possess equal probability of advancing from one position to another forward position. This probability is governed by a transition intensity parameter for which two mathematical interpretations are examined. A simplified crack growth rate equation, employing one of the definitions, is derived and applied to A17075-T6 material for different loading conditions. Results of this application are compared with those experimentally obtained.

INTRODUCTION

THE WORK of Ghonem *et al.*[1, 2] describes a probabilistic crack growth model based on the assumption that fracture history can be established by employing a particular discontinuous Markovian process which takes into account the fundamental aspects of the crack growth mechanism. This approach leads to the description of the sample curve of the crack growth process in terms of a constant-probability criterion. When considering that the crack growth curve given by any continuum crack growth model coincides with the median growth curve, the probabilistic model would then be sufficient to describe the evolution of the crack length and associated scatter at any stress level[3, 4]. The present paper is an attempt to extend the concepts of the model by including a different definition for the transition intensity probability of the growth process. This will lead to the derivation of a simple and explicit probabilistic crack growth rate equation similar in structure to the Paris–Erdogan equation.

The first part of the paper focuses on the constant probability crack growth curve concept and its model derivation, while the second part will deal with the application of the proposed law.

MODEL

The basic model is based on the assumpion the crack front in the crack propagation stage, as shown in Fig. 1, can be approximated by a large number M of arbitrarily chosen points α, $\alpha = 1, \ldots, M$. Each of these points in terms of the theory of probability, identifies a statistical "trial" or "experiment" conducted under identical conditions. The fracture state of the αth trial at cycle "i" is given by the crack length or random variable ${}^{\alpha}a_i(x_1, x_2, x_3)$ whose evolution with time shall then be established.

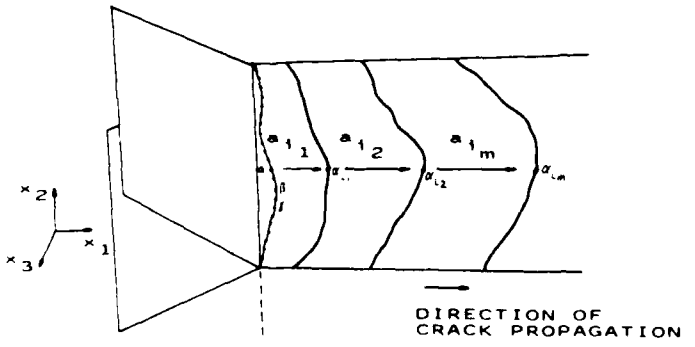

Fig. 1. Schematic of crack front positions along the fracture surface.

The following observations can be made regarding ${}^{a}a_i$:

1. The evolution of ${}^{a}a_i$ in the x_1, x_2 and x_3 directions are statistically independent of each other.

2. The statistical evolution of ${}^{a}a_i(x_1)$ is different from those of ${}^{a}a_i(x_2)$ and ${}^{a}a_i(x_3)$ in that the former consistently increases while the latter may be described as a type of random-walk phenomenon.

3. For an external load applied in the x_1 direction, the crack evolution in the x_2 and x_3 directions are orders of a lesser magnitude than that in the x_1 direction.

On the basis of these observations this model is limited to the evolution of ${}^{a}a_i(x_1)$ by assuming that the crack growth distributions of ${}^{a}a_i(x_2)$ and ${}^{a}a_i(x_3)$ can be described by Dirac–Delta functions. So, ${}^{a}a_i$ will hereafter be referred to as a_i.

Due to the built-in limitations of all experimental techniques in crack measurement, the observed value of a_i can only be specified within a range of:

$$x < a_i < x + \Delta x,$$

where Δx is the experimental error and x is the crack position calculated as (see Fig. 2):

$$x = r\Delta x; \quad r_0 < r < r_f. \tag{1}$$

Here "r" identifies the observable zone or state along the fracture surface; r_0 is the initial propagation state, r_f is the state just prior to catastrophic failure of the specimen and $r_1, r_2, \ldots, r_{f-1}$ are the intermediate zones, all zones having the same width.

Given that the crack is in state r, then after i cycles from the instant of reaching r, one of

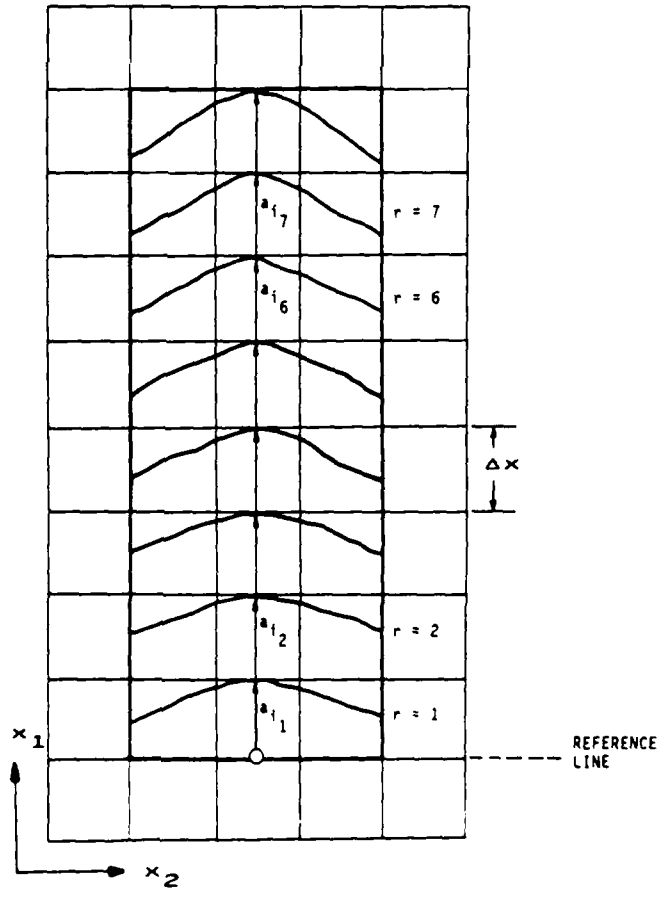

Fig. 2. Schematic of the proposed fatigue crack propagation along the fracture surface states.

two events will occur. Either a_i will remain in state r (event ${}^{r}E_i$) or a_i will not be in state r (event ${}^{s}E_i$). The following points should now be noted.

(a) The crack propagation process is irreversible (i.e. there is no rewelding of crack surfaces). Hence the crack, if it is not in state r after i cycles, must exist in a state greater than r

(b) Since it is not possible for the crack to propagate from one state to another state without penetrating the adjacent one, the crack can be identified by the number of cycles (i) required to advance from a given state to the immediately following state.

Based on these observations, events ${}^{r}E_i$ and ${}^{s}E_i$ can be seen as elements of a measurable space (Ω) (see ref. [3]) and the following definition of the probability measure of a_i becomes possible. At any fatigue cycle i, the probability that a_i is in state r, i.e. the probability of ${}^{r}E_i$, is defined as:

$$P\{a_i \in {}^{r}E_i\} = P\{x < a_i < x + \Delta x\}, \tag{2}$$

i.e.

$$P({}^{r}E_i) = P_r(i). \tag{3}$$

Therefore, the probability of a_i not falling within r, i.e. the probability of ${}^{s}E_i$ is,

$$P({}^{s}E_i) = 1 - P_r(i). \tag{4}$$

It can be seen that, $P_r(i)$ should continuously decrease as the number of cycles increases. Before proceeding further to identify the parameters that define $P_r(i)$, it is necessary to make these comments.

Under conditions of constant amplitude loading, where no overloading effects are considered, the growth of a crack from a particular state depends only on its present mechanical and microstructural details. More specifically, the probability of a_i propagating from state r to $r+1$ in the cycle interval $(i, i+\Delta i)$ depends on the event (${}^{r}E_i$) and is independent of the events prior to i, (${}^{r}E_j$, $j < i$). To elaborate, let (${}^{r+1}E_i$) be the event of a_i jumping to $(r+1)$ from r in the interval $(i, i+\Delta i)$. This represents a future event if (r_{E_i}) is an event in the present. Clearly, the future event is conditional on the occurrence of the present event. Given that the present has occurred, the probability of the future is not affected by the probability of the occurrence of the past (${}^{r}E_j$, $j < i$). Also, the occurrence of (${}^{r}E_i$) precludes the occurrence of the (${}^{s}E_j$, $j < i$, $s > r$) due to the irreversible nature of the crack growth process.

The above feature is similar to that of a pure birth Markovian process in which the future is determined only by the present and not by the past, and in which the discrete space variable never decreases in magnitude with increase of time. This analogy helps to define a transition probability that is also a Markovian property and introduce the condition probability function that governs the crack growth process as:

$$\begin{aligned} P\{{}^{r+1}E_i/{}^{r}E_i, \ldots, {}^{r}E_j, \ldots, {}^{r}E_0\} &= P\{{}^{r+1}E\Delta i/{}^{r}E_i\} \\ &= P_{rt}(i); \quad ij, \end{aligned} \tag{5}$$

where $P_{rt}(i)$ is the transition probability linking the probability measures of two consecutive states "r" and "t" ($t = r+1$) along the fracture surface and "/" denotes the conditional probability. This property, together with the evolution of a_i within the two event sample space (Ω), describes a discrete space continuous time Markov process.

Since the analogy to the Markovian process has been shown, the criteria attached to this process can be assumed to be valid for the crack growth as well.

1. The probability that a_i propagating to a state different from r in Δi cycles, where Δi is very small, after i cycles elapse in state r is:

$$\begin{aligned} P_s(\Delta i) &= P\{{}^{t}E\Delta i/{}^{r}E_i\} + 0(\Delta i), \\ &= \lambda_r \Delta i + 0(\Delta i); \quad t = r+1. \end{aligned} \tag{6}$$

Here, λ_r is a positive variable indicating the probability transition rate. It describes the transition rate from state r to $r+1$ in i cycles.

In this analysis, λ_r is assumed to be a material parameter which in addition to being a function of crack position r, should depend explicitly on both initial cycle i, and duration Δi. The propagation process thus becomes time-inhomogeneous.

2. The corresponding probability that a_i will be in state r during the cycle interval Δi is:

$$P_r(\Delta i) = P\{{}^rE_{\Delta i}/{}^rE_i\} + 0(\Delta i)$$
$$= (1 - \lambda_r \Delta i) + 0(\Delta i). \tag{7}$$

3. The probability that a_i is in a state different from $r+1$ is:

$$P_{\pi}(\Delta i) = P\{{}^{\pi}E_{\Delta i}/E_i\}$$
$$= 0(\Delta i); \quad \pi \neq r+1. \tag{8}$$

The time interval Δi is so small that the probability of advancing from r to a state greater than $r+1$ is almost zero. By definition, $0(\Delta i)$ is such that,

$$\lim_{\Delta i \to 0} \frac{0(\Delta i)}{\Delta i} = 0.$$

Now, let

$$A = {}^rE_i \quad \text{and} \quad B = {}^rE_{\Delta i}.$$

Then

$$A \cap B = {}^rE_{i+\Delta i}.$$

Since

$$P(A \cap B) = P(B/A) \cdot P(A).$$

Therefore

$$P\{{}^rE_{i+\Delta i}\} = P\{{}^rE_{\Delta i}/{}^rE_i\} \cdot P\{{}^rE_i\}. \tag{9}$$

Substituting eqs (6), (7) and (8) in (9) we get,

$$P\{{}^rE_{i+\Delta i}\} = (1 - \lambda_r \Delta i) \cdot P\{{}^rE_i\} + 0(\Delta i), \tag{10}$$

which can be written as

$$P_r(i + \Delta i) = (1 - \lambda_r \Delta i) \cdot P_r(i) + 0(\Delta i). \tag{11}$$

By transposing the term $P_r(i)$, dividing by Δi and passing to the limit $\Delta i \to 0$, eq. (11) becomes

$$\frac{dP_r(i)}{di} = -\lambda_r P_r(i). \tag{12}$$

The solution of this equation is:

$$\ln P_r(i) = -\int \lambda_r \, di + L_1, \tag{13}$$

where L_1 is a constant.

This equation describes the crack growth probability from state r, after i cycles elapse, in terms of the constant L_1 and the transition rate λ_r which is discussed below.

The parameter λ_r was introduced in this model as the transition intensity by which a_i propagates from one state to the next. Adopting the notion that the crack growth process is a discrete one, the crack transition from a specific state can be viewed as being governed by a critical threshold energy at the crack tip. When such a threshold (which is environmental, material, stress and crack-length dependent) is satisfied by cyclic energy accumulation, a crack tip transition can be said to occur. Therefore the larger the cycle duration associated with the crack in a specific state, the greater the probability that the propagation threshold is satisfied and the greater the probability that the crack advances to the following state.

The transition intensity, λ_r, can be assumed to have several physical interpretations, however, the primary concern at this point is whether λ_r is a material property present only when there is application of cyclic loads or whether it exists even when there is no cycling.

If λ_r is a property that owes its existence to cyclic loading, then it could represent a dislocation accumulation rate, a microvoid growth rate, a ductility exhaustion rate or a rate at which any physical phenomenon occurs in the grain structure of a polycrystalline material to aid the propagation of a crack. In that case, the magnitude of λ_r should be zero at any instant there is no cycling. Specifically, its magnitude should be equal to zero at $i = 0$, the instant at which the load cycling is about to begin, after the crack has reached a particular state, r. Keeping in mind the fact that λ_r should monotonically increase with i, the following expression for λ_r can then be chosen.

$$\lambda_r(i) = L(r) i^{\alpha(r)}, \tag{14}$$

where $L(r)$ and $\alpha(r)$ are functions of the crack state.

If, on the other hand, λ_r is a property present even when there is no cyclic loading, the physical analogy for λ_r would be completely different. λ_r would then represent a dislocation density in the microstructure or a microvoid density in the microstructure of a material. Thus while the property λ_r does increase in magnitude during cycling, it does not cease to exist when the cycling is absent. Hence, from this point of view, λ_r should have a value corresponding to $i = 0$, the instant at which the cycling is about to begin after the crack has reached a specified state, r. The following expression could then be considered.

$$\lambda_r = L(r)\, e^{\alpha(r) i}. \tag{15}$$

From a purely mathematical point of view expression (15) was first selected to be utilized in the present model. By substituting eq. (15) in (13), it yields:

$$\ln P_r(i) = -B\, e^{Ci} + L_1, \tag{16}$$

where $B = L/C$.

The upper and lower limits of $P_r(i)$ in the above equation are:

$$1 \geq P_r(i) \geq 0. \tag{17}$$

The form of eq. (15) suggests that i has a lower boundary that satisfies the upper limit condition of $P_r(i)$. Equation (16) thus becomes:

$$\begin{aligned} \ln P_r(i) &= B(e^{CI_0} - e^{Ci}) \quad && i > I_0 \\ &= 0 && i \leq I_0 \end{aligned} \tag{18}$$

where the parameters B, C and I_0, the incubation time, are found to be:

$$B = C_1 a_r^{n_1}; \tag{19}$$

$$C = C_2 a_r^{n_2} \tag{20}$$

and

$$I_0 = C_3[a_{r+1}^{n_2} - a_r^{n_3}] \tag{21}$$

C_1, C_2, C_3, n_1, n_2 and n_3 are material-, stress- and environment-dependent parameters.

The application of the above eq. (18) to different steel and aluminum alloys is detailed in ref. [3].

In this paper the interpretation concerning λ_r, as given in eq. (14), will be examined. By substituting this equation in (13) and setting the upper and lower limits of $P_r(i)$ to:

$$1 \geq P_r(i) \geq 0,$$

one can arrive at the following solution

$$\Delta i = A(-\ln P_r(i))^{\beta}, \tag{22}$$

where

$$A = \left(\frac{1+\alpha}{L}\right)^{1/(1+\alpha)} \quad \text{and} \quad \beta = \frac{1}{1+\alpha}.$$

A and B are considered here to be material-, stress- and crack-position dependent.

The above equation identifies the duration of fatigue cycles required for a crack at position r to propagate with a specific constant probability $P_r(i)$, to a position $r+1$ along the fracture surface. By calculating such durations for states r_1 to r_{f-1}, the history of the entire constant-probability crack growth curve can be obtained. If an assumption is made that the crack growth curve generated by a continuum model coincides with the median growth curve, i.e., the $P_r(i) = 0.5$ curve, parameters A and β can be determined and eq. (22) becomes fully defined for a particular material and a particular constant amplitude stress condition. The work described below explains the procedure for determining the expressions of both A and β.

Following the approach detailed in ref. [3], work of Virckler *et al.*[5], which combines crack growth data of 68 replicate tests of A12024-T3, shown in Fig. 3(a) was arranged in 9 constant probability crack growth curves as shown in Fig. 3(b). Data points representing cycle intervals corresponding to similar discrete crack propositions along three different constant-probability curves; $P_r(i) = 0.05$, 0.5 and 0.95, were used as input to eq. (22) to determined the parameters A and β. Using curve regression analysis parameter β was found to be constant for all state positions with a value of 0.166. The parameter A varied as function of r in a pattern shown in Fig. 3 which is fitted into the form:

$$A = 1.5 \times 10^7((r-1)^{-1} - r^{-1}). \tag{23}$$

Similarly, data of Yang *et al.*[6], Fig.4, which consist of the distribution of crack size as function of load cycles for IN-100 tested for two different load conditions, were used to obtain the expressions for A and β. These expressions were obtained as:

Test condition I

$$A = 4.3 \times 10^6((r-1)^{-0.70} - r^{-0.7}).$$
$$\beta = 0.155. \quad \text{(average)} \tag{24}$$

Test condition II

$$A = 4.06 \times 10^6((r-1)^{-1.4} - r^{-1.4}).$$
$$\beta = 0.266. \quad \text{(average)} \tag{25}$$

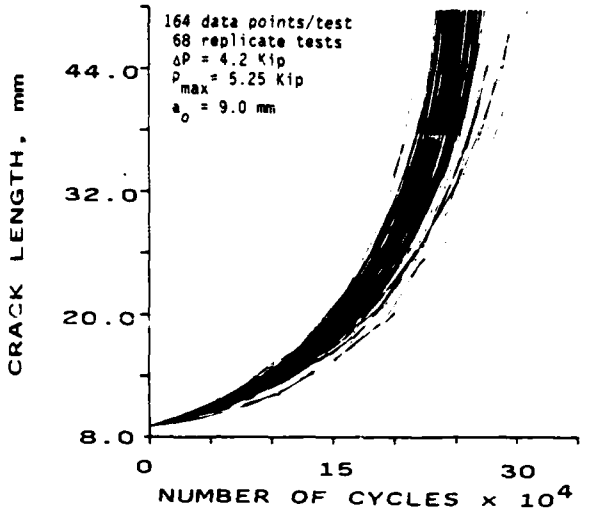

Fig. 3(a). Sample curves of data set from Virckler's study.

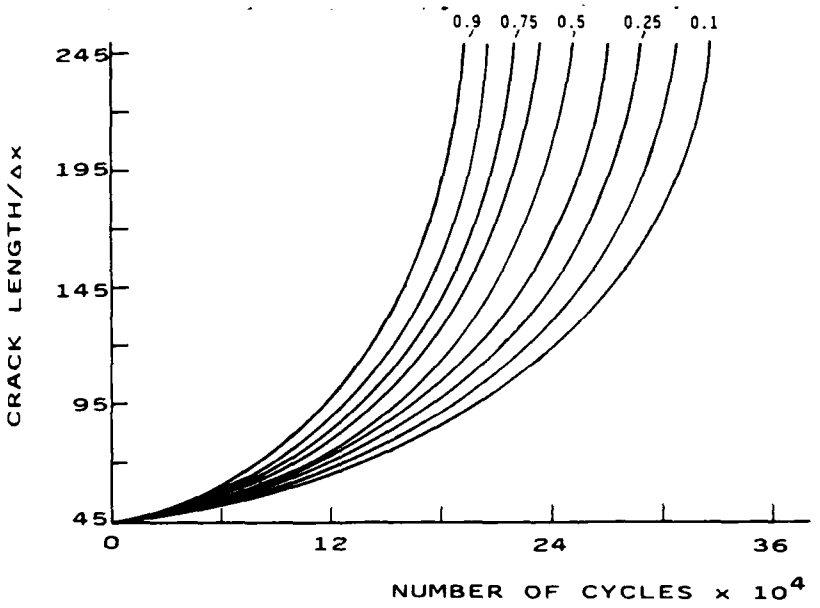

Fig. 3(b). Experimental constant-probability crack growth curves generated from the data in Fig. 3(a); $\Delta x = 0.2$ mm.

By observing the forms of A and β, as expressed in eq. 23–25, obtained from two different types of alloys, one can conclude that, while β seems to depend mainly on the material and stress condition, a general form of A depends on the crack position and can be written as:

$$A = C_1((r-1)^\gamma - r^\gamma),$$

where C_1 and γ are material- and stress-dependent parameters. Therefore, one can write eq. (21) as:

$$\Delta i = C_1((r-1)^\gamma - r^\gamma)(-\ln P(i))^\beta$$

$$= \frac{C_1}{\Delta x^\gamma}[\Delta x^\gamma (r-1)^\gamma - \Delta x^\gamma r^\gamma](-\ln P)^\beta \tag{26}$$

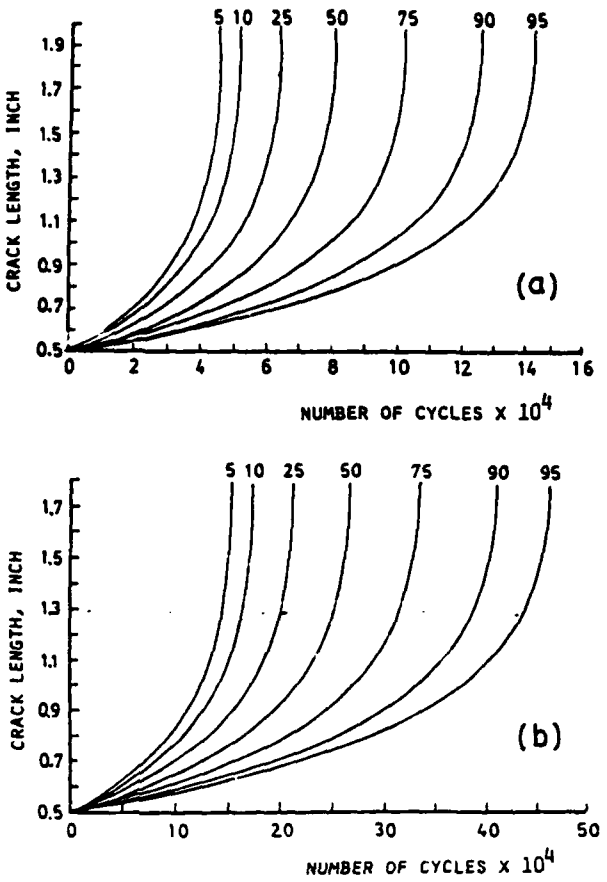

Fig. 4. Experimental constant-probability growth curves for (a) Test condition I and (b) Test condition II[6].

since the crack length a_r can be written as $a_r = \Delta x \cdot r$, thus, eq. (26) becomes

$$\Delta i = C_2(a_{r-1}^{\gamma} - a_r^{\gamma})(-\ln P)^{\beta}, \tag{27}$$

where $C_2 = C_1/\Delta x^{\gamma}$. One should remember here that Δi is the number of cycles counted from the instant the crack tip reaches state r and P is the probability that the crack will not propagate from state r to the following state within Δi cycles. For the same value of $P_r(i)$, i.e. operating on a single crack growth curve, eq. (27) can be manipulated as follows:

$$\Delta i_1 = i_1 - 0 = C_2(a_0^{\gamma} - a_1^{\gamma})(-\ln P)^{\beta},$$

where a_0 is a constant that represents the initial crack length.

$$\Delta i_2 = i_2 - i_1 = C_2(a_1^{\gamma} - a_r^{\gamma})(-\ln P)^{\beta}$$

. . . . . .

. . . . . .

. . . . . .

$$\Delta i_r = i_{r-1} - i_r = C_2(a_{r-1}^{\gamma} - a_r^{\gamma})(-\ln P)^{\beta}.$$

By summing $\Delta i_1 + \Delta i_2 + \cdots + \Delta i_r$ one obtains

$$i_r = C_2(a_0^{\gamma} - a_r^{\gamma})(-\ln P)^{\beta}.$$

Differentiating both ends w.r.t. i; thus:

$$l = C_2\left(-\gamma a_r^{\gamma-1}\frac{da}{di}\right)(-\ln P)^{\beta}.$$

This equation can be rearranged as:

$$\frac{da}{di} = C_3 a^{\delta}(-\ln P)^{-\beta}, \tag{28}$$

where

$$C_3 = \frac{-1}{C_2\gamma} \quad \text{and} \quad \delta = 1-\gamma.$$

By multiplying and dividing eq. (28) with $\Delta\sigma^{2\delta}\pi^{\delta}$; where $\Delta\sigma$ is the stress range, one can obtain:

$$\frac{da}{di} = C\Delta\sigma^{2\delta}\pi^{\delta}a^{\delta}(-\ln P)^{-\beta}, \tag{29}$$

where $C = C_3/\Delta\sigma^{2\delta}\pi^{\delta}$.

Equation (29) could then be written as:

$$\frac{da}{di} = C_I(\Delta K)^{\delta}(-\ln P)^{-\beta} \tag{30}$$

which represents a crack growth rate equation for a crack progressing from one state to the following state along the fracture surface with a constant probability P.

As mentioned before a basic assumption in the work of ref. [2] is that the median of the constant probability crack growth equation, i.e., the curve with $P_r(i) = 0.5$, can be described using a continuum crack growth law. By invoking this assumption the validity of eq. (30) could be examined using results of tests carried out on A17075-T6 specimens (3). In this work the crack length versus number-of-cycles was obtained for three different stress conditions. Each condition was tested by using sixty identical center-notched flat specimens (320.67 × 50.8 × 3.175 mm) resulting in sixty crack-growth curves, each consisting of 25 points generated through the use of an automated photographic technique detailed in ref. [3]. The results of this study and the corresponding experimental constant probability crack growth curves are shown in Figs 5–8. Following an argument discussed in the above mentioned study, Forman's eq. (6) was selected as a suitable continuum crack-growth law since it recognizes the effect of the stress ratio R and is well documented for A17075-T6; it is written as

$$\frac{da}{di} = \frac{C\Delta K^m}{(1-R)(K_c - K_{max})}, \tag{31}$$

where

$$K_c = 74 \text{ MPa } m^{1/2},$$
$$C = 1.63 \times 10^{-17}$$
$$m = 3.065.$$

The results of the comparison of this equation with those experimentally obtained for $P_r(i) = 0.5$ are shown in Fig. 9; they indicated close agreement.

The above equation could now be equated to eq. (30) in which $P_r(i) = 0.5$. In this equality the parameter δ is set equal to m of Formann equation, i.e., $\delta = 3.065$. Using an iterative

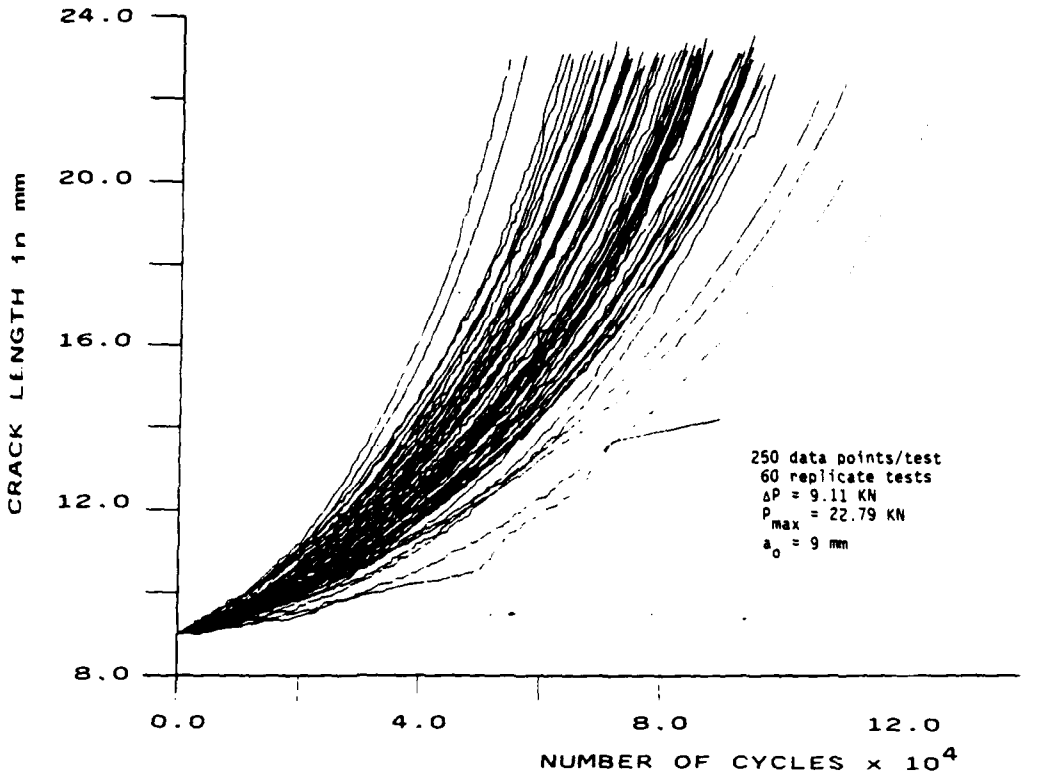

Fig. 5(a). Sample curves of test condition I ($\Delta X = 0.2$ mm).

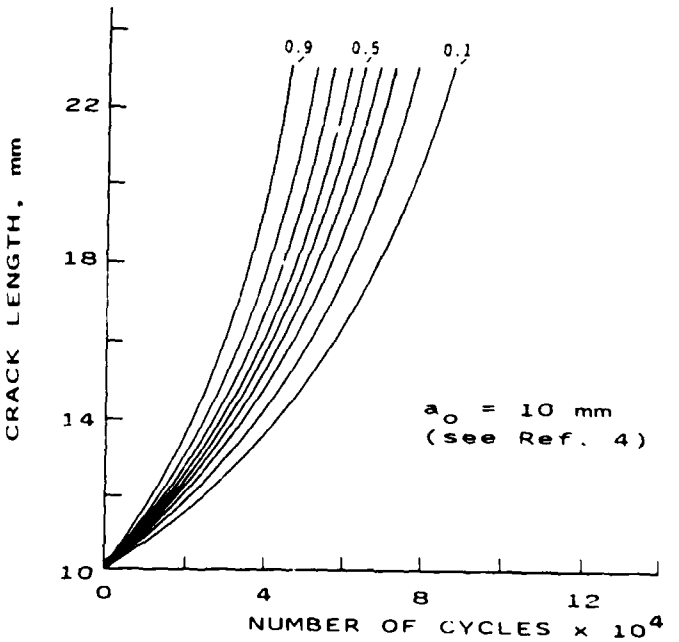

Fig. 5(b). Constant-probability curves generated from Fig. 5(a).

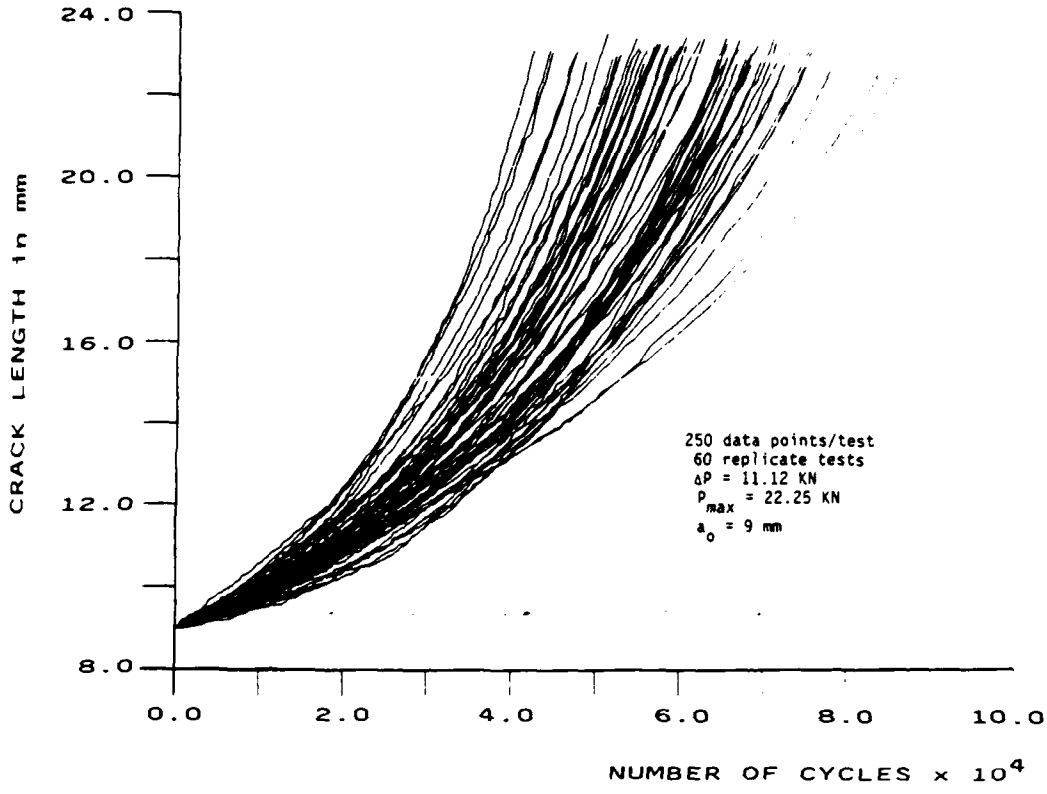

Fig. 6(a). Sample curves of test condition II ($\Delta X = 0.2$ mm).

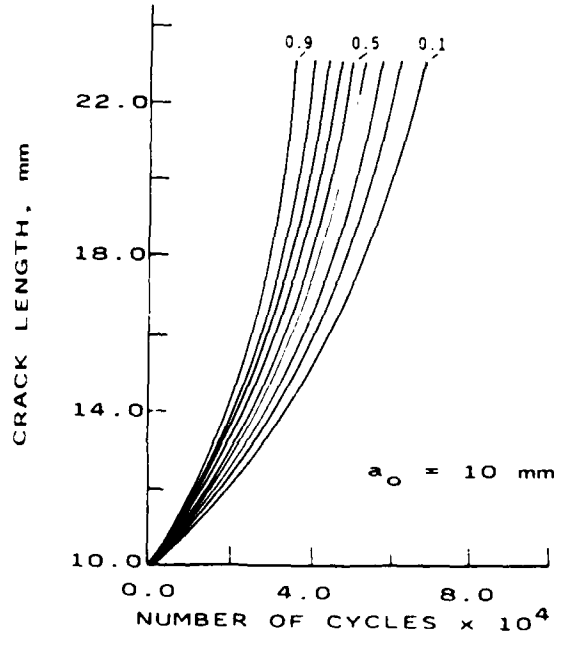

Fig. 6(b). Constant-probability curves generated from data in Fig. 6(a).

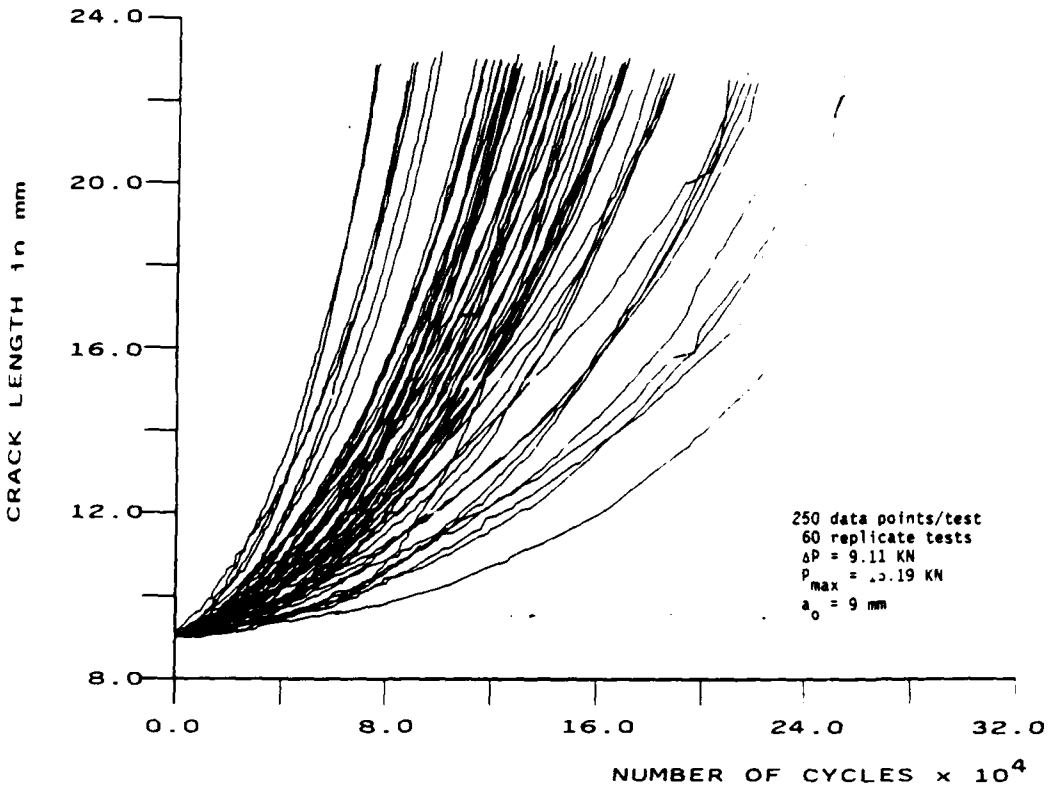

Fig. 7(a). Sample curves of test condition III ($\Delta X = 0.2$ mm).

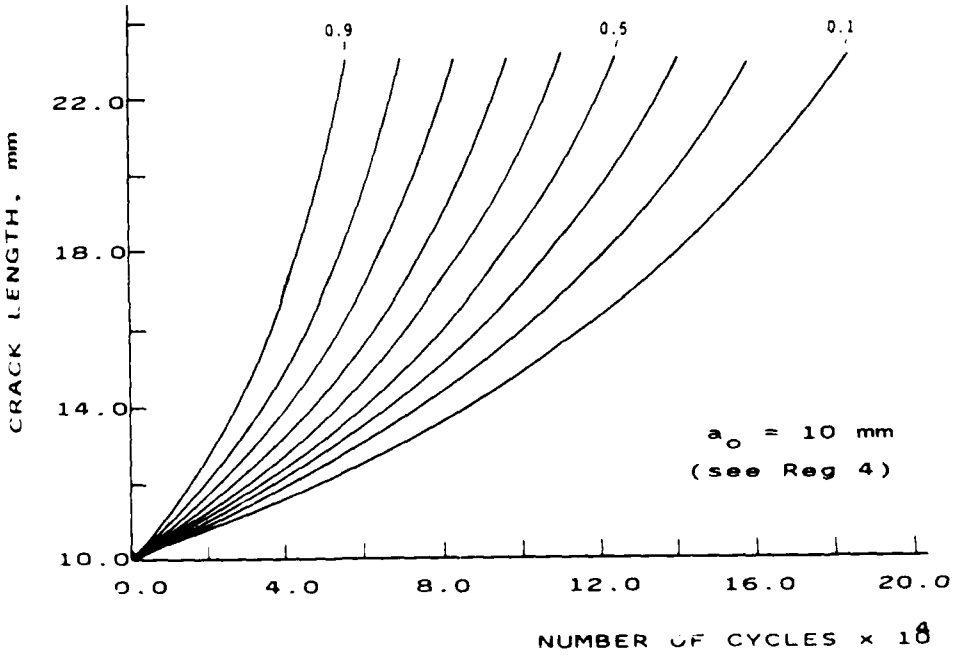

Fig. 7(b). Constant-probability curves generated from data in Fig. 7(a).

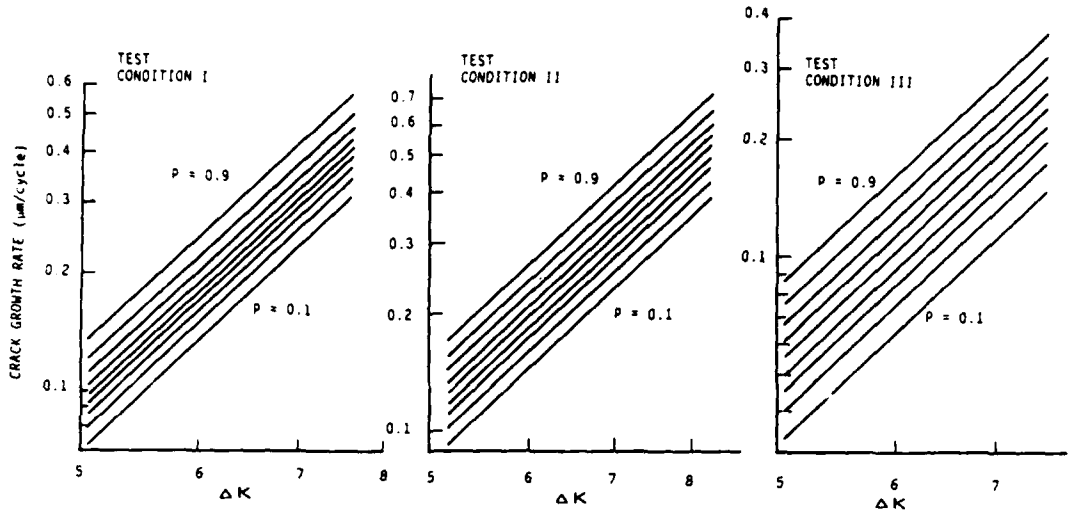

Fig. 8. Experimental crack growth rate vs ΔK for the three test conditions shown in Figs 5–7 (ΔK in MPa $m^{1/2}$).

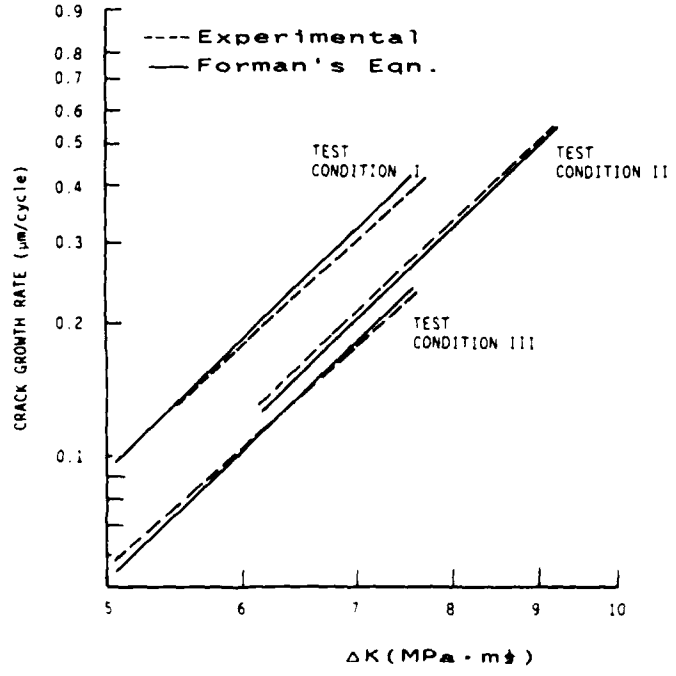

Fig 9 Comparison between median curves obtained experimentally and those calculated using Forman's equations.

numerical technique that employs the Newton–Raphston method, values of C_l and β for the three different load conditions were obtained:

	Test condition I	*Test condition* II	*Test condition* III
C_l	2.64×10^{-4}	1.65×10^{-4}	1.42×10^{-4}
β	0.195	0.203	0.299

The parameters C_l and β were then substituted in eq. (30) to generate, for each load condition, the entire spectrum of the constant probability crack growth rate curves. These curves were compared to those experimentally obtained in Fig. 8. Results of this comparison, in the form of percentage-of-error of number-of-cycles corresponding to a similar crack length, are summarized in Fig. 10. These results show that the error of the model under test conditions I, II and III are ±2.5%, ±5% and ±8% respectively. This degree of error is similar to that obtained when λ_r is expressed by eq. (15), see ref. [3]. Furthermore, a comparison between both the theoretical and experimental cumulative distribution function for selected crack lengths, at the three different loading conditions, are shown in Fig. 11; they indicate a very close agreement.

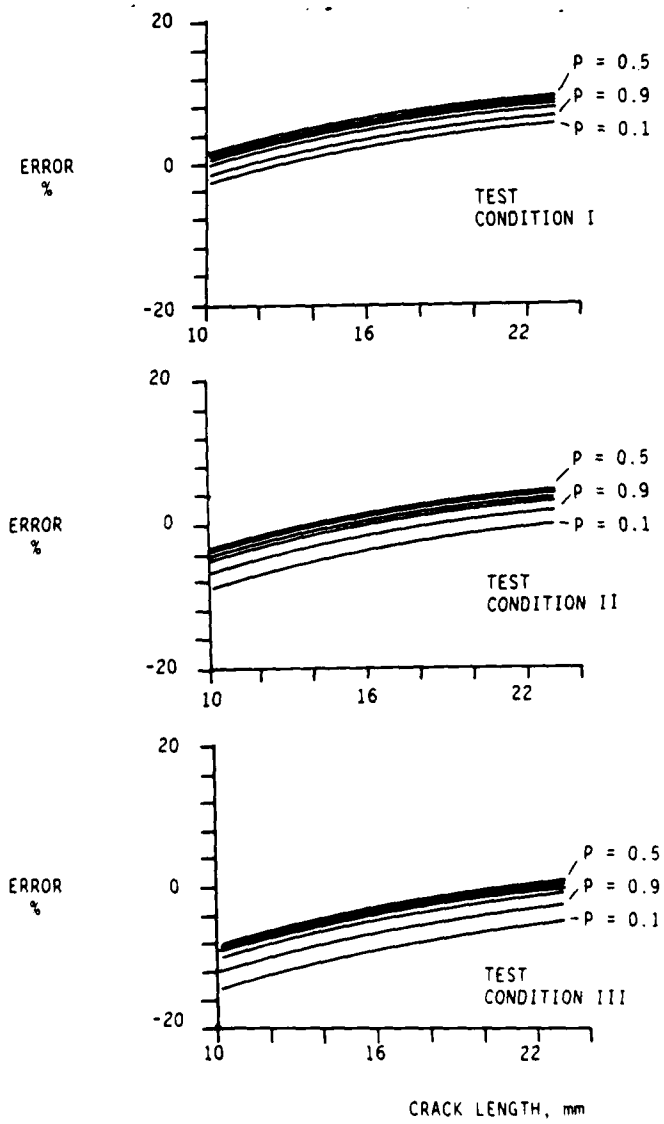

Fig. 10. Error in per cent between constant-probability crack growth curves generated using the mathematical model and those obtained experimentally in Figs 5–7

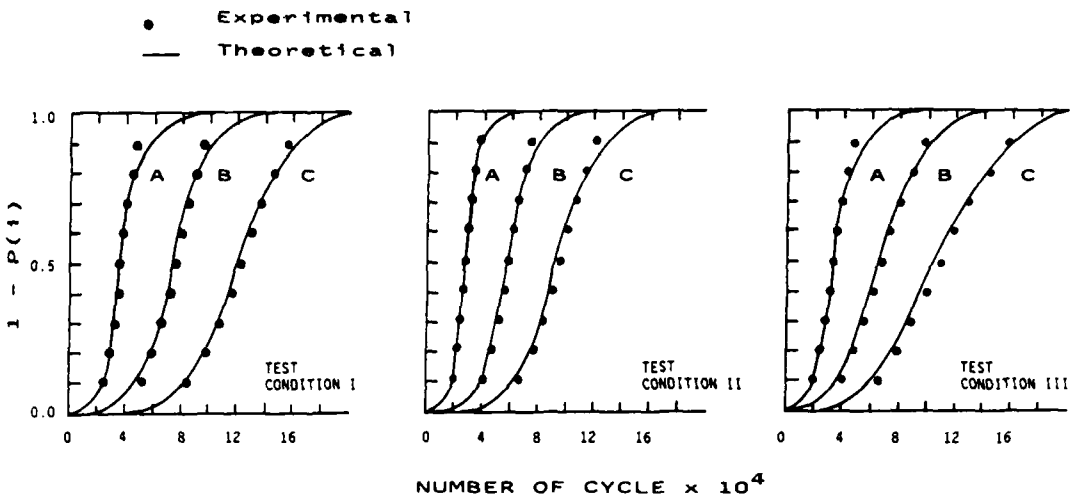

Fig. 11. Cumulative distribution functions for three crack length positions; $A = 12$ mm, $B = 15$ mm, and $C = 21$ mm obtained for the three test conditions in Figs 5–7.

CONCLUSIONS

This paper has outlined the principle of a stochastic model aimed at describing crack growth and its variability due to random characteristics of the microstructure of polycrystalline solids. The model was built by developing an analogy to a discontinuous Markovian process. This treatment leads to the calculation of the cycle duration required for a point along the crack tip to advance with a particular probability to a forward state along the fracture surface. This probability is governed by a transition intensity parameter, λ_r, which is viewed here as material- and cycle-dependent. In the absence of a definite physical interpretation of this parameter, it has been given two mathematical expressions which differ in that one expression, λ_r, possesses a value when Δi approaches zero, while in the other expression λ_r becomes zero as $\Delta i \rightarrow 0$. The paper examined the latter condition which then led to the derivation of a crack growth rate equation in which a probability term is explicit. Comparison of the results of this equation, when applied to A17075-T6 for three different loading conditions, indicates agreement with experimental results obtained by the author for the same loading conditions.

Acknowledgement—This work was supported by the U.S. Air Force Office of Scientific Research under Contract AFOSR-85-0362 monitored by Dr G. Haritos.

REFERENCES

[1] H. Ghonem and J. W. Provan, Micromechanics theory of fatigue crack initiation and propagation, *Engng Fracture Mech.* **13**, 963–977 (1980).
[2] H. Ghonem and S. Dore, Probabilistic description of fatigue crack propagation in polycrystalline solids, *Engng Fracture Mech.* **21**, 1151–1168 (1985).
[3] H. Ghonem and S. Dore, Probabilistic description of fatigue crack growth in aluminum alloys, AFOSR-83-0322 (April 1986).
[4] H. Ghonem and S. Dore, Experimental study of the constant-probability crack growth curves under constant amplitude loading, *Engng Fracture Mech.* **27**, 1–25 (1987).
[5] D. A. Virckler, B. M. Hillberry and P. K. Goel, The statistical nature of fatigue crack propagation, *J. Engng Mater Technol.* **101**, 148–153 (1979).
[6] J. N. Yang and R. C. Donath, Statistics of crack growth of a super-alloy under sustained load, *J. Engng Mater. Technol.* **106**, 79–83 (1984).
[7] R. G. Forman, V. E. Kearney and R. M. Engle, Numerical analysis of crack propagation in cyclic loaded structures, *J. Basic Engng*, 459–464 (September 1967).

(*Received* 17 *August* 1987)

APPENDIX D

POTENTIAL DROP MEASUREMENT

APPENDIX D

Potential Drop Measurement

1. Potential Drop

The crack measurement technique used in this report is the d.c. electrical potential drop method which is a widely accepted method of monitoring crack initiation and growth in controlled lab tests. In its simplest form it involves passing a constant current through the specimen and then measuring the electrical potential across the crack plane. As the crack propagates the resistance of the specimen, and hence the potential drop (P.D.) increases due to the reduction in uncracked cross sectional area of the specimen.

The P.D. technique has many advantages over optical measurements of crack length. It provides a total measurement inclusive of crack front curvature, and because it does not require visual accessibility, tests may conducted in any sealed environment. The output is continuous which permits automatic data collection and processing together with a 24 hours usage of testing machine capacity. The block diagram of our d.c. potential system is illustrated in Fig. D-1.

In order to obtain a relation of potential and crack length, which is independent of current and temperature variations, the potential measurements are modified and compared using the ratio of two measurement V_R, which is expressed as:

$$V_R = \frac{V_1 - V_1^0}{V_2 - V_1^0}$$

where V_1 and V_2 are two potential measurements as shown in Fig D-2 and V_1^0 and V_2^0 are the null voltage of V_1 and V_2 respectively measured when current is shut off, both of which account for the thermocouple effects. V_R instead of V_1 is used here to allow compensation for temperature, current and material variations with time.

The crack length in calibration was observed by optical microscope as shown in Fig. D-3. The relationship between d.c. potential and crack length for the specimen shown in Fig. D-4 was obtained through calibration test in which data pairs of crack length and potential were recorded during crack propagation. The dimension of the specimen used in this study is shown in Fig. D-5.

2. Computer hardware and software

The control system has constructed around a IBM-PC. Machine control, data acquisition and storage, and output of results are affected via a computer interface which includes DASH-16, a multifunction high speed analog/digital I/O expansion board for the IBM Personal Computer.

The test machine cyclic load and frequency are controlled through a 410 Digital Function Generator.

The application software has been written in BASIC and its operation is summarized in the flow diagram shown in Fig. D-6. The programs are also attached to this appendix in Fig. D-7.

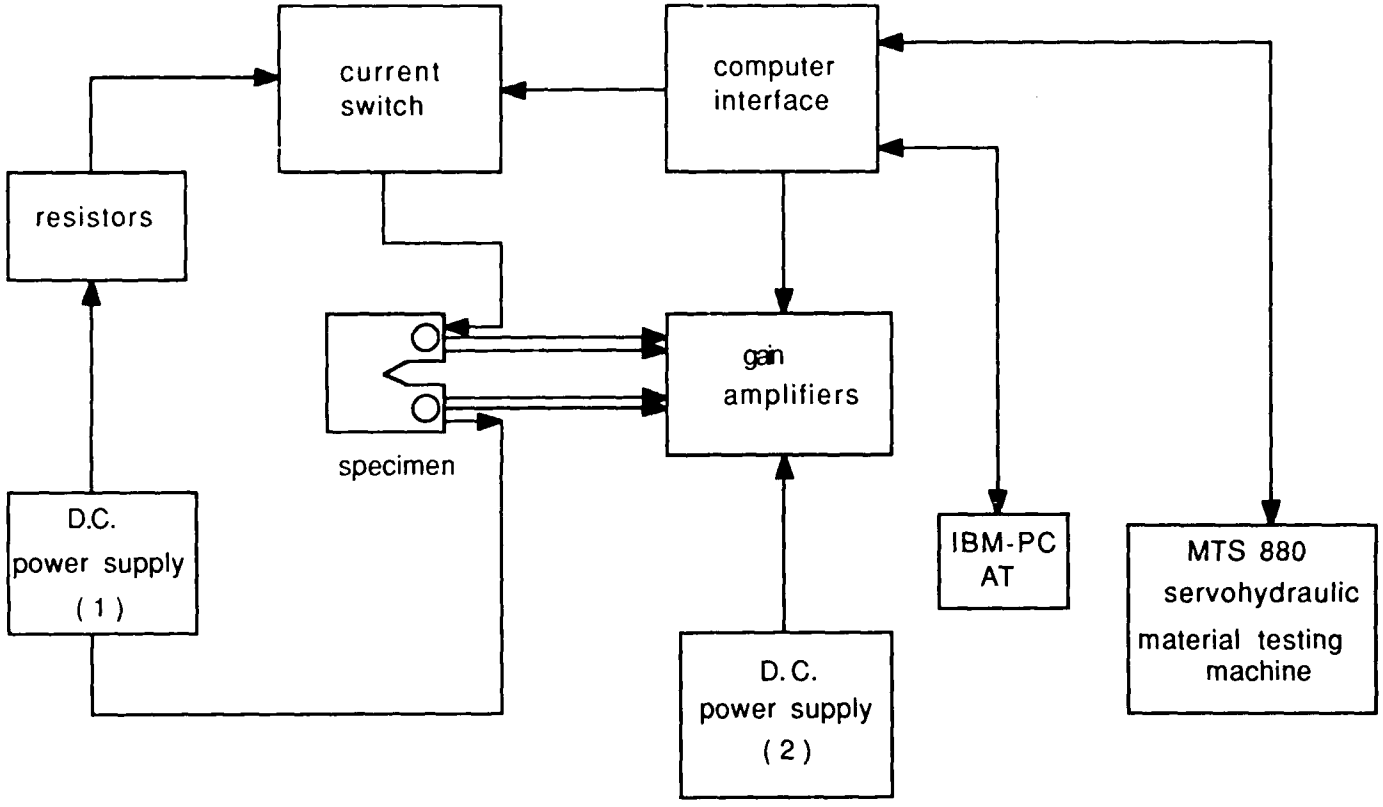

Fig. D-1 Schematic sketch of system for d.c. potential drop measurement and servohydraulic test machine control

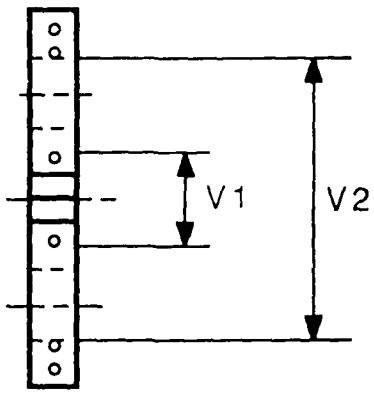

Fig. D-2 Two potential measurements

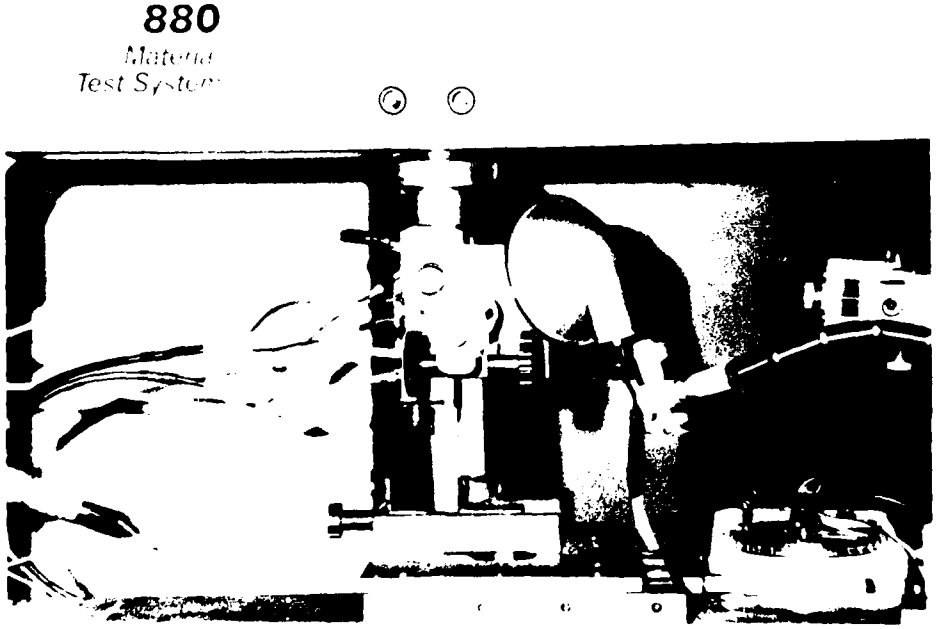

Fig. D-3 Optical microscope observation of crack length in the calibration

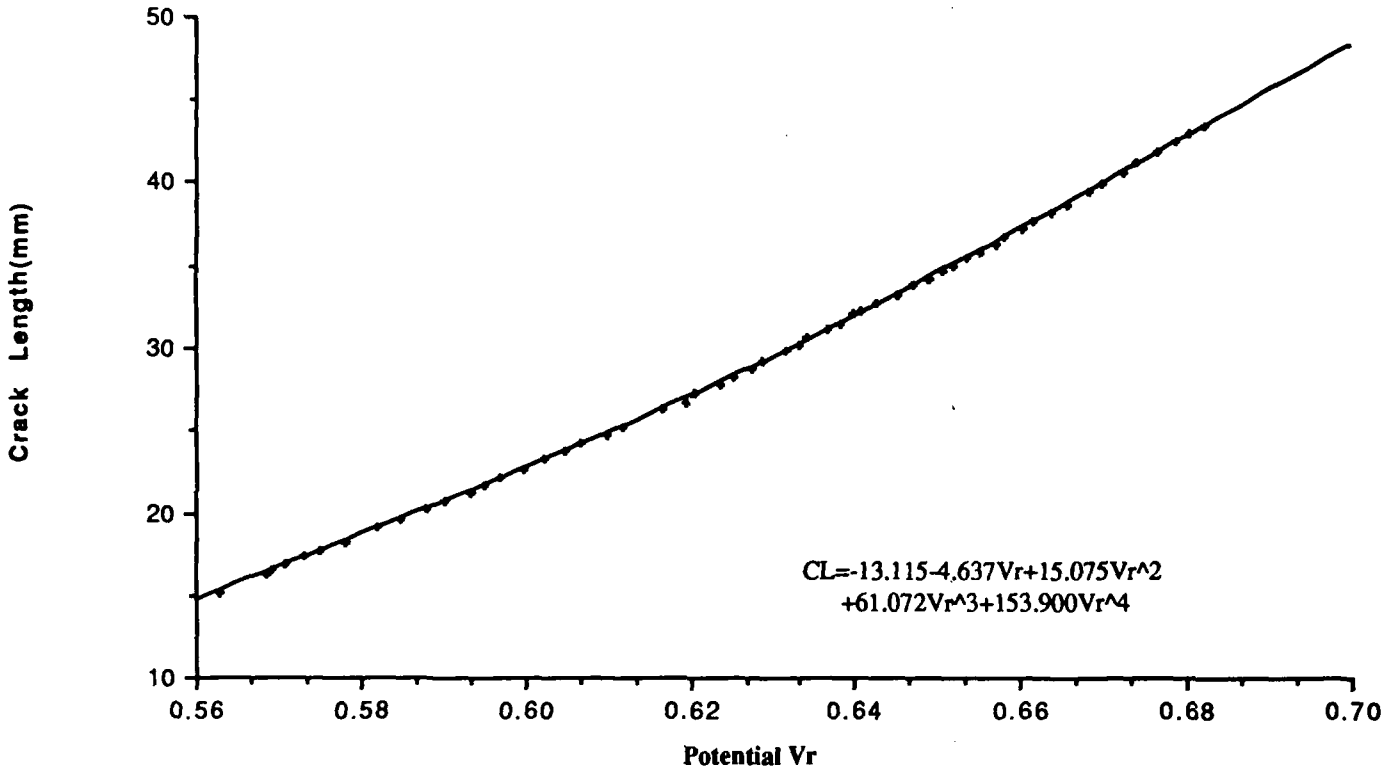

Fig.D-4 Calibration curve and equation

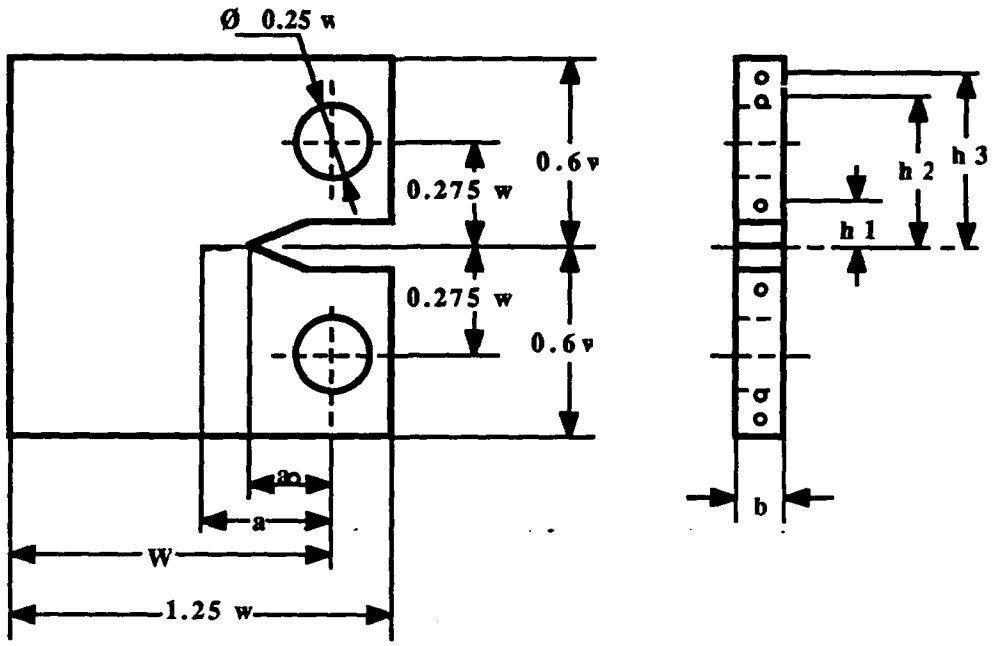

w=76.1mm
ao(length of notch)=15mm
b=7.2mm
h1=6.1mm
h2=34.4mm
h3=43.3mm

Fig. D-5 Test specimen used in the present study

D-7 Flow chart of the main program used in the experiment

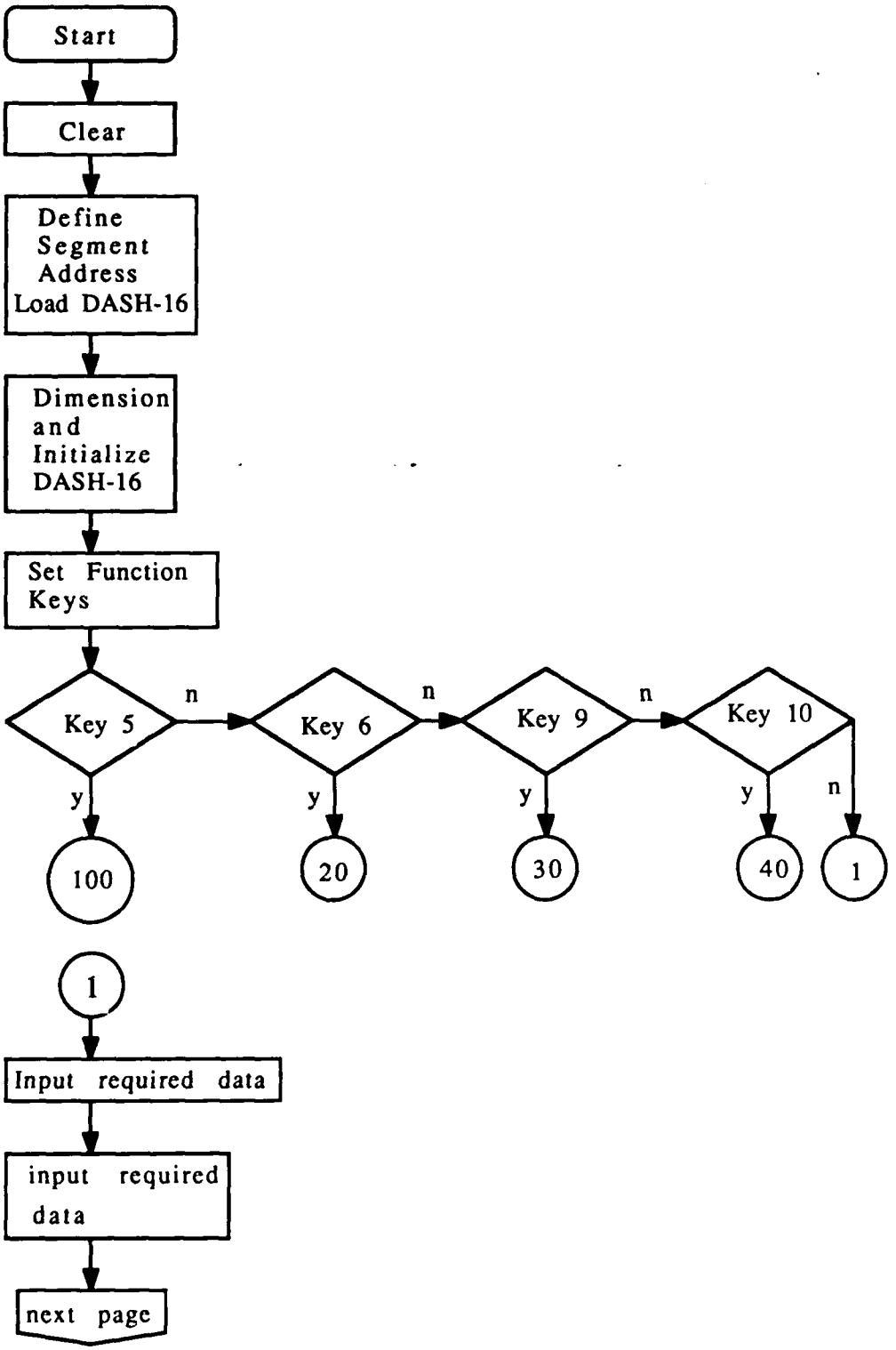

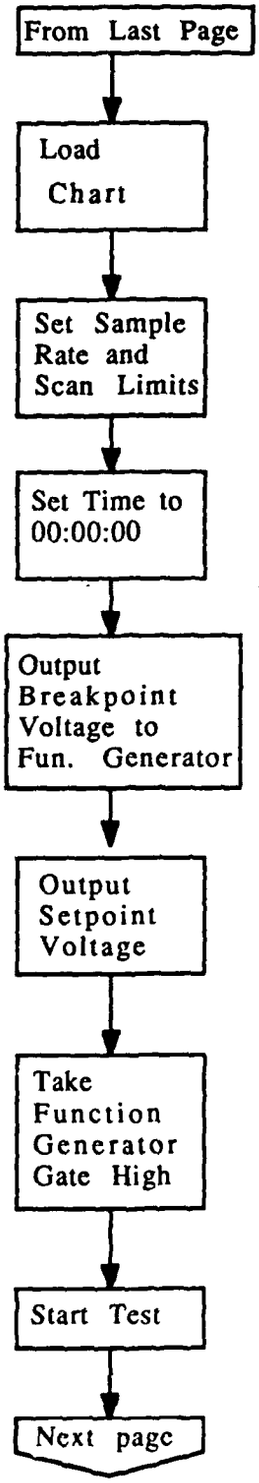
From Last Page
Load Chart
Set Sample Rate and Scan Limits
Set Time to 00:00:00
Output Breakpoint Voltage to Fun. Generator
Output Setpoint Voltage
Take Function Generator Gate High
Start Test
Next page

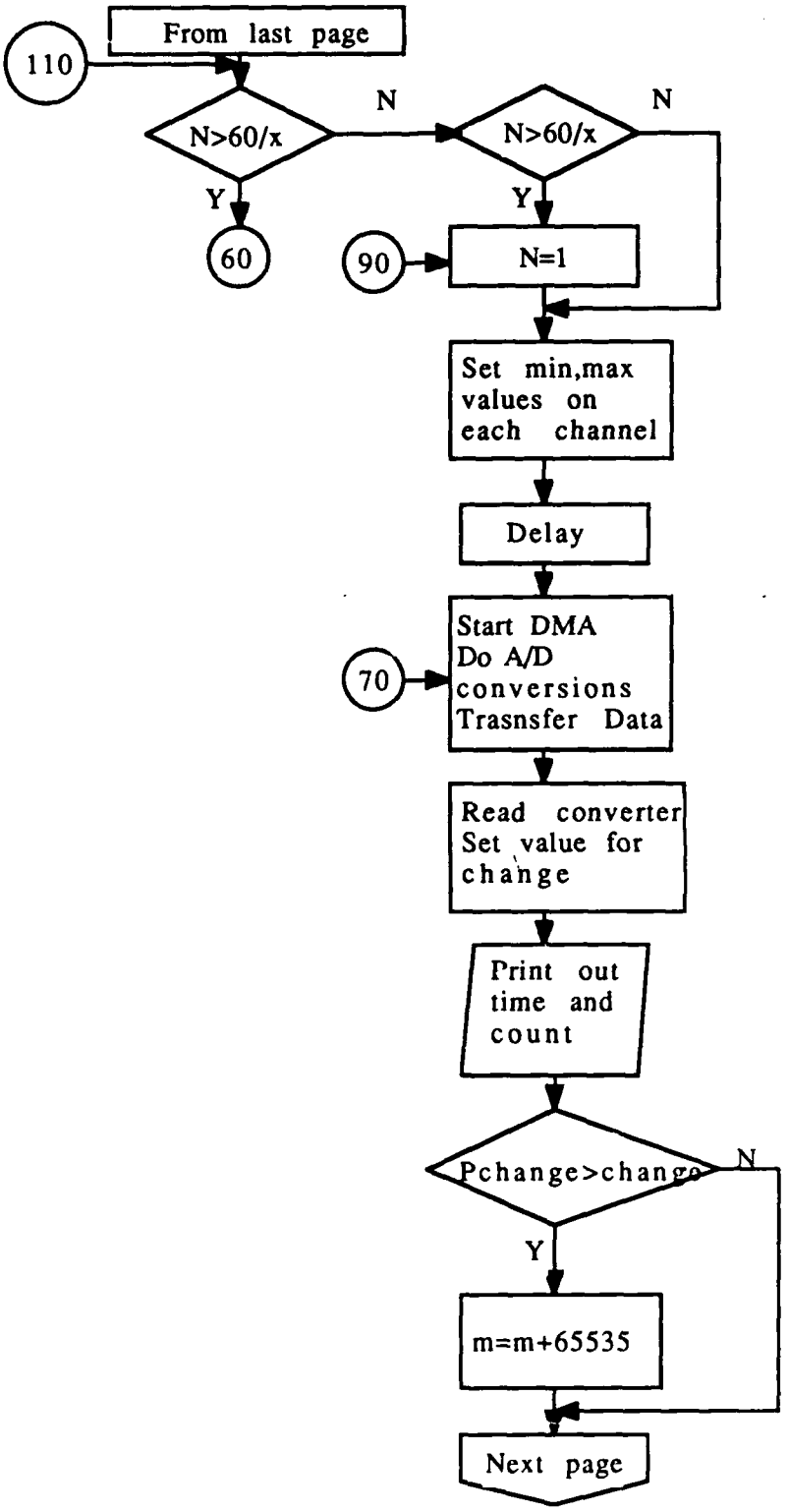
From last page
110
N>60/x
N
N>60/x
N
Y
60
Y
90
N=1
Set min,max values on each channel
Delay
Start DMA
Do A/D conversions
Trasnsfer Data
70
Read converter
Set value for change
Print out time and count
Pchange>change
N
Y
m=m+65535
Next page

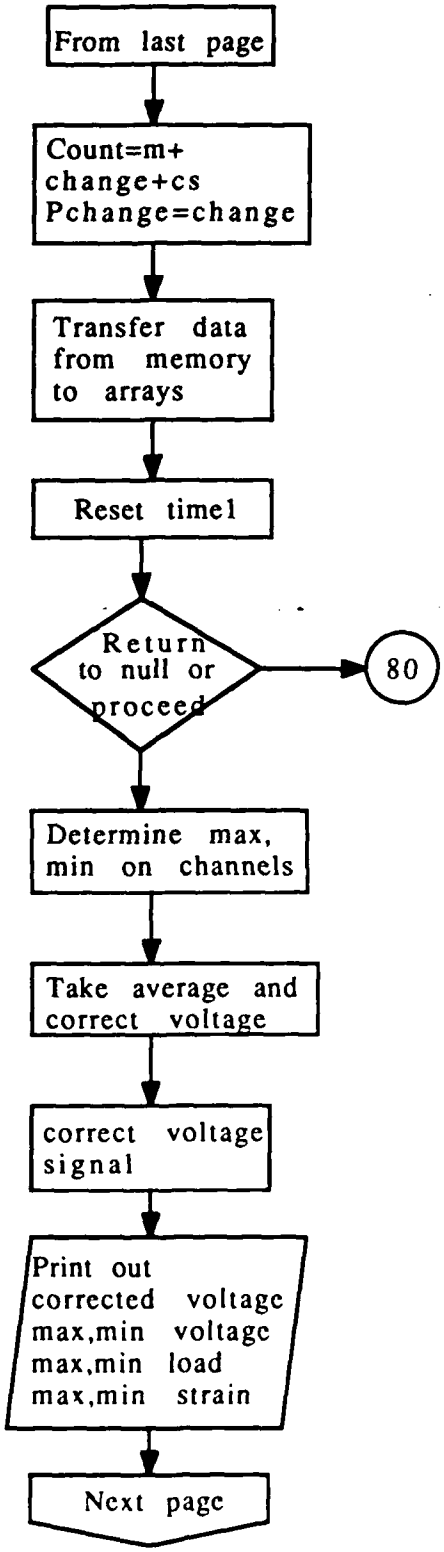
From last page
Count=m+
change+cs
Pchange=change
Transfer data
from memory
to arrays
Reset time1
Return
to null or
proceed
80
Determine max,
min on channels
Take average and
correct voltage
correct voltage
signal
Print out
corrected voltage
max,min voltage
max,min load
max,min strain
Next page

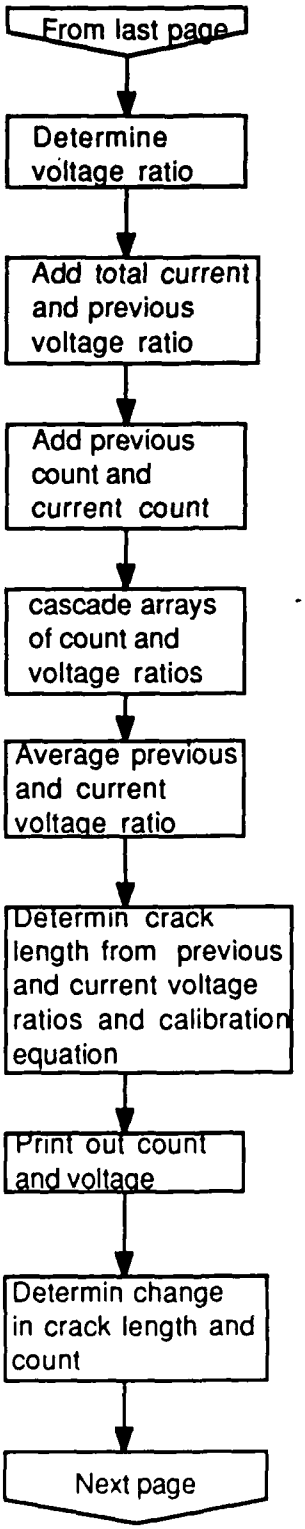
From last page
Determine voltage ratio
Add total current and previous voltage ratio
Add previous count and current count
cascade arrays of count and voltage ratios
Average previous and current voltage ratio
Determin crack length from previous and current voltage ratios and calibration equation
Print out count and voltage
Determin change in crack length and count
Next page

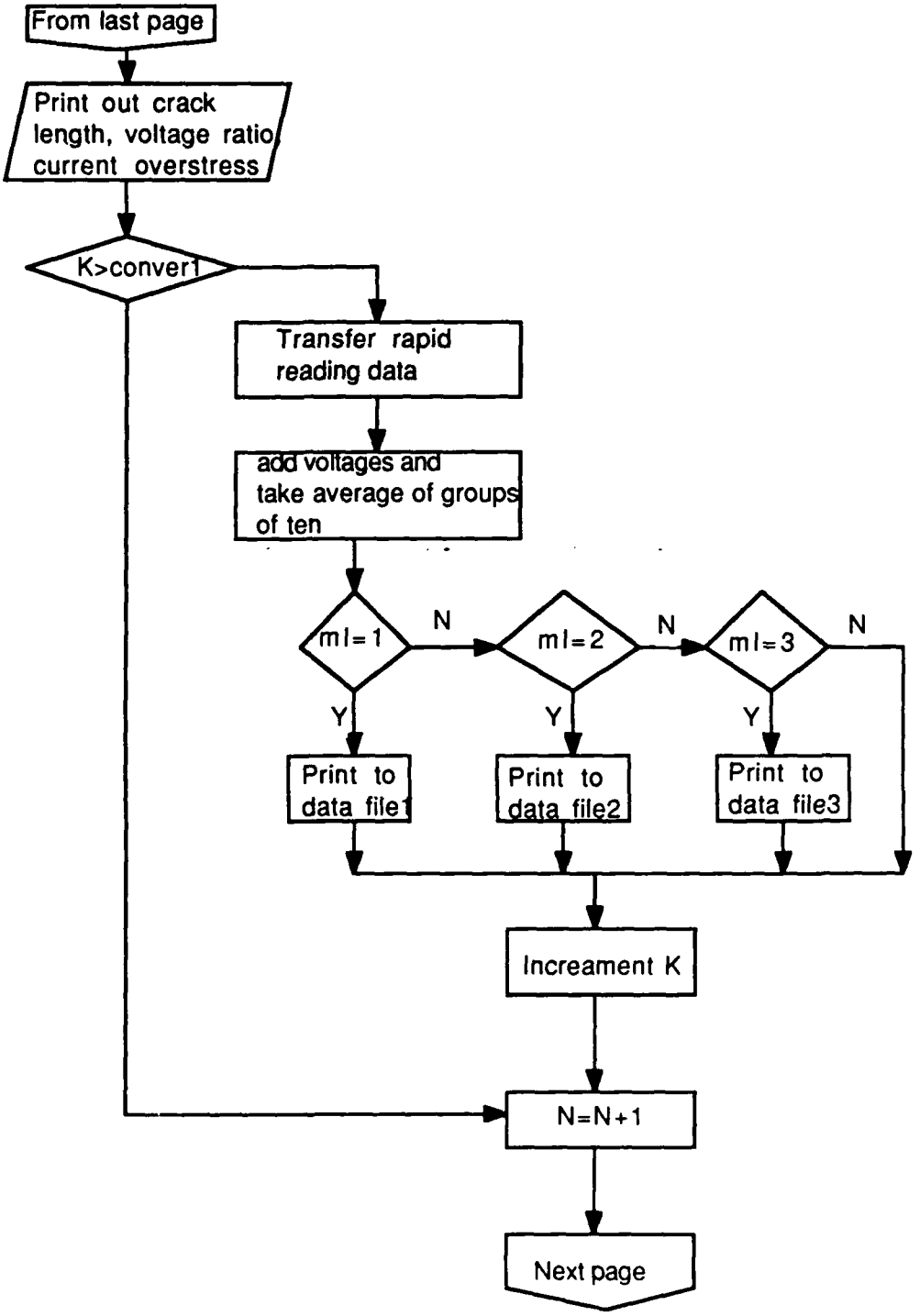
From last page
Print out crack length, voltage ratio current overstress
K>conver1
Transfer rapid reading data
add voltages and take average of groups of ten
ml=1
N
ml=2
N
ml=3
N
Y
Y
Y
Print to data file1
Print to data file2
Print to data file3
Increament K
N=N+1
Next page

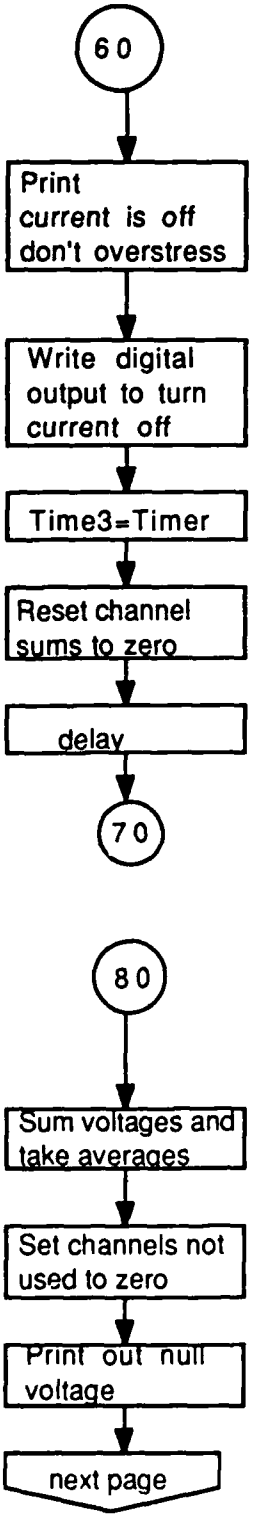
60
Print
current is off
don't overstress
Write digital
output to turn
current off
Time3=Timer
Reset channel
sums to zero
delay
70
80
Sum voltages and
take averages
Set channels not
used to zero
Print out null
voltage
next page

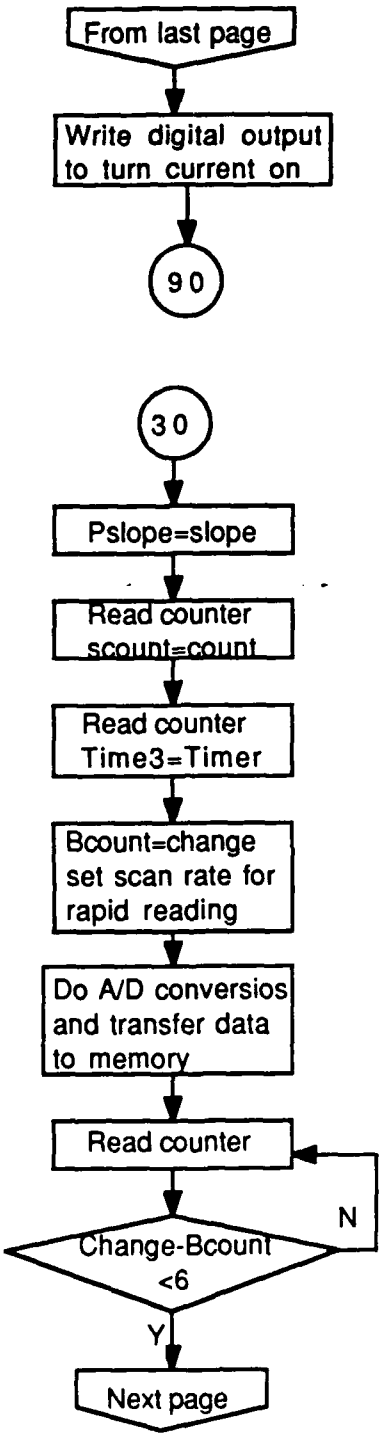
From last page
Write digital output to turn current on
90
30
Pslope=slope
Read counter scount=count
Read counter Time3=Timer
Bcount=change set scan rate for rapid reading
Do A/D conversios and transfer data to memory
Read counter
N
Change-Bcount <6
Y
Next page

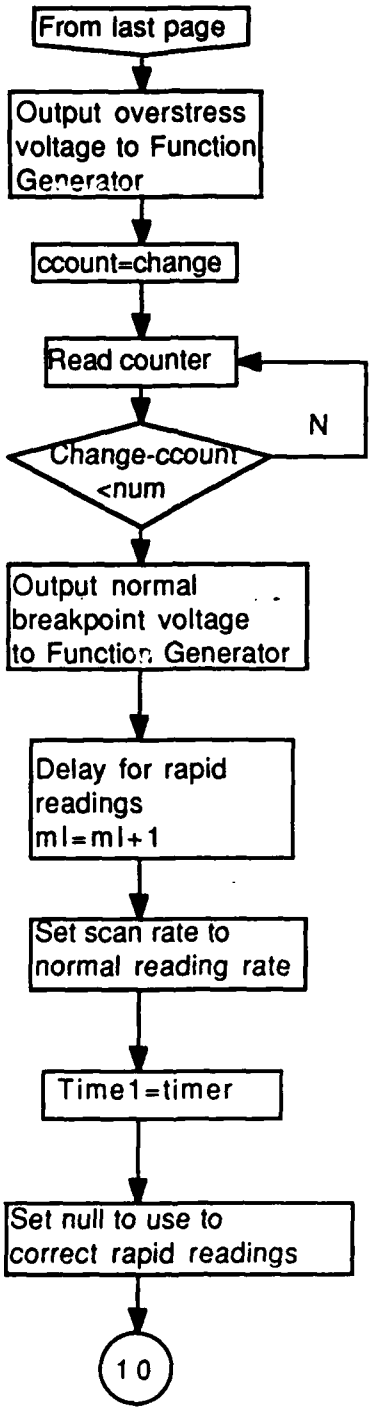
From last page
Output overstress voltage to Function Generator
ccount=change
Read counter
N
Change-ccount <num
Output normal breakpoint voltage to Function Generator
Delay for rapid readings
ml=ml+1
Set scan rate to normal reading rate
Time1=timer
Set null to use to correct rapid readings
10

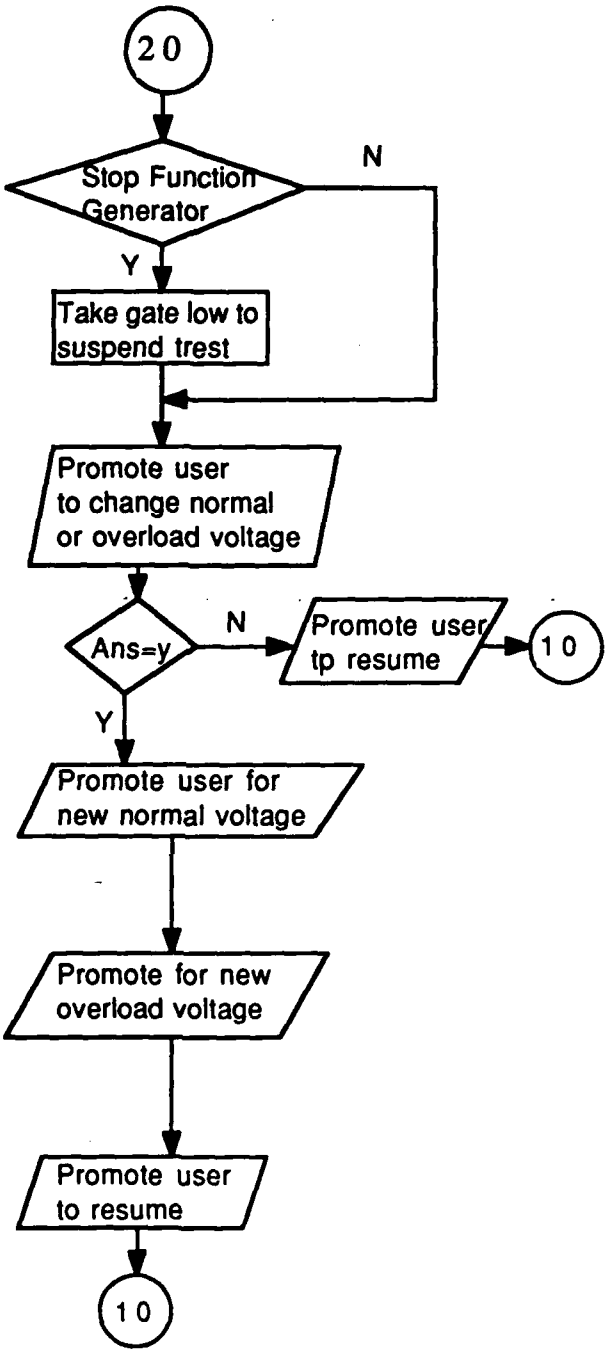
20
Stop Function Generator
N
Y
Take gate low to suspend trest
Promote user to change normal or overload voltage
Ans=y
N
Promote user tp resume
10
Y
Promote user for new normal voltage
Promote for new overload voltage
Promote user to resume
10

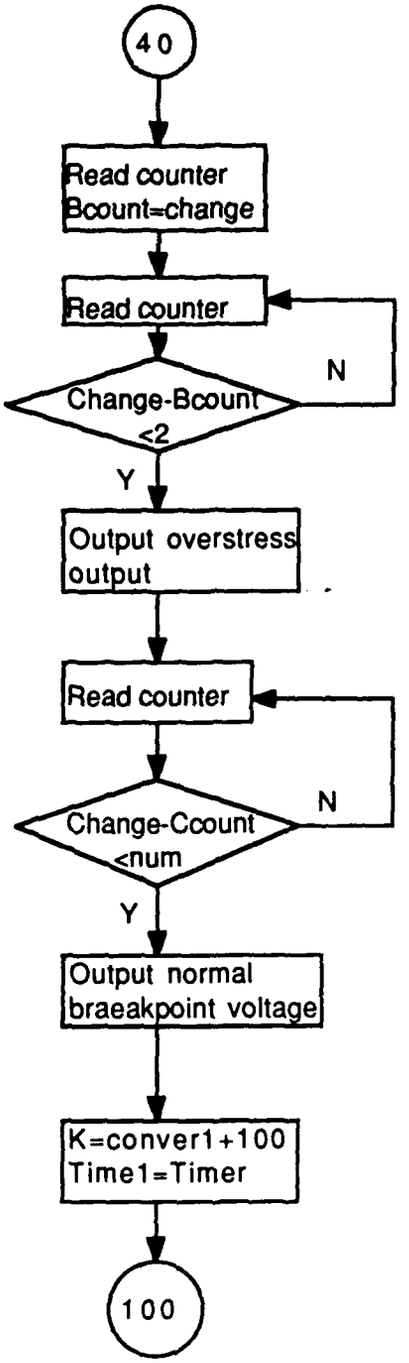
40
Read counter
Bcount=change
Read counter
N
Change-Bcount
<2
Y
Output overstress
output
Read counter
N
Change-Ccount
<num
Y
Output normal
braeakpoint voltage
K=conver1+100
Time1=Timer
100

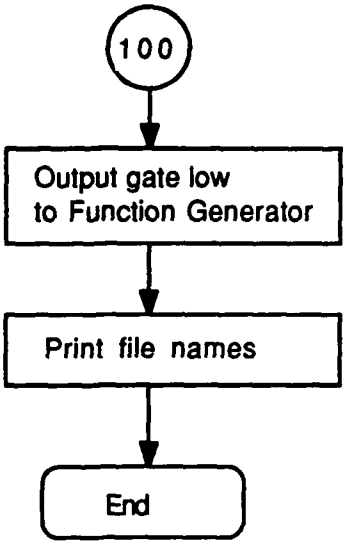
100
Output gate low
to Function Generator
Print file names
End

PROGRAM

Program for test control

```
10 'THIS IS THE FINAL VERSION OF THE TEST PROGRAM
20 ' AS OF 6-02-88 AND
50 ' IS STORED AS NEWNUL11.BAS
100 '   THIS NEWNUL11.BAS IS FOR COLLECTING AND RECORDING THE DATA
FROM
120 '   MTS MACHINE,EXTENSOMETER AND POTENTIONAL DROP
150 '
200 '
250 '
300 CLEAR
350 DEF SEG=0
400 SG=256*PEEK(&H511)+PEEK(&H510)
450 SG=SG+49152!/16
500 DEF SEG=SG
550 BLOAD "DASH16.BIN",0
600 '
650 'INITIALIZE PROGRAM
700 '
750 DIM DIO%(4),DT%(2000!),CH%(2000!),DAVG(10),DSUM(10),VOLT(10),BSUM(100)
800 DIM PVR(100),PCOUNT(100)
850 DIO%(0)=832
900 DIO%(1)=2
950 DIO%(2)=1
1000 MD%=0
1050 FLAG%=0
1100 DASH16=0
1150 CALL DASH16 (MD%,DIO%(0),FLAG%)
1200 IF FLAG% <>0 THEN PRINT "INITIALIZATION ERROR #";FLAG% :STOP
1250 ML=0
1300 N=1
1310 ON ERROR GOTO 22000
1350 KEY (5) ON
1400 KEY (6) ON
1450 KEY (2) ON
1470 KEY (9) ON
1500 KEY (10) ON
1550 ON KEY (5) GOSUB 19050
1600 ON KEY (6) GOSUB 17100
1650 ON KEY (2) GOSUB 14900
1670 ON KEY (9) GOSUB 21000
1700 ON KEY (10) GOSUB 18100
1750 CLS:INPUT"NAME FOR NORMAL RATE DATA FILE";F$
1800 INPUT"NAME FOR FIRST RAPID RATE DATA FILE";G$
```

```
1850 INPUT"NAME FOR SECOND RAPID RATE DATA FILE";H$
1900 INPUT"NAME FOR THIRD RAPID RATE DATA FILE";E$
1950 INPUT"STARTING NUMBER OF CYCLES";CS
2000 OPEN F$ FOR APPEND AS #1
2050 OPEN G$ FOR OUTPUT AS #2
2100 OPEN H$ FOR OUTPUT AS #3
2150 OPEN E$ FOR OUTPUT AS #4
2160 METAL$=LEFT$(F$,1)
2170 IF METAL$="T" OR METAL$="t" THEN
C1=-17.12129:C2=-15.72081:C3=9.748079:C4=175.5466:C5=29.25841
2180 IF METAL$="S" OR METAL$="s" THEN
C1=-12.41537:C2=-6.551828:C3=13.0006:C4=61.65978:C5=169.0192
2190 PRINT TAB(10)"The coefficients:"
2200 PRINT TAB(10) USING" #####.#####";C1,C2,C3
2210 PRINT TAB(10) USING" #####.#####";C4,C5
2250 INPUT"SETPOINT LOAD AS % OF FULL RANGE";SETPOINT
2300 SET=4095*(SETPOINT/50)
2350 SET2=SET
2400 INPUT"NORMAL LOAD AS % OF FULL RANGE";NORM
2450 NORM1=4095*(NORM/50)
2500 NORM2=NORM1
2550 INPUT"OVERLOAD AS % OF FULL RANGE";OVER
2600 OVER1=4095*(OVER/50)
2640 NUM=1:X=20:LL%=1:UL%=5:RATE=5000:CONVER=1000:RATE2=32000:SEC=1
2650 PRINT"NUMBER OF OVERLOAD CYCLES";NUM
2700 PRINT"TIME BETWEEN AUTOREADINGS";X
2750 PRINT"LOWER CHANNEL LIMIT";LL%
2800 PRINT"UPPER CHANNEL LIMIT";UL%
2850 PRINT"NORMAL READING RATE";RATE
2900 PRINT"NUMBER OF NORMAL RATE READINGS PER SAMPLE";CONVER
2950 PRINT"RAPID READING RATE";RATE2
3000 PRINT "SECONDS OF RAPID READINGS";SEC
3050 CONVER1=SEC*RATE2
3100 XX=0
3150 K=CONVER1+100
3200 INC=((UL%-LL%)+1)*10
3205 INPUT"HYDRAULICS ON";DUMB
3210 INPUT"FAN ON";DUMB
3215 INPUT"DC POWER SUPPLY DCR40-35A AT 10 AMPS";DUMB
3220 INPUT"CURRENT SWITCH, DC POWER SUPPLY AND OSCILLOSCOPE
ON";DUMB
3225 INPUT"EVENT COUNTER SET TO ZERO FOR A NEW TEST";DUMB
3230 INPUT"TEST MACHINE RANGE SET TO DESIRED NUMBER (10,20,50 OR
100)";DUMB
3250 INPUT "PUSH RETURN TO BEGIN TEST";DUMB$
3260 LPRINT"NORMAL RATE DATA FILE: ";F$
3265 LPRINT"STARTING NUMBER OF CYCLES: ";CS
```

```
3270 LPRINT"FIRST RAPID RATE DATA FILE: ";G$
3275 LPRINT"SECOND RAPID RATE DATA FILE: ";H$
3280 LPRINT"THIRD RAPID RATE DATA FILE: ";E$
3285 LPRINT"SETPOINT LOAD AS % OF FULL RANGE: ";SETPOINT
3290 LPRINT"NORMAL LOAD AS % OF FULL RANGE: ";NORM
3295 LPRINT"OVERLOAD AS % OF FULL RANGE: ";OVER:LPRINT:LPRINT
3300 FOR I=1000 TO 10 STEP -10
3350 SET3=(SET*10)/I
3400 MD%=15:DIO%(0)=1:DIO%(1)=SET3:FLAG%=X
3450 CALL DASH16 (MD%,DIO%(0),FLAG%)
3500 IF FLAG% <>0 THEN PRINT "ERROR IN D TO A #";FLAG% :STOP
3550 NEXT I
3600 '
3650 '
3700 'INITIALIZE COUNTER
3750 '
3800 MD%=11:DIO%(0)=-1
3850 CALL DASH16 (MD%,DIO%(0),FLAG%)
3900 IF FLAG% <>0 THEN PRINT "COUNTER ERROR #";FLAG% :STOP
3950 '
4000 '
4050 'SET SAMPLE RATE
4100 '
4150 SAMPLE RATE= 1,0,0/DIO%(0)*DIO%(1)
4200 DIO%(0)=2
4250 DIO%(1)=500000!/RATE
4300 MD%=17
4350 CALL DASH16 (MD%,DIO%(0),FLAG%)
4400 IF FLAG% <>0 THEN PRINT "ERROR IN TIMER #";FLAG% :STOP
4450 '
4500 '
4550 'SET SCAN LIMITS
4600 '
4650 '
4700 '
4750 DIO%(0)=LL%
4800 DIO%(1)=UL%
4850 MD%=1
4900 CALL DASH16 (MD%,DIO%(0),FLAG%)
4950 IF FLAG% <>0 THEN PRINT "ERROR IN SCAN LIMITS #";FLAG% :STOP
5000 '
5050 '
5100 ' START AND RUN TEST
5150 '
5200 TIME$="00:00:00"
5220 TIME1=TIMER
5250 MD%=15:DIO%(0)=0:DIO%(1)=NORM2:FLAG%=X
```

```
5300 CALL DASH16 (MD%,DIO%(0),FLAG%)
5350 IF FLAG% <>0 THEN PRINT "ERROR IN D TO A #";FLAG% :STOP
5400 MD%=15:DIO%(0)=1:DIO%(1)=SET2:FLAG%=X
5450 CALL DASH16 (MD%,DIO%(0),FLAG%)
5500 IF FLAG% <>0 THEN PRINT "ERROR IN D TO A #";FLAG% :STOP
5550 MD%=13:DIO%(0)=1:FLAG%=X
5600 CALL DASH16 (MD%,DIO%(0),FLAG%)
5650 IF FLAG% <>0 THEN PRINT "ERROR IN DIGITAL OUT #";FLAG% :STOP
5750 IF N>(60/X) THEN GOSUB 13100
5780 IF N>(60/X) THEN LPRINT USING"#######  ########  ##.####  ##.##########
##.##########";COUNT,TIME5,CL,PSLOPE,SLOPE
5800 IF N>(60/X) THEN N=1
5830 IF N>(60/X) THEN LPRINT USING"#######  ########  ##.####  .##########
.##########";COUNT,TIME5,CL,PSLOPE,SLOPE
5850 FOR I= LL% TO UL%
5900 DSUM(I)=0
5950 MIN(I)=10000
6000 MAX(I)=-10000
6050 BMIN(I)=10000
6100 BMAX(I)=-10000
6150 NEXT I
6200 IF (TIMER-TIME1)<(X-.25) THEN GOTO 6200
6250 GOSUB 6350
6300 GOTO 8200
6350 'START DMA
6400 DIO%(0)=CONVER
6450 DIO%(1)=&H2000
6500 DIO%(2)=1
6550 DIO%(3)=0
6600 MD%=6
6650 CALL DASH16 (MD%,DIO%(0),FLAG%)
6700 IF FLAG% <>0 THEN PRINT "ERROR IN DMAN #";FLAG% :STOP
6750 GOSUB 6850
6800 GOTO 7050
6850 MD%=12:DIO%(0)=1:DIO%(1)=0
6900 CALL DASH16 (MD%,DIO%(0),FLAG%)
6950 IF DIO%(1)<0 THEN CHANGE=-1-DIO%(1) ELSE CHANGE=65535!-DIO%(1)
7000 RETURN
7050 PRINT ""
7100 PRINT ""
7150 PRINT USING"    ELAPSED TIME       = ########.## SEC";TIMER
7200 TIME5=TIMER
7250 IF PCHANGE>CHANGE THEN M=M+65535!
7300 COUNT=M+CHANGE+CS
7350 'PRINT USING "#######.";PCOUNT(1)
7400 PCHANGE=CHANGE
7450 PRINT USING"    NUMBER OF CYCLES   =   #######";COUNT
```

```
7500 PRINT ""
7550 TIME2=TIMER
7600 DEL=(CONVER/RATE)+.05
7650 IF (TIMER-TIME2)<DEL THEN GOTO 7650
7700 'RETRIVE DATA
7750 DIO%(0)=CONVER
7800 DIO%(1)=&H2000
7850 DIO%(2)=0
7900 DIO%(3)=VARPTR(DT%(0))
7950 DIO%(4)=VARPTR(CH%(0))
8000 MD%=9
8050 CALL DASH16 (MD%,DIO%(0),FLAG%)
8100 TIME1=TIMER
8150 RETURN
8200 'DISPLAY DATA
8250 FOR I=0 TO (CONVER-1)
8300 DSUM(CH%(I))=DSUM(CH%(I))+DT%(I)
8350 IF MAX(CH%(I))<DT%(I) THEN MAX(CH%(I))=DT%(I)
8400 IF MIN(CH%(I))>DT%(I) THEN MIN(CH%(I))=DT%(I)
8450 NEXT I
8500 FOR I=LL% TO (LL%+1)
8550 DAVG(I)=DSUM(I)/(CONVER/((UL%-LL%)+1))
8600 VOLT(I)=(DAVG(I)/2048)*10
8650 CVOLT(I)=VOLT(I)-NVOLT(I)
8700 PRINT USING"    VOLTAGE CHANNEL##  = ###.##### VOLTS";I,CVOLT(I)
8750 NEXT I
8800 FOR I = (LL%+2) TO UL%
8850 VMAX(I)=(MAX(I)/2048)*10
8900 VMIN(I)=(MIN(I)/2048)*10
8950 NEXT I
9000 NORM2=NORM2-((((MAX(5)-MIN(5))*4)-NORM1)/2)
9050 SET2=SET2-(((MIN(5)*4)-SET)/2)
9100  PRINT  USING"        MAX-MIN  VOLTAGE  FG      ###.####      ###.####
VOLTS";VMAX(3),VMIN(3)
9150 MAXLOAD = VMAX(5)*5
9200 MINLOAD = VMIN(5)*5
9250  PRINT  USING"        MAX-MIN  LOAD              ###.####      ###.####
KN";MAXLOAD,MINLOAD
9300 MAXSTRAIN =VMAX(4)
9350 MINSTRAIN =VMIN(4)
9400  PRINT  USING"        MAX-MIN  COD               ###.####      ###.####
MM";MAXSTRAIN,MINSTRAIN
9450 VR=CVOLT(LL%+1)/CVOLT(LL%)
9500 TPVR=0
9550 TPCOUNT=0
9600 TCVR=0
9650 TCCOUNT=0
```

```
9700 PVR(5)=VR
9750 PCOUNT (5)=COUNT
9800 FOR NN=1 TO 5
9850 TPVR =TPVR+PVR(NN-1)
9900 TCVR=TCVR+PVR(NN)
9950 TPCOUNT=TPCOUNT+PCOUNT(NN-1)
10000 TCCOUNT=TCCOUNT+PCOUNT(NN)
10050 NEXT NN
10100 FOR NN=0 TO 4
10150 PVR (NN)=PVR(NN+1)
10200 PCOUNT (NN)= PCOUNT(NN+1)
10250 NEXT NN
10300 APVR=TPVR/5
10350 ACVR=TCVR/5
10400 APCOUNT=TPCOUNT/5
10450 ACCOUNT=TCCOUNT/5
10500 CL=C1+(C2*(VR))+(C3*(VR^2))+(C4*(VR^3))+(C5*(VR^4))
10550 PCL=C1+(C2*(APVR))+(C3*(APVR^2))+(C4*(APVR^3))+(C5*(APVR^4))
10600 CCL=C1+(C2*(ACVR))+(C3*(ACVR^2))+(C4*(ACVR^3))+(C5*(ACVR^4))
10650'LPRINT USING"###.#####";VOLT(1),CVOLT(1),NVOLT(1),VOLT(2),
CVOLT(2),NVOLT(2),VR,CL
10700 'LPRINT USING "########.";COUNT,TIME5
10750 PRINT #1,USING "########.#";COUNT,TIME5
10800 PRINT#1,USING"###.#####";CVOLT(1),NVOLT(1),CVOLT(2),NVOLT(2),
VR,CL
10810 PRINT #1,USING"###.#####";VMAX(3),VMIN(3),VMAX(4),VMIN(4),
VMAX(5),VMIN(5)
10850 DELCL=CCL-PCL
10900 DELCOUNT=ACCOUNT-APCOUNT
10950 SLOPE=DELCL/DELCOUNT
11000 PRINT USING"    CRACK LENGTH       = ###.####";CL
11050 PRINT USING"    VOLTAGE RATIO      = ###.####";VR
11100 'LPRINT DELCL,DELCOUNT
11150 PRINT"    CURRENT dA/dN     = ";SLOPE
11200 PRINT"  OVER STRESS dA/dN   = ";PSLOPE
11210 IF FLAG(1)=0 AND CL>17 THEN FLAG(1)=1:FLBEEP=1
11220 IF FLAG(2)=0 AND CL>23 THEN FLAG(2)=1:FLBEEP=1
11230 IF FLAG(3)=0 AND CL>28 THEN FLAG(3)=1:FLBEEP=1
11233 IF FLAG(4)=0 AND CL>40 THEN FLAG(4)=1:FL40=1
11237 IF CL>45! THEN GOSUB 19050
11240 IF FLBEEP=1 THEN BEEP:BEEP:PRINT"* * * * CHECK dA/dN BEFORE
OVERSTRESS (Hit F9 to stop message) * * * *":BEEP:BEEP
11245 IF FL40=1 THEN BEEP:BEEP:PRINT"* * * THIS TEST WILL AUTOMATICALLY
END AT 45mm * * *"
11250 'LPRINT SLOPE
11260 PRINT #1,SLOPE,PSLOPE
11300 '
```

```
11350 'THIS PORTION TRANSFERS RAPID READINGS
11400 'AND AVERAGES IN GROUPS OF 10
11450 '
11500 IF K>CONVER1 THEN GOTO 12750
11550 DIO%(0)=(INC*30)
11600 DIO%(1)=&H3000
11650 DIO%(2)=K
11700 DIO%(3)=VARPTR(DT%(0))
11750 DIO%(4)=VARPTR(CH%(0))
11800 MD%=9
11850 CALL DASH16 (MD%,DIO%(0),FLAG%)
11900 IF FLAG% <>0 THEN PRINT "ERROR DATA RETRIVAL #";FLAG% :STOP
11950 FOR Y = 0 TO (INC*29) STEP INC
12000 FOR B =Y TO (Y+(INC-1))
12050 BSUM(CH%(B))=BSUM(CH%(B))+DT%(B)
12100 NEXT B
12150 FOR L = LL% TO UL%
12200 BAVG(L)=BSUM(L)/10
12250 RVOLT(L)=(BAVG(L)/2048)*10
12300 BVOLT(L)=RVOLT(L)-NNVOLT(L)
12350 BSUM(L)=0
12400 IF ML=1 THEN PRINT #2, L, BVOLT(L),SCOUNT,XX
12450 IF ML=2 THEN PRINT #3, L, BVOLT(L),SCOUNT,XX
12500 IF ML=3 THEN PRINT #4, L, BVOLT(L),SCOUNT,XX
12550 NEXT L
12600 XX=XX+1
12650 NEXT Y
12700 K=K+(INC*30)
12750 N=N+1
12800 GOTO 5250
12850 '
12900 '
12950 'THIS PORTION TURNS OFF THE CURRENT
13000 'AND TAKES NULL READINGS
13050 '
13100 PRINT ""
13150 PRINT ""
13200 PRINT "******* CURRENT IS OFF WAIT DO NOT OVERSTRESS *******"
13250 MD%=13:DIO%(0)=3:FLAG%=X
13300 CALL DASH16 (MD%,DIO%(0),FLAG%)
13350 IF FLAG% <>0 THEN PRINT "ERROR IN DIG OUT #";FLAG% :STOP
13400 TIME3=TIMER
13450 FOR I = LL% TO UL%
13500 NSUM(I)=0
13550 NEXT I
13600 IF (TIMER-TIME3)<10 GOTO 13600
13650 GOSUB 6350
```

```
13700 FOR I=0 TO (CONVER-1)
13750 NSUM(CH%(I))=NSUM(CH%(I))+DT%(I)
13800 NEXT I
13850 PRINT " "
13900 FOR I=LL% TO UL%
13950 NAVG(I)=NSUM(I)/(CONVER/((UL%-LL%)+1))
14000 NVOLT(I)=(NAVG(I)/2048)*10
14050 NEXT I
14100 NVOLT(UL%)=0!
14150 NVOLT(UL%-1)=0!
14200 NVOLT(UL%-2)=0!
14250 FOR I= LL% TO (LL%+1)
14300 PRINT USING"   NULL VOLTAGE CHANNEL##  = ##.##### VOLTS";I,NVOLT(I)

14350 NEXT I
14400 PRINT " "
14450 PRINT "*** CURRENT BACK ON WAIT TILL AFTER NEXT READING ***"
14500 MD%=13:DIO%(0)=1:FLAG%=X
14550 CALL DASH16 (MD%,DIO%(0),FLAG%)
14600 IF FLAG% <>0 THEN PRINT "ERROR IN DIG OUT #";FLAG% :STOP
14650 RETURN
14700 '
14750 '
14800 'TAKE RAPID READINGS WITH OVERSTRESS
14850 '
14900 PSLOPE=SLOPE
14950 GOSUB 6850
15000 COUNT=M+CHANGE+CS
15050 SCOUNT=COUNT
15100 GOSUB 6850
15150 TIME3=TIMER
15200 BCOUNT=CHANGE
15250 DIO%(0)=2
15300 DIO%(1)=500000!/RATE2
15350 MD%=17
15400 CALL DASH16 (MD%,DIO%(0),FLAG%)
15450 DIO%(0)=CONVER1
15500 DIO%(1)=&H3000
15550 DIO%(2)=1
15600 DIO%(3)=0
15650 MD%=6
15700 CALL DASH16 (MD%,DIO%(0),FLAG%)
15750 GOSUB 6850
15800 IF (CHANGE-BCOUNT)<6 GOTO 15750
15850 MD%=15:DIO%(0)=0:DIO%(1)=OVER1:FLAG%=X
15900 CALL DASH16 (MD%,DIO%(0),FLAG%)
15950 CCOUNT=CHANGE
```

```
16000 GOSUB 6850
16050 IF (CHANGE-CCOUNT)<NUM THEN GOTO 16000
16100 MD%=15:DIO%(0)=0:DIO%(1)=NORM1:FLAG%=X
16150 CALL DASH16 (MD%,DIO%(0),FLAG%)
16200 IF FLAG% <>0 THEN PRINT "ERROR IN A TO D  #";FLAG% :STOP
16250 IF (TIMER-TIME3)<(SEC+.05) THEN GOTO 16250
16300 ML=ML+1
16350 K=0
16400 DIO%(0)=2
16450 DIO%(1)=500000!/RATE
16500 MD%=17
16550 CALL DASH16 (MD%,DIO%(0),FLAG%)
16600 IF FLAG% <>0 THEN PRINT "ERROR IN TIMER #";FLAG% :STOP
16650 TIME1=TIMER
16700 FOR I=LL% TO UL%
16750 NNVOLT(I)=NVOLT(I)
16800 NEXT I
16850 RETURN 5250
16900 '
16950 '
17000 'THIS PORTION SUSPENDS OPERATION
17050 '
17100 INPUT "DO YOU WANT TO STOP THE FUNCTION GEN.(Y,N)";GEN$
17110 LPRINT:LPRINT:LPRINT"FUNCTION KEY 6 HAS BEEN ACTIVATED.":BEEP
17120 LPRINT" HAS THE FUNCTION GENERATOR BEEN STOPPED? ";GEN$
17150 IF GEN$="N" THEN GOTO 17350
17200 MD%=13:DIO%(0)=0:FLAG%=X
17250 CALL DASH16 (MD%,DIO%(0),FLAG%)
17300 IF FLAG% <>0 THEN PRINT "ERROR IN DIGITAL OUT#";FLAG% :STOP
17350 INPUT "DO YOU WANT TO CHANGE THE SETPOINT,NORMAL LOAD OR
OVERLOAD (Y,N)?";V$
17400 IF V$="N" THEN GOTO 17800
17410 INPUT "NEW SET POINT LOAD AS % OF FULL RANGE:";SETPOINT
17415 LPRINT"NEW SET POINT LOAD AS % OF FULL RANGE: ";SETPOINT
17420 SET2=4095*(SETPOINT/50)
17430 SET=SET2
17450 INPUT"NEW NORMAL LOAD AS % OF FULL RANGE:";NORM
17455 LPRINT"NEW NORMAL LOAD AS % OF FULL RANGE: ";NORM
17500 NORM1=4095*(NORM/50)
17550 NORM2=NORM1
17600 INPUT"NEW OVERLOAD AS % OF FULL RANGE:";OVER
17605 LPRINT"NEW OVERLOAD AS % OF FULL RANGE: ";OVER
17650 OVER1=4095*(OVER/50)
17800 INPUT "PRESS ENTER TO RESUME";DUMB
17810 BEEP:LPRINT:LPRINT
17850 RETURN 5250
17900 '
```

```
17950 '
18000 'THIS PORTION OVERSTRESSES WITHOUT RAPID READINGS
18050 '
18060 PSLOPE=SLOPE
18100 GOSUB 6850
18150 BCOUNT=CHANGE
18200 GOSUB 6850
18250 IF (CHANGE-BCOUNT)<2 GOTO 18200
18300 MD%=15:DIO%(0)=0:DIO%(1)=OVER1:FLAG%=X
18350 CALL DASH16 (MD%,DIO%(0),FLAG%)
18400 GOSUB 6850
18450 CCOUNT=CHANGE
18500 GOSUB 6850
18550 IF (CHANGE-CCOUNT)<NUM THEN GOTO 18500
18600 MD%=15:DIO%(0)=0:DIO%(1)=NORM1:FLAG%=X
18650 CALL DASH16 (MD%,DIO%(0),FLAG%)
18700 K=CONVER1+100
18750 TIME1=TIMER
18800 RETURN 5750
18850 '
18900 '
18950 ' THIS PORTION ENDS THE TEST
19000 '
19050 MD%=13:DIO%(0)=0:FLAG%=X
19100 CALL DASH16 (MD%,DIO%(0),FLAG%)
19150 IF FLAG% <>0 THEN PRINT "ERROR IN DIGITAL OUT #";FLAG% :STOP
19200 FOR I=1 TO 100
19250 SET3=SET/I
19300  MD%=15:DIO%(0)=1:DIO%(1)=SET3:FLAG%=X
19350 CALL DASH16 (MD%,DIO%(0),FLAG%)
19400 IF FLAG% <>0 THEN PRINT "ERROR IN D TO A #";FLAG% :STOP
19450 NEXT I
19500  MD%=15:DIO%(0)=1:DIO%(1)=0:FLAG%=X
19550 CALL DASH16 (MD%,DIO%(0),FLAG%)
19600 PRINT ""
19650 PRINT ""
19700 PRINT "************************************************"
19750 PRINT "   YOUR NORMAL RATE DATA FILE IS NAMED  ";F$
19800 PRINT "   YOUR FIRST RAPID RATE DATA FILE IS NAMED  ";G$
19850 PRINT "   YOUR SECOND RAPID RATE DATA FILE IS NAMED  ";H$
19900 PRINT "   YOUR THIRD RAPID RATE DATA FILE IS NAMED  ";E$
19950 PRINT "    WRITE THEIR NAMES DOWN !!!!!! "
20000 PRINT"************************************************"
20050 CLOSE
20060 LPRINT USING"#######  ########  ##.####  ##.########## ##.##########  TEST
ENDED";COUNT,TIME5,CL,PSLOPE,SLOPE
20070 LPRINT:LPRINT:LPRINT:LPRINT
```

```
20100 END
21000 FLBEEP=0:RETURN
21010 END
22000 PRINT"ERROR: ";ERR;" OCCURED":LPRINT"ERROR: ";ERR;" OCCURED":GOTO
19050
```

Program for calibration

```
50 'THIS PROGRAM IS STORED AS NEWCAL.BAS
100 'used for calibration
150 '
200 '
250 '
300 CLEAR
350 DEF SEG=0
400 SG=256*PEEK(&H511)+PEEK(&H510)
450 SG=SG+49152!/16
500 DEF SEG=SG
550 BLOAD "DASH16.BIN",0
600 '
650 'INITIALIZE PROGRAM
700 '
750 DIM DIO%(4),DT%(2500!),CH%(2500!),DAVG(10),DSUM(10),VOLT(10),
      BSUM(100)
800 DIO%(0)=832
850 DIO%(1)=2
900 DIO%(2)=1
950 MD%=0
1000 FLAG%=0
1050 DASH16=0
1100 CALL DASH16 (MD%,DIO%(0),FLAG%)
1150 IF FLAG% <>0 THEN PRINT "INITIALIZATION ERROR #";FLAG%:STOP
1200 ML=0
1250 N=7
1300 KEY (6) ON
1350 KEY (5) ON
1400 KEY (10) ON
1450 ON KEY (6) GOSUB 9200
1500 ON KEY (5) GOSUB 9900
1550 ON KEY (10) GOSUB 4700
1600 INPUT"NAME FOR DATA FILE";F$
1650 OPEN F$ FOR OUTPUT AS #1
1700 INPUT"NORMAL LOAD AS % OF FULL RANGE";NORM
1750 NORM1=(4095*(NORM/100))*2
1800 INPUT"LOWER CHANNEL LIMIT";LL%
1850 INPUT"UPPER CHANNEL LIMIT";UL%
1900 INPUT"READING RATE";RATE
1950 INPUT"NUMBER OF READINGS PER SAMPLE";CONVER
2000 XX=0
2050 X=10
2100 '
```

```
2150 'INITIALIZE COUNTER
2200 '
2250 MD%=11:DIO%(0)=-1
2300 CALL DASH16 (MD%,DIO%(0),FLAG%)
2350 IF FLAG% <>0 THEN PRINT "COUNTER ERROR #";FLAG% :STOP
2400 '
2450 '
2500 'SET SAMPLE RATE
2550 '
2600 'SAMPLE RATE= 1,000,000/DIO%(0)*DIO%(1)
2650 DIO%(0)=2
2700 DIO%(1)=500000!/RATE
2750 MD%=17
2800 CALL DASH16 (MD%,DIO%(0),FLAG%)
2850 IF FLAG% <>0 THEN PRINT "ERROR IN TIMER #";FLAG% :STOP
2900 '
2950 '
3000 'SET SCAN LIMITS
3050 '
3100 '
3150 '
3200 DIO%(0)=LL%
3250 DIO%(1)=UL%
3300 MD%=1
3350 CALL DASH16 (MD%,DIO%(0),FLAG%)
3400 IF FLAG% <>0 THEN PRINT "ERROR IN SCAN LIMITS #";FLAG%:STOP
3450 '
3500 '
3550 ' START AND RUN TEST
3600 '
3650 MD%=15:DIO%(0)=0:DIO%(1)=NORM1:FLAG%=X
3700 CALL DASH16 (MD%,DIO%(0),FLAG%)
3750 IF FLAG% <>0 THEN PRINT "ERROR IN D TO A #";FLAG% :STOP
3800 MD%=13:DIO%(0)=1:FLAG%=X
3850 CALL DASH16 (MD%,DIO%(0),FLAG%)
3900 IF FLAG% <>0 THEN PRINT "ERROR IN DIG OUT #";FLAG% :STOP
3950 TIME$="00:00:00"
4000 FOR I= LL% TO UL%
4050 DSUM(I)=0
4100 NEXT I
4150 TIME1=TIMER
4200 IF N>(60/X) THEN GOSUB 7600
4250 IF N>(60/X) THEN N=2
4300 IF N=3 THEN PRINT " ****  OK F10 TO TAKE READING  ****"
4350 IF N=3 THEN PRINT"              F6 TO SUSPEND F5 TO END"
4550 IF (TIMER-TIME1)<(X-.25) THEN GOTO 4550
4600 N=N+1
```

```
4650 GOTO 4150
4700 GOSUB 4800
4750 GOTO 6600
4800 'START DMA
4850 DIO%(0)=CONVER
4900 DIO%(1)=&H2000
4950 DIO%(2)=1
5000 DIO%(3)=0
5050 MD%=6
5100 CALL DASH16 (MD%,DIO%(0),FLAG%)
5150 IF FLAG% <>0 THEN PRINT "ERROR IN DMAN #";FLAG% :STOP
5200 GOSUB 5300
5250 GOTO 5550
5300 MD%=12:DIO%(0)=1:DIO%(1)=0
5350 CALL DASH16 (MD%,DIO%(0),FLAG%)
5400 IF FLAG% <>0 THEN PRINT "ERROR IN READING COUNTER #";FLAG%
          :STOP
5450 IF DIO%(1)<0 THEN CHANGE=-1-DIO%(1) ELSE
   CHANGE=65535!-DIO%(1)
5500 RETURN
5550 PRINT ""
5600 PRINT ""
5650 PRINT USING"    ELAPSED TIME    = ########.## SEC";TIMER
5700 IF Y>CHANGE THEN M=M+65535!
5750 COUNT=M+CHANGE+CS
5800 Y=CHANGE
5850 PRINT USING"    NUMBER OF CYCLES    = #######";COUNT
5900 PRINT ""
5950 TIME2=TIMER
6000 DEL=(CONVER/(1000000!/RATE))+.05
6050 IF (TIMER-TIME2)<DEL THEN GOTO 6050
6100 'RETRIVE DATA
6150 DIO%(0)=CONVER
6200 DIO%(1)=&H2000
6250 DIO%(2)=0
6300 DIO%(3)=VARPTR(DT%(0))
6350 DIO%(4)=VARPTR(CH%(0))
6400 MD%=9
6450 CALL DASH16 (MD%,DIO%(0),FLAG%)
6500 TIME1=TIMER
6550 RETURN
6600 'DISPLAY DATA
6650 FOR I=0 TO (CONVER-1)
6700 DSUM(CH%(I))=DSUM(CH%(I))+DT%(I)
6750 NEXT I
6800 INPUT"CRACK LENGTH";CL
6850 CL=CL+15.2
```

```
6855 LPRINT
6860 LPRINT USING"                    CL      ###.####";CL
6900 FOR I=LL% TO UL%
6950 DAVG(I)=DSUM(I)/(CONVER/((UL%-LL%)+1))
7000 VOLT(I)=(DAVG(I)/2048)*10
7050 CVOLT(I)=VOLT(I)-NVOLT(I)
7100 PRINT USING"    VOLTAGE CHANNEL##  = ###.##### VOLTS";I,
      CVOLT(I)
7150 PRINT #1, CVOLT(I),
7200 NEXT I
7225 VR=CVOLT(2)/CVOLT(1)
7230 PRINT USING"                   VR      ###.####";VR
7235 INVR=1/VR
7240 PRINT USING"                 INVR      ###.####";INVR
7245 LPRINT USING"                  VR      ###.####";VR
7246 LPRINT USING"                INVR      ###.####";INVR
7250 PRINT #1,COUNT,CL,VR
7300 RETURN 4000
7350 '
7400 '
7450 'THIS PORTION TURNS OFF THE CURRENT
7500 'AND TAKES NULL READINGS
7550 '
7600 PRINT ""
7650 PRINT ""
7700 PRINT "******* CURRENT IS OFF WAIT *******"
7750 MD%=13:DIO%(0)=3:FLAG%=X
7800 CALL DASH16 (MD%,DIO%(0),FLAG%)
7850 IF FLAG% <>0 THEN PRINT "ERROR IN DIG OUT #";FLAG% :STOP
7900 TIME3=TIMER
7950 FOR I = LL% TO UL%
8000 NSUM(I)=0
8050 NEXT I
8100 IF (TIMER-TIME3)<10 GOTO 8100
8150 GOSUB 4800
8200 FOR I=0 TO (CONVER-1)
8250 NSUM(CH%(I))=NSUM(CH%(I))+DT%(I)
8300 NEXT I
8350 PRINT " "
8400 FOR I=LL% TO UL%
8450 NAVG(I)=NSUM(I)/(CONVER/((UL%-LL%)+1))
8500 NVOLT(I)=(NAVG(I)/+2048)*10
8550 NVOLT(UL%)=0!
8600 NVOLT(UL%-1)=0!
8650 PRINT USING" NULL VOLTAGE CHANNEL##  = ##.##### VOLTS";I,
       NVOLT(I)
8700 NEXT I
```

```
8750 PRINT " "
8760 MD%=13:DIO%(0)=1:FLAG%=X
8770 CALL DASH16 (MD%,DIO%(0),FLAG%)
8780 IF FLAG% <>0 THEN PRINT "ERROR IN DIG OUT #";FLAG% :STOP
8800 PRINT "*** CURRENT BACK ON WAIT 10 SEC FOR NEXT READING ***"
8850 PRINT " "
8900 PRINT " "
8950 RETURN 4250
9000 '
9050 '
9100 'THIS PORTION SUSPENDS OPERATION
9150 '
9200 MD%=13:DIO%(0)=0:FLAG%=X
9250 CALL DASH16 (MD%,DIO%(0),FLAG%)
9300 IF FLAG% <>0 THEN PRINT "ERROR IN DIG OUT #";FLAG% :STOP
9301 INPUT"DO YOU WANT TO CHANGE THE DELTA LOAD (Y,N)";V$
9302 IF V$="N" THEN GOTO 9350
9303 INPUT "NEW DELTA LOAD";NORM
9304 NORM1=4095*(NORM/50)
9305 MD%=15:DIO%(0)=0:DIO%(1)=NORM1:FLAG%=X
9306 CALL DASH16 (MD%,DIO%(0),FLAG%)
9307 IF FLAG% <>0 THEN PRINT "ERROR IN D TO A #";FLAG% :STOP
9350 INPUT "PRESS ENTER TO RESUME";DUMB
9400 MD%=13:DIO%(0)=1:FLAG%=X
9450 CALL DASH16 (MD%,DIO%(0),FLAG%)
9500 IF FLAG% <>0 THEN PRINT "ERROR IN DIG OUT #";FLAG% :STOP
9550 RETURN 4000
9600 '
9650 '
9700 '
9750 '
9800 ' THIS PORTION ENDS THE TEST
9850 '
9900 MD%=13:DIO%(0)=0:FLAG%=X
9950 CALL DASH16 (MD%,DIO%(0),FLAG%)
10000 IF FLAG% <>0 THEN PRINT "ERROR IN DIG OUT #";FLAG% :STOP
10050 PRINT ""
10100 PRINT ""
10150 PRINT "*******************************************"
10200 PRINT "   YOUR  DATA FILE IS NAMED  ";F$
10250 PRINT "    WRITE THE NAME DOWN !!!!!! "
10300 PRINT "*******************************************"
10350 CLOSE
10400 END
```